Application of Polymer Ageing Models to Cable Geometry and Time-To-Failure Distributions

Thesis submitted for the degree of

Doctor of Philosophy

at the University of Leicester

by

Elizabeth Susan Cooper MPhys (Hons)

Department of Engineering

University of Leicester

October 2002

Acknowledgements

I would like to thank my supervisors Professors John Fothergill and Len Dissado for all their help, guidance and support during this project. I am grateful to the EPSRC and BICC Cables for initially funding the project, and to Pirelli cables for continuing the funding after taking over BICC. I'd like to thank Nigel Hampton, John Lewis, Mark Dickinson, Fanggao Chang and Steven Betteridge for some very useful input at various stages of the project. I'm also grateful to everyone I've worked with in the HV lab of the engineering department.

Huge thanks must go to my husband Richard, for love, encouragement and proofreading way above and beyond the call of duty. I'm also very grateful for the support of my family, who have all been very encouraging. I'd like to thank some very good friends - especially Virginia and Anita for putting up with a lot of moaning. Thanks also to Suzanne, Kelham, Catherine, Eve, Simon, Dobbo, Tolcher, Taylor, Twiddle, Rich T and Steve for providing welcome distractions.

Application of Polymer Ageing Models to Cable Geometry and Time-To-Failure Distributions

by
Elizabeth Susan Cooper

Abstract

Polymer ageing models predict the working lifetime of polymeric insulation in terms of the electrical and thermal stresses to which it is subjected. Two such models are investigated in this thesis and are found to be mathematically similar even though they are based on different mechanisms for the way in which an electric field accelerates the ageing process. It is shown that both models can successfully fit characteristic time-to-failure data from ageing experiments involving thin films. A new method is developed to allow the ageing models to be applied to cable insulation, where the field and temperature are not spatially constant. This method is used to apply one of the models to characteristic lifetime data from experiments involving cables. The fits to data are found to be good, and resulting parameter values are used as the basis for a discussion of the possible effects of specimen volume on ageing.

The distribution of failure times observed when thin films and cable insulation are aged at a given experimental condition has also been investigated. This has been carried out using distributions of the activation free energy of ageing within one of the ageing models. It is established that small changes in the minimum activation energy from specimen to specimen could be responsible for the observed failure statistics. Changes in the activation energy distributions with ageing condition suggest that ageing may involve conformational re-arrangements of chain segments in the crystalline-amorphous interface. This is in broad agreement with the conclusions of other workers.

Table of Contents

1. Introduction

Polymeric materials are used as electrical insulators in a wide range of forms and applications, from thin films in capacitors to thick insulation layers in high voltage power cables. Insulation failure in such systems often means failure of the whole structure, and manufacturers and users are therefore concerned with calculating how long insulation will last under working conditions. Consequently, various functions exist for trying to calculate the working lifetimes of polymers under electrical and thermal stress [e.g. 1,2,3,4 – see also further references in chapter 2]. Some are purely empirical, and others have more of a theoretical basis.

A widely used empirical model is known as the inverse power law, or IPL. This predicts the lifetime of a polymeric specimen in terms of the voltage applied to it, and two empirical constants – a multiplier and an exponent. This model tends only to hold over fairly narrow voltage ranges. In order for extrapolation between temperature and voltage regimes to be possible, as well as a feeling that a lifetime prediction would benefit from a better understanding of the physical processes at work during ageing, various theory-based lifetime models have also been developed. Many of these (including those described in 1-4) are based on the idea that ageing can be described in terms of chemical rate reactions, which was first suggested by Dakin in 1948 [5].

Two of the theory-based models (called here the DMM and the Lewis models) are discussed in some detail in the next chapter. Previously, both of these models have been successfully fitted to characteristic lifetime data from ageing experiments involving thin film specimens [6,7]. In this thesis, application of the DMM model is extended to characteristic lifetime data from ageing experiments involving cable specimens. The model is shown to be able to fit such data well, and the method derived to fit the models to cable data introduces some interesting questions about the role of specimen volume in polymeric ageing. The DMM model is also applied to complete time-to-failure data sets for both thin film and cable ageing experiments, to try to get a better understanding of the physical reasons for the statistical nature of time-to-failure distributions.

The two models used in this thesis aim to predict the time-to-failure of any polymeric specimen as a function of the field, E and temperature, T it experiences. The model lifetime equations are therefore dependent on E and T, and each also contains various parameters. Values for these parameters can be obtained from fitting the model equations to data from ageing experiments at known E and T conditions. Once parameter values are obtained for specimens of a certain type, the lifetime of other specimens of the same type can be predicted at any given field and temperature. Here, specimens of a certain 'type' are those of the same size, shape and material aged under an electrical field with the same frequency.

Used only this way, the models can be seen to be semi-empirical – parameter values obtained by experiment are used to predict insulation lifetime in much the same was as functions that have no theoretical basis at all. An entirely empirical approach to lifetime prediction is often considered adequate – after all, the aim of all the functions is basically to accurately predict service lifetimes of insulation systems. However, an understanding of the physical processes at work during ageing is likely to lead ultimately to a much better method of lifetime prediction.

It is possible to make steps towards a better understanding of ageing using the DMM and Lewis models. This can be done by analysis of parameter values obtained from fitting the models to different sets of ageing data. This is because the derivations of both of the lifetime functions are such that each parameter has a physical meaning relating to the ageing process. The values obtained for the parameters in different types of ageing experiment - *e.g.* in AC and DC ageing experiments, experiments involving different materials, or specimens of different sizes and shapes -can therefore reveal some information about how the ageing process differs with frequency, material, size or volume.

It should be noted that both of the models mentioned here are concerned with the *ageing* part of insulation failure. 'Breakdown' is used throughout this thesis to refer to the process by which a polymer ultimately fails, and this is assumed to be a short-lived, catastrophic event. 'Ageing', on the other hand, is used to describe a lengthy process that precedes breakdown. Ageing is considered to be a process that alters the polymer on a microscopic level in such a way as to make the breakdown process

possible, and sometimes inevitable. The models therefore strictly describe the time to the beginning of a breakdown process, rather than a time-to-failure. Ageing, however, is assumed throughout to be the time-limiting part of failure, so that the time-to-failure is approximately equal to the time predicted by the models. The good fits to data achieved seem to justify this assumption.

To date, both models have been successfully fitted to data from ageing experiments involving thin film specimens of various polymer materials [6,7], and an example of this is given in chapter 3. Work has also been carried out to investigate the electrical field frequency effects of ageing, through examination of differences in DMM parameter values between AC and DC ageing experiments [6,8]. However, the effects of volume, size or shape of specimens on lifetime and ageing have been less thoroughly addressed in the literature, and these factors are not explicitly taken into account by either of the models.

One situation in which shape must affect ageing is if a specimen's shape is such that E and/or T is not spatially constant throughout the material. Application of the ageing models, which depend on E and T, is then not straightforward. This is a common real-life situation – an example being cable insulation, where cylindrical geometry leads to radial E and T variations. A method for applying the models to cable geometry is developed in chapter 4. Such a method is important so that cable manufacturers can use ageing models to accurately predict in a non-phenomenological way the working lifetime of the cables they produce. The method developed in chapter 4 is applied to some cable ageing data in chapter 5. The resulting parameter values are then used as the basis for a discussion of the possible effects of volume on ageing.

As mentioned before, both of the ageing models discussed in this thesis (along with other ageing models) predict time-to-failure in terms of the electrical stress and temperature experienced by a specimen. This means that at any given E and T condition they all predict a single time-to-failure. In reality, in a group of nominally identical specimens tested under the same E and T conditions, each specimen will tend to fail at a different time. This distribution of failure times at a given experimental condition is investigated in chapter 6 in terms of the implied distributions of DMM parameter values within the model equation. The way that the DMM parameter

distributions change with ageing condition is then discussed, and this gives further insight into the ageing process.

In order to try to understand the physics of the ageing process in polymers, it is first necessary to have an understanding of polymeric morphology and structure. The process of charge trapping in polymers under electrical stress is also important to ageing. A brief introduction to these subjects is therefore given in the next sections.

1.1 Polymer Structure

Polymers are made up of long-chain molecules, which comprise many identical repeating units, called monomers. The simplest example of a polymer chain unit is that of polyethylene (PE), which is shown below [e.g. 9].

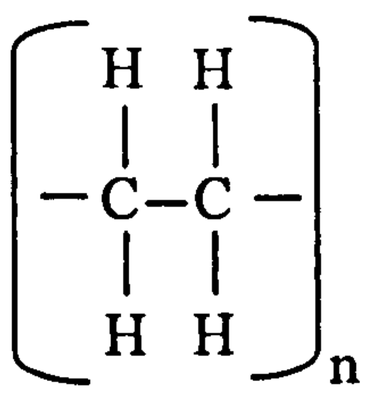

Figure 1.1

Polymer chains necessarily have molecular units different from the monomer at either end. Since each chain may contain of the order of 10^3-10^5 monomer units [10], the influence of end groups on many of the bulk properties of the material is minimal, but they can have a significant effect upon net space charge since they are charge trapping centres.

An example of a polymer with a more complicated structure is polyethylene-terephthalate (PET), the repeating unit, or monomer of which is shown in figure 1.2. [e.g. 10]

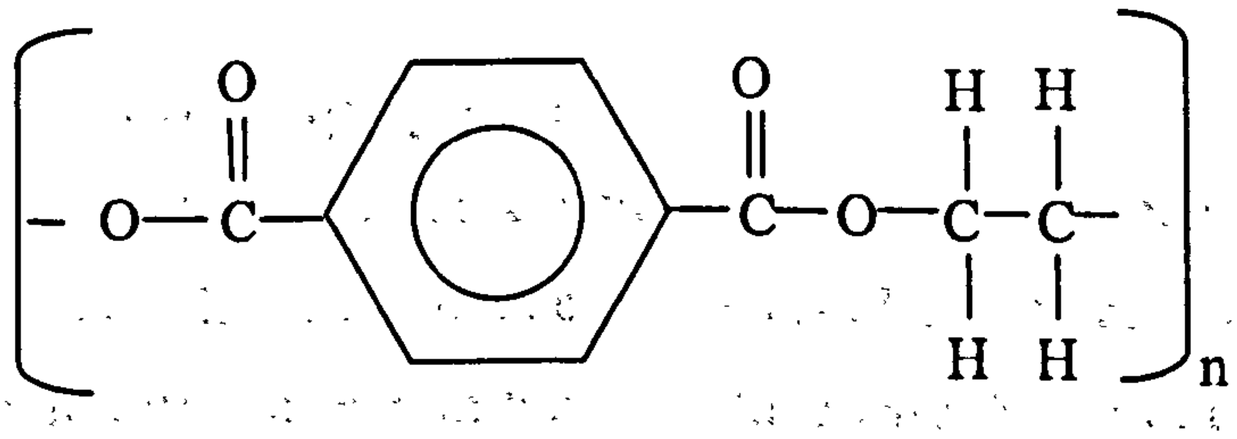

Figure 1.2

The materials above are chosen as examples because they are good illustrations of a simple and a more complicated monomer structure. They are also both very relevant here, since the data the models are fitted to in the rest of the thesis are from ageing experiments carried out on PE and PET specimens. In fact, the PE examined later in the thesis is actually cross-liked PE, known as XLPE. XLPE is PE that has been treated to join PE polymer chains together, so that in an extreme case the whole structure could actually comprise one single molecule.

The shape of the constituent monomer and the degree of cross-linking are some of the factors that affect how the polymer chains in a solid fit together. Many polymers are said to be semi-crystalline in structure, containing both crystalline and amorphous regions.

1.1.1 Crystalline structure

Crystalline solids have an atomic structure based on a regular, 3-dimensional repeating pattern. Because of this long-range periodicity, direct measurements of the crystal structure can be made by X-ray diffraction [e.g. 9,12,13], and processes such as thermal and electrical conduction are relatively easy to understand and model [e.g. 9].

Crystalline solids have well-defined melting temperatures. When heated through the melting temperature, T_m, crystalline solids melt, and above T_m exist in liquid form. While the material is molten, the constituent molecules have sufficient energy to be able to move freely past one another. Below T_m the material is in solid, crystalline form and the molecules are rigidly bound in place by attractive forces between them. The existence of the sharp melting temperature is due to the fact that the forces keeping each molecule bound in the crystalline matrix are very similar due to the material's periodic nature. The attractive forces between molecules can all therefore be broken with the same addition of heat energy, leading to global melting at T_m.

1.1.2 Amorphous structure

Amorphous structures are those with no regular long-range order, such as glasses. Examination and characterisation of these disordered structures by experimental means is much more difficult than in the crystalline case. Some information about structure can be inferred from spectroscopy experiments (including mechanical and dielectric

relaxation spectroscopy, NMR, IR, FIR, Raman and X-ray emission techniques [14]), but such information necessarily applies only over very short ranges. X-ray, neutron and electron diffraction have also been used to try to probe amorphous structures, but experimental data requires extensive analysis to be useful, and can again only be relevant over short distances. [15]. Glassy structures tend to lead to more complicated thermal conduction and charge movement processes than crystalline ones.

Glassy solids do not have a well-defined melting temperature – instead they undergo a 'glass transition' upon heating or cooling within a certain temperature range, T_g. This is due to the fact that in a disordered, glassy solid, the forces between molecules, which keep them in place, vary. As an amorphous structure is heated through the range T_g, attractive forces between different molecules are therefore overcome at slightly different temperatures. The transition from a solid glass to a liquid therefore takes place over a range of temperatures described by T_g.

1.1.3 Semi-crystalline structure

Polymers such as PE and PET are made up of regions that can be said to be crystalline, and regions that are amorphous. Such semi-crystalline systems necessarily display characteristics of both crystalline and amorphous systems – for instance on heating they can be seen to undergo both a glass transition in their amorphous regions and melting of their crystalline parts.

Crystalline regions in polymers form as long ribbons called lamellae, which can then form into spherulites [e.g. 10]. Lamellae are sheet-like in geometry, comprising aligned, parallel chain segments. These aligned segments may be parts of chains that are folded back and forth many times (with the folds outside of the lamellae as they would disturb the regular structure). Aligned segments may be part of chains that also pass through the amorphous regions and possibly then also go on to form parts of other lamellae. These are termed 'tie molecules' by some workers [16]. Spherulites are structures that form if many lamellae nucleate from the same point, and then grow outwards in all directions.

The relative number and size of lamellae present in a polymer specimen is described by its degree of crystallinity, and this depends on a number of factors. One of these is the structure of the constituent chains. Polymer chains can only crystallise if they can assume a closely-packed, regularly repeating structure. This is not possible for polymers that have no regular structure, such as random copolymers (polymers made up of more than one type of monomer, with the monomers in a random order) and atactic polymers (polymers which have an asymmetric monomer unit, with the monomers randomly aligned) [10,17]. In the cases of PE and PET, the chains are such that they can fit together in a close and orderly structure. A relatively high degree of crystallinity is therefore possible for each on morphological grounds –crystalline proportions of up to 50% have been observed for PET [18] and over 90% for PE [19]. In XLPE, however, the degree of crystallinity is likely to be significantly reduced by the physical constraints involved in many of the chains being linked together.

A major factor affecting the degree of crystallinity in a semi-crystalline polymer is the rate at which it was cooled to solidification from the melt. The solidification process can be described in terms of specific volume, V. Specific volume is the reciprocal of density, and can be thought of as a measure of how much space, on average, a polymer chain takes up with thermal motions. This decreases as a polymer solidifies from the melt, as shown in figure 1.3 [reproduced from 20].

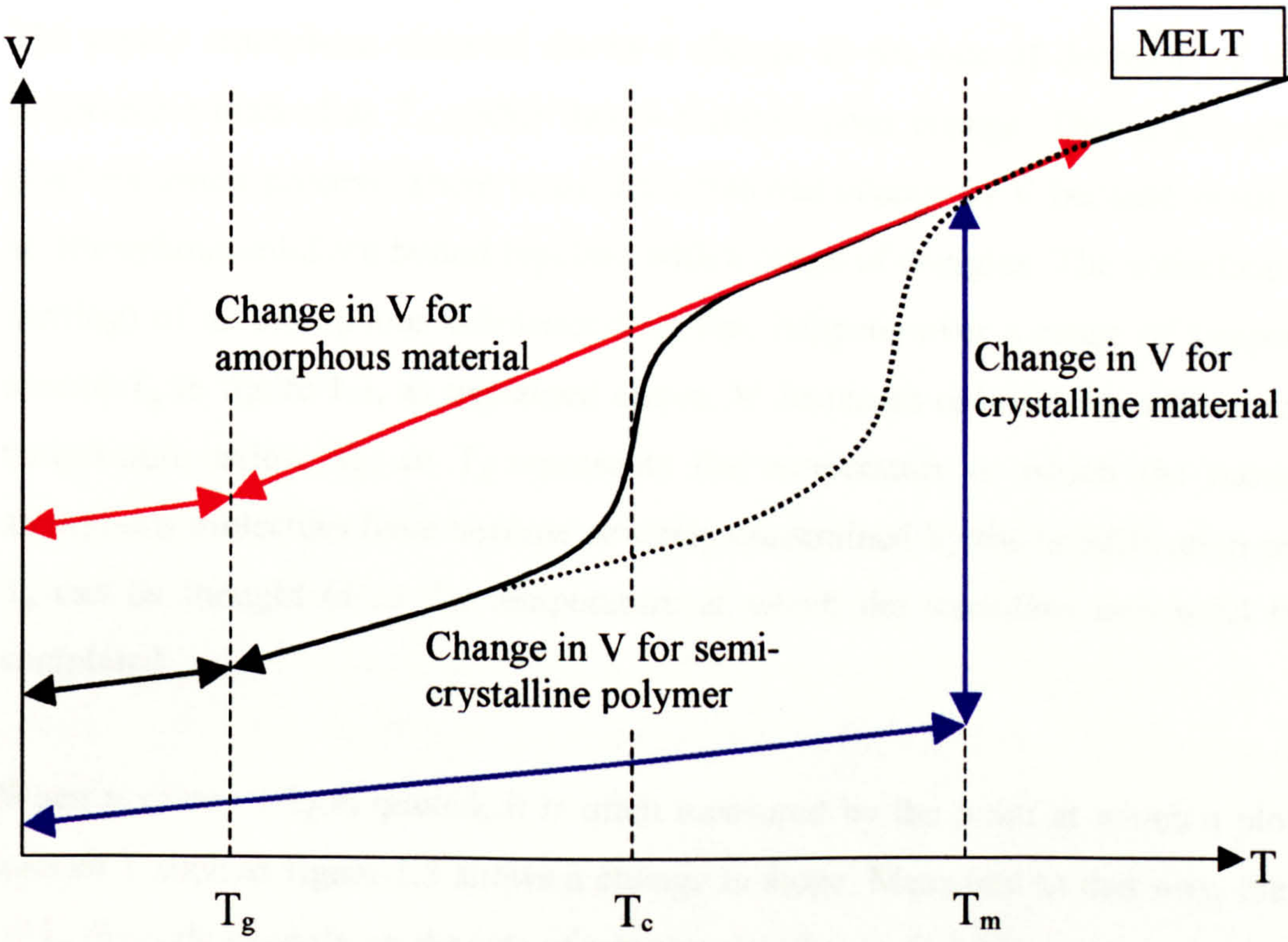

Figure 1.3

The solid black line in figure 1.3 shows the decrease in specific volume, V, with temperature, T, of a semi-crystalline polymer on solidification. For comparison, the decrease in specific volume with temperature is also shown for an ideal purely crystalline substance (in blue) and an ideal purely amorphous substance (in red).

For the purely amorphous and purely crystalline materials, the increase in V on heating the material through the range shown in figure 1.3 would follow the line shown for solidification in reverse. This is not so for the semi-crystalline polymer - the dotted line shows the increase in V with heating through T_m and T_g for this case.

On cooling from the melt, V initially decreases at the same rate for all structures, as molecules lose energy and therefore occupy less space with thermal motions. At T_m, the purely crystalline structure solidifies, leading to a discontinuous decrease in V. A discontinuity occurs because the whole structure solidifies at T_m as explained above. Below T_m, V decreases much more slowly with decreasing temperature, as the thermal

motions molecules change only very slightly once the structure has solidified and the molecules are frozen into place.

The purely amorphous material shows a change in the rate of decrease of V at the temperature marked as T_g, rather than a discontinuous change. This is a feature of a glass transition process. There is no discontinuous change in V because molecules in an amorphous solid are bound together with a range of energies. The solidification (or melting) of an amorphous substance therefore happens over a range of temperatures around T_g in figure 1.3, as explained above. V decreases only slowly with decreasing temperature below T_g, so T_g represents the temperature at which the motions of amorphous molecules have become severely constrained by the solidification process. T_g can be thought of as the temperature at which the transition into solid form is completed.

When a value of T_g is quoted, it is often measured by the point at which a plot of V against T such as figure 1.3 shows a change in slope. Measured in this way, the value of T_g depends strongly on the rate of temperature change [10,20].

V for semi-crystalline polymers can be seen to lie between the limits of ideal crystalline and ideal amorphous materials at all points in figure 1.3. On solidification, the decrease in V follows the same pattern as for amorphous material until the temperature range around T_c. At this temperature, the crystalline parts of the polymer solidify, leading to a sharp decrease in V. The change in V with crystallisation is not discontinuous as for the ideal crystalline solid, as lamellae in polymers are likely to contain imperfections. The environment of each molecule will therefore not be exactly the same, and the binding energies between them will be slightly different.

Once all crystallite lamellae are formed in the polymer, V continues to decrease at a uniform rate until the temperature falls to T_g. At this temperature the remaining un-crystallised chains are rigidly bound in place, leading to a change in the rate of decrease in V, just as for the purely amorphous structure. T_g is the temperature of the glass transition for amorphous regions of the polymer.

On heating a semi-crystalline polymer, T_g of the amorphous part occurs in the same temperature region as on cooling. The crystallites then melt at a temperature between T_c and T_m, causing a large increase in V with T.

The rate of cooling has a large effect on the measured value of T_g and on the degree of crystallinity in solids. Though a crystalline structure is thermodynamically the most stable arrangement, molecules take a finite time to re-arrange into the crystalline structure. If a melt is cooled very rapidly, few polymer chains will have time to re-arrange into a regular crystalline structure. Most chains will be frozen into the positions they occupy in the melt, leading to a solid polymeric structure with a low degree of crystallinity. Cooling a melt very slowly enables more polymer chains to assume the crystalline structure and results in a solid with a higher degree of crystallinity. The process of annealing is one where a semi-crystalline material is heated to a temperature range where crystallites can form (around T_c in figure 1.3) to promote further crystal growth.

1.2 Charge trapping and transport in polymers

Charge carriers can enter and leave polymers at electrode interfaces by such processes as Schottky and Fowler-Nordheim injection [10, 21], but are usually unable to travel very far in the bulk of the polymer by normal diffusive conduction. Consequently, the conductivities of insulating polymers are generally very low. For example, the conductivity of PE at 40°C is quoted as $2\times10^{-18}\ \Omega^{-1}m^{-1}$ and that of PET is quoted as less than $1\times10^{-19}\ \Omega^{-1}\ m^{-1}$ at 80°C [9].

Conduction along polymer chains is possible, but unlikely. Intra-chain bonds in polymers are primary, covalent bonds. Sufficient electron wave-function overlap therefore exists between constituent atoms that a band-gap energy model is applicable along chains. However, the band gap is generally too large for thermal excitation to create free charge carriers [10].

Inter-chain bonds are weaker, secondary bonds, as there is insufficient wave-function overlap to form a continuous valence band between chains. This alters the standard band gap model in the case of polymeric materials, and restricts the flow of current

even further; though a limited amount of conduction may be possible along polymer chains, charge cannot easily move between chains.

The flow of charge in polymers is hindered even further by the existence of sites that can trap and hold charge. Charge trapped at such sites makes a major contribution to the net 'space charge', and is observable experimentally by such means as pulsed electro-acoustic measurements [e.g 22, 23]. Trapping sites modify band-gap theory for polymer structure further by introducing electron energy levels inside the band gap region [10]. These sites act as traps because they are often separated in both energy and distance from energy levels in the valence and conductions bands. Electrons or holes may remain trapped in them for long times as a consequence. Hopping and tunnelling of charges between traps is, however, possible [10,21].

Charge trapping sites can be classified as physical traps – due to irregularities of structure, and chemical traps – impurities in the polymer left over from manufacturing processes. Modelling work [24,25] shows that physical traps in polymers are likely to be numerous compared to chemical traps, but that chemical traps are 'deeper' –i.e. electrons require more energy to be released from them, and will therefore tend to remain in them longer.

Space charge is significant in terms of electrothermal ageing. Local concentrations of charge in a polymeric specimen must alter an applied field distribution locally, and since both models assume a field dependence of time-to-failure, this is likely to be important. In fact, space charge is assumed by the DMM model to be the mechanism by which an electrical field accelerates ageing in polymers. This is discussed further in the next chapter.

2. Polymer Ageing Models

The aim of polymer ageing models is to predict the working lifetime of polymeric insulation subject to thermal and electrical stresses. Such theories have been developed by *e.g.* L.A. Dissado, G.C. Montanari and G. Mazzanti [1-4], T.J. Lewis, P.J. Llewellyn, C.L. Griffiths, P.W. Sayers and S. Betteridge [5-13], J.P Crine and J. Parpal [14,15], L. Simoni [16], and J. Artbauer [e.g. 17]. The two that have been used in this work are those developed by Dissado *et al* – abbreviated here to the DMM model - and Lewis *et al* – abbreviated to the Lewis model.

The DMM and Lewis models try to predict polymer lifetime by mathematically describing an ageing process in terms of applied field and temperature, and by specifying an endpoint at which this process is considered to have ended the life of the polymer [1-7,9]. Both models consider failure to comprise a lengthy ageing process, followed by short-lived catastrophic breakdown. The predictions of the models are therefore not strictly lifetime predictions; rather they predict the time to the beginning of a breakdown process such as treeing or crack formation and partial discharge. The models can therefore only be applied to situations in which it is reasonable to assume that once underway, the breakdown process will be very swift.

In both models, the ageing process is assumed to be a thermally activated one, which is accelerated by the application of an electrical field. The acceleration occurs due to charge distributed in the polymer according to the DMM model, [1-4], and via a mechanical force resulting from an applied electrical field in the Lewis model [5,7-9,12].

2.1 DMM Model

The derivation of the DMM model does not assign any specific physical process to ageing [1-4]. It could therefore be used to describe many different candidate ageing processes so long as they can be described by chemical rate reactions as described in [18]. Such processes must be reversible, and could include bond breaking or polymer chain untangling.

2.1.1 Ageing in absence of an electrical field

The polymer is considered to be made up of many moieties, or groups of atoms. The ageing process is a thermally activated one where these moieties move from one free energy configuration to another. Movement between these energy configurations is assumed to be reversible for each moiety, since product and reactant states will not be separated in either space or in phase [1,2]. Each moiety with sufficient energy can therefore move back and forwards between two energy states over an energy barrier as shown in fig 2.1.

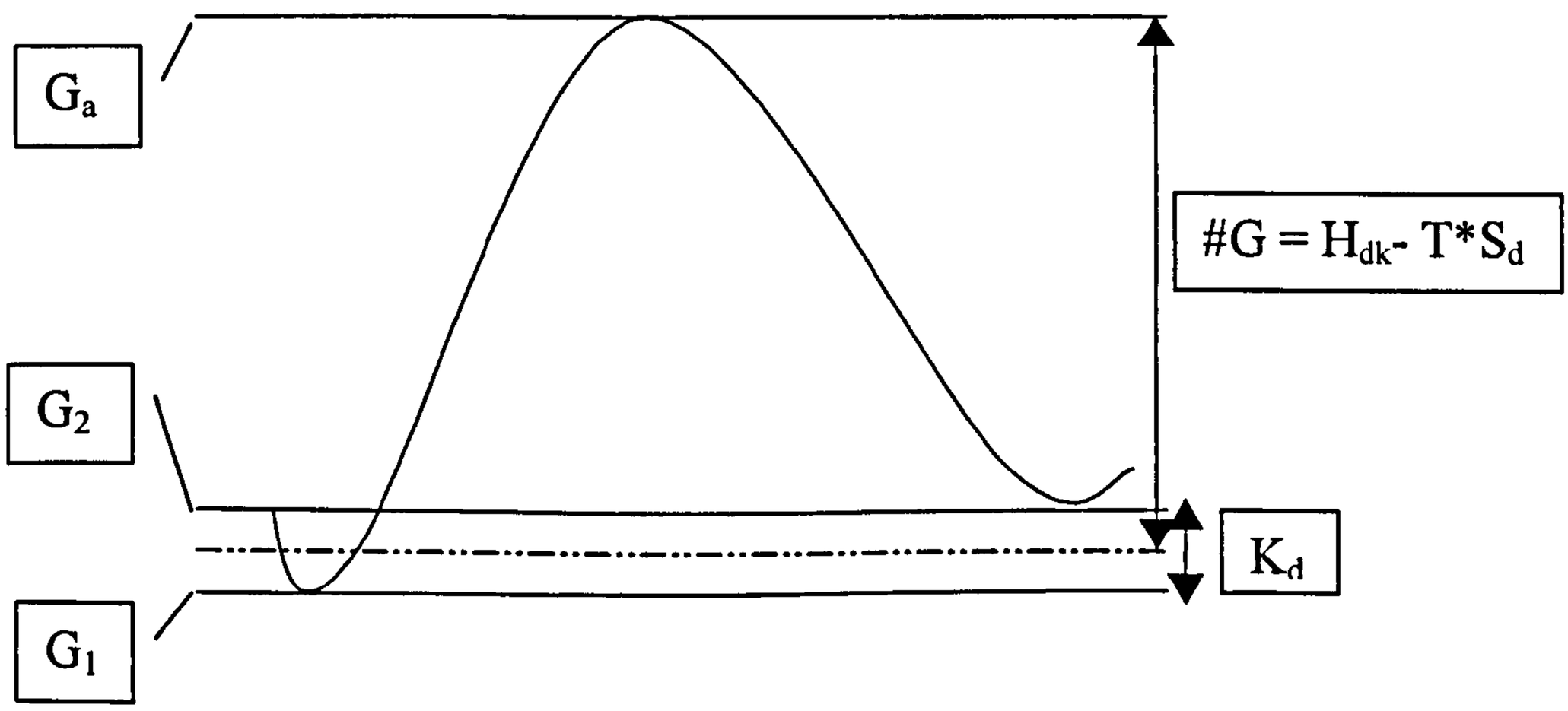

Figure 2.1

The free energy of the unaged state is called G_1 and the free energy of the aged state G_2. The difference between these is called K_d. The short-lived activated state has free energy G_a, and the activation energy barrier #G is defined to be the difference between G_a and the mean of G_1 and G_2. This activation energy is made up of an enthalpy part, H_{dk}, and an entropy part, S_d.

Due to the microstructural inhomogeneity of most polymers, each moiety in a polymer is actually likely to have a different activation barrier height. Some moieties will have smaller barriers to ageing than others, and the value of #G must therefore actually be different from moiety to moiety. This is discussed further in Chapter 6, but for most purposes single parameter values are used in the models, and this approximation has been seen to fit data well [1-4, Chapter 3].

Initially, the polymer is assumed to be in a non-equilibrium state, with all of the moieties in the unaged state and with free energy G_1. Each moiety in the polymer which is energetically able to take part in the reaction will then start to move back and forwards between the two states. As time goes on, the polymer moves towards a dynamic equilibrium in terms of the fraction of moieties in the unaged and aged states. It is this move towards equilibrium that is described as ageing, and the movement is irreversible

The model supposes that if a sufficient fraction of moieties is in the aged state in any local area then an irreversible breakdown process can begin. This critical fraction of aged moieties is called A*, and for breakdown to start it needs to be exceeded only on a local scale – not throughout the whole polymer Once the breakdown process is initiated, the polymer lifetime is limited by the breakdown process and likely to be very short.

It is likely that at low temperatures the fraction of moieties in the aged state can never exceed A*, even when thermal equilibrium has been reached. This leads to situations in which the lifetime predicted by the model is infinite, and the definition of a threshold temperature below which polymer lifetime is infinite. In effect, this just means that the ageing process does not limit the lifetime of the specimen below a threshold temperature.

The fraction of moieties in the aged state depends on several factors. Increased temperature increases the fraction of moieties in the aged state by increasing the number of moieties with sufficient energy to take part in the reaction. The fraction of moieties in the aged state will also depend on the barrier height, which may be different from material to material, depending on the details of the ageing process.

The ageing process is assumed to be governed by Eyring's rate theory [1,2]. This means that a rate constant, K_f, describes the movement of moieties from the unaged state into the aged state and another one, K_b, describes the reverse process. These rate constants are given by

$$K_f = B \times \exp\left(\frac{-(G_a - G_1)}{kT}\right)$$
$$K_b = B \times \exp\left(\frac{-(G_a - G_2)}{kT}\right) \qquad 2.1 \text{ and } 2.2$$

In the rate equations, k is Boltzmann's constant and T is temperature. The factor B in the rate equations is an attempt frequency. It is assumed that

$$B = \frac{kT}{h}\exp\left(\frac{S'_d}{k}\right) \qquad 2.3$$

Where k is Boltzmann's constant as before, h is Planck's constant, and T is temperature. The factor S'_d allows for the fact that not all moieties with energy kT will be able to take part in the ageing reaction due to entropy constraints.

The movement of moieties between the aged and unaged states with time can then be described in terms of these rate constants and the concentrations of reacting moieties in each state, C_1 and C_2.

$$\frac{dC_1}{dt} = -C_1K_f + C_2K_b$$
$$\frac{dC_2}{dt} = -C_2K_b + C_1K_f \qquad 2.4 \text{ and } 2.5$$

In equations 2.4 and 2.5, t is time. Letting $N=C_1+C_2$, where N is the total concentration of reacting moieties, introducing a new variable $X=C_2/N$, and then subtracting dC_1/dt from dC_2/dt gives that

$$\frac{dX}{dt} = K_f - (K_f - K_b)X \qquad 2.6$$

As mentioned above, the condition for breakdown is that a certain fraction of reacting moieties are in state 2 – i.e. C_2 must reach a critical value, C*, for the polymer life to be ended by a breakdown process. At the start of ageing t=0, and all the moieties are assumed to be in the unaged state, so $C_2=0$, and X=0. At the end of the polymer life, $C_2=C^*$, and $X=C^*/N$.

Therefore, rearranging equation 2.6 and integrating from X=0 to X=A*=C*/N gives a time t_c, which describes the lifetime of the polymer.

$$t_c = \frac{1}{K_b + K_f} \times \left[-\ln\left(\frac{A_{eq} - A^*}{A^*} \right) \right] \qquad 2.7$$

Where A_{eq} is the value of X at thermal equilibrium, and is equal to

$$A_{eq} = \frac{K_f}{K_f + K_b} \qquad 2.8$$

The log part of equation 2.7 shows mathematically the threshold behaviour of the equation: if the equilibrium value of X, A_{eq} does not reach the value of A* - *i.e.* the fraction of moieties in the aged state does not reach the critical value, then the predicted lifetime becomes infinite. Equation 2.7 is therefore more correctly given as

$$t_c = \frac{1}{K_b + K_f} \times \left[-\ln\left(\frac{A_{eq} - A^*}{A^*} \right) \right] \qquad A_{eq} \geq A^* \qquad 2.9$$

$$t_c = \infty \qquad A_{eq} < A^*$$

2.1.2 Effects of electrical field

In the DMM model, application of an electrical field is assumed to modify the ageing process described above. This is assumed to happen via space charge trapping within the polymer [1,2]. Charge injection into polymer specimens has been experimentally observed at both anode and cathode interfaces, and it has also been seen to travel into the bulk. Charge is likely to be trapped at morphological defects in polymers, and in the regions between crystalline and amorphous regions as well as at sites of chemical impurities and inclusions [1,19-21].

At any site at which space charge is trapped within a polymer, the local field distribution will be altered. Electrostatic and electromechanical forces will be set up, which will have maximum values at the boundaries of these space charge regions [1].

The electrostatic forces generated at space charge sites are assumed to affect all the energy levels involved in the ageing process by the same amount, and will not therefore affect #G, the rate constants or polymer lifetime. The electromechanical

forces, however, are assumed to only affect the energy level of the unaged state, G_1. Electromechanical strains therefore affect the polymer lifetime through #G and the rate equations [1,2]. The effect of a change in G_1 on the energy level diagram is shown in fig 2.2.

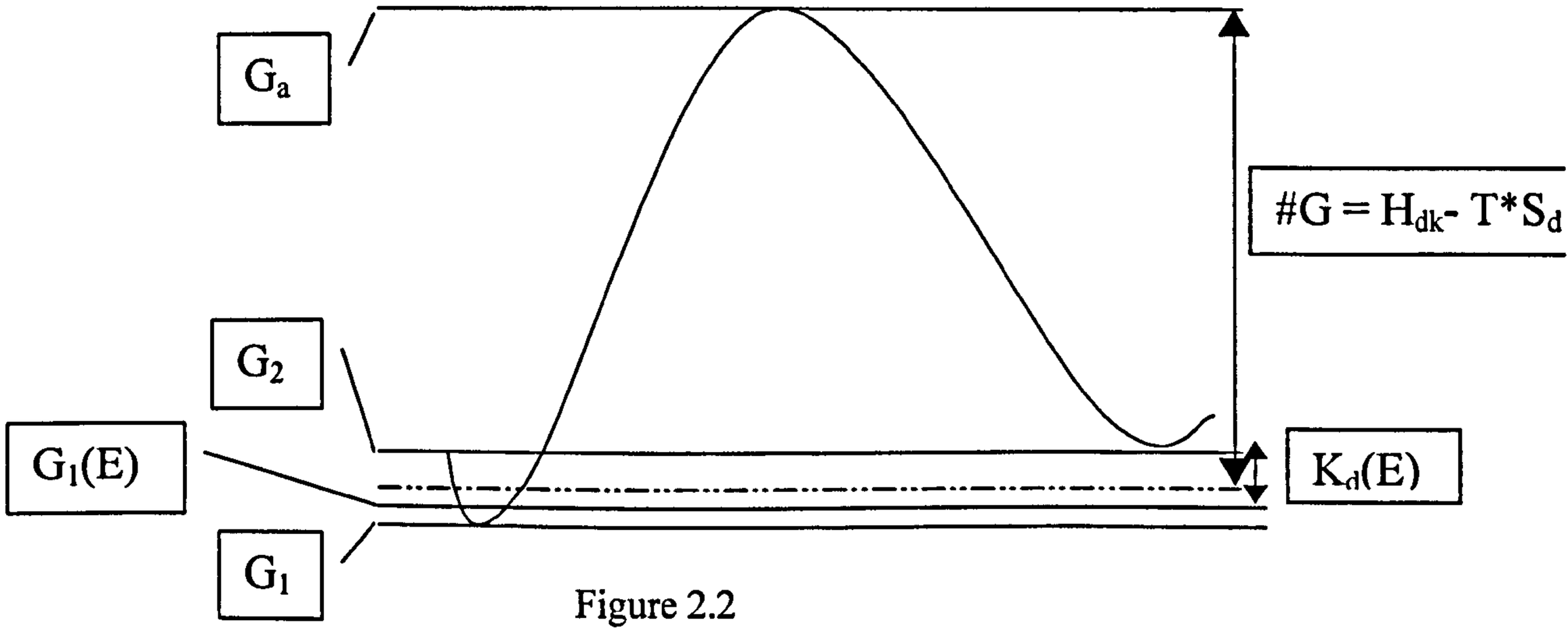

Figure 2.2

The model assumes that only the electromechanical forces affect ageing due to an assumption that any electrostatic forces present at a space charge centre will not be released when a moiety undergoes the ageing reaction. According to the model, the space charge will not be removed or neutralised on ageing, so the electrostatic force will remain constant. Electromechanical strains, on the other hand, are assumed to be released when moieties at the space charge site change from state 1 to state 2. The ageing process is therefore essentially one of local creep. Electromechanical forces cause a strain, which is released when the moiety increases its free energy to G_2 by changing its free energy in some way under the influence of the strain. If the electromechanical force at a space charge site is such that enough moieties undergo this process then the A* fraction is exceeded, and a breakdown process such as micro-crack or tree formation can begin.

The macroscopic applied field must also generate global electromechanical forces in the polymer. However, the DMM model assumes that they are unlikely to affect the ageing process [1].

The amount of free energy added to G_1 on application of a field must be related to the amount of charge trapped at the charge centres. The amount of charge in a centre is not governed by a well developed relationship, but is assumed in the DMM model to be a function of the magnitude of the applied field. The energy addition must also depend on the susceptibility of the polymer to the electromechanical forces resulting from this space charge. The field dependent value of G_1 is assumed to be of the form

$$G_1(E) = G_1 + C \times E^{4b} \qquad 2.10$$

In equation 2.10, C is a function of material parameters such as the Young's modulus, the electrostriction coefficient and the permittivity. It is also a function of the radius of the space charge centre. The amount of charge present is linked to the applied field, E, through a power law [1,2]. The use of a power law here is based on the fact that many complicated expressions with field dependencies approximate to power laws over limited ranges of field values. Given that the lifetime function has been shown to fit a fairly wide range of experimental data, the power law here seems justified.

By substituting the field dependent value for G_1 from equation 2.10 into K_f, and substituting for both K_b and K_f from 2.1 and 2.2 into the equation for t_c, the following expression for the lifetime is derived:

$$t_c = \frac{1}{\frac{kT}{h}\exp\left[\frac{-S'_d}{k}\right]\left\{\exp\left(\frac{-\left(G_a-\left(G_1+CE^{4b}\right)\right)}{kT}\right)+\exp\left(\frac{-\left(G_a-G_2\right)}{kT}\right)\right\}} \times \left[-\ln\left(\frac{Aeq-A^*}{Aeq}\right)\right]$$

2.11

Defining K_d in terms of the difference between the energies of the unaged and aged states

$$K_d = \frac{G_2 - G_1}{k} \qquad 2.12$$

Defining C_d such that

$$C_d = \frac{C}{k} \qquad 2.13$$

Letting K_{dd} be the difference between the free energy of the activated state and the mean of the free energies of the aged and unaged states

$$K_{dd} = \frac{G_a - \left(\frac{G_1 + G_2}{2}\right)}{k} \qquad 2.14$$

Equation 2.11 can then be rearranged to give:

$$t_c = \frac{\frac{h}{kT}\exp\left[\frac{-S'_d}{k}\right]\exp\left[\frac{K_{dd} - \frac{C_d E^{4b}}{2}}{T}\right]\left[-\ln\left(\frac{A_{eq} - A^*}{A_{eq}}\right)\right]}{\exp\left(\frac{-\left(K_d - C_d E^{4b}\right)}{2T}\right) + \exp\left(\frac{\left(K_d - C_d E^{4b}\right)}{2T}\right)} \qquad 2.15$$

The denominator then reduces to a cosh term, and the following substitutions can be made, where H_a, H_1 and H_2 are the enthalpy of the activated, unaged and aged states respectively. S_a, S_1 and S_2 are the same values for entropy:

$$K_{dd} = \frac{H_a - \left(\frac{H_1 + H_2}{2}\right)}{k} - T\left(\frac{S_a - \left(\frac{S_1 + S_2}{2}\right)}{k}\right) \qquad 2.16$$

Letting

$$H_{dk} = \frac{H_a - \left(\frac{H_1 + H_2}{2}\right)}{k} \quad \text{and} \quad S''_d = S_a - \left(\frac{S_1 + S_2}{2}\right) \qquad 2.17 \text{ and } 2.18$$

It then follows that

$$K_{dd} = H_{dk} - \frac{TS_d''}{k} \qquad 2.19$$

Substituting for H_{dk} and S_d into 1.13 makes the temperature dependence of the equation fully explicit by separating out enthalpy and entropy contributions to the activation energy. The final lifetime equation is:

$$t_c = \frac{\frac{h}{2kT}\exp\left[\frac{-S_d}{k}\right]\exp\left[\frac{H_{dk}-\frac{C_d E^{4b}}{2}}{T}\right]\left[-\ln\left(\frac{Aeq-A^*}{Aeq}\right)\right]}{\cosh\left[\frac{K_d - C_d E^{4b}}{2T}\right]} \qquad 2.20$$

Where $S_d = S'_d + S''_d$, and from 2.1, 2.2 and 2.8,

$$A_{eq} = \frac{1}{1+\exp\left(\frac{K_d - C_d E^{4b}}{T}\right)} \qquad 2.21$$

2.1.3 Parameters - material and frequency dependence

The derived lifetime equation 2.19 contains six parameters whose meanings have been briefly discussed above. The physical meanings of the parameters are summarised below. The meanings and values of the parameters offer an insight into the physical processes at work during ageing.

The lifetime expression is such that all field and temperature dependence of lifetime is explicitly expressed; the parameters should therefore have no dependence on either of these. Fittings to experimental lifetime data have shown that the parameters vary from material to material and from AC to DC situations [3,4].

- H_{dk} describes the activation enthalpy of a moiety changing between free energy levels. As shown in equation 2.16 it is the difference between the enthalpy of the short-lived activated state and the mean of the enthalpies of states one and two. This parameter is likely to be material dependent, since the barrier to ageing may depend upon material morphology or chemistry.

- S_d is the entropy parameter analogous to H_{dk} as described above. This is also likely to be material dependent.
- K_d is the difference in free energy between the aged and the unaged states, and like the other two energy barrier parameters is likely to be material dependent.
- A* is the critical fraction of moieties that need to be in the aged state in any localised area for the ageing process to cause breakdown of the polymer. This is likely to be a function of material.
- C_d is the multiplier in the term which links the applied electrical field, E, to the change in free energy of the unaged moiety state. This depends on many material characteristics as described above.
- b is the exponent in the power law linking the applied electrical field to the increase in free energy of the unaged moiety state.

The model was initially proposed just to describe DC ageing, since it requires charge to be trapped at sites in the polymer long enough to influence the ageing process. At higher applied frequencies, space charge is less likely to be trapped in one place for a very long time. However, it has been shown that the model can also fit AC data well, and the frequency and material dependence of all of the above parameters has been observed through fitting the model to experimental data from AC and DC ageing experiments [3,4].

As expected from their physical meanings, the parameters related to the microstructure and morphology of a material, C_d, A* and b exhibit almost no changes between AC and DC fittings for the same materials, but vary from material to material [3,4]. The parameters relating to the energy barrier, H_{dk}, S_d and K_d, however, do show a marked frequency dependence [3,4]. The main changes from DC to AC are that the enthalpy barrier to the process significantly decreases, and an entropy barrier is set up. In fact, the entropy barrier in the DC case is so small as to be insignificant – in the DC case, the barrier to ageing can be considered to be an enthalpy barrier mainly.

The change in the energy barrier parameters between AC and DC fittings offers an insight into the differences in the ageing process between AC and DC. The lowering of the enthalpy barrier in AC is likely to be due to the fact that the polymer matrix will be

mechanically driven under AC stress, thus making changes in free energy of moieties effectively easier. More atoms must be involved in the process in the AC, case, however, and this accounts for the setting up of an entropy barrier.

A frequency dependent version of the DMM model is developed and shown to fit data well in [4], but for most industrial applications only AC 50Hz and DC parameter values are needed.

2.2 Lewis Model

The Lewis model deals with polymer moieties experiencing a change in free energy in a similar way to the DMM model. In this case, however, the change between the aged and unaged states is assigned to one particular physical process – namely the way that the chemical bonds linking the moiety to the rest of the polymer matrix change with time [5,6]. The unaged state therefore corresponds to an unbroken bond between two molecules in the polymer, and the aged state to a broken or weakened bond.

2.2.1 Ageing in absence of an electrical field

As in the DMM model, the polymeric ageing process is assumed to be a reversible, thermally activated one which progresses even without the application of electrical stress to the material. The electrical stress merely acts to accelerate the process.

The mathematical details of the process are very similar to those in the DMM model as described above. Rate equations are devised in the same way, so that K_f and K_b are defined as [5,6].

$$K_f = B \times \exp\left(\frac{-(U_B)}{kT}\right)$$

$$K_b = B \times \exp\left(\frac{-(U_R)}{kT}\right) \qquad \text{2.22 and 2.23}$$

K_f is now the rate at which bonds are broken or weakened, and K_b the rate at which bonds can be repaired. U_B is equivalent to G_a-G_1 in the DMM model, and U_r equivalent to G_a-G_2. U_B is the energy required to break a bond – i.e. the energy needed to take the a moiety from the unaged state over the energy barrier into the aged state.

U_R is the energy required to repair a bond and to therefore take the moiety back into the unaged free energy configuration. B is again an attempt frequency, but in this case does not include any entropy considerations, and is just given by

$$B = \frac{kT}{h} \qquad 2.24$$

Where k is Boltzmann's constant, h is Planck's constant and T is temperature. An energy barrier picture corresponding to fig 2.1 is shown in fig 2.3.

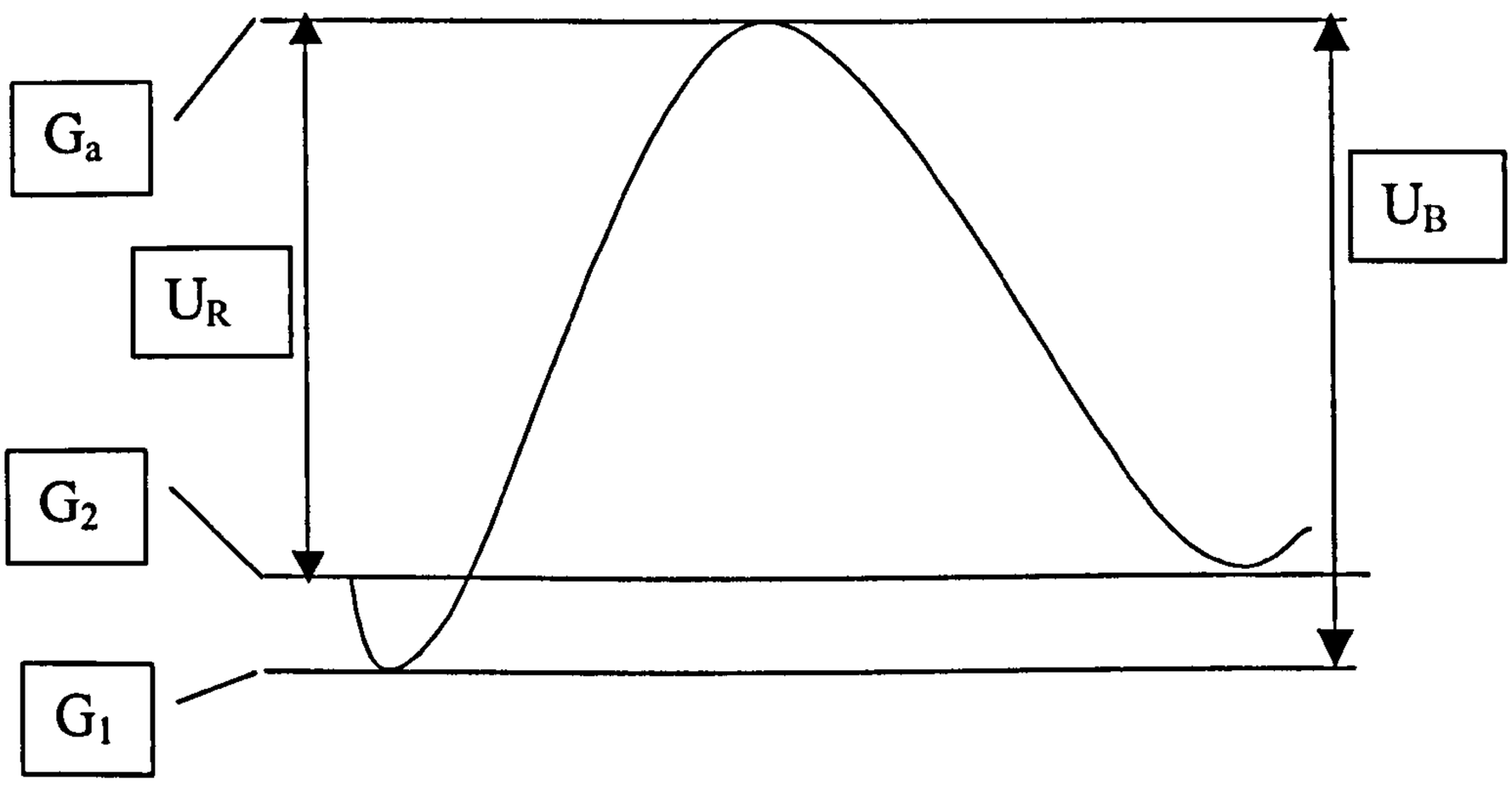

Figure 2.3

Following the derivation in section 2.1.1, with N representing all bonds taking part in the ageing process, C_1 now represents the concentration of unbroken bonds and C_2 the concentration of broken bonds. X represents the fraction of broken bonds (=C_2/N), and as before

$$\frac{dX}{dt} = K_f - (K_f - K_b)X \qquad 2.25$$

Equation 2.25 therefore gives an expression for the change in the fraction of broken bonds with time, t. The threshold behaviour of the Lewis model works in the same way as for the DMM model – breakdown is assumed to begin once a critical fraction of bonds are broken. This means that X must reach a critical fraction equivalent to A*, and in the Lewis model this is usually called b. Here it will be called b* to differentiate from the b factor in the DMM model and to highlight the equivalence of A* and b*.

2.2.2 Effect of electrical field

As before, the application of an electrical field is assumed to accelerate the ageing process described above. The mechanism by which this is assumed to occur is different from that assumed in the DMM model. The Lewis model uses a generalised form of the Lippmann electro-capillary equation applied to a macroscopic dielectric system to show that a macroscopic electrical field generates a mechanical stress everywhere in the polymer, which acts to expand the polymer against its cohesive forces [5,7,8]. This mechanical stress is shown to act in directions orthogonal to electrical field lines, and evidence of the stress has been experimentally observed [7,9,10,22]. The mechanical stress, σ, is given by

$$\sigma = \varepsilon E^2 \qquad 2.26$$

Where ε is the permittivity of the polymer and E is the applied electrical field. The expanding action of the mechanical stress is assumed in the Lewis model to reduce the amount of energy needed to break bonds, and to increase the amount of energy required to repair bonds. The application of an electrical field to a polymer therefore accelerates the ageing process by reducing U_B and increasing U_R.

The amount by which these energies are changed is assumed to be proportional to the mechanical force, so that the field dependent energy barriers are as given below.

$$U_B(E) = U_B - \gamma_B \varepsilon E^2$$
$$U_R(E) = U_R + \gamma_R \varepsilon E^2 \qquad 2.27 \text{ and } 2.28$$

The energy barrier picture represented by fig 2.3 is changed as in fig 2.4

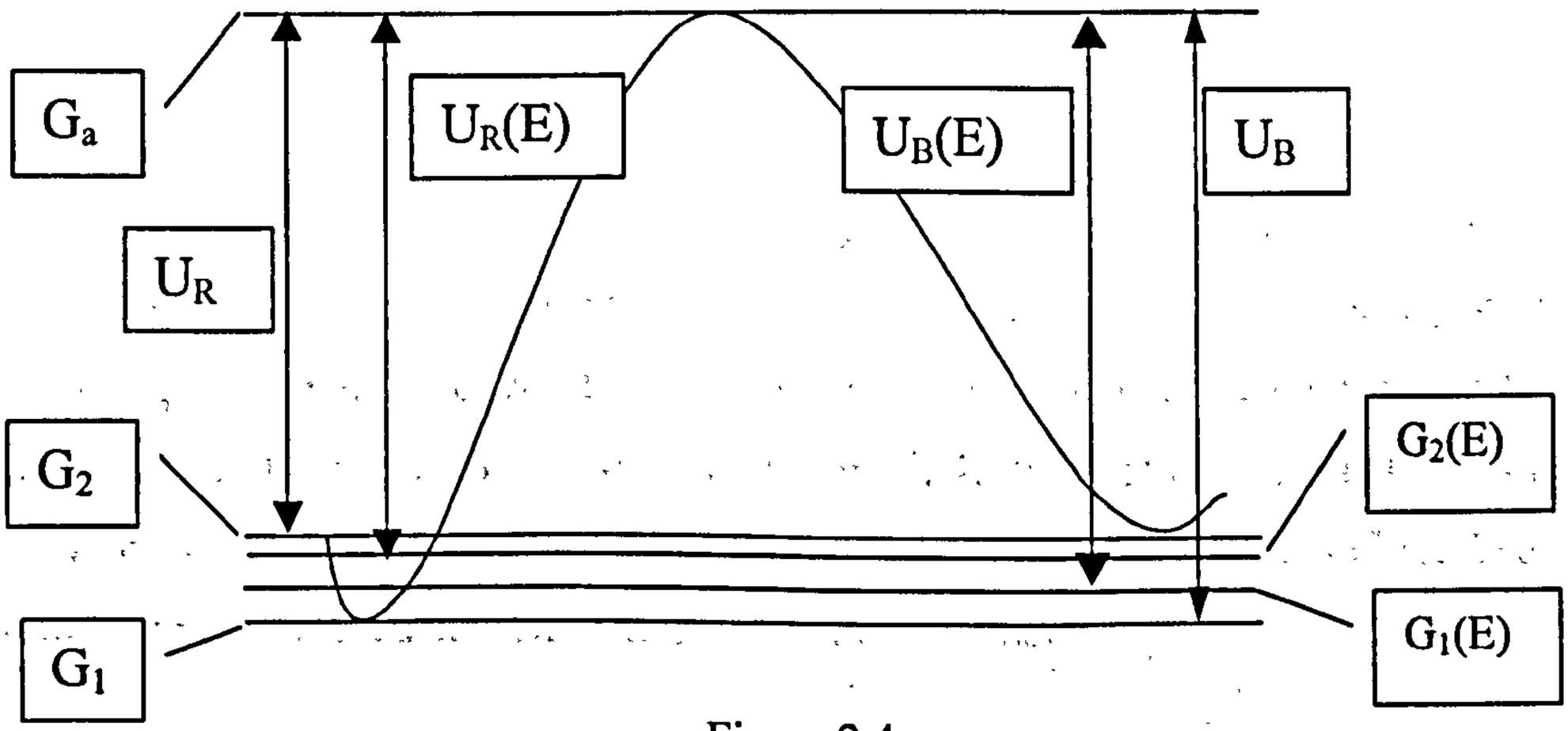

Figure 2.4

This leads to field modified rate equations such that

$$K_f = B \times \exp\left(\frac{-\left(U_B - \gamma_B \varepsilon E^2\right)}{kT}\right)$$

$$K_b = B \times \exp\left(\frac{-\left(U_R + \gamma_R \varepsilon E^2\right)}{kT}\right) \qquad 2.29 \text{ and } 2.30$$

In section 2.1.2, equation 2.6 was integrated to give equation 2.7. Equivalently integrating 2.24 from X=0 to X=b* gives an equation for t_c very similar in form to equation 2.7:

$$t_c = \frac{1}{K_b + K_f} \times \left[-\ln\left(\frac{b_{eq} - b^*}{b^*}\right)\right] \qquad 2.31$$

Where b_{eq} is the equilibrium fraction of broken bonds equivalent to A_{eq} in the DMM model.

The above integration, however, assumes that neither γ_B nor γ_R are dependent on X. In fact, in [5] it is suggested that these factors must be a function of X, since they represent the strain at a bond site due to the electromechanical stress σ. This macroscopic stress is assumed to be experienced by all bonds in the material so that when one bond breaks, there will be a resulting increase in stress and strain experienced by all other unbroken bonds in the material. This idea is also discussed in [23]. Here ageing according to the Lewis model is attributed to the electromechanical stress causing tie molecules between crystalline lamella to break free from one lamella. This would increase the stress on remaining tie molecules between the lamella, and may lead to bond scission.

If the γ factors are both functions of X as suggested, equation 2.31 no longer holds. The integration of 2.25 becomes possible only by numerical means, and an equation equivalent to 2.7 cannot be devised. Fits of the Lewis model to data have been reported in the literature [11] and in BICC company reports [24]. It is not clear in [11] how the γ factors have been dealt with, while in [24] a numerical integration method has been used in some cases, and a constant value of γ values in others.

2.2.3 Parameters – material and frequency dependence

The Lewis model contains five parameters. Two of these are activation energy parameters, which in the DMM model are considered in terms of enthalpy and entropy contributions. In the Lewis model this is not the case, so both U_B and U_R are likely to have temperature dependence. They can therefore also be described as made up of three activation energy parameters analogous to those in the DMM model, and this is considered in the next chapter.

The parameters are summarised below.

- U_B describes the energy needed for a bond to be broken. This is likely to be material dependent, and also to be temperature dependent.
- U_R is the energy needed to repair or create a bond. This will have the same dependences as above.
- γ_B is the term which links the applied field to the decrease in energy needed to break a chemical bond. It represents the strain at a bond site caused by the field-induced mechanical stress, and must have the dimensions of volume. As mentioned above, if this is a function of the fraction of unbroken bonds, the Lewis lifetime equation is not solvable except numerically, and extra parameters will need to be introduced into the Lewis model equation.
- γ_R links the applied field to the increase in energy needed to create a bond. It also represents a strain, and must have the same units.
- b* specifies the endpoint of the ageing process, i.e. the point at which breakdown can begin. It is the critical fraction of bonds involved in ageing that must be broken for breakdown to begin.

No comparisons between parameter values obtained for fits to AC and DC lifetime data are available in the literature. Through the equivalence of the parameters between the models, however (see section 2.3.2), it is possible to relate the frequency behaviour of the DMM parameters to those of the Lewis model.

2.3 Comparison of the models

2.3.1 Threshold conditions

Both models have a threshold condition that has to be met before the electrothermal ageing process can have an effect on the lifetime of a polymer specimen. In the DMM

model A_{eq} must exceed A* for ageing to occur, and in the Lewis model b_{eq} must exceed b*.

In the DMM model, the threshold takes the form of a critical fraction of moieties in the aged, less energetically favourable state, which has to be exceeded for ageing to be important. The physical meanings of these two states is left unspecified, so that the change in free energy could be applied to various different processes. In the Lewis model, the analogous condition in the original model was that a critical fraction of the bonds in the material had to be broken [5,6], and experimental evidence is available in [12,23] to support the theory that during electro-thermal ageing, polyethylene C-C bonds are indeed broken. In another publication, [13], the ageing process has been slightly re-defined, so that the physical interpretation of this condition is different. Here it is postulated that the ageing process is one of polymer tie-chain untangling and polymer yield, and this is also discussed in [23]. This process would still involve the breaking or weakening of some chemical bonds in the polymer.

The threshold conditions are directly mathematically analogous so long as equation 2.31 holds – i.e. as long as the γ factors are not dependent on X. A physical difference is that that in the DMM model the condition is a local one, rather than a global one. This means that in the Lewis model a critical fraction of bonds have to be broken throughout the whole polymer volume for the breakdown process to begin. In the DMM model, a critical fraction of moieties in the aged state only needs to be exceeded in any localised area.

2.3.2 Effect of electrical field

The biggest difference between the two models is in the way in which an applied electrical field changes the activation energy of the ageing process, and the mechanism by which this is assumed to happen. Both models, however, yield a threshold field below which no ageing can occur, and evidence for such electrical thresholds in polymers have been inferred by experimental means [25,26].

In the DMM model, an applied field raises G_1 by an amount equal to C_dE^{4b}, where C_d and b are factors that depend on material (and possibly specimen size or geometry – see Chapters 5 and 6). The C_dE^{4b} term links the macroscopic field, E, to the effect of

locally trapped space charge. The effect of applying a field is therefore to make the transition from state one to state two more likely by reducing (G_a-G_1). The transition from state two to state one is unaffected, though G_1 becomes less energetically stable relative to G_2 after a field is applied.

In the Lewis model an applied field raises the energy of state one, G_1, by $\gamma_B \varepsilon E^2$. It also lowers G_2 by an amount $\gamma_R \varepsilon E^2$, where ε is the permittivity of the material, and E is the macroscopic field as before. This means that on application of a field, the transition from state one to state two becomes more likely, as G_a-G_1 is reduced. The transition from state two to state one also becomes less likely on application of a field, since G_a-G_2 is increased.

The physical mechanisms by which the ageing process is assumed to be altered in the presence of an electrical field are also very different between the models. The DMM assumes a relationship between applied field and trapped space charge, and it is charge that accelerates ageing through the electromechanical forces generated by it. The Lewis model assumes that the applied field causes a macroscopic electromechanical stress throughout the whole polymer, and that it is this that accelerates ageing. The DMM also makes allowance for the existence of this macroscopic force, but does not consider this to be the most important effect of field. Similarly, in the Lewis model, the existence of any space charge in the polymer must affect the macroscopic stress in the locality of the space charge site, but this effect is not considered to be the main one.

2.3.3 Mathematical Equivalence of Parameters

As mentioned above, b* and A* are exactly mathematically equivalent in the models so long as equation 2.31 holds. Assuming that the models do actually describe the same ageing process, and comparing the energy level diagrams in figs 2.1-2.4, it can be seen that certain mathematical equivalences also exist between the activation energy parameters, and between the parameters describing the effects of electrical field.

These mathematical relationships include the following, which relate the parameters that apply when no electrical field is present:

$$U_B = H_{dk} - TS_d + \frac{K_d}{2}$$

$$U_R = H_{dk} - TS_d - \frac{K_d}{2} \qquad \text{2.32, 2.33 and 2.34}$$

$$U_B - U_R = K_d$$

It is also possible to compare the effect of an applied field, since in the DMM model,

$$K_d(E) = K_d - C' E^{4b} \qquad \text{2.35}$$

while in the Lewis model,

$$U_B(E) - U_R(E) = \left(U_B - \gamma_B \varepsilon E^2\right) - \left(U_R + \gamma_R \varepsilon E^2\right) \qquad \text{2.36}$$

Equation 2.36 is equivalent (through equation 2.34) to:

$$K_d(E) = K_d - (\gamma_R + \gamma_B)\varepsilon E^2 \qquad \text{2.37}$$

Equating the right hand sides of equations 2.34 and 2.36 is can be seen that

$$C' E^{4b} = (\gamma_R + \gamma_B)\varepsilon E^2 \qquad \text{2.38}$$

The only way that equation 2.38 can be always true is if b in the DMM model is equal to 0.5, and if the sum of the γ factors multiplied by the permittivity of the material in the Lewis model is equal to the C' factor in the DMM model. This latter constraint cannot be satisfied if the γ factors are functions of the number of remaining unaged moieties in the polymer, unless they change to compensate one another, leaving their sum always the same.

The fact that the functional forms of the effect of field are different between the models is not surprising, since they assume that electrical field affects ageing via different mechanisms. For them both to successfully fit data, however, there must be a reasonable degree of agreement between them.

2.3.4 Functional form of the lifetime equations

The functional forms of the lifetime expressions derived in equations 2.10 and 2.31 are similar. They can yield similar lifetime predictions depending on the values of the parameters chosen to go in them. The equations can be used to generate lifelines.

Lifelines predict the lifetime of insulation with applied field at a particular temperature, or alternatively, are lines that show the predicted lifetime with temperature for a particular applied field. Examples of the first kind are given in fig 2.5, and examples of the second in fig 2.6.

Fig 2.5 shows both Lewis and DMM lifetime equations vs. field at two constant temperatures. Field threshold behaviour is observable in all four lifelines, with the Lewis model displaying a higher threshold field for the sets of parameter values used. At applied fields lower than these thresholds, the models predict infinite lifetime.

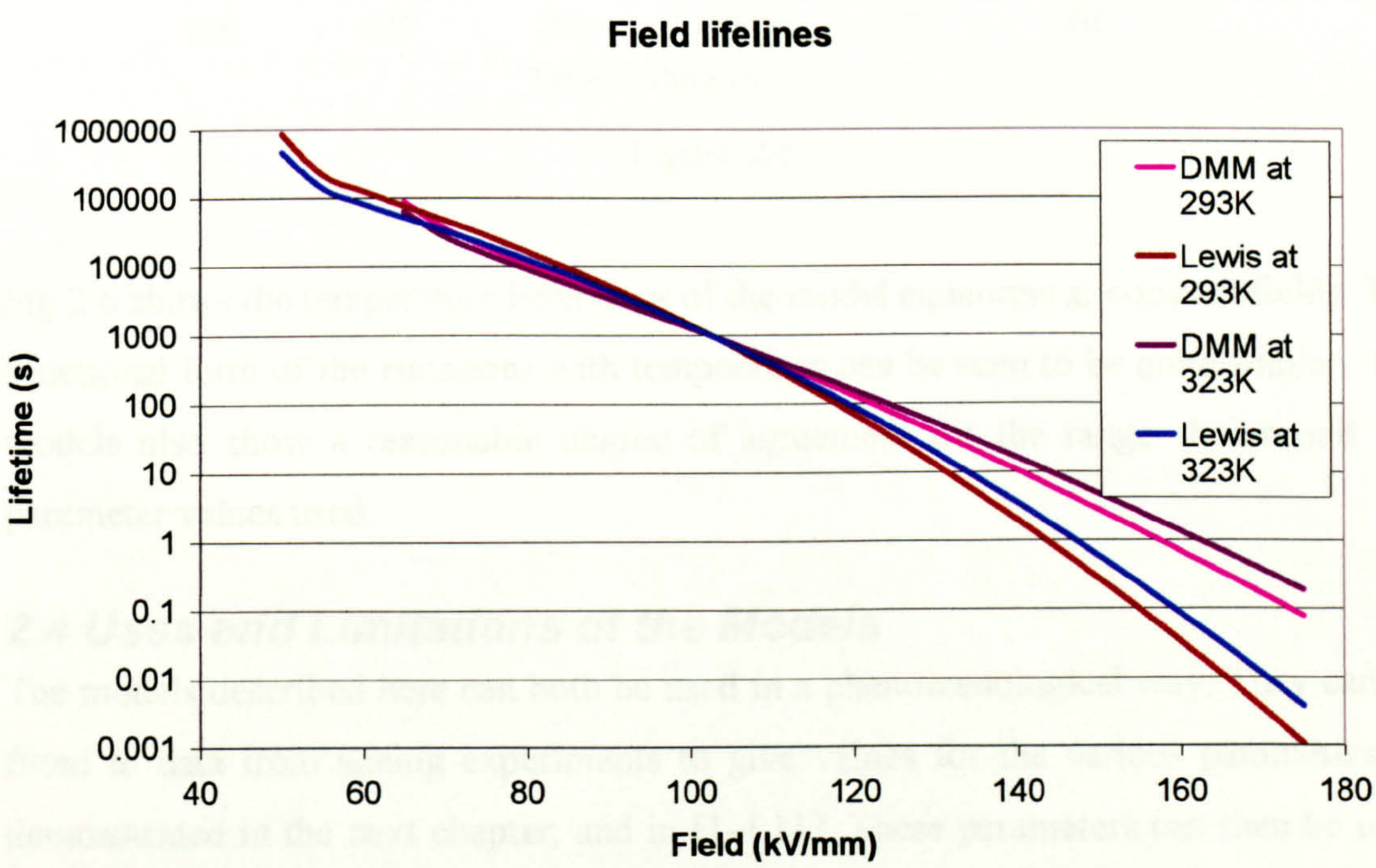

Figure 2.5

The functional forms of the model equations with field can be seen to be quite similar, and there is reasonably good agreement between the predicted lifelines in the field range above both thresholds up to about 110kV/mm

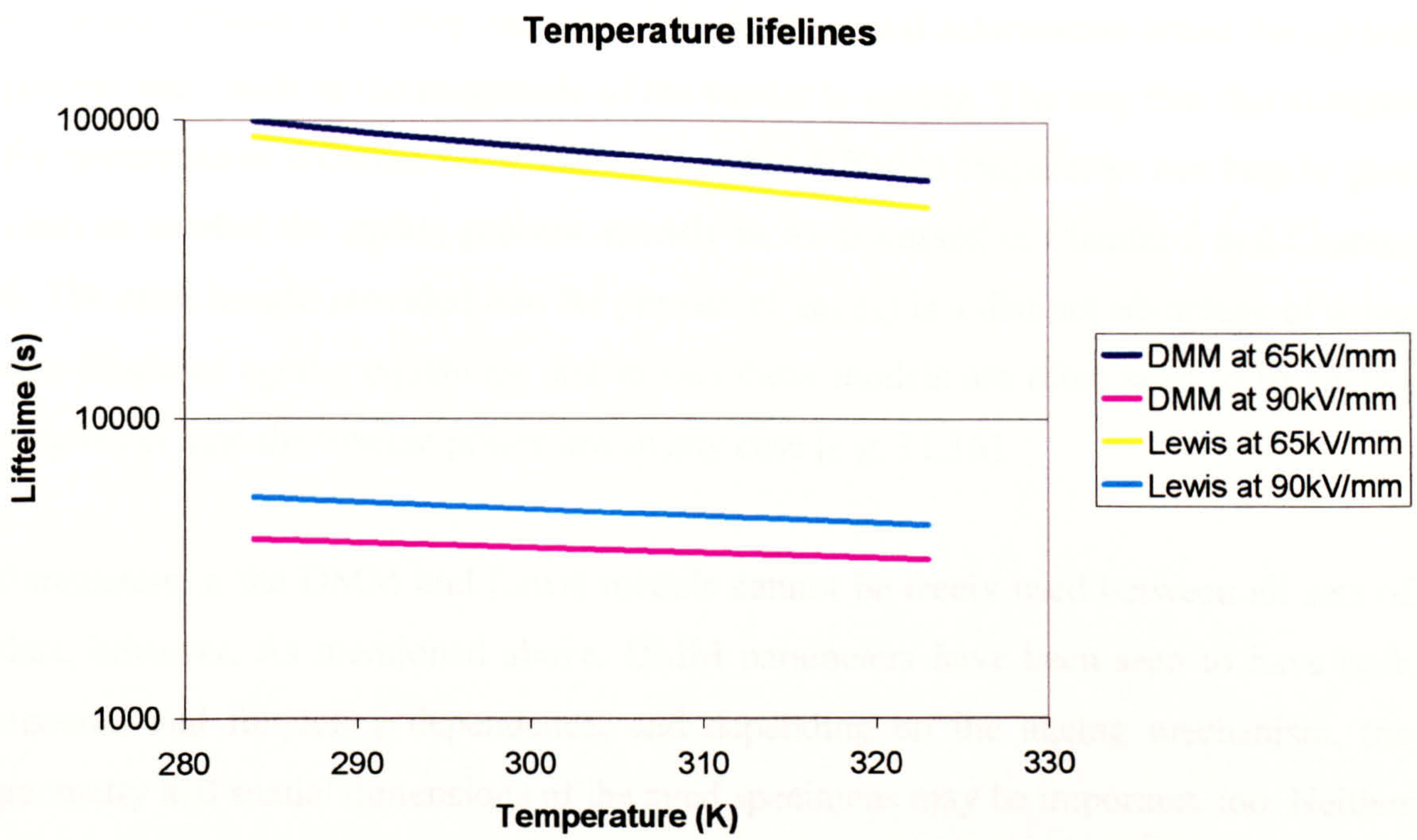

Figure 2.6

Fig 2.6 shows the temperature behaviour of the model equations at constant fields. The functional form of the equations with temperature can be seen to be quite similar. The models also show a reasonable degree of agreement for the range shown and the parameter values used.

2.4 Uses and Limitations of the Models

The models described here can both be used in a phenomenological way. They can be fitted to data from ageing experiments to give values for the various parameters as demonstrated in the next chapter, and in [1-4,11]. These parameters can then be used along with the lifetime equations to give lifetime predictions for other ageing conditions. This is very useful, since it means that ageing experiments can be carried out at high fields and temperatures, and the resulting parameters used for conditions that would take much longer to test.

In this sort of application, the models are not novel – cable manufacturers have been using *e.g.* the inverse power law [*e.g.* 11,16] to predict cable lifetime in this way for many years, and the inverse power law has the advantage of only 2 parameters, compared with up to 6 for these models. The models described here, however, are not just empirical like the inverse power law, and the parameter values, are not only useful

in further predictions – they can also yield fundamental information about the ageing process itself such as the magnitude of the barrier to ageing. The way that this changes for specimens of different sizes, materials and at different frequencies can help to give clues as to what the ageing process actually is, as discussed in Chapter 5 and Chapter 6. The extra insight provided into the physics of ageing is a distinct advantage of using non-empirical ageing equations, and in fact these models are often seen to fit ageing data better than the inverse power law in any case [*e.g.* 11,16].

Parameters in the DMM and Lewis models cannot be freely used between all sets of data, however. As mentioned above, DMM parameters have been seen to have both material and frequency dependence, and depending on the ageing mechanism, the geometry and spatial dimensions of the aged specimens may be important, too. Neither model makes any sort of allowance for specimen volume or thickness, and this is discussed further in Chapters 4 and 5. Caution must therefore be used in applying parameter values from one set of experiments to another.

Another drawback of the models is that they both assume that polymers are homogeneous. On a microscopic level this is not the case, but given the good fits to data achieved in the literature and in chapters 3 and 5 of this thesis, the approximation seems to be justifiable for this purpose.

3. Application of Models to Thin Film Data

The DMM and Lewis models predict the lifetime of polymeric insulation according to equations 2.7 and 2.30 derived in the last chapter. In order to obtain values for the various parameters in the lifetime equations, it is necessary to fit the equations to experimental field, temperature and lifetime data. It is hoped that once the models have been fitted to data from ageing experiments of a certain type (i.e. specimens of the same size and material aged at one frequency) the parameter values obtained should be applicable to specimens of the same type at any other field and temperature. The advantage of this is that ageing tests can be performed under a few high field and temperature conditions, the results from which are quick to produce. The equations and the parameters obtained can then be applied to service field and temperature conditions to predict the working lifetime of real insulation systems.

Used in this way, the models are phenomenological; after observing behaviour under one set of conditions, the models can be used to predict behaviour under different conditions. The fact that the parameters all have physical meanings, however, means that the models are not limited to this phenomenological approach. The values of parameters found during such fittings have physical implications for the ageing process, and can therefore aid in understanding it.

3.1 Experimental Data

When a set of seemingly identical polymeric specimens is aged under the same experimental conditions –i.e. under the same field and temperature- a distribution of lifetimes is produced; each specimen in the set fails at a different time. The distribution of failure times is often observed to be a Weibull distribution [1-4], and analysis of the failure times is usually therefore carried out using Weibull statistics.

This involves ranking the failure times in order from smallest to largest. For small data sets such as those used here, the accuracy of the distribution parameters can also be improved by weighting each failure time according to the number of data in the set. These weightings are given in [2]. The cumulative probability of failure corresponding

to each failure time can then be worked out using Weibull probability equations [1,2,5], and failure time versus cumulative probability of failure can then be plotted on a Weibull graph. The time at which 63.2% of the specimens has failed can be worked out using *e.g.* linear regression or a 'by eye' method [1,2]. This time is the characteristic lifetime of the specimens and is known as B63. It can also be regarded as the time at which any specimen in the set has a 63.2% chance of failing, and can be considered as analogous to the mean value of a Normal distribution, though it is not directly equivalent.

The spread in each set of lifetime data can also be characterised by Weibull statistics, and this is done via the Weibull parameter β. Its reciprocal is analogous to standard deviation of the Normal distribution, since a larger value of β indicates a narrower spread of values in the distribution. This value can also be calculated via linear regression or 'by eye' methods.

Statistical confidence limits can be derived for each B63 and β value as detailed in [2]. Limits between particular confidence percentiles for B63 values will be wider for broader sets of data. The uncertainty in the characteristic lifetime must be greater if there is a greater spread of lifetimes around it.

'Identical' polymer specimens are necessarily used in ageing tests of this type. Lifetime is dependent on material, so the specimens all need to be of the same material. Specimen volume, geometry and size may also have an effect on lifetime, and this effect is not well understood (as discussed further in following chapters). Using geometrically identical specimens results in lifetimes and hence model parameters that are characteristic of that particular geometry.

3.2 Method of fitting the models

In order to get parameter values for the models, the equations can be fitted to B63 values. This yields parameter values that correspond to characteristic failure times - the parameter values must therefore also be 'characteristic' values, though not in the strict statistical sense in which the B63 times are the characteristic failure times of the

experimental lifetime distributions. The exact meanings of these 'characteristic' parameter values are discussed further in Chapter 6.

To ensure the parameter values are as 'good' as possible, it is best to fit the data to B63 values from experiments under as many different conditions as possible. This ensures that the parameter values will be applicable to a range of field and temperature conditions. It is also best to have as many specimens as possible in each ageing experiment, to try to ensure that the characteristic failure times and hence the parameter values are as representative as possible. Ideally, then, ageing experiments will be carried out at many different fields and temperatures, and each experiment will involve ageing many polymer specimens.

In this investigation, the models have been fitted to characteristic lifetime data from experiments where PET thin films have been aged under various different conditions [6]. PET is not a polymer generally used for cable insulation, but the data was used in this case since it was readily available, and comprised results from a wide range of field and temperature conditions. Data from both AC and DC ageing experiments have been used, and data from the two different frequencies has been fitted separately to allow for frequency dependences of parameters as outlined in Chapter 2 and described in the literature [7,8].

The DC ageing experiments were carried out on PET films with a thickness of 36μm. Specimens were aged at nineteen different experimental conditions, with seventeen PET specimens aged at each condition. The test temperatures were in the range 383K to 458K, and the applied voltages in the range 1kV to 3kV. The AC experiments were carried out on 50μm-thick films, with nine specimens aged under each of 30 different conditions. The AC tests were carried out under applied voltages from 0.65kV to 2.5kV r.m.s and temperatures from 293K to 423K.

The lifetime data from each experimental condition were analysed as described in section 3.1 to give a characteristic lifetime or B63 value for each condition using a linear regression method. The model lifetime equations were then fitted to the B63 values using a fitting algorithm. Both lifetime equations are extremely non-linear, so

are best suited to a non-linear fitting algorithm. The algorithm used in this chapter is the Levenberg-Marquardt algorithm as implemented in MATHCAD.

MATHCAD can fit equations to data using 'solve blocks'. These consist of the word 'Given' followed by a series of logical constraints – in this instance the constraints are lifetime expressions set equal to experimental lifetime data. The solve block is finished with a 'Minerr(arguments)' statement, which instructs MATHCAD to minimise the error for the given constraints by changing the value of the arguments of minerr in the constraints. In this case the arguments are the DMM or Lewis parameters. The algorithm used to minimise the error for the constraints can be chosen by the user. Part of the solve block for fitting the DMM equation to the DC PET experimental lifetime data is shown in box 3.1.

In box 3.1, the initial guess values for each parameter are defined at the top, as well as the values of the constants needed in the DMM lifetime expressions. The given loop contains some sample constraints, each with a DMM life expression on the left hand side, and an experimental characteristic lifetime on the right hand side. For the actual fitting, all 19 of the DC PET experimental lifetimes were equated to corresponding DMM life expressions; only three constraints are shown here for brevity. The miner function is then set to minimise the difference between the DMM expressions and the experimental data by changing the values of the six DMM parameters.

Values for the experimental characteristic lifetimes, fields and temperatures must already have been defined in the MATHCAD worksheet for the solve block to work. In this example, the fields are contained in a vector called 'DCE', the temperature values in 'DCT' and the lifetimes in 'DCa'. The vector names with subscripts – as shown in Box 3.1 - refer to corresponding elements in these vectors, so that the lifetime denoted DCa_1 was obtained under experimental field DCE_1 and temperature DCT_1.

Initial guess values for parameters:

$Hdk := 17762$

$Kd := 305.9$

$Sd := -9.1 \cdot 10^{-25}$

$Cd := 1.582$

$b := 0.389$

$Astar := 0.485$

Constants

$h := 6.626 \cdot 10^{-34}$

$k := 1.381 \cdot 10^{-23}$

The 'given loop' containing sample constraints:

Given

$$\frac{\frac{h}{k \cdot 2 \cdot DCT_1} \cdot \exp\left(\frac{Sd}{k}\right) \cdot \exp\left[\frac{Hdk - \frac{Cd \cdot (DCE_1)^{4 \cdot b}}{2}}{DCT_1}\right] \cdot \left[-\ln\left[\left[\frac{1}{1 + \exp\left[\frac{Kd - Cd \cdot (DCE_1)^{4 \cdot b}}{DCT_1}\right]} - Astar\right]\right]\right]}{\cosh\left[\frac{Kd - Cd \cdot (DCE_1)^{4 \cdot b}}{2 \cdot DCT_1}\right]} = DCa_1$$

$$\frac{\frac{h}{k \cdot 2 \cdot DCT_2} \cdot \exp\left(\frac{Sd}{k}\right) \cdot \exp\left[\frac{Hdk - \frac{Cd \cdot (DCE_2)^{4 \cdot b}}{2}}{DCT_2}\right] \cdot \left[-\ln\left[\left[\frac{1}{1 + \exp\left[\frac{Kd - Cd \cdot (DCE_2)^{4 \cdot b}}{DCT_2}\right]} - Astar\right]\right]\right]}{\cosh\left[\frac{Kd - Cd \cdot (DCE_2)^{4 \cdot b}}{2 \cdot DCT_2}\right]} = DCa_2$$

$$\frac{\frac{h}{k \cdot 2 \cdot DCT_3} \cdot \exp\left(\frac{Sd}{k}\right) \cdot \exp\left[\frac{Hdk - \frac{Cd \cdot (DCE_3)^{4 \cdot b}}{2}}{DCT_3}\right] \cdot \left[-\ln\left[\left[\frac{1}{1 + \exp\left[\frac{Kd - Cd \cdot (DCE_3)^{4 \cdot b}}{DCT_3}\right]} - Astar\right]\right]\right]}{\cosh\left[\frac{Kd - Cd \cdot (DCE_3)^{4 \cdot b}}{2 \cdot DCT_3}\right]} = DCa_3$$

etc.....

$Minerr(Hdk, Sd, Kd, Astar, b, Cd) =$

Box 3.1

The Levenberg-Marquardt algorithm is a non-linear least squares method, which is a variation of a steepest descent method [9,10]. The algorithm needs initial guess values for each of the parameters, and the results are very sensitive to these initial guesses. This sensitivity means that the initial guess values are very important.

In this case, finding initial guess values for the parameters in the DMM model was not difficult, since the model had already been fitted to very similar data in the past. The parameter values for fits to both AC and DC PET thin film data are therefore available in [7](Levenberg-Marquardt fitting for PET AC and DC data), [11](Simplex fitting method for PET dc data) and [12] (Levenberg Marquardt used for PET DC data). The values from [7] were used as the initial guess values for the fitting algorithm. In a first fitting, guess values could be derived from the physical meanings of each parameter, and to test the robustness of the parameters obtained, the algorithm could be provided with different initial guess values. Convergence to the same solution would then indicate that a global minimum between the life function and the data had been found, rather than just a local minimum.

For the Lewis model, no PET parameter values were available. Initial guess values for each parameter were therefore obtained from equivalences with the DMM parameters as outlined in Chapter 2. The Lewis parameters U_b and U_r were split into enthalpy and entropy parts as in the DMM derivation, so that their temperature dependence could be explicitly examined. Equivalent parameters were then obtained from modified versions of equations 2.31-2.33, as shown below in equations 3.1-3.3

$$U_B = LH_{dk} - TLS_d + \frac{LK_d}{2}$$

$$U_R = LH_{dk} - TLS_d - \frac{LK_d}{2} \qquad \text{3.1-3.3}$$

$$U_B - U_R = LK_d$$

LH_{dk}, LS_d, LK_d are therefore the Lewis model equivalents of the DMM parameters H_{dk}, S_d and K_d, and guess values from previous DMM fittings can be used directly as input for these in the solving algorithm. Initial values for the γ parameters were

estimated so that equation 2.37 was approximately satisfied at a few test fields in the range at which the experimental data was obtained.

In both AC and DC cases it should be noted that the models were fitted to all of the experimental data simultaneously. In other words only one set of parameters was obtained which gave the best fit to the data from all the different experimental conditions. This is important, since the good fits to data then imply that the E and T dependencies in the model have indeed all been explicitly expressed, as they must have been if many of the assumptions made about the ageing process are good ones. The models could alternatively have been fitted to each point in turn – giving different parameter values for each experimental condition. This would inevitably result in a better fit between experiment and data, but to agree with the theory used the parameters should be temperature and field independent.

3.3 Results from fitting the models

3.3.2 Results from fitting of models to AC PET data

The predictions of both models were found to fit the characteristic data from AC ageing experiments well, as shown in fig 3.1. Over half of the DMM model predictions and over a quarter of the Lewis model predictions are within the 90% confidence limits of the corresponding data points. The graph shows the experimental characteristic lifetime data as black diamonds with 90% confidence limits shown on each point as error bars. The predictions of the DMM model are shown as blue squares, and those of the Lewis model as red triangles. The y-axis of the graph shows lifetime in seconds, and the x-axis just shows experiment number – there is no particular significance to values on this axis.

The fact that the DMM model gives a better fit to the data is not entirely surprising given that the DMM model is inherently more flexible; the Lewis model assumes a field squared dependence in the change in the activation barrier, whereas the DMM model allows the field exponent to be one of the fitted model parameters.

As well as looking at the fit between the data points and the model predictions, it is possible to generate lifelines using the parameter values. Field lifelines show the predicted lifetime of the polymer specimen with field at any particular temperature. Fig

3.2 shows field lifelines of the DMM model with the PET AC data, and fig 3.3 shows the Lewis field lifelines with the data.

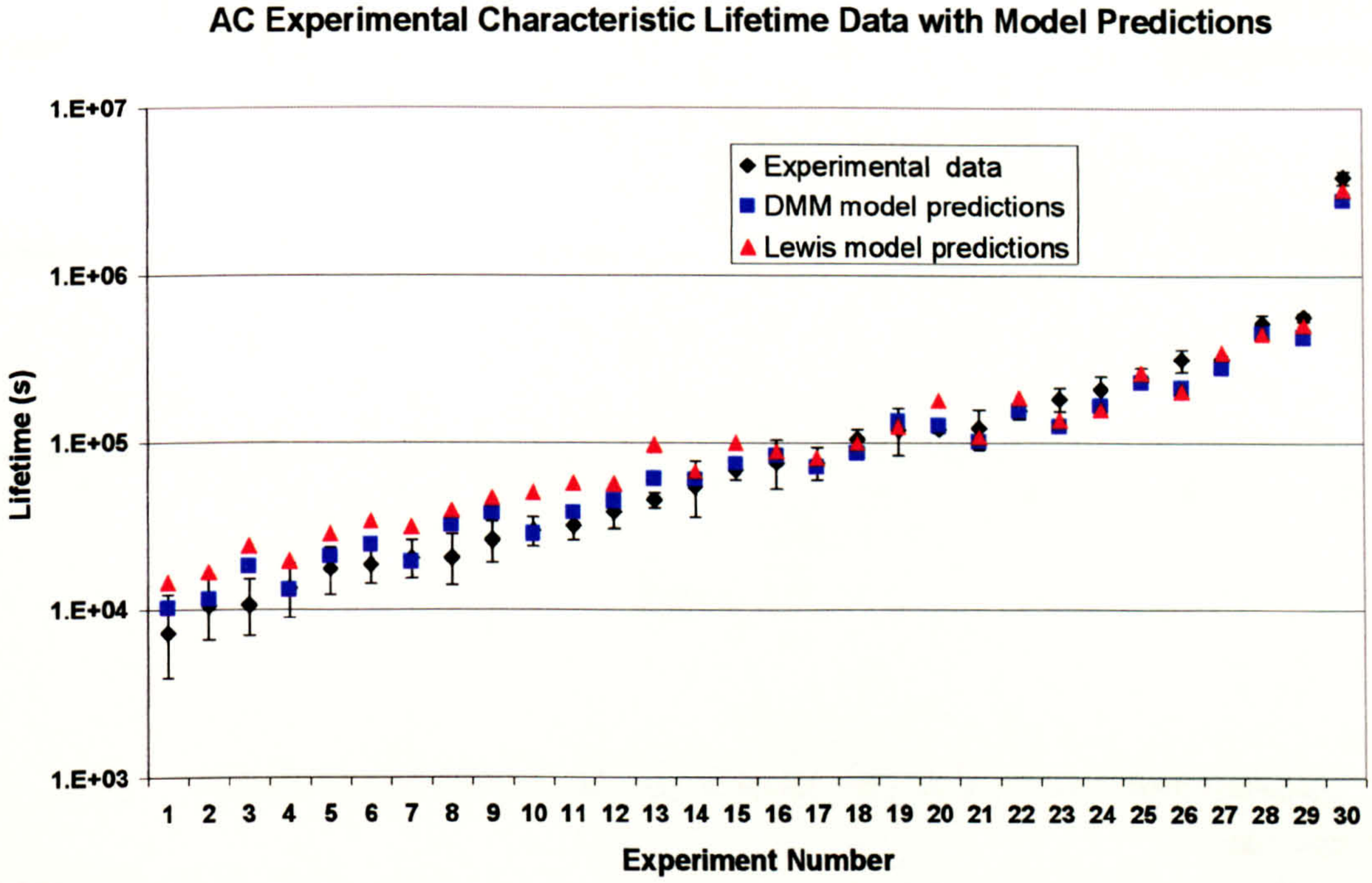

Figure 3.1

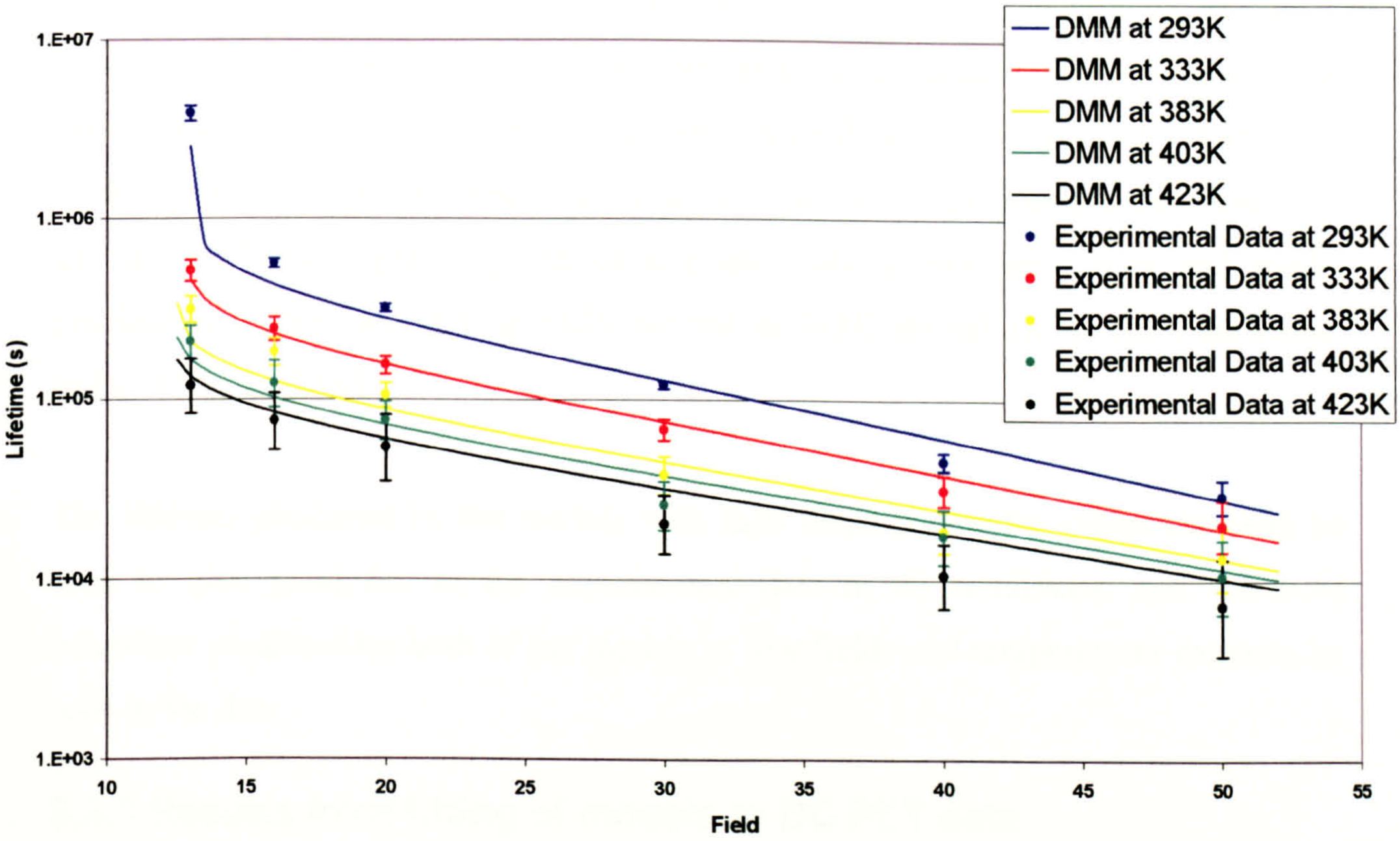

Figure 3.2

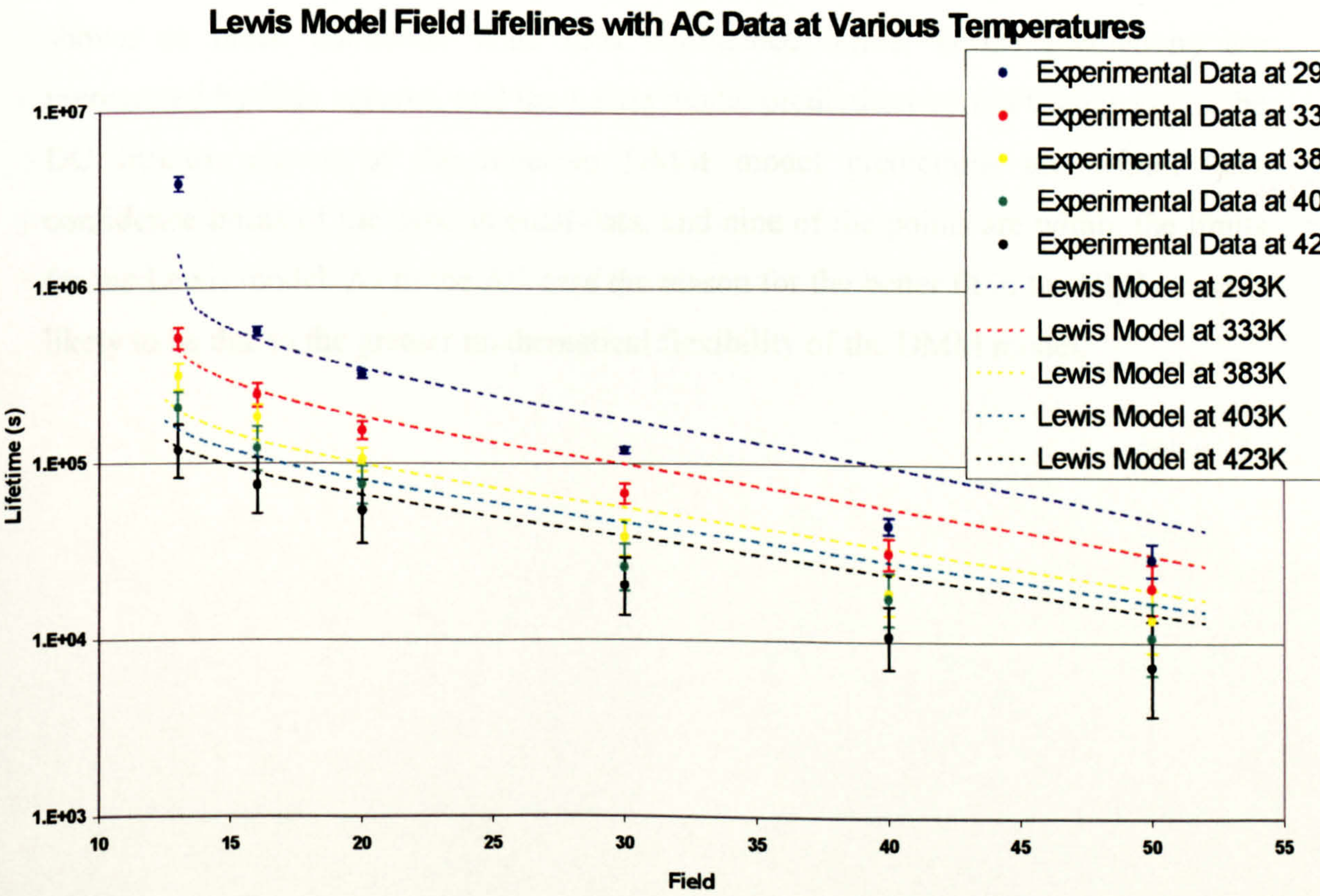

Figure 3.3

In figures 3.2 and 3.3, the y-axes show lifetime of the specimens in seconds, and the x-axes show applied field. In the AC case, the r.m.s applied field is used throughout. The experimental characteristic lifetimes are shown as data points with 90% confidence limits shown by error bars. The DMM and Lewis model predictions are shown as solid and dotted lines respectively. In each graph, data points, error bars and model predictions at 293K are blue, at 333K are red, at 383K are yellow, at 403K are green, and at 423K are black.

The lifelines produced by the models with their fitted parameter values can both be seen to give good fits to the experimental data at all conditions, and threshold behaviour predicted by both of the models at low fields and temperatures can also be seen in the data.

3.3.3 Results from fitting of models to DC PET data

The predictions of the two models were also found to give good fits to the data from DC ageing experiments, as shown in fig 3.4. As in fig 3.1, the y-axis shows lifetime in seconds, and the x-axis just denotes experiment number. The experimental data are shown as black diamonds with 90% confidence limits, DMM predictions are represented by blue squares, and the Lewis model predictions by red triangles. For the DC fittings, eleven of the nineteen DMM model predictions are within 90% confidence limits of the experimental data, and nine of the points are within the limits for the Lewis model. As in the AC case the reason for the better fit in the DMM case is likely to be due to the greater mathematical flexibility of the DMM model.

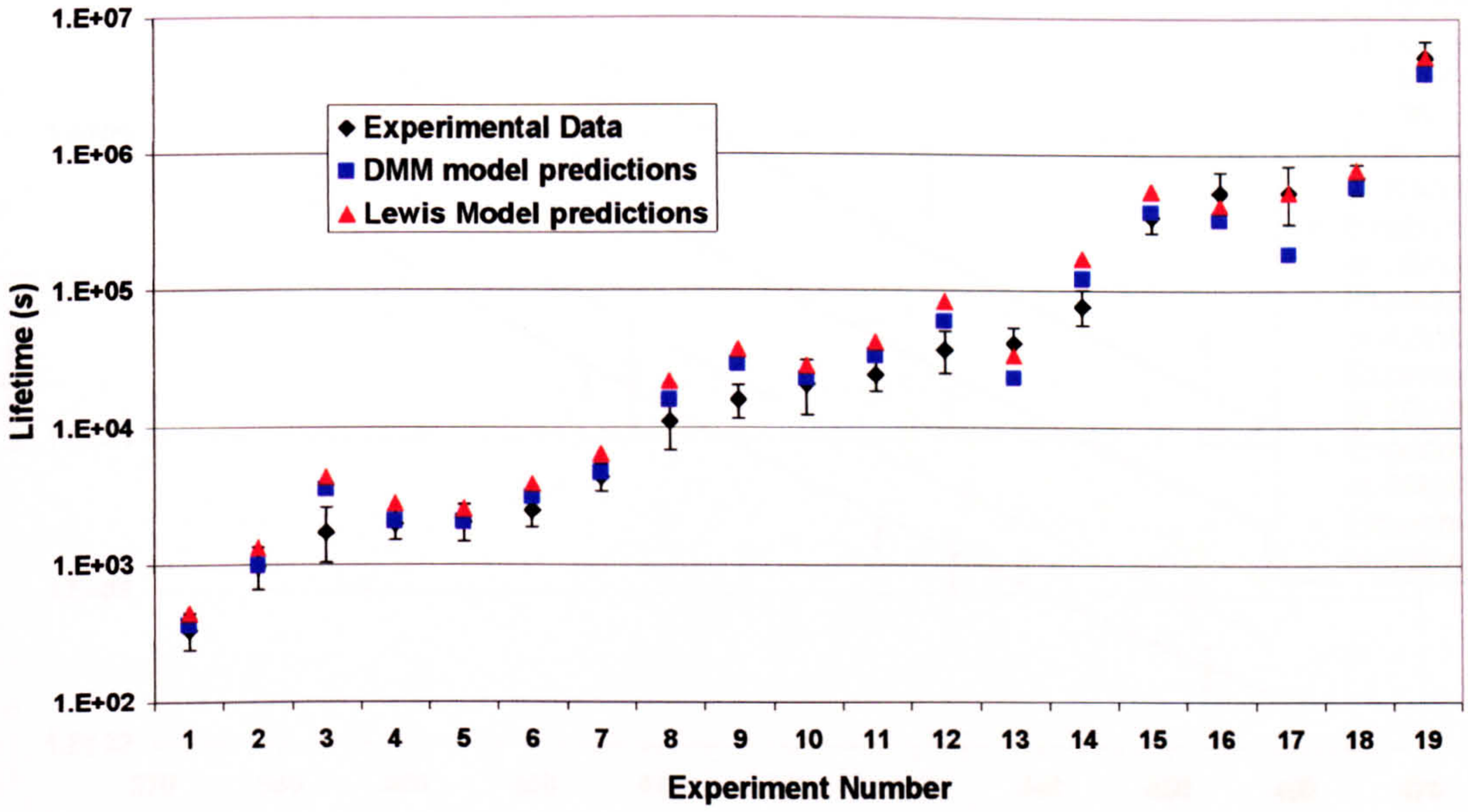

Figure 3.4

Lifelines can again be produced, though for the DC case field lifelines are more difficult, since while the AC experiments were carried out at each of 6 fields and 5 temperatures to give 30 experimental conditions, the conditions under which the DC experiments were carried out were less ordered. In fact the temperature of each experiment was different. Only five fields were used, however, so in the DC case the data are shown with temperature lifelines. Temperature lifelines show lifetime with temperature for any given field. Temperature lifelines are shown with the DC experimental data in fig 3.5 for the DMM model, and in fig 3.6 for the Lewis model.

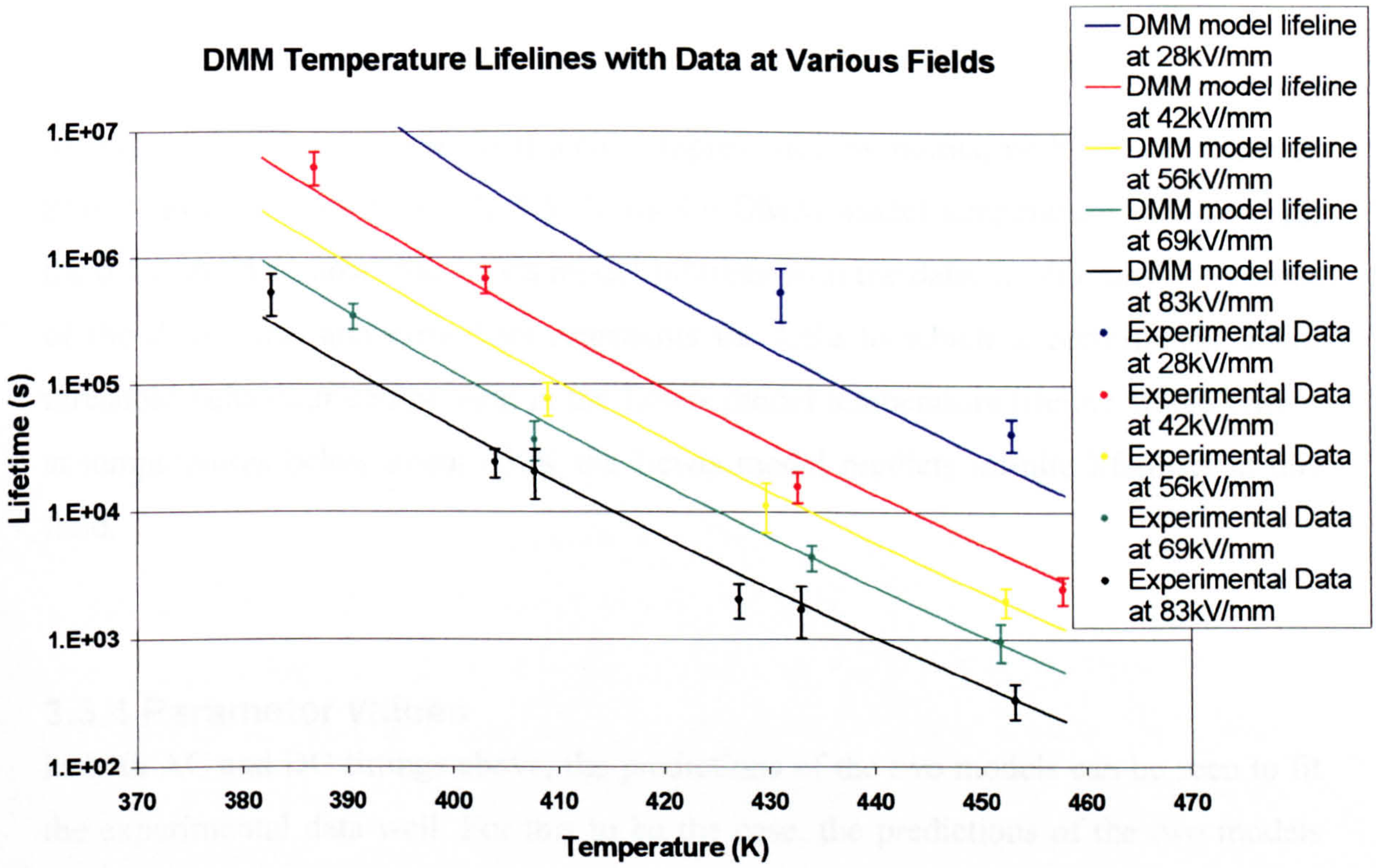

Figure 3.5

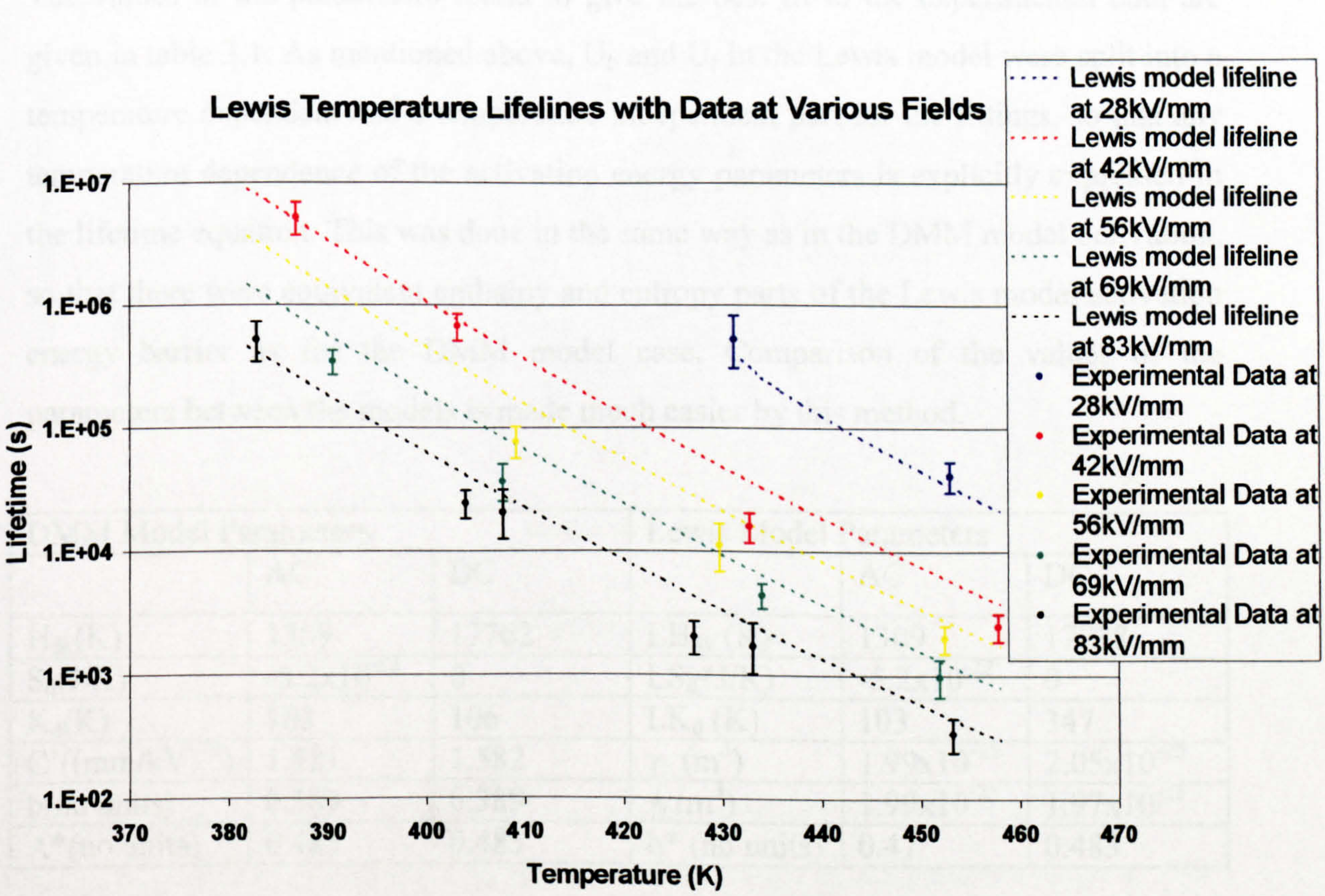

Figure 3.6

In figs 3.5 and 3.6, experimental data is represented by points, with 90% confidence limits shown as error bars. Fig 3.5 shows the DMM model temperature lifelines with the data, and 3.6 shows the Lewis model lifelines with the data. In all cases, the colour of the data, lines and error bars represents the field to which it corresponds. Field threshold behaviour can be seen in the Lewis model temperature lifeline at 28kV/mm; at temperatures below about 430K the Lewis model predicts infinite lifetimes at this field.

3.3.4 Parameter values

In both AC and DC fittings above, the predictions of the two models can be seen to fit the experimental data well. For this to be the case, the predictions of the two models must be very similar to one another. Given the mathematical similarities of the model functions as discussed in the previous chapter, and the fact that the fitting algorithm was given very similar initial conditions in both cases, this result is not very surprising.

The values of the parameters found to give the best fit to the experimental data are given in table 3.1. As mentioned above, U_b and U_r in the Lewis model were split into a temperature dependent and a temperature independent part for the fittings, so that any temperature dependence of the activation energy parameters is explicitly expressed in the lifetime equation. This was done in the same way as in the DMM model derivation, so that there were equivalent enthalpy and entropy parts of the Lewis model activation energy barrier as for the DMM model case. Comparison of the values of the parameters between the models is made much easier by this method.

DMM Model Parameters			Lewis Model Parameters		
	AC	DC		AC	DC
H_{dk}(K)	1309	17762	LH_{dk} (K)	1309	17738
S_d(J/K)	-5.2×10^{-22}	0	LS_d (J/K)	-5.2×10^{-22}	0
K_d(K)	103	106	LK_d (K)	103	347
C'((mm/kV)^{4b})	1.581	1.582	γ_b (m^3)	1.99×10^{-25}	2.05×10^{-25}
b(no units)	0.389	0.389	γ_r (m^3)	1.99×10^{-25}	1.97×10^{-25}
A*(no units)	0.485	0.485	b* (no units)	0.47	0.483

Table 3.1

The activation energy parameters for the two models in the AC case are identical, and there are only slight differences between them in the DC case. For the lifetime equations to both fit the same experimental data, this is not surprising. Values of A* and b* are also very similar for the two models, which is also as expected given the mathematical equivalence of these parameters between the models.

As mentioned in chapter 2, the biggest difference between the models is the way in which an applied field affects the activation energy of the ageing process. This is described by $C'E^{4b}$ in the DMM model and $(\gamma b+\gamma r)E^2$ in the Lewis model. These two terms are shown plotted with field in fig 3.7 for both AC and DC parameter values. The change in barrier height is shown in the y-axis with applied field on the y-axis. The difference between the changes in barrier height predicted by the models increases as the applied field increases.

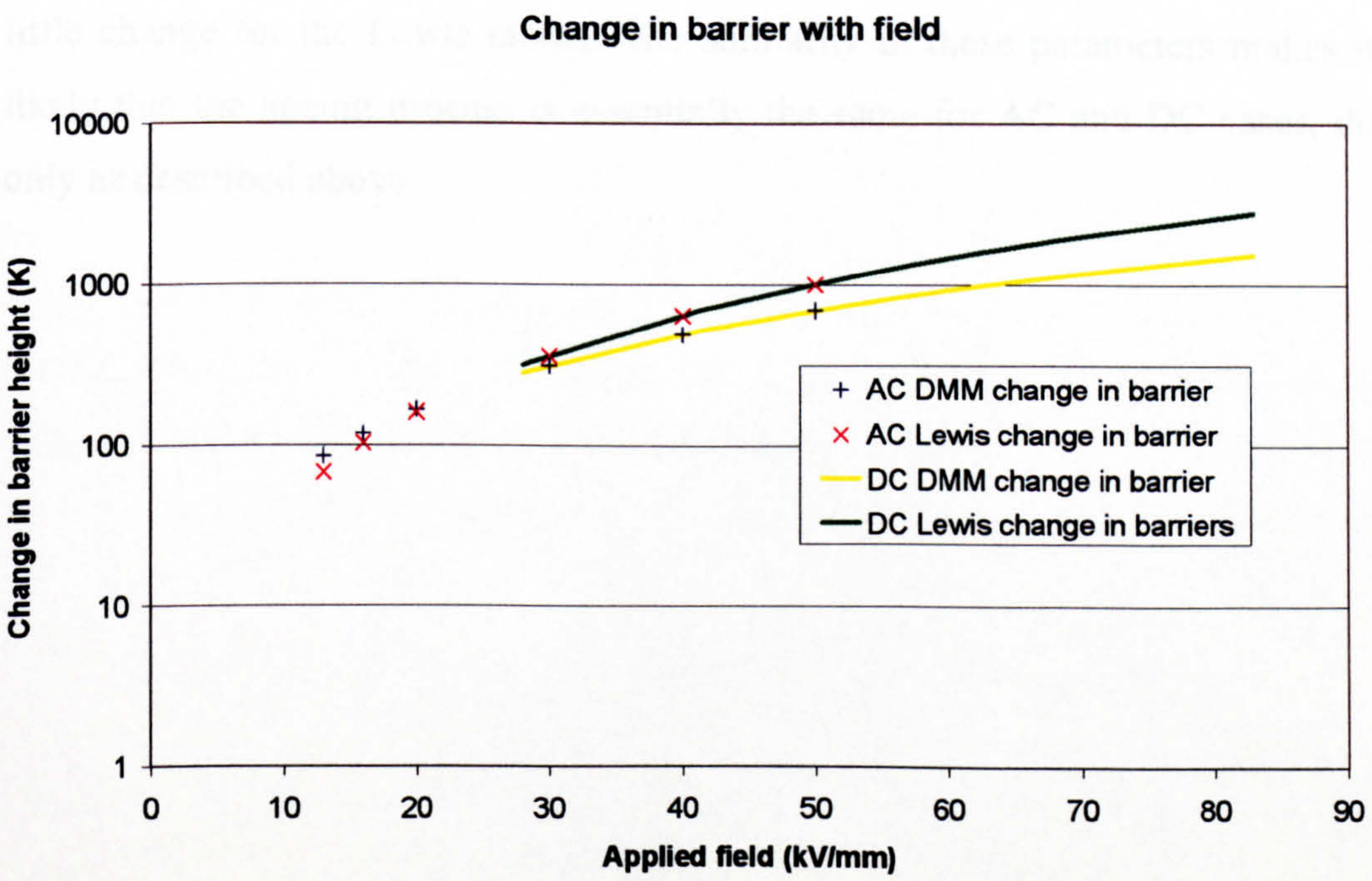

Figure 3.7

The difference between DMM parameter values obtained from AC fittings and DC fittings has been described in [7,8], and briefly discussed in the previous chapter. The values found here are consistent with previous results in that from AC to DC the entropy part of the activation energy reduces to zero, while the enthalpy part of the

activation energy increases in magnitude. This holds here for both the DMM and the Lewis models, agreeing with the hypothesis mentioned in Chapter 2, and discussed in [7,8]. This hypothesis states that because in the AC case the ageing reaction is taking place in a polymer matrix being driven at AC frequency, less enthalpy is needed for the moieties to become involved in ageing. However, an entropy constraint is introduced – there is less chance that an AC driven moiety will be in such an arrangement as to make the ageing reaction possible.

The parameters relating to polymer morphology and microstructure (rather than activation energy) are observed not to change significantly between AC and DC, as has been seen before for the DMM model. These parameters are C' and b for the DMM model, and γ_b and γ_r in the Lewis model, and they describe how the macroscopic field magnitude affects the barrier to ageing for moieties involved in ageing. There is actually no change at all in these DMM parameters between AC and DC, and very little change for the Lewis model. The similarity in these parameters makes it seem likely that the ageing process is essentially the same for AC and DC cases, different only as described above.

4. Application of Models to Power Cable Data – Theory

The previous chapter demonstrates how the DMM and Lewis polymer ageing models can be fitted to data from ageing experiments involving thin films. For the thin film case, the temperature and field experienced by each film were considered to be spatially constant. In systems such as power cable insulation this assumption cannot be made. The insulation of a power cable under load experiences a radially varying temperature distribution due to Joule heating in the core as shown in section 4.2.1 below. The insulation also experiences a radially varying electrical stress distribution, as shown in section 4.2.2 for the AC case and section 4.2.3 for the DC case. This makes fitting the ageing models to lifetime data from cable ageing experiments more difficult than in the thin film case.

A brief outline of power cable design is given in section 4.1. A method of using the ageing models for power cable geometry is then described in section 4.3, and some results of using the method are given in Chapter 5.

4.1 Power Cable Structure

Power cables vary widely in design and structure according to manufacturer and intended use. A general overview is briefly presented here.

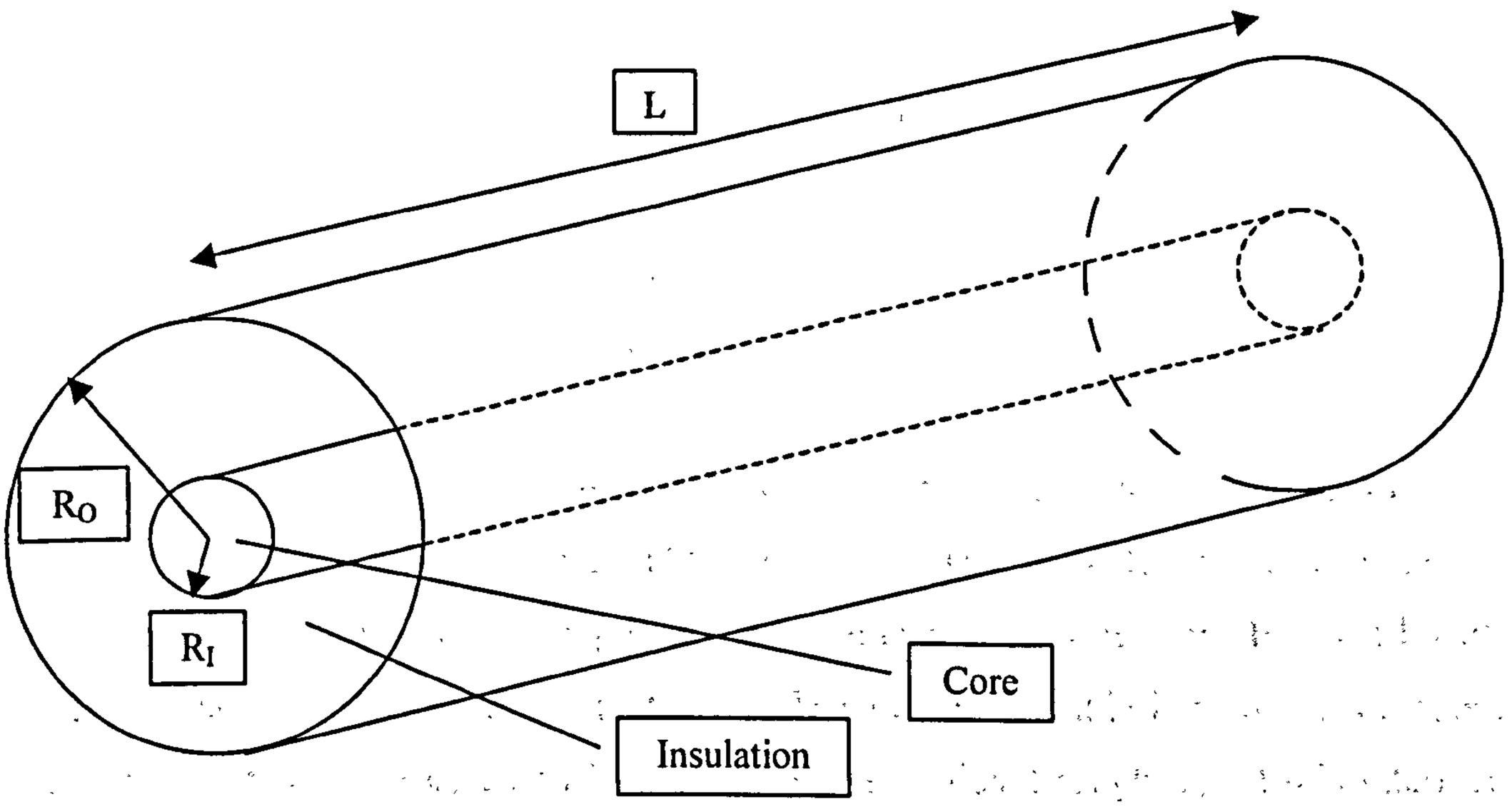

Figure 4.1

Fig 4.1 shows a simple co-axial cable design. The cable has length L, and a central current-carrying core with a circular cross section of radius R_I. The core is surrounded by an insulation layer with circular cross section of radius R_O as measured from the centre of the cable core. The subscripts I and O are used to refer to the inner and outer radii of the cable insulation respectively, since it is the insulation that concerns this investigation.

Common cable core materials are copper and aluminium, which both have high electrical conductivity. Copper also has the advantage of being very easy to manipulate into rods and wires, though financial factors have promoted the use of aluminium since the 1950s, when the price of copper rose substantially [1]. Cores are not always solid cylinders as shown in fig 4.1 – segmented cores are common for high voltage cables [1,2]. The simplest geometry (as shown above) is assumed in this chapter, firstly for simplicity. This geometry is also applicable here since the cable ageing data used in the next chapter is from cables of this type.

Insulation types fall into three main categories:

1. Paper and oil insulation.
2. Paper and polymer laminate insulation.
3. Polymeric insulation.

Details of all of these types can be found in [1] and [2], but in this chapter only polymeric insulation is considered, since the ageing models described in chapter 2 can only strictly be applied to polymeric insulation. Polymeric insulating materials include polyvinyl chloride (PVC), polypropylene (PP) and commonly polyethylene (PE). Thermoset polymers such as ethylene-propylene rubbers (EPR) are also used, with the choice of polymer depending on the specific application [1,2].

In addition to the core and insulation layers shown above, many cables also have a 'semicon' layer between the core and the insulation. This is made from an extrudeable polymer, compatible with and possibly the same as the insulation, but filled with carbon black to make it more conductive. The function of this is to make a smooth interface between the core and insulation. Any significant roughness at this interface could lead to localised field enhancements when voltage is applied to the core, and this could be very damaging to the insulation. Cables usually also comprise a semicon

layer outside the insulation, and then various sheaths. The sheaths are designed to protect the cable from physical damage and water ingress in service, so vary according to the intended use.

4.2 Field and Temperature Distributions in Cable Insulation

Theoretical expressions for field and temperature distributions in power cable insulation are derived below. The derivations are all for a steady state situation –i.e. are valid only after the temperature distribution has stabilised and any transient electrical effects due to the initial application of voltage and current to the cable core have died away. This assumption is particularly important in the DC case where any polarisation of the insulation material due to the applied voltage is assumed to have already occurred for the field expression to be valid. Though not considered here, the form of the DC field distribution at various stages during DC voltage application, removal and polarity reversal is discussed in [3]. The changes in AC electrical field distribution on application of a current are discussed in [4].

The derivations that follow also involve the assumption that no charge is injected into the insulation under cable operation, and that the field distribution is therefore due only to a voltage applied to the cable core. Any charge injected into the material must modify the field distribution significantly, and space charge measurements on cable specimens do tend to reveal the existence of space charge injection under both AC and DC conditions [e.g. 5-9]. This is discussed further in section 4.3.1.

The derivations assume that the field and temperature vary only with distance from the cable core, r, and not with distance along the length of the cable. In a perfectly homogeneous insulation system this might be the case, but in real systems slight variations in polymer properties that affect temperature and field magnitude (electrical and thermal resistivity, permittivity, morphology etc.) are possible along the cable length. The main dependence, however, is likely to be a radial one as assumed here.

4.2.1 Temperature Distribution

Temperature gradients occur across the thickness of cable insulation due to Joule heating in the core when it is loaded by a current. Assuming conductive heat transfer in

the insulation, the dependence of temperature, T, upon radius, r, measured from the centre of the core can be given by [10,11]

$$T(r) = T_1 + \left(\frac{W \times Th}{2\pi} \ln\left(\frac{R_o}{r} \right) \right) \qquad 4.1$$

T_1 is the ambient temperature outside of the cable, and Th is the combined thermal resistivity of the insulation material and any outer cable layers such as semicon and protective layers. R_o is the outer radius of the insulation and r is radius from the centre of the core. W is the power dissipated per unit length by the loading of the core, so can be approximately given by

$$W = I^2 R \qquad 4.2$$

I is the current in the cable core and R is the electrical resistance of the core per unit length. For AC cases, the RMS value of I must be used in equation 4.2.

The form of the temperature distribution across the insulation of a cable as described in equation 4.1 is shown in fig 4.2 for various values of applied current. The cable dimensions and insulation material characteristics have been chosen according to information pertaining to a typical XLPE insulated BICC cable designed to operate at 33kV. All the relevant information is taken from [1], and is given in table 4.1. Two values are given for the current rating. This is the maximum current that the cable is designed to carry, and depends on insulation material; the two values in table 4.1 correspond to different grades of XLPE.

TABLE 4.1 Dimensions and insulation characteristics for 33kV cable	
Core radius, R_I	18mm
Insulation radius, R_O	35mm
Thermal resistivity of XLPE, Th	3.5m°C/W
Electrical resistivity of core, R	$3.5x10^{-5}\Omega/m$
Current rating (maximum design current)	1420 or 1930 A

Figure 4.2 shows the temperature variation with radius for various values of applied current. In each case the ambient temperature, T_1 was assumed to be 15°C. For the zero current case, there is no heating, and the temperature in the insulation is therefore everywhere equal to 15°C. For the highest current of 1930A, the temperature at the inside edge of the insulation reaches 63°C, which is not an unrealistic situation. In fact, core temperatures of up to 70-90°C are not unusual for cables with PE or PP insulation [1,2].

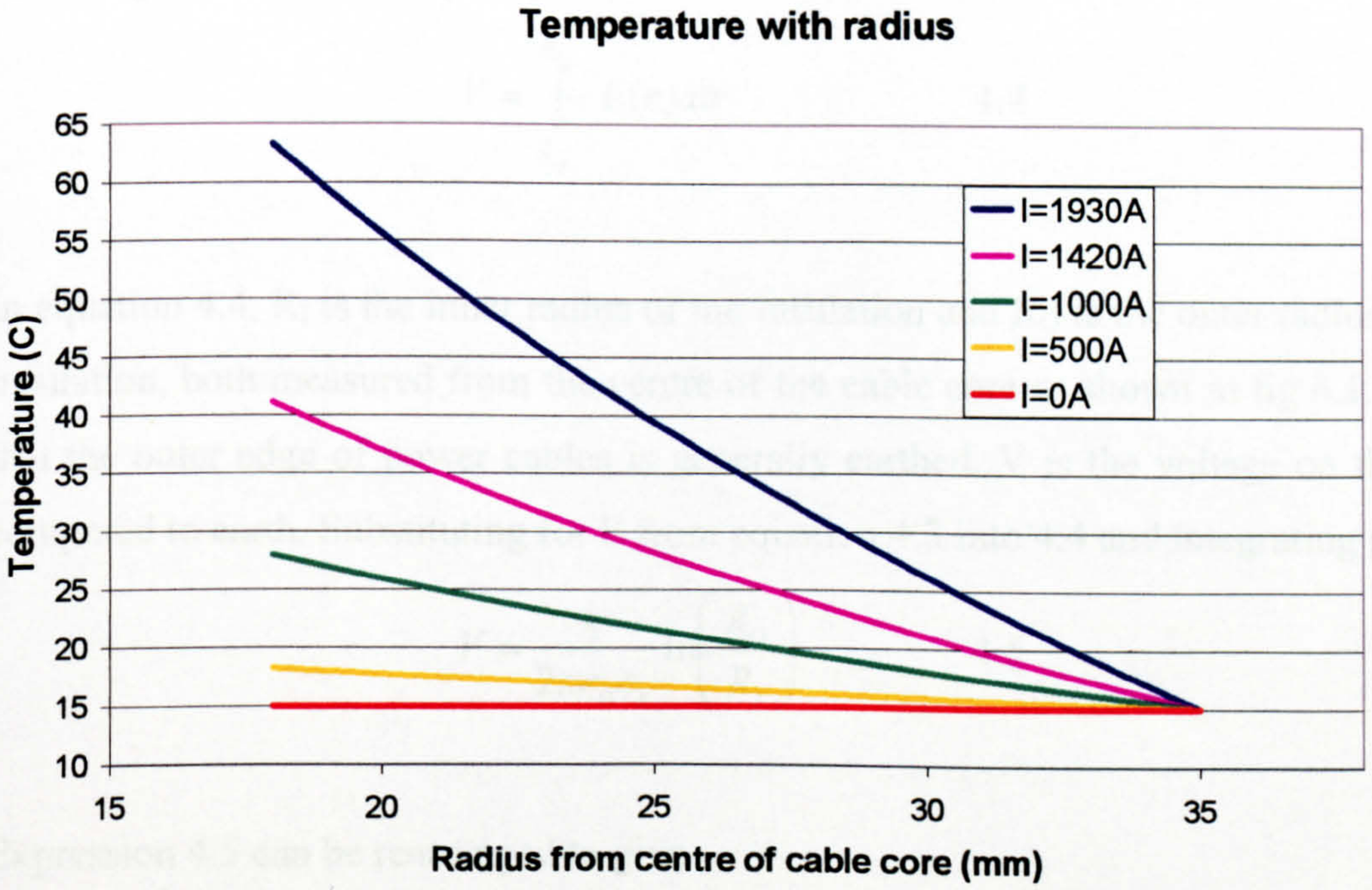

Figure 4.2

Additional heating may also occur directly in cable insulation due to leakage currents and dielectric losses in the insulation. This effect is likely to be very small, but is discussed further in [10].

4.2.2 AC Field Distribution

In the AC case, the field distribution in cable insulation is a function of time, since the applied voltage varies cyclically with time. The instantaneous radial field strength can be found from the following reasoning [1]. If the instantaneous charge per unit length on the conductor is given by q, Gauss's Law gives

$$E(r) = \frac{q}{2\pi\varepsilon_0\varepsilon_r r} \qquad 4.3$$

E(r) is the instantaneous magnitude of the electrical field at radius r; ε_0 is the permittivity of free space and ε_r is the permittivity of the insulation material at the frequency of the applied AC voltage.

An expression for the potential difference between the inner and outer edge of the insulation, V, can be derived from the relationship between potential difference, V and field, E: Here V and E must both be instantaneous values, since in an AC application their magnitudes constantly vary.

$$V = \int_{R_O}^{R_I} -E(r).dr \qquad 4.4$$

In equation 4.4, R_I is the inner radius of the insulation and R_O is the outer radius of the insulation, both measured from the centre of the cable core as shown in fig 4.1. Given that the outer edge of power cables is generally earthed, V is the voltage on the core compared to earth. Substituting for E from equation 4.3 into 4.4 and integrating gives

$$V = \frac{q}{2\pi\varepsilon_0\varepsilon_r}\ln\left(\frac{R_O}{R_I}\right) \qquad 4.5$$

Expression 4.5 can be rearranged to give

$$\frac{q}{2\pi\varepsilon_0\varepsilon_r} = \frac{V}{\ln\left(\frac{R_O}{R_I}\right)} \qquad 4.6$$

Comparing equation 4.6 with equation 4.3, it can be seen that

$$E(r) = \frac{V}{r \ln\left(\frac{R_O}{R_I}\right)} \qquad 4.7$$

Where r, R_o and R_I all have their previous meanings.

AC electrical stress at any radius and time is therefore dependent on

- Voltage across the insulation
- Inner and outer insulation radii.

The form of the AC field distribution is shown in fig 4.3 for cable characteristics as in table 4.1. The field distribution is shown at various stages during a voltage cycle with a peak value of V of 33kV.

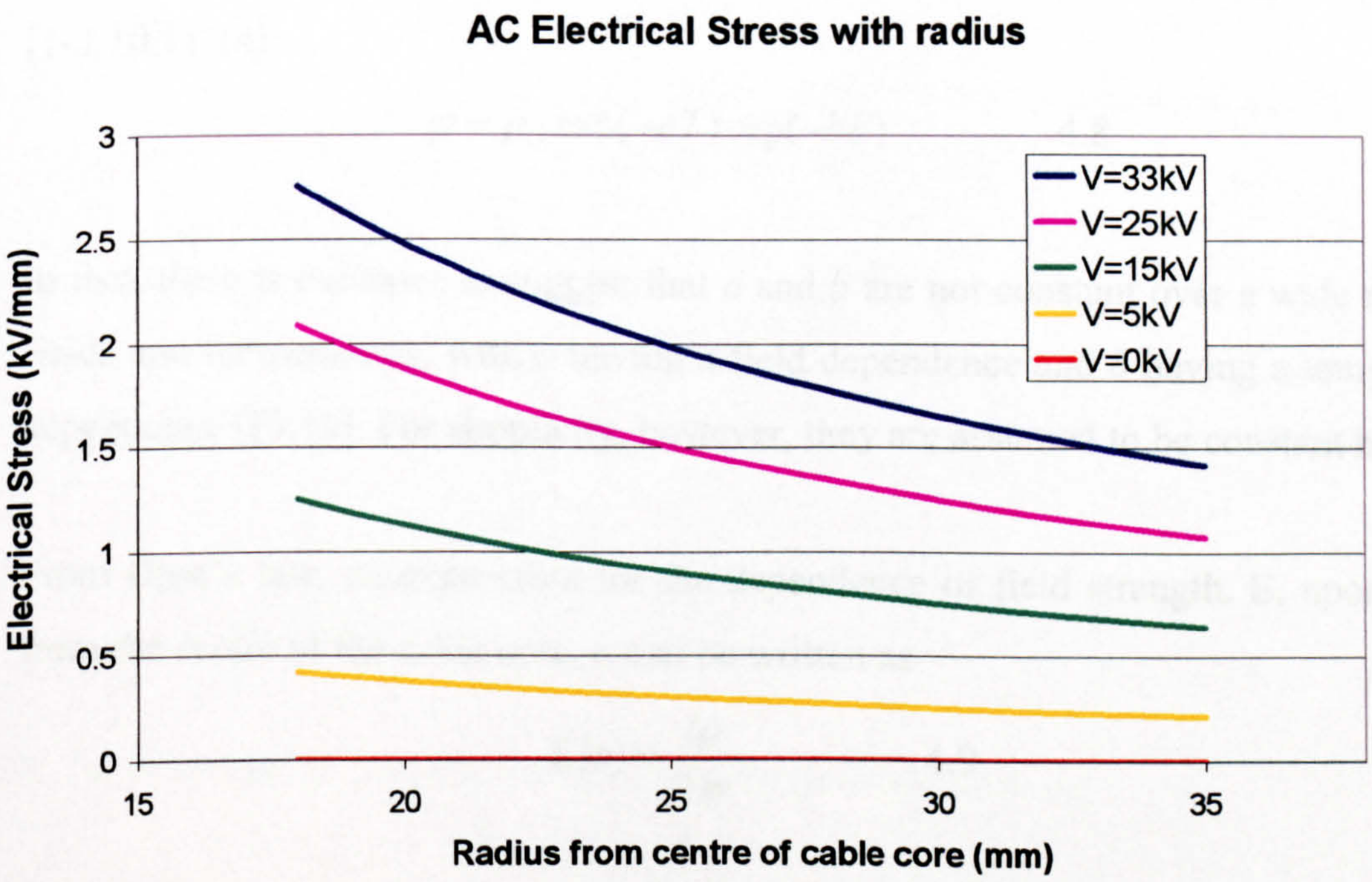

Figure 4.3

In Figure 4.3 it can be seen that the electrical stress is always highest closest to the cable core in AC applications. For a negative value of V, the stress profile is essentially as it would be if the stress distribution due to positive V of the same magnitude were reflected in the x-axis. The magnitude of the field strength is therefore

still greatest close to the cable core. The stress profiles shown in figure 4.3 are not affected by the applied current

4.2.3 DC Field Distribution

For cables carrying DC current, the electric field distribution is more complicated than in the AC case. The steady-state field distribution is dominated by the electrical resistivity of the insulation in the DC case, rather than permittivity as in the AC case. The insulation permittivity can be considered constant over the working temperature ranges of cables, whereas the resistivity of most polymers, ρ, varies strongly with both temperature, T and electrical stress, E. Various methods have been devised to model the field distribution in DC cable insulation [e.g. 2,3,10-15], but the model used here is that developed in [10] and quoted in [1].

Resistivity can be described by the semi-empirical equation 4.8, where a and b are constants, and ρ_0 is the resistivity of the material at a reference field and temperature. [1-3,10,11,14].

$$\rho = \rho_O \exp(-aT)\exp(-bE) \qquad 4.8$$

In fact, there is evidence to suggest that a and b are not constant over a wide range of fields and temperatures, with a having a field dependence and b having a temperature dependence [15,16]. For simplicity, however, they are assumed to be constant here.

From Ohm's law, an expression for the dependence of field strength, E, upon radius from the centre of the cable core, r, can be written as

$$E(r) = \frac{i\rho}{2\pi r} \qquad 4.9$$

Where i is the leakage current through the cable insulation per unit length of cable. The resistivity, ρ, in 4.9 can be replaced with the expression in equation 4.8, and also substituting for T from equation 4.1 gives

$$E(r) = \frac{i}{2\pi r}\rho_0 \exp\left[-aT_1 - aC\ln\left(\frac{R_O}{r}\right) - bE\right] \qquad 4.10$$

Where

$$C = \frac{W \times Th}{2\pi} \qquad 4.11$$

Equation 4.10 can be rearranged to give

$$E(r) = \frac{i}{2\pi r}\rho_0\left(\frac{r}{R_o}\right)^{\alpha C}\exp[-aT_1 - bE] \qquad 4.12$$

Which can also be written as

$$E(r) = \frac{i}{2\pi R_o}\rho_0\left(\frac{r}{R_o}\right)^{\alpha C-1}\exp[-aT_1]\exp[-bE] \qquad 4.13$$

This expression has the disadvantage that the field at radius r is strongly dependent on itself. Iterative numerical methods such as those in [13] can be used to solve 4.13, but in order to solve the equation analytically an approximation needs to be made. One option is simply to remove the field dependence of the conductivity altogether. This is done in [3], where 4.8 is used without the field dependent term. Here, the approximation in [2,10,14] is used, where

$$\exp(-bE) \approx \left(\frac{E(r)}{E_0}\right)^{-\gamma} \qquad 4.14$$

And

$$E_0 = \frac{\overline{E}}{\exp(1)} \qquad \text{and} \qquad \gamma = b\overline{E} \qquad 4.15 \text{ and } 4.16$$

In the above expressions, $\bar{E}$ is a kind of average field, given by

$$\overline{E} = \frac{V}{R_O - R_I} \qquad 4.17$$

In equation 4.17, V is the voltage difference between the cable core and the earthed outer edge of the insulation –i.e. the voltage drop across the insulation.

Making the substitution of 4.14 into 4.13 and rearranging gives

$$E(r) = E_0\left(\frac{i\rho_0}{2\pi R_O E_0}\right)^{\frac{1}{1+\gamma}}\left(\frac{r}{R_O}\right)^{\delta-1}\exp\left(\frac{-aT_1}{1+\gamma}\right) \qquad 4.18$$

Where δ is defined as

$$\delta = \frac{aC+\gamma}{1+\gamma} \qquad 4.19$$

In order to eliminate i, the current leaking through the insulation per unit length, the relationship given in equation 4.4 can be used. This involves integration of equation 4.18 with respect to r between the limits of R_I and R_O. Setting this equal to V, an expression for i can be determined and this can be substituted back into 4.14 to give a final expression for E(r).

The expression for i is

$$i = \frac{2\pi}{\rho_0 (E_0 R_O)^{\gamma}}\left[\frac{V\delta}{1-\left(\frac{R_I}{R_O}\right)^{\delta}}\right]^{1+\gamma}\exp(aT_1) \qquad 4.20$$

Substituting this back into 4.18 and rearranging gives

$$E(r) = \frac{V\delta\left(\frac{r}{R_O}\right)^{\delta-1}}{R_O\left(1-\left(\frac{R_I}{R_O}\right)^{\delta}\right)} \qquad 4.21$$

Using equations 4.11, 4.16, 4.17and 4.19, δ can be more clearly expressed as

$$\delta = \frac{a\frac{W\times Th}{2\pi}+\frac{bV}{R_O-R_I}}{\frac{bV}{R_O-R_I}+1} \qquad 4.22$$

The DC electrical field strength at any radius is therefore a function of the following characteristics of the insulation material:

- Thermal resistivity
- Electrical resistivity at a known temperature
- Field and temperature coefficients in the electrical resistivity equation 4.8.

It also depends on:

- The inner and outer radii of the insulation
- The current in the cable core
- The voltage applied to the cable core

The form of the DC field distribution is shown in fig 4.4 for the cable described in table 4.1, with an outside temperature of 15°C as before. The value of V used is 33kV, and the effect of various values of applied current is shown. The current values are the same as for the temperature profiles in figure 4.2, so the temperature and DC field profiles can be compared.

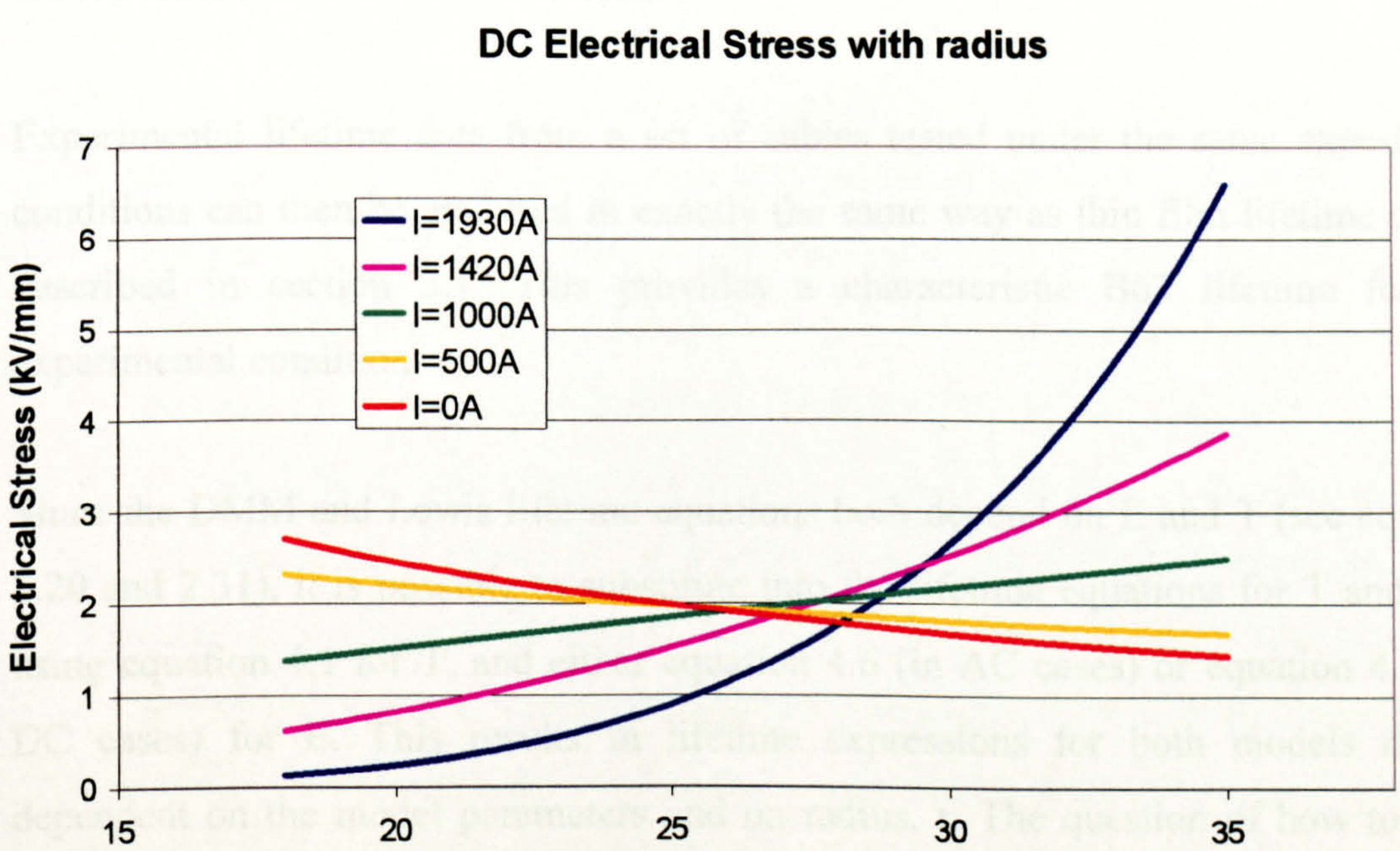

Figure 4.4

Comparison of figures 4.3 and 4.4 shows that while the AC electrical stress is highest closest to the core, this is not always so for the DC case. At currents of 1000A and

higher for the cable described in table 4.1, the so-called 'temperature inversion' effect can be seen. This refers to the fact that due to heating of the insulation as described in section 4.2.1, the conductivity of insulation close to the core increases. This leads to a fall in the electric field strength close to the core, and a corresponding rise in the outer layers of insulation. This can be seen clearly in figure 4.4.

4.3 Method of Fitting Models to Power Cable Data

Section 4.2 provides theoretical expressions for the dependence of field, E and temperature, T upon radius in cable insulation. This radial dependence of E and T means that in ageing tests, the insulation of a cable, or set of cables, cannot be subjected to a unique field, E, or temperature, T. An 'experimental condition' for an ageing test on a set of cables must therefore be redefined from the thin film case, in which identical specimens tested under one experimental condition were all subjected to the same E and T. Cables tested under the same conditions must all experience the same voltage, current and ambient temperature so that the E(r) and T(r) distributions are the same in the insulation of each.

Experimental lifetime data from a set of cables tested under the same experimental conditions can then be analysed in exactly the same way as thin film lifetime data, as described in section 3.1. This provides a characteristic B63 lifetime for each experimental condition.

Since the DMM and Lewis lifetime equations both depend on E and T (see equations 2.20 and 2.31), it is possible to substitute into the lifetime equations for T and for E, using equation 4.1 for T, and either equation 4.6 (in AC cases) or equation 4.21 (for DC cases) for E. This results in lifetime expressions for both models that are dependent on the model parameters and on radius, r. The question of how to fit the models to lifetime data from cable experiments is then more complicated than in the thin film case, since a continuous, radially dependent model lifetime expression needs to be fitted to a single experimental B63 value for each experimental condition. This is addressed in section 4.3.2, 4.3.3 and 4.3.4. Section 4.3.1 discusses the implications of charge injection into cable insulation.

4.3.1 Charge injection considerations

As mentioned previously, the expressions for the radial dependence of field given above assume that no charge is injected into the insulation. This has been shown not to be the case for both polymeric cable insulation [e.g. 5-9], and oil-impregnated paper insulation [3]. Space charge injection and distribution has been seen to vary with the material chosen as the semicon layer [16], and also with insulation material. This latter dependence has resulted in investigations into the use of fillers in PE insulation to discourage space charge growth in DC applications e.g. [18-21]

Any injected charge must significantly change the field distributions as derived above. A much more accurate way to approach the problem would therefore be to experimentally determine the field or charge distribution within the cable insulation as in [e.g. 5-9]. Experimentally determined expressions for field (or charge) dependence on radius can be formulated into radius dependent field (or space charge) expressions. These expressions could then be input directly into the model lifetime equations in place of theoretical expressions 4.7 or 4.21. This would have to be done in slightly different ways for each model due to the different ways in which the field is assumed to affect ageing.

- For the Lewis model, an experimentally determined field distribution with radius could be input directly into the model in place of E. An experimentally determined field distribution would naturally include the effect of any space charge distribution within the insulation, and within the model equation would generate corresponding mechanical forces as described in chapter 2.
- For the DMM model, an experimentally determined charge distribution would be more useful, since the field term in the DMM lifetime expression is an assumed one; the field term is due to the field dependence of charge density. Removing the $C'E^{4b}$ term and replacing it with a term directly dependent on charge density would therefore be a much more accurate way of predicting lifetime in any insulation system according to the DMM model.

The distinction between the experimental determination of either E or charge distribution is obviously slightly artificial, since determination of one of these readily yields the other. The distinction is really just in the way that the expression would need to go into the models.

Experimentally determined field or space charge distributions are not easily obtainable, and were not available for the specimens corresponding to the lifetime data used in this investigation. The theoretical expressions derived above were therefore used to give radially dependent lifetime expressions. The results in the next chapter show that good fit to some AC cable lifetime data can be obtained even with all the approximations and assumptions involved in the derivations of the ageing models and of equations 4.1 and 4.21.

4.3.2 Dividing the cable into shells

Substituting radially dependent expressions for T (4.1) and E (4.7 or 4.21) into the lifetime model equations results in a lifetime expression for each model that is also dependent on radius. Experimental ageing tests result in a characteristic lifetime for any given condition. In order to fit a theoretical lifetime continuum to an experimental B63 lifetime, the cable is first divided into 'shells' or 'layers'.

E and T, and therefore lifetime are assumed only to vary with distance from the cable core. Considering the insulation as a series of infinitely thin shells which form cylinders as shown in fig 4.5 therefore results in shells which each experience a constant field and temperature.

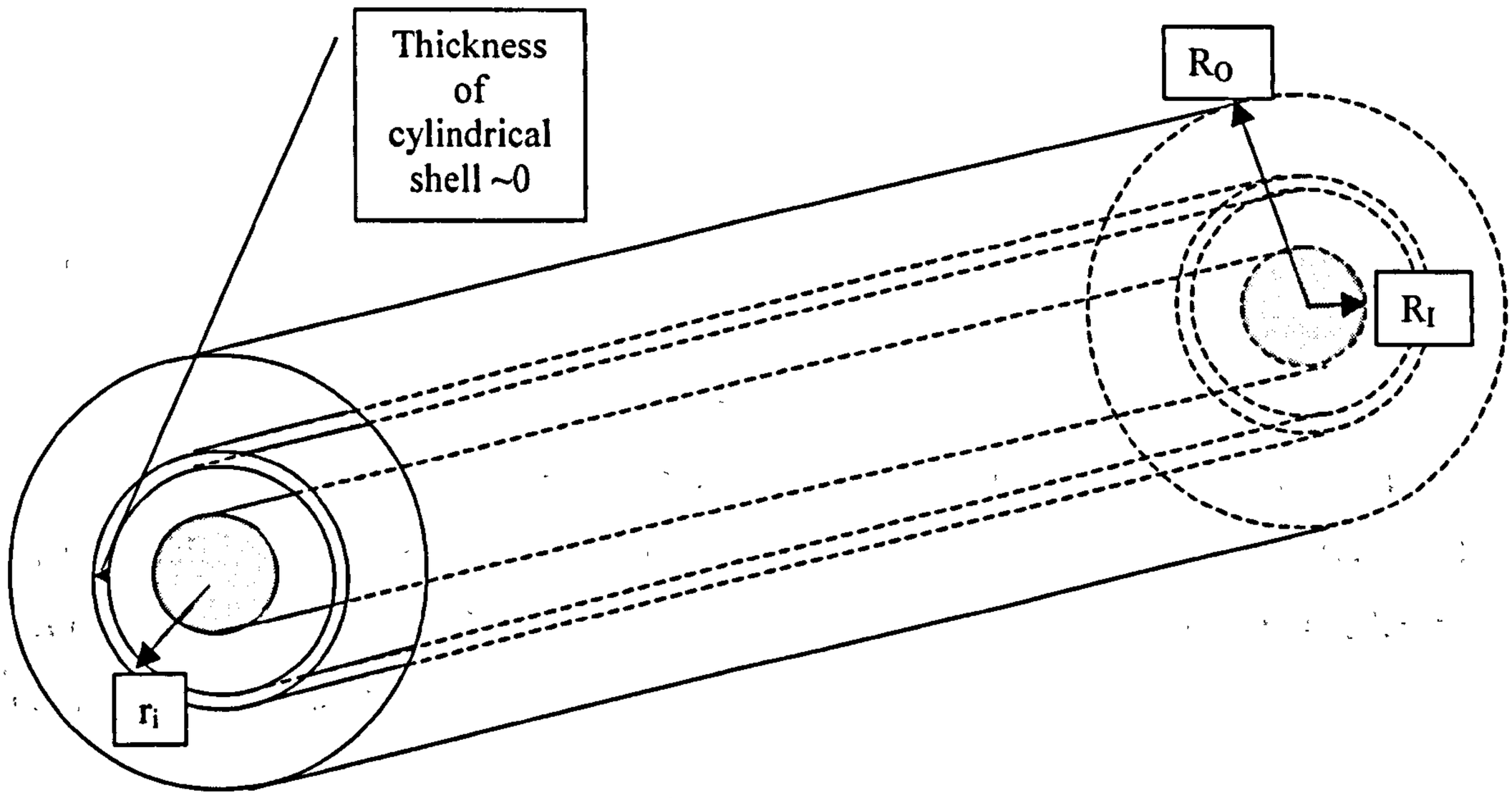

Figure 4.5

Figure 4.5 shows a cable of the same geometry as that in figure 4.1. An example 'shell' at radius r_i is shown. Sufficiently thin shells of this shape but with finite thickness can be assumed to have constant field and temperature over their volume.

If the cable is divided into shells of constant thickness, each layer will have a different volume. Neither the DMM nor the Lewis ageing model takes account of any of the spatial dimensions of the polymer specimen, or those of the test electrodes. In fact, depending on the mechanisms of ageing, at least one of these factors is likely to be important to the lifetime of a polymer specimen. Both models used here are based on the assumption that ageing is a bulk process, in which case it is often argued that the volume of a specimen must affect its lifetime. [e.g. 22]

The reasoning behind this is that a greater volume of polymer may correspond to increased likelihood of extreme conditions within it. Extreme conditions relevant to ageing may be areas of the polymer that are 'weaker' – i.e. more susceptible to the ageing process – or areas where the local field or temperature are able to reach higher values. For specimens under identical E (or V for cables) and T conditions, a polymer specimen with a greater volume would therefore have a higher probability of breakdown after a certain time than one with smaller volume. This translates into a shorter working lifetime for longer cables under the same conditions as shorter ones, and this assumption is often made by e.g. cable manufacturers.

The precise physics of the effect of specimen volume on ageing are not well understood, and there is little data in the literature from ageing experiments where volume is the primary variable. Experiments to gauge the electrical strength of polymers as a function of volume are more common [e.g. 23,24], and these seem to show that electrical strength is reduced as specimen volume increases. It seems likely that this indicates a reduction in lifetime with volume, as electrical strength and probability of survival with time are likely to be linked, but more data is needed to confirm this hypothesis.

If polymer lifetime is volume dependent as suggested, this must mean that some of the parameter values in each of the models are also volume dependent. The question must then be raised as to which of the parameter values depend on specimen volume. This is

addressed in the next chapter by comparing DMM parameter values from a range of specimen types, and considering the likely effect of volume on the ageing process.

Since the effect of volume is not well understood, the cable is divided into shells of equal volume, rather than shells of equal thickness. This ensures that any effect on ageing and lifetime due to volume is the same for each shell, and this approach was used here. Equal volumes, however, have physical disadvantages for cable geometry, as the shells closest to the core must be the thickest layers. Since the field is most divergent here, the inner shells need to be thin enough to fulfil the requirement that E and T can be considered constant over each shell, and this leads to the need for many shells.

4.3.3 Lifetime of each shell

Each of the above shells must experience an electrical stress and temperature according to its positional radius, r_i. The temperature and field values for each shell at radius r_i are given by 4.1 and 4.6 or 4.21. A lifetime expression for each shell, L_i, can then be obtained simply by substituting the relevant field and temperature values for that shell into a model lifetime equation as shown below.

The DMM equation gives an expression for the lifetime of the 'i'th shell, L_i, as in equation 2.20 – i.e.

$$L_i = \frac{\frac{h}{2kT_i}\exp\left[\frac{-S_d}{k}\right]\exp\left[\frac{H_{dk}-\frac{C_d E_i^{4b}}{2}}{T_i}\right]\left[-\ln\left(\frac{Aeq-A^*}{Aeq}\right)\right]}{\cosh\left[\frac{K_d - C_d E^{4b}}{2T_i}\right]} \qquad 4.23$$

Where L_i is the predicted lifetime of the 'i'th shell, which is situated at radius r_i. T_i and E_i are the temperature and field at r_i.

The Lewis model gives the following expression for L_i from equations 2.29, 2.30 and 2.31

$$L_i = \frac{1}{B\exp\left(\frac{-\left(U_R + \gamma_R \varepsilon E_i^2\right)}{kT_i}\right) + B\exp\left(\frac{-\left(U_B - \gamma_B \varepsilon E_i^2\right)}{kT_i}\right)}\left[-\ln\left(\frac{b_{eq} - b^*}{b^*}\right)\right] \quad 4.24$$

Where L_i is again the lifetime of the 'i'th shell, and T_i and E_i are the temperature and field for that layer –*i.e.* the field and temperature at radius r_i.

In each case, E_i is given by either 4.7 for an AC situation or 4.21 for a DC situation. T_i is given by equation 4.1.

4.3.4 Combining lifetimes of shells and fitting to data

Using the previous sections it is possible to consider a continuous cable insulation system as a series of N shells, and formulate a lifetime expression for each. The lifetime expression for each shell is a function of the field and temperature experienced by that shell, which are in turn a function of the radius at which the shell is situated, r_i. The lifetime expressions are also functions of the ageing model parameters, and to find values for the parameters, the expressions need to be fitted to ageing data as in the thin film case.

A method for combining N lifetime expressions in order to fit them to one B63 value per experimental condition is described below. The method uses probability equations, and involves a number of assumptions, which are also explained below.

Assuming that any insulation system can be considered as made up of many smaller insulation volumes, and that failure in any one of the constituent volumes will cause the entire insulation to fail, the following equation can be used.

$$PS(L) = \prod_{i=1}^{N} PS(S)_i \quad 4.25$$

In equation 4.25, PS(L) is the probability of survival at time t of a large volume of insulation, made up of N components. $PS(S)_i$ is the probability of survival at time t of the ith, smaller component. If the values of PS(S) are all the same, this leads to

$$PS(L) = PS(S)^N \qquad 4.26$$

In terms of a cable insulation volume, VC, made up of N shells each with volume VS=VC/N, these equations become

$$PS(VC) = \prod_{i=1}^{N} PS(VS) \qquad 4.27 \text{ and } 4.28$$

$$PS(VC) = PS(VS)^N$$

The time to failure distributions resulting from ageing tests on polymer specimens are commonly assumed to be Weibull distributions with shape parameters, β, which are characteristic of the ageing process. Assuming, therefore, that PS(VC) and PS(VS) are Weibull distributions with the same β values, they can be given by [e.g.25].

$$PS(VC) = \exp\left(-\left[\frac{t}{B63}\right]^{\beta}\right) \qquad 4.29 \text{ and } 4.30$$

$$PS(VS) = \exp\left(-\left[\frac{t}{L_i}\right]^{\beta}\right)$$

Here t is time. B63 is the characteristic lifetime of a set of cables aged under the same experimental conditions and L_i is the characteristic lifetime of a set of shells of insulation all aged under one particular condition. β in equation 4.29 is the shape parameter of the time-to-failure distribution from the cable ageing experiments, and in 4.30 is the shape parameter of the distribution of the shell times-to-failure. It is reasonable to assume that the values of β in the above equations are the same, since the ageing process is likely to be the same in each shell.

Substituting 4.29 and 4.30 into 4.27, an expression for the characteristic lifetime of cable insulation, B63 in terms of the characteristic lifetimes of a set of shells of insulation, L_i can be derived.

$$\frac{1}{B63^{\beta}} = \sum_i \left(\frac{1}{L_i^{\beta}}\right) \qquad 4.31$$

In this case, B63 is the characteristic lifetime of a cable set, and L_i can be replaced with an expression for the lifetime of the 'i'th shell. Using 4.23 or 4.24 for each L_i, equation 4.31 can then be used to fit either of the models to experimental B63 values and obtain parameter values.

Parameter values obtained from fitting equation 4.31 will necessarily depend on the volume of the cable insulation through B63 in the same way as for thin films. However, they will also have a dependence on the shell volume (or equivalently a dependence on N), since the probabilities in 4.27 are volume dependent. Parameters that depend on both VC and N have the disadvantage that direct comparisons between cable and film experiments are then difficult, since parameters from film experiments will only depend on the total film insulation volume –equivalent to VC.

To get parameter values from cable experiments that only depend on VC, it is necessary to 'scale up' the probability of failure of each shell to the total insulation volume. In other words, it is necessary to determine an expression for the probability of failure that each shell would have if it had the volume of the whole insulation. This can be obtained using 4.26.

$$PS(SS) = PS(VS)^N \quad 4.32$$

Where PS(SS) is the probability of survival of the scaled up shell, and PS(VS) is the probability of survival of the shell. Equation 4.25 shows that taking the product of the PS(SS) values would then give the probability of survival of a volume of insulation N times bigger than VC. Using 4.25 and 4.32 therefore gives

$$\prod_{i=1}^{N} PS(SS)_i = \prod_{i=1}^{N} [PS(VS)]^N{}_i = PS(NVC) \quad 4.33$$

Where PS(NVC) is the probability of survival of an insulation specimen with volume N times bigger than VC. To get the probability of survival of insulation of volume VC (i.e. of the total cable insulation), 4.26 can be used again with 4.33 to give

$$PS(VC) = PS(NVC)^{\frac{1}{N}} = \left[\prod_{i=1}^{N} PS(SS)_i\right]^{\frac{1}{N}} \quad 4.34$$

Where PS(VC) is the probability of survival of the cable. Using this equation, and assuming again that the probabilities of survival are all Weibull distributions with the same shape parameter, the following equation is derived

$$\frac{1}{B63^{\beta}} = \frac{1}{N}\sum_{i}\left(\frac{1}{L_i^{\beta}}\right) \qquad 4.35$$

L_i is now an expression for the lifetime of a scaled up shell – i.e. an expression for the lifetime that a shell would have if it had volume VC. Substituting 4.23 or 4.24 for each L_i and fitting the equation to experimental B63 data, results in parameter values that have no dependence on N, and depend only on the total volume of insulation, VC through B63.

Equation 4.35 is used to fit the DMM model to ageing data from cables insulated with XLPE insulation in the next chapter.

5. Application of Models to Power Cable Data – An Example

Chapter 3 shows how the DMM and Lewis models can be fitted to experimental data from thin film ageing experiments. For the DMM model this is essentially done by finding parameter values that minimise the error in the following equation for each experimental ageing condition:

$$B63 = \frac{\frac{h}{2kT}\exp\left[\frac{-S_d}{k}\right]\exp\left[\frac{H_{dk} - \frac{C_d E^{4b}}{2}}{T}\right]\left[-\ln\left(\frac{Aeq - A^*}{Aeq}\right)\right]}{\cosh\left[\frac{K_d - C_d E^{4b}}{2T}\right]} \qquad 5.1$$

Here B63, E and T are the experimental characteristic lifetime, field and temperature of a set of aged films respectively, h and k are Planck's and Boltzmann's constants, and the model parameters are as defined in chapter 2.

Equivalently, this equation must be satisfied as closely as possible for the Lewis model:

$$B63 = \frac{1}{B\exp\left(\frac{-\left(U_R + \gamma_R \varepsilon E_i^2\right)}{kT_i}\right) + B\exp\left(\frac{-\left(U_B - \gamma_B \varepsilon E_i^2\right)}{kT_i}\right)}\left[-\ln\left(\frac{b_{eq} - b^*}{b^*}\right)\right] \qquad 5.2$$

Again, B63, E and T are experimental characteristic lifetime, field and temperature for a set of films. ε is the permittivity of the film material, and the model parameters are as described in chapter 2.

Chapter 4 explains that in the case of cable geometry 5.1 and 5.2 can no longer be applied to ageing data, due to the spatial variation of E and T in the insulation. A new method of fitting the models to data from ageing tests involving cables is therefore hypothesised, which involves considering the cable insulation as made up of N shells.

The new equation to be used to find model parameter values and predict insulation lifetime is shown below.

$$B63 = \left(\left[\frac{N}{\sum_i \left(\frac{1}{L_i^{\beta}} \right)} \right]^{\frac{1}{\beta}} \right) \qquad 5.3$$

B63 is experimental characteristic lifetime as above, and β is a shape parameter characteristic of the ageing process, which can be obtained from lifetime data. L_i is a lifetime expression for the 'i'th shell as given by the RHS of either equation 5.1 or 5.2. N is the number of shells considered.

5.1 Solving equations simultaneously – the error function

To be consistent with the physics behind the derivations of both the DMM and Lewis models, parameter values obtained from fitting the model equations to data should be applicable at all experimental conditions. This means that in the thin film case, either 5.1 or 5.2 needs to be satisfied simultaneously for all available B63, E and T data. In the thin film case in chapter 3 this was achieved by using the Levenberg Marquardt algorithm as implemented in MATHCAD. This method takes initial values for each parameter and computes an error function according to the algorithm. This error function represents the difference between the predicted lifetimes according to the model and the experimental lifetimes from ageing experiments. The algorithm then seeks to minimise this difference, by changing the parameter values so that the error function is minimised. The error function used by the algorithm involves all the constraints given to it – each of which is an equation like 5.1 or 5.2. The fitting therefore involves all available B63, E and T data, and in this way, parameter values are optimised for all experimental data simultaneously.

Unfortunately, the MATHCAD Levenberg-Marquardt method cannot be used for cable ageing data. The reason for this is that for some experimental conditions, the models predict that some of the shells have infinite lifetimes – *i.e.* they predict some infinite values of L_i (discussed further in section 5.4.3). This happens when the field and/or

temperature experienced by some shells are below the thresholds for ageing. This is a physically reasonable situation for the outer-most shells where the field and temperature are lowest. Infinite L_i values, however, result in MATHCAD resorting to parameters that have complex values. This cannot be the case, due to the physical meanings of the parameters.

An alternative method of finding parameter values was therefore devised, with a new error function to represent the difference between the data and the model predictions. The error function to be minimised is as shown below.

$$\sum_J \left[\left\{ \ln(B63_J) - \ln\left(\left[\frac{N}{\sum_i \left(\frac{1}{L_i^{\beta}} \right)} \right]^{\frac{1}{\beta}} \right)_J \right\}^2 \right] \qquad 5.4$$

Above, J is the number of B63 values available. For each B63 value, the error function takes the difference between the log of the B63 value and the log of the hypothesised cable lifetime expression as in equation 5.3. Each difference is squared, and the squares of the differences are summed over all experimental conditions to give the final error value for the whole data set. Natural logarithms are used in the error function due to the extreme non-linearity of the DMM and Lewis lifetime equations. The square of the differences is used to avoid fits where the fit is good for most B63 values but very poor in one or two cases.

This error function is less complex than the function used by the Levenberg-Marquardt algorithm, but the good fits to data achieved and the extra level of complexity involved in using equation 5.3 rather than equation 5.1 or 5.2 justify its use here.

5.2 Grid Search for Minimum Error

The error function shown above must be minimised for a set of ageing data to produce model parameter values that match the data. The simplest way to do this is by using a grid search method. This involves choosing several sets of model parameter values and computing the error function for the data and each of the chosen parameter sets. Some

parameter sets will produce lower error function values than others. Parameter sets that produce low error function values can be considered good fits to the data.

Further parameter sets with similar values to those which give low error functions can then be chosen, and the error function re-calculated for those sets. Repetition of this process results in reducing the error further and further and thus results in better and better parameter values for the ageing data set. This process can be thought of as effectively searching 'parameter space' for the lowest error function value. Wide ranges of parameter values can be chosen at first, progressing to narrower limits each time, to try to gradually pinpoint the lowest error function value.

The error function has complicated dependencies on each of the parameters. Care therefore has to be taken to try to find a global error function minimum rather than local minima. To try to avoid this, the homing-in process can be carried out in several 'areas' of parameter space where the initial error was found to be low. Convergence to the same (or similar) set(s) of parameter values from different areas of parameter space then implies that a global minimum has been found.

5.3 Application to XLPE cable data

The fitting method outlined above has been applied to data from AC ageing tests performed on cables insulated with XLPE, using the DMM model. This model was chosen over the Lewis model due to its greater mathematical flexibility, and due to the fact that parameter values from other fittings are available for comparison in the literature. The method would, however, be equally applicable to the Lewis model or to any other lifetime model, such as those mentioned in chapter 2.

5.3.1 Ageing Data Used

Data was used from ageing experiments carried out for BICC Cables Ltd (now owned by Pirelli Cables Ltd.) [1]. Cables insulated with extruded XLPE of thickness 4.4mm were aged under nine different experimental conditions, and the times to failure recorded. Twelve cables were aged under each condition, and the tests were stopped after eight cables had failed. Data of this kind, where the test is stopped before all of the specimens in a set fail, is called top censored data. The Weibull probability

equations used to get B63 and β values are therefore slightly different than for complete, non-censored data such as that used in chapter 2 [2]. A Weibull analysis applicable to top censored data was carried out, resulting in B63 and β values for each of the nine experimental conditions.

The cables were 15kV medium rated cables, with aluminium cores and values of R_I and R_O of 5.9mm and 10.3 mm respectively. They were all 9.14m long. The cables also contained thin semicon layers between the core and the insulation, though these were ignored for the purposes of the fitting. This is justifiable here, since the only effect of an extra layer would be to change the mean thermal and electrical resistivities of the insulation/semicon layer. In all cases here, the cables were aged under constant temperature and AC voltage, with no current applied to the cable cores. There was therefore no temperature gradient across the insulation – only a field gradient, which is independent of both electrical and thermal resistivity of the insulating layer as shown in chapter 4

Cables were aged at constant temperatures of 60°C, 75°C and 90°C and the temperature of each shell was just set equal to the applied temperature. The AC field gradient equation 4.7 was used to determine the field experienced by each shell. Cables were aged at applied r.m.s. voltages of 34.6kV, 26kV and 17.3kV.

5.3.2 FORTRAN Code

A FORTRAN program was written to carry out a grid search, as described in section 5.2, for the data described above. The program is briefly described below, and the code is presented in Appendix A. The code is designed such that the user can input a maximum and minimum value for each of the DMM parameters, and specify the number of values that the program should test in that range. The program then works out the error function for each set of values within the ranges specified, using a series of nested loops. The user can also specify N, the number of shells to be used.

For each parameter set specified by the user, the code calculates a value of L_i for each of the N shells. It then calculates the error function according to equation 5.4. The code tests whether each value of L_i is infinite by looking at the threshold condition for each parameter set and the E and T conditions of each shell. When it encounters infinite L_i

values it sets the reciprocal of L_i equal to zero, and this avoids the problems encountered in MATHCAD.

In FORTRAN it is possible to use a structured programming approach, where a main program calls other functions or subprograms to perform calculations as needed. One of the advantages of this is that the modules can all be edited and tested separately. The program is therefore made up of several separate functions and a main program, which uses each of the other modules in turn. The different modules of the program are summarised below. The code for each is presented in Appendix A.

- RADIUS. This module reads in the cable dimensions and the number of shells required, N, from the main program, and splits the cable insulation into N equal volume shells. It then gives the radius value for each shell, r_i back to the main program.
- FIELD. This works out the field for each of the shell radii calculated above. It reads in each radius, the experimental V and T conditions and the cable dimensions from the main program, and gives back the relevant field values. Equation 4.7 is used to work out field values, since the data used is from AC ageing experiments.
- LIFETIME. This module reads in the field for each shell and the model parameters from the main program. It then calculates the reciprocal of the lifetime for each cylinder (i.e. $1/L_i$, with each L_i given by equation 5.1). This inverse lifetime is set to zero if the infinity condition in the model is encountered – thus avoiding the problems found using MATHCAD.
- ERROR. This works out the error function for each predicted lifetime and its associated B63 as in equation 5.4.
- MAIN PROGRAM. This uses all the modules above to calculate shell radii, field values, L_i values and consequently the predicted lifetime for each experimental condition at which there is lifetime data. It then calculates an error function for each specified parameter set. It does this for many different sets of parameter values by having the main code and all the modules inside seven nested loops – one for each parameter. Parameter values are therefore changed for each calculation in a systematic way, and an error value calculated for each different set. If the error is the lowest value so far, the error and the parameter values are recorded. The final output of the program is therefore the

optimal parameter set within the defined range, and this can be used to define a new parameter range. The whole process can then be repeated.

5.3.3 Details of fitting method

For each of the nine experimental conditions under which cables were aged, voltage and temperature values were known, as were B63 and β values. These values were all put into text files for the FORTRAN program to read in.

The value of N in the fitting is user-specified. In this case a value of N=100 was chosen for several reasons. Firstly, N=100 corresponds to the thickest shells in the cable being roughly the same thickness as the PET films for which the fitting was carried out in chapter 3. Since the models were designed originally to work only for thin films, ensuring that the shells are sufficiently thin for the model to be applied to each one may be important. Secondly, N was chosen to be high enough to give a good a fit as possible to the data. Since the N dependence of the model parameters was eliminated in the fitting function, the only effect of increasing N should be to increase the quality of the fits due simply to the improved accuracy involved in splitting a continuous system into as many parts as possible. This effect was found to reach saturation at a value of N of approximately 100, with no further improvement in fit being found for values of N larger than this. The third criterion for a value of N is that it cannot be too large that the computation takes too much time.

A value for β also had to be chosen, since the error function requires only one value of beta. Each experimental condition yields its own value of β, and for the data used here the β values ranged from 2.4 to 8.5 – each with fairly wide confidence limits. Theoretically, each of these values should be the same so long as the ageing process is the same for each cable set, so an average of all the β values was used. This average was weighted towards the smaller end, since the highest β was much higher than the other values and was therefore deemed atypical.

5.4 Results of fit to XLPE cable data

5.4.1 Fit to data

As mentioned above, the best way to carry out a grid-search type fitting is to begin with a wide range of parameter values, and then slowly home in where the error function is small. This was carried out for the BICC cable data, and the resulting lifelines using parameter values for which the error function is very low (=0.674) are shown in figure 5.1 with the B63 data. The parameter values are shown in the first column of table 5.1.

Other sets of parameters that gave similarly low error functions tended to have values for the parameters that were very similar to those shown in table 5.1. This suggests that this parameter set corresponds to a global minimum in the error function, rather than a local one.

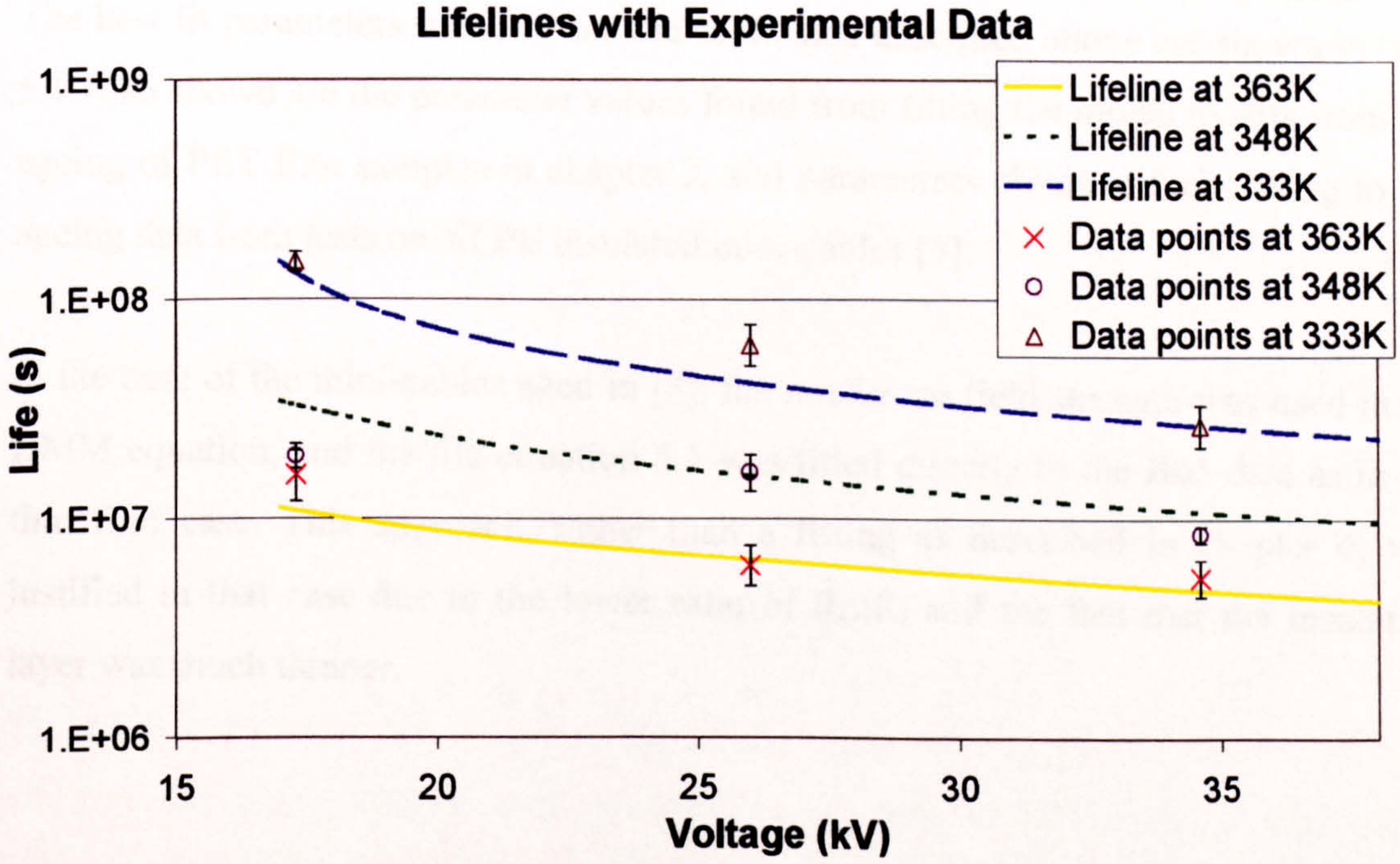

Figure 5.1

In figure 5.1, the y-axis represents time in seconds, and the B63 values from each of the nine conditions under which cables were aged are shown as crosses, circles and triangles corresponding to tests at 363K, 348K and 333K respectively. The 90% confidence limits for each B63 are shown as error bars. The lifelines shown are equivalent to figures 3.2 and 3.5 for thin film data, except that the x-axis now

represents applied voltage rather than applied field. Each of the lines shown is at a different temperature corresponding to one of the three temperatures under which cable sets were aged. The lines show voltage threshold behaviour in the same way that field lifelines show field threshold behaviour in the thin film case. For films, the predicted lifetime becomes infinite if the field and temperature experienced by the film are below the threshold for that material. The cable lifetime only becomes infinite if the field and temperature experienced everywhere in the insulation – i.e. by each of the constituent shells - is below the threshold for the material.

The fit in figure 5.1 can be seen to be good, with the DMM predicted lifetimes being within the 90% confidence limits of the experimental data for four out of the nine conditions. This is comparable with the thin film AC case in chapter 3, in which sixteen out of the thirty DMM predictions were within 90% limits.

5.4.2 Comparison of parameter values – volume considerations

The best fit parameters obtained for the cable data described above are shown in table 5.1 Also shown are the parameter values found from fitting the model to data from AC ageing of PET film samples in chapter 3, and parameters obtained from fitting to AC ageing data from tests on XLPE insulated mini-cables [3].

In the case of the mini-cables aged in [3], the maximum field strength was used in the DMM equation, and the life equation 5.1 was fitted directly to the B63 data as in the thin film case. This approach, rather than a fitting as described in chapter 4, was justified in that case due to the lower ratio of R_O:R_I and the fact that the insulation layer was much thinner.

TABLE 5.1	Parameters from this investigation	Parameters for AC ageing of thin film PET from chapter 3	Parameters for AC ageing of XLPE insulated mini-cables [3]
Sd (J/K)	-3.8E-22	-5.2E-22	-5.6E-22
Hdk (K)	6333	1274	1448
Kd (K)	292	103	229
C_d (J(mm/kV)^{4b})	3.833	1.593	1.376
A*	0.325	0.485	0.38
b	0.400	0.39	0.425
#G (J) at T=20°C and T=100°C	2.0E-19 2.3E-19	1.7E-19 2.1E-19	1.8E-19 2.3E-19

In the FORTRAN grid search, the DMM parameters were allowed to vary over wide ranges. The magnitudes of the model parameters obtained are nevertheless all similar in magnitude to those obtained in previous fittings to AC ageing data of XLPE mini-cables and PET thin films. This suggests that the cable fitting method works well, and supports the theory that the ageing process is the same for each of the materials studied.

The parameters in table 5.1 were obtained from fits to AC ageing data involving very different specimen types. In this investigation, the cables were insulated with XLPE with a volume of $5.6\text{x}10^{-4}\text{m}^3$ and a thickness of 4.4mm. The mini-cables for which parameter values are quoted had an insulation volume of approximately $2.8\text{x}10^{-6}\text{m}^3$, and a thickness of 1.5mm. The volume of the PET films is not known, but the thickness of each was $50\text{x}10^{-6}$mm – implying a volume many times smaller than in either of the cable cases.

Any dependence of specimen lifetime on volume must be reflected in the magnitudes of the DMM parameter values obtained from fitting to data involving specimens of different volumes. The question of how specimen volume affects parameter values in table 5.1, however, is not clear, since the parameters obtained are all for different materials, as well as for different volumes. This is true even of the XLPE cables used here and the XLPE insulated mini-cables, since the XLPE was made by different cable manufacturers in each case, and there are therefore likely to be significant differences in composition between the two. It is therefore not possible to separate out differences in parameter values due to volume, from differences due to material morphology and chemical composition. The volume of insulation of the cables used here, however, is considerably larger than in the other two cases – almost 200 times larger than the mini-cable insulation, and likely to be much larger again for the PET films.

Despite the problems associated with the parameter sets in table 5.1 being from different materials, it is still possible to speculate about which of the DMM parameter values might be affected by volume. The common assumption that a larger volume of insulation will fail faster than a smaller volume is essentially based on the fact that a larger volume must contain more moieties that can take part in the ageing process. Thus the likelihood of finding moieties that are in some way more susceptible to ageing, or can age faster is increased.

Following this logic, it is possible that a larger volume of polymer may contain more moieties with very low energy barriers to ageing, and this may be responsible for the shorter lifetimes observed in larger polymer specimens. The values in table 5.1, however, show that the characteristic value of #G (= H_{dk}-TS_d as shown in chapter 2) is actually very similar for all three of the parameter sets. Over a range of temperatures from 20°C to 100°C the ratio of the free energy barrier magnitudes is never more than 1.2:1, in spite of the differences in the magnitudes of H_{dk} and S_d between this investigation and the others. This difference – that H_{dk} is rather larger than for the other specimens, and that S_d is smaller in magnitude - may be due more to the different fitting method used (i.e. a grid search as opposed to Levenberg-Marquardt algorithm) than any physical reason. The similarity in values for #G for the different specimen types seems to imply that the ageing process is very similar in each regardless of material or volume. However it should be noted that because #G appears in an

exponential form in the DMM lifetime equation, a small decrease in its value will reduce the characteristic lifetime substantially.

It is also possible that A* may be affected by volume. A* is the fraction of moieties that must be in the aged state for breakdown to occur in any localised area, and it seems likely that this fraction might vary from area to area of specimen. This means that in a larger volume of polymer there may be an increased likelihood of finding regions where fewer moieties need to be in the aged state for breakdown to be initiated. As a result, a specimen with a larger volume will require less local energy concentration to convert sufficient moieties into the product state so that failure can be initiated. The differences in characteristic A* found so far seem to support the hypothesis that the specimens with larger volumes require fewer moieties to be in the aged state, and therefore lower energies, to initiate breakdown. They therefore experience a reduction in lifetime.

C_d and b describe the effect of a field on the barrier to ageing, #G. On the application of an electrical field of magnitude E, #G is reduced by an amount equal to C_dE^{4b}, and this acts to accelerate the ageing reaction. Large values of C_d and b for a set of specimens therefore indicate that the ageing reaction is accelerated strongly by the electrical field. A greater volume of polymer is more likely to contain sites at which this is the case – i.e. sites at which the field can have a strong influence on the ageing process. In the DMM model such sites will be those that have greater ability to trap charge and store electro-mechanical energy. They may therefore be sites that have a bigger electrostriction coefficient than the average for the specimen. Such sites may also (or instead) have a smaller bulk modulus or relative permittivity than average. Microscopic variations in macroscopic material characteristics such as these seem very likely, which makes these two parameters the most likely to have a volume dependency.

The data in table 5.1 seems to support this to some extent, with the largest polymer volume showing by far the largest values of C_d. The values of b are all quite similar, however, with no observable pattern with volume. Overall, the C_dE^{4b} term for fields from 0 to 20kV/mm is always largest for the XLPE cable parameters. The same term is larger for the mini-cables than for the thin film parameter values for all fields above

about 3kV/mm. Below this field, at which fields the ageing process is unlikely to be accelerated significantly, the values are very similar. These parameters are also likely to be strongly material dependent, however, so this is by no means conclusive.

5.4.3 Lifetime with radius

The method described in chapter 4 provides a way of predicting the lifetime of cable insulation. However, it is also interesting to look at the variation of predicted lifetime with radius for each experimental condition. As mentioned above, for some experimental conditions, the model predicts that the outermost layers of cable insulation will not undergo any ageing due, to the low field and temperature conditions they experience. Therefore these shells with infinite lifetime prediction do not directly influence the total insulation lifetime at all, since they add zero to the sum of $1/L_i$ values in equation 5.3.

This has further implications for the role of volume effects in ageing, since for those conditions in which the infinity life condition is found for some of the shells, only part of the cable insulation was directly involved in the ageing process. The number of moieties taking part in the ageing process is therefore reduced, and, by reducing the likelihood of moieties than can age very quickly as explained in the last section, this could have the effect of increasing the probability of survival with time of the insulation as a whole.

The voltage and temperature conditions under which each of the nine cables were aged are shown in table 5.2. In each case the temperature was constant across the entire insulation, rather than varying according to equation 4.1.

Cable number	1	2	3	4	5	6	7	8	9
Temperature (°C)	363	348	333	363	348	333	363	348	333
Voltage r.m.s (kV)	34.6	34.6	34.6	26	26	26	17.3	17.3	17.3

Table 5.2

The electrical stress profiles for the three applied voltages are shown below. The r.m.s. voltage was used in equation 4.7 to produce these plots, which means that the electrical

field strength at each radius is also an r.m.s value. The r.m.s. field value is shown since this is the value used in the DMM model [3].

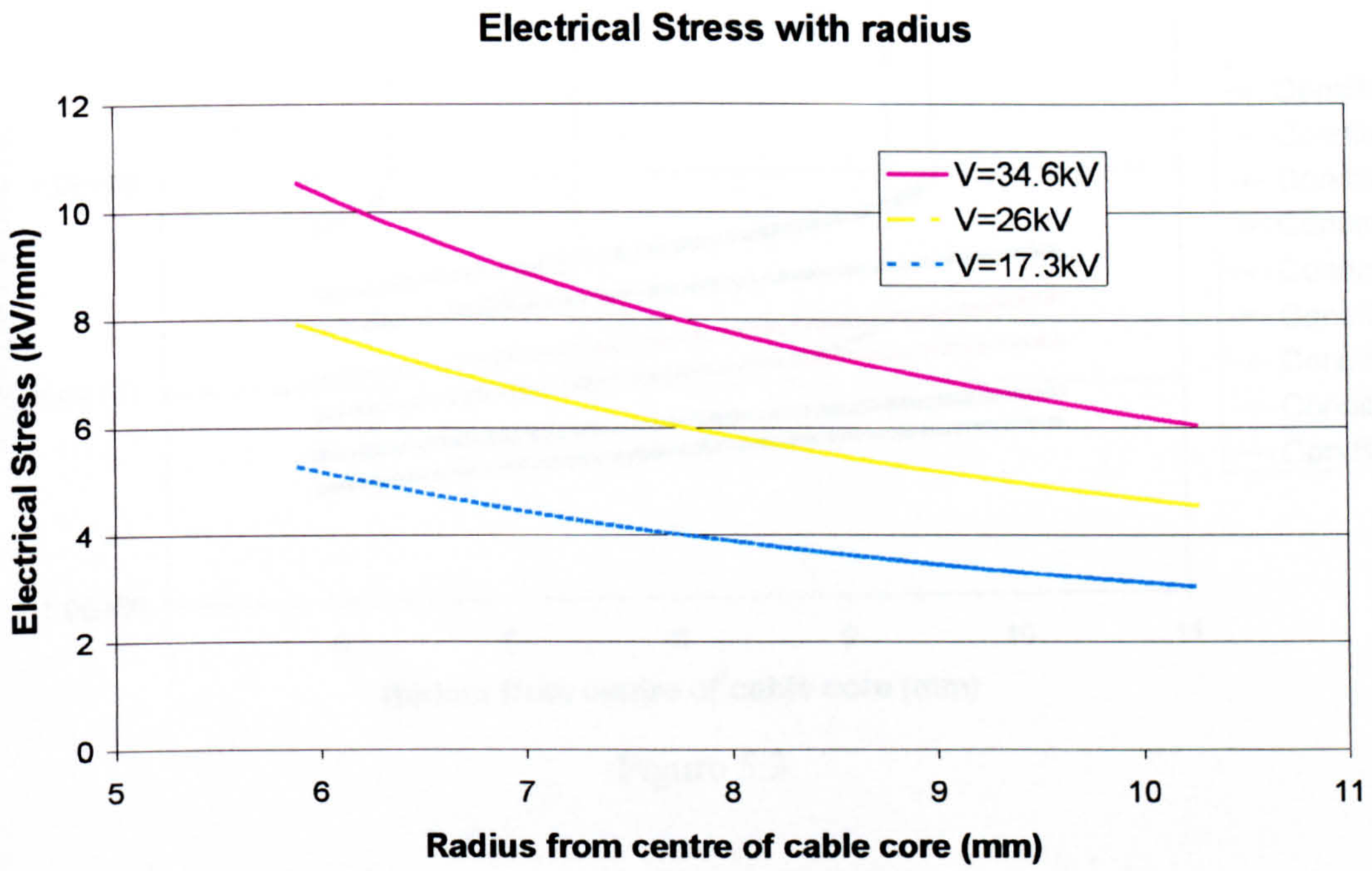

Figure 5.2

In figure 5.2, the y-axis represents electrical stress, and the x-axis shows radius from the centre of the core –*i.e.* r_i. The field at each r_i is therefore the field experienced by the shell situated at radius r_i. The solid pink line shown the stress distribution for conditions 1, 2 and 3; the dash-dot yellow line shows the stress for conditions 4, 5 and 6; conditions 7, 8 and 9 are represented by the dashed cyan line.

The predicted lifetime with radius for the nine different experimental conditions is shown below. The plots are labelled 1 to 9 to correspond to the conditions shown in table 5.2.

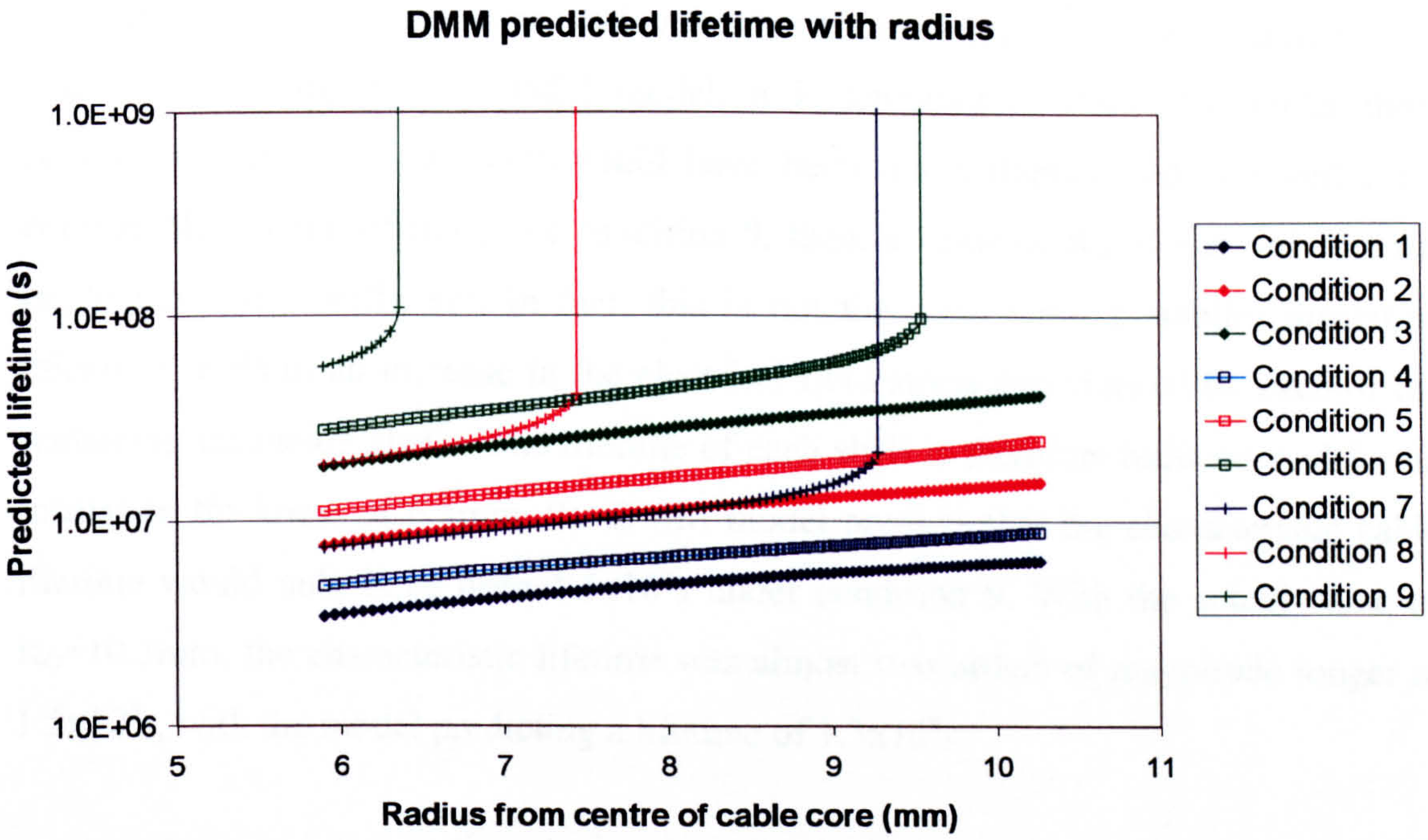

Figure 5.3

Figure 5.3 shows predicted lifetime on the y-axis for each of 100 shells of insulation. Each shell is situated at radius r_i, which is represented on the x-axis. The blue lines are all for an ageing temperature of 363K, the red lines are for 348K and the green lines for 333K. Solid lines with diamonds are for an ageing voltage of 34.6kV, unfilled squares are for V=26kV and the crosses are for V=17.3kV.

In figure 5.3, it can be seen that for all cases where the ageing voltage was the lowest value of 17.3kV, some of the outer insulation shells are predicted to have an infinite life by the DMM model. Infinite lifetimes are also predicted for condition 6, the lowest test temperature at 26kV, at all radii above approximately 9.55mm. For condition 7, where T=363K, all shells situated more than 9.28mm from the centre of the cable core are predicted infinite lifetime and the moieties in them were therefore not involved in the ageing process. For condition 8, where the temperature is T=333K, all shells outside 7.45mm are uninvolved in ageing, and for condition 9, where T=333K, all shells outside a radius of 6.36mm are uninvolved. This effectively means that the volumes undergoing ageing in these three cases are different from each other, and from in the other six cases.

Since the outermost shells were not involved in the ageing process for conditions 6, 7, 8 and 9 according to the DMM model, it is tempting to think that under these conditions, the cable insulation could have been made thinner and survived for a comparable amount of time. For condition 9, then, a value of R_O of e.g. only 6.5mm might have been sufficient. In fact, this is not the case, since a smaller insulation thickness leads to an increase in the electrical field stress experienced by each of the remaining insulation shells. The lifetime of each shell is therefore reduced, and for an insulation thickness of 6.5mm, the DMM model predicts that the characteristic cable lifetime would only have been $1.5x10^6$s under condition 9. With the actual value of R_O=10.3mm, the characteristic lifetime was almost two orders of magnitude longer at $1.5x10^8$s, with the model predicting a lifetime of $1.3x10^8$s.

6. Application of models to time-to-failure distributions

When a set of nominally identical polymeric specimens is aged under a particular experimental condition, each specimen in the set generally fails at a different time. Polymer lifetime models, however, give a single lifetime prediction for any given experimental condition. In the previous chapters, the model lifetime predictions have been equated to the characteristic failure times of sets of specimens aged under the relevant condition. Fitting the models to these characteristic lifetimes necessarily provides 'characteristic' or 'typical' values for each of the parameters in the model.

In reality, as discussed in the last chapter with reference to volume effects, many of the parameters in both the DMM and Lewis models are likely to vary within any particular specimen, and some may actually be different for every moiety or bond involved in the ageing process. For example, the parameters describing the energy barrier to ageing are likely to be different for each reacting moiety, since in the DMM model no two moieties in any material are likely to require exactly the same amount of energy to make them move into the product state. Equivalently, for the Lewis model, no two bonds are likely to need exactly the same amount of energy to be broken, formed or altered.

In this chapter it is hypothesised that the different times-to-failure observed in nominally identical polymer specimens aged under the same conditions, may be directly attributed to differences in the moieties which cause failure in each specimen. With this in mind, the possibility of modelling the time-to-failure distribution for a set of specimens is investigated. This is done by distributing some of the DMM model parameters in the lifetime equation. Changes in the forms of the parameter distributions with experimental conditions then yield some information about the ageing process.

6.1 Theory

The DMM parameters investigated here are those describing #G, the energy barrier to ageing for moieties involved in the ageing process. The magnitude of this barrier is likely to be different for each moiety in a polymer. Differences in #G from moiety to

moiety could be due to a number of factors, depending on the processes at work during ageing. However, microscopic inhomogeneity in terms of physical structure and chemical makeup are two factors that are likely to affect any physical process, and these generally exist in any polymeric specimen. Chemical inhomogeneities could include by-products of manufacturing processes. For cables such processes include curing and cross-linking, the by-products of which have been found to be unevenly distributed throughout the cable insulation [1]. Morphological inhomogeneity is a more fundamental characteristic of polymeric materials due simply to the non-uniform arrangement of polymer chains in crystalline and/or amorphous structures [e.g. 2].

According to the DMM model, only a fraction of moieties (equal to the value of A*) need to be in the product state in any localised area of a specimen for breakdown to be initiated. This means that in the specimen as a whole, the number of moieties in the product state when breakdown occurs is likely to be extremely small – very much smaller than typical values of A* of around 40%. Since the moieties with the smallest barriers to ageing will be the moieties which reach the product state first, it seems likely that the moieties with the smallest energy barriers in each specimen will be those that are ultimately responsible for the breakdown of that specimen.

This means that the time-to-failure of each specimen is likely to be directly related to the magnitude of the ***smallest*** values of #G it contains. Therefore, in the DMM model, a more accurate way to describe the parameter #G is as a *minimum* barrier to ageing. #G is made up of an enthalpy barrier, the magnitude of which is described by H_{dk}, and an entropy barrier, whose magnitude is described by $|S_d|$. A small value of H_{dk}, or a small value of $|S_d|$ corresponds to a small barrier to ageing, so the values of H_{dk} and $|S_d|$ found when fitting to B63 lifetime values are actually *minimum* enthalpy and entropy barriers characteristic of the specimens aged.

Each experimental ageing condition yields a time-to-failure for each specimen tested under that condition, and these form a distribution. If each of the times-to-failure corresponds to a different value of minimum energy barrier, #G, each experimental condition can therefore also yield a distribution of minimum #G values, or a distribution of minimum H_{dk} or $|S_d|$ values. Distributions of the enthalpy and entropy parameter values are investigated separately here. By looking at how these

distributions vary with experimental conditions, an insight can be gained into the distribution of times-to-failure at each experimental condition.

In the following it is assumed that it is the extreme smallest #G in a specimen which directly relates to the time-to-failure. This is actually unlikely to be the case, but the approximation is reasonable as long as very few moieties need to be in the aged state to cause breakdown of a specimen. This seems likely – firstly due to the small values of A* and b* found from fitting of the DMM and Lewis models to lifetime data. Secondly, large structural or chemical changes are not generally observed away from the breakdown site in failed polymers, which implies that only a small amount of ageing can cause a polymer to fail. The good fits to data achieved here also justify the use of the approximation.

Distributions of other factors that affect ageing, and therefore other DMM parameters, could well be equally responsible for the observed time-to-failure distributions, either instead of, or in conjunction with distributions of the H_{dk} and S_d parameters. The effect of assuming distributed C_d and A* on the time-to-failure distributions, for example, is investigated in [3].

6.1.1 Extreme value statistics

According to the theory above, a distribution of minimum H_{dk} or $|S_d|$ values can be obtained for each experimental condition at which time-to-failure data are available. Each of the H_{dk} or $|S_d|$ values in each distribution represents the smallest H_{dk} or $|S_d|$ present in one of the specimens. The distributions of smallest H_{dk} (or smallest $|S_d|$) values at each condition represent the probability density of smallest H_{dk} (or smallest $|S_d|$) values in specimens at that experimental condition. The distributions are therefore well suited to being modelled by an extreme value distribution.

Extreme value statistics can be used to describe the probability distributions of extreme largest or smallest values. The distribution applicable to smallest (rather than largest) values, such as those described above, is the Weibull distribution [2,4,5,6]. This distribution was mentioned in chapter 3 with reference to the time-to-failure distributions obtained when ageing polymer specimens. The Weibull distribution is often found to fit time-to-failure and breakdown data well, and the physical reasons for

choosing this particular distribution for failure times are well accepted [e.g 7,8,9] and outlined below.

Extreme value statistics are used where the extreme (smallest or largest) value of a parameter (or a local property) determines the behaviour of a system. They are described through functions for the probability that the largest (smallest) value in the global distribution is less than a chosen value. These distributions obey a stability criterion, *i.e.* the form of the distribution for the extremes in a set of n samples is retained for a set of Nn samples. This imples that the functional form of the statistics remains invariant to changes in sample size [2,4,5,6].

In the case of polymer lifetimes, each specimen can be thought of as containing N regions. Each of these regions will be different on a microscopic level, and each is therefore likely to take a different time to reach the breakdown criterion. In other words, each region will take a different time to reach a situation in which a sufficient number of moieties are aged for breakdown to proceed. Each region can therefore be assigned its own breakdown time.

Each of n specimens in a set of ageing tests therefore contains a distribution of N values of the variable of interest, which is time-to-failure. The global distribution in this case contains all possible failure times for regions of the material considered. The shape of this distribution is unknown, but is not important. In fact, the global distribution of times-to-failure can just be thought of as time, t, since any value of t is also a possible value of time-to-failure for a region of polymer. The Weibull cumulative probability function can then be used to find the probability at any given time, t, that the ***smallest*** time-to-failure in any one of n specimens aged under a particular condition is less than t. This can clearly be equated to the probability that one of the n specimens will fail, since if the smallest time-to-failure in a specimen is less than t, it must fail.

This approach assumes that the region with the smallest time-to-failure will cause breakdown of each specimen. This is valid as long as breakdown in any one region can cause the whole specimen to fail, and this is assumed to be the case here. It is therefore only the extreme smallest breakdown time present in each specimen that is of interest.

In this investigation, the Weibull distribution is used to model the probability distributions of extreme smallest H_{dk} or $|S_d|$ values in each specimen according to the method described below. The theory outlined above is still applicable – it is the smallest value of H_{dk} or $|S_d|$ in each specimen which is assumed to cause the specimen to break down, just as above it was the region with the smallest time-to-failure which was important. Each region is now assigned an H_{dk} or $|S_d|$ rather than a time-to-failure, and the H_{dk} and $|S_d|$ values corresponding to the specimen time-to-failures are assumed to be distributed according to the Weibull probability distribution. The H_{dk} or $|S_d|$ value obtained from a failure time is the smallest value in that specimen, and is called mH_{dk} or mS_d to indicate a minimum value.

Since the mH_{dk} or mS_d probability distributions can be assumed to be Weibull distributions, the distribution at each experimental condition can be characterised in exactly the same way as described for the times to failure distributions in chapter 3. Each experimental condition therefore yields a distribution of mH_{dk} or mS_d with a characteristic value, α, and a shape parameter, β. The characteristic value of a Weibull distribution represents the value of the variable for which there is a 63% probability that the value of mH_{dk} or mS_d present in one of the specimens is smaller than a specified value of the variable from the global distribution. Equivalently, the characteristic B63 time used in chapters 3 and 5 is the time at which the probability of failure (i.e. the probability that the smallest time-to-failure in one of the specimens is less than time, t) is 63%. The characteristic value of each mH_{dk} (or mS_d) distribution corresponds to the characteristic smallest mH_{dk} (or mS_d) value present in the specimens at that condition, and is called α.. The shape parameter of each distribution, β, describes the spread in values of mH_{dk} or mS_d around the characteristic value.

6.2 Application to thin film Data

The time-to-failure data used here were those described in chapter 3 from PET thin film AC and DC ageing experiments [10]. AC time-to-failure data were available in the range 293K to 423K and 10 to 50 kV/mm. DC lifetime data were available in the range 28 to 83kV/mm and from 382K to 453K.

6.2.1 Method

As explained above, it was assumed that each time-to-failure of a thin film specimen was due to the smallest H_{dk} or $|S_d|$ present in that specimen, called mH_{dk} or mS_d respectively. By rearranging the DMM lifetime equation, it was therefore possible to obtain a value of mH_{dk} or mS_d for each specimen. The equations to give each mH_{dk} and mS_d are rearrangements of the DMM lifetime equation as shown below:

$$mH_{dk} = T\ln\left[\frac{\cosh\left(\frac{K_d - C_d E^{4b}}{2T}\right)\times TTF}{\frac{h}{2kT}\exp\left(\frac{-Sd}{k}\right)\left(-\ln\left(\frac{Aeq - A^*}{Aeq}\right)\right)}\right] + \frac{C_d E^{4b}}{2}$$

$$mS_d = T\ln\left[\frac{\cosh\left(\frac{K_d - C_d E^{4b}}{2T}\right)\times TTF}{\frac{h}{2kT}\exp\left(\frac{H_{dk} - \frac{C_d E^{4b}}{2}}{T}\right)\left(-\ln\left(\frac{Aeq - A^*}{Aeq}\right)\right)}\right] \qquad 6.1 \text{ and } 6.2$$

In 6.1 and 6.2 k is Boltzmann's constant, h is Planck's constant, E is field and T is temperature. TTF is the time-to-failure of an individual polymer specimen aged at E and T. C_d, b, A* and Aeq are parameters of the DMM model as explained in chapter 2. All DMM parameters on the RHS of the above equations were assumed to have their typical values from the fits to the B63 data from the same experiments – i.e. the values found in chapter 3.

At each ageing condition, several TTF values were obtained, since each specimen failed at a different time. Equations 6.1 and 6.2 therefore produce several values of mH_{dk} or mS_d at each experimental condition. These form a distribution at each experimental condition, each of which can be characterised by its α and β values as described above, producing a value of α and β for each experimental condition. Using these α and β values, 'idealised' mH_{dk} and mS_d distributions with 10,000 elements

were then produced for each experimental condition. This was done using the 'rweibull' function in MATHCAD to generate a distribution of the Weibull form.

These calculated mH_{dk} and mS_d distributions were then substituted back into the DMM lifetime equation to provide 10,000 time-to-failure values at each condition. These were plotted together with the experimental time-to-failure data at each condition, to enable comparison of the generated and experimental time-to-failure distributions. A good match between these distributions would indicate that distributing the activation energy parameters within the DMM lifetime equation is a good way of modelling the time-to-failure distributions. Some results are presented below.

6.2.2 AC results

Graphs showing time-to-failure distributions produced by the mH_{dk} and mS_d distributions and the experimental time-to-failure data at each ageing condition are presented in section B1 of Appendix B. An example of the results is shown in fig 6.1.

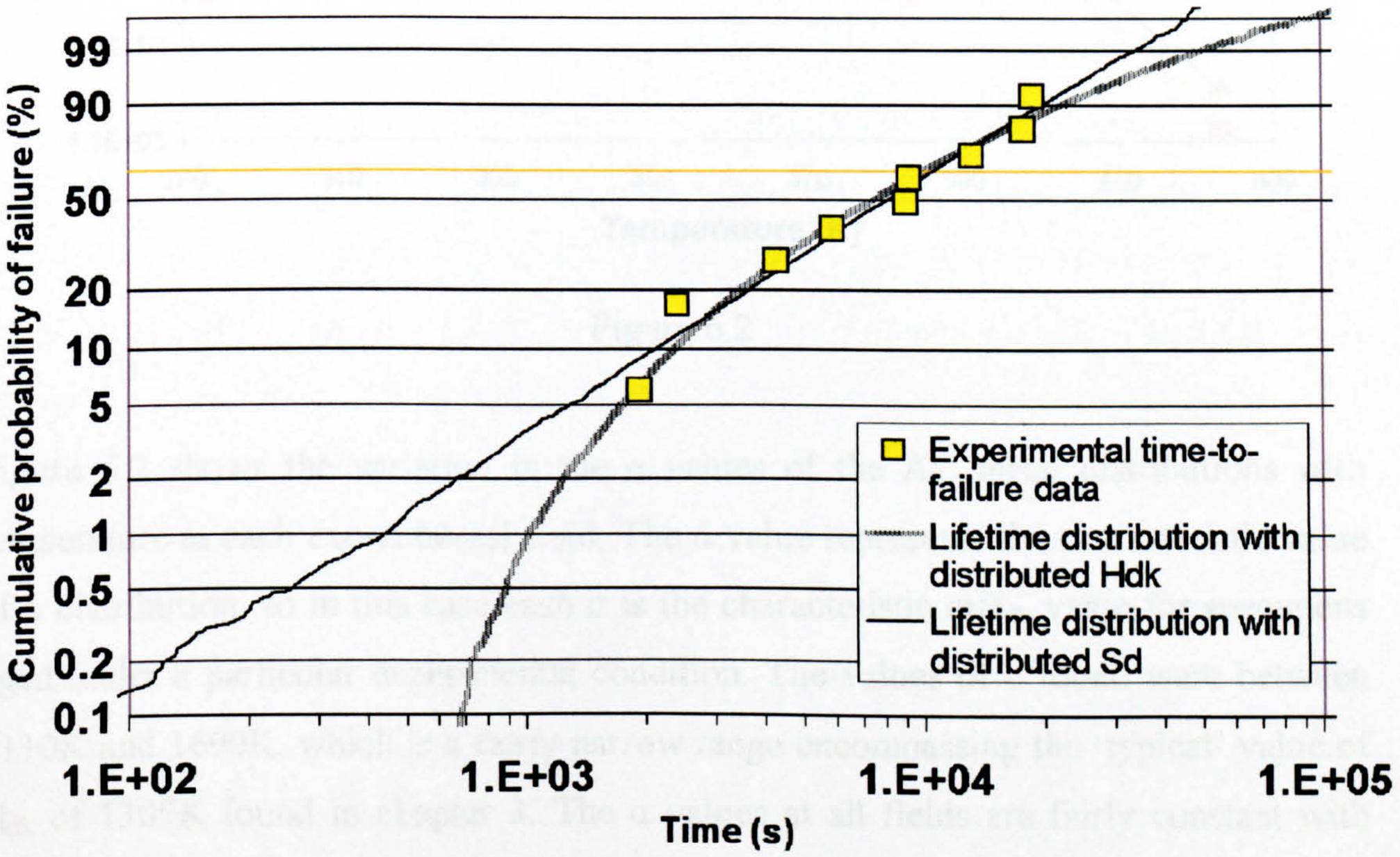

Figure 6.1

Figure 6.1 shows Weibull cumulative probability of failure on the y-axis against time in seconds on the x-axis. The square points are experimental time-to-failure data at E=50kV/mm and T=403K. The thin black line shows the lifetime distribution (with 10,000 elements) generated from assuming a distribution of mS_d values within the

DMM model. The thicker grey line shows the lifetime distribution resulting from a distribution of mH_{dk} values.

It is also interesting to look at the changes in the mH_{dk} and mS_d distributions with applied field, E and temperature, T. Figure 6.2 shows the change in the characteristic value of the H_{dk} distributions, α, with T. No particular pattern was seen in the change of the H_{dk} alpha values with E.

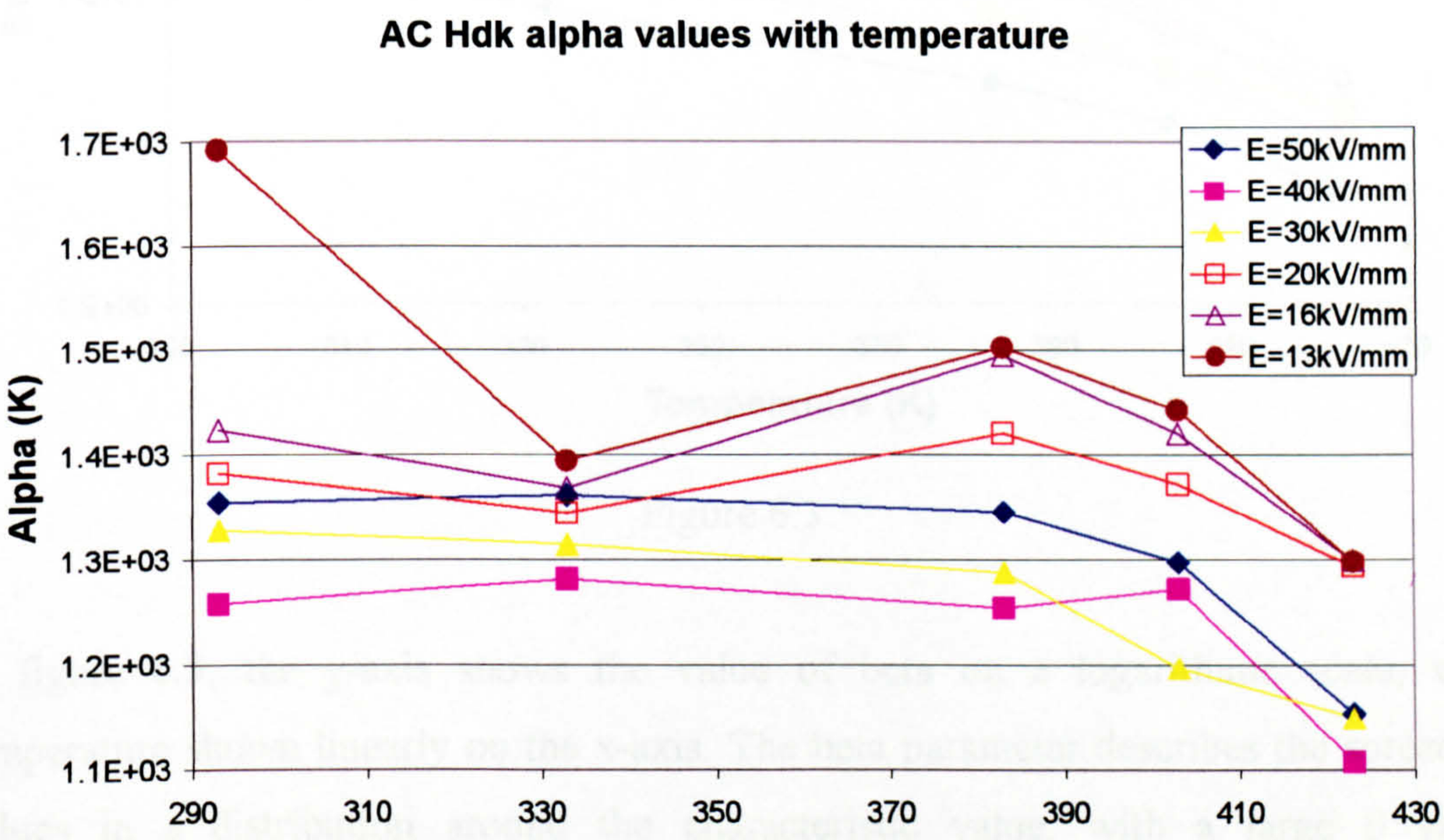

Figure 6.2

Figure 6.2 shows the variation in the α values of the AC mH_{dk} distributions with temperature at each experimental field. The α value represents the characteristic value of a distribution, so in this case each α is the characteristic mH_{dk} value for specimens aged under a particular experimental condition. The values of α found were between 1110K and 1690K, which is a fairly narrow range encompassing the 'typical' value of H_{dk} of 1309K found in chapter 3. The α values at all fields are fairly constant with temperature below about 383-403K. Above this temperature range, the characteristic values in the distributions appear to fall off with temperature at every field.

Figure 6.3 shows the change in the β parameter of the mH_{dk} distributions with T.

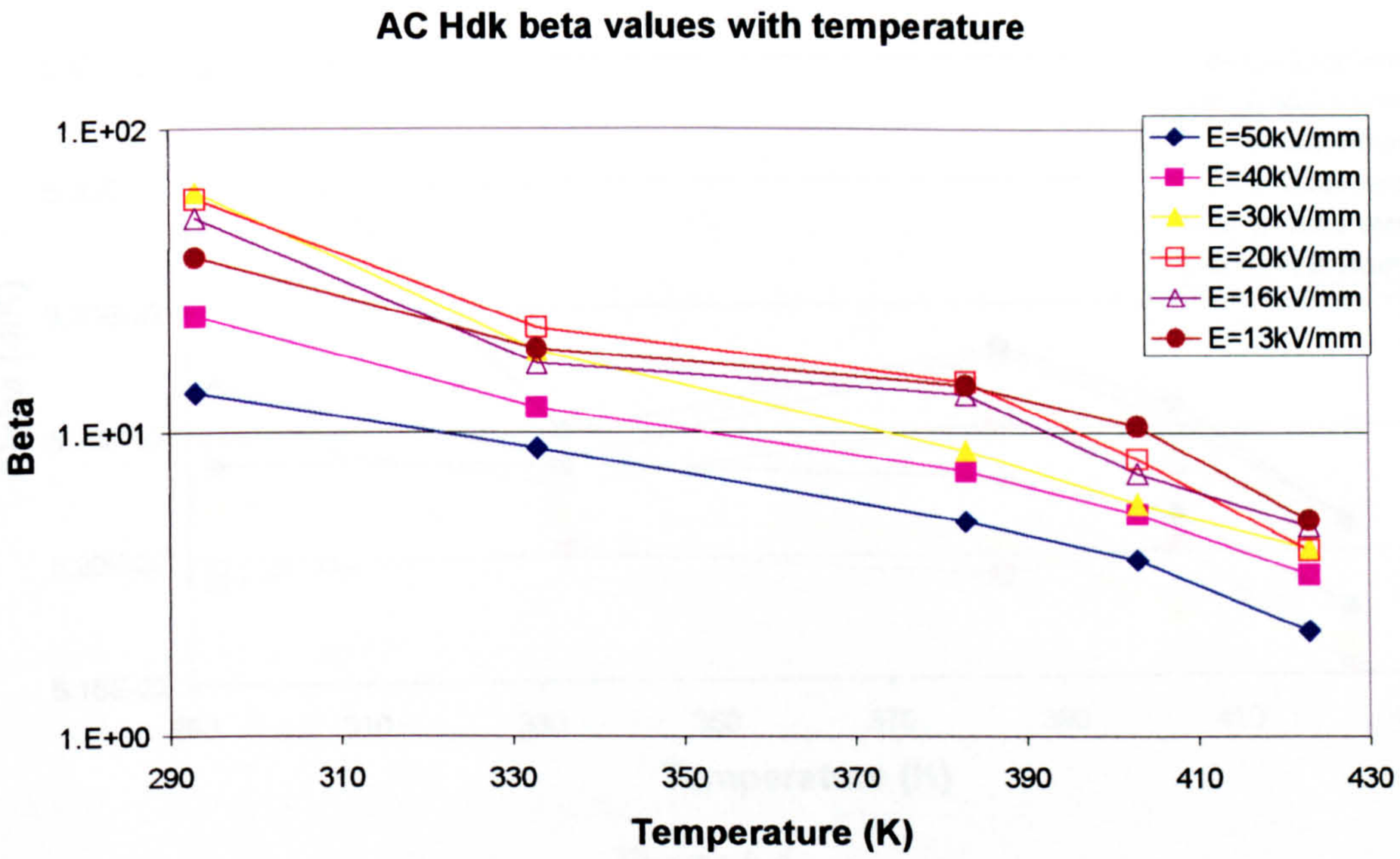

Figure 6.3

In figure 6.3, the y-axis shows the value of beta on a logarithmic scale, with temperature shown linearly on the x-axis. The beta parameter describes the spread of values in a distribution around the characteristic value, with a large β value corresponding to a narrow distribution and a small value of beta corresponding to a broad distribution. The beta values for the mH_{dk} distributions are all quite large, with values ranging from 2.2 to 62. Figure 6.3 shows the beta parameter for the distributions falling off sharply with temperature for all fields. The β values of the AC mH_{dk} distributions showed no pattern with field.

The α and β values for the AC mS_d distributions show similar trends to the mH_{dk} distributions. Figure 6.4 shows the change of the mS_d α value with temperature, and figure 6.5 shows the change of the mS_d β values with temperature. Graphs of these parameters with field reveal no obvious trend.

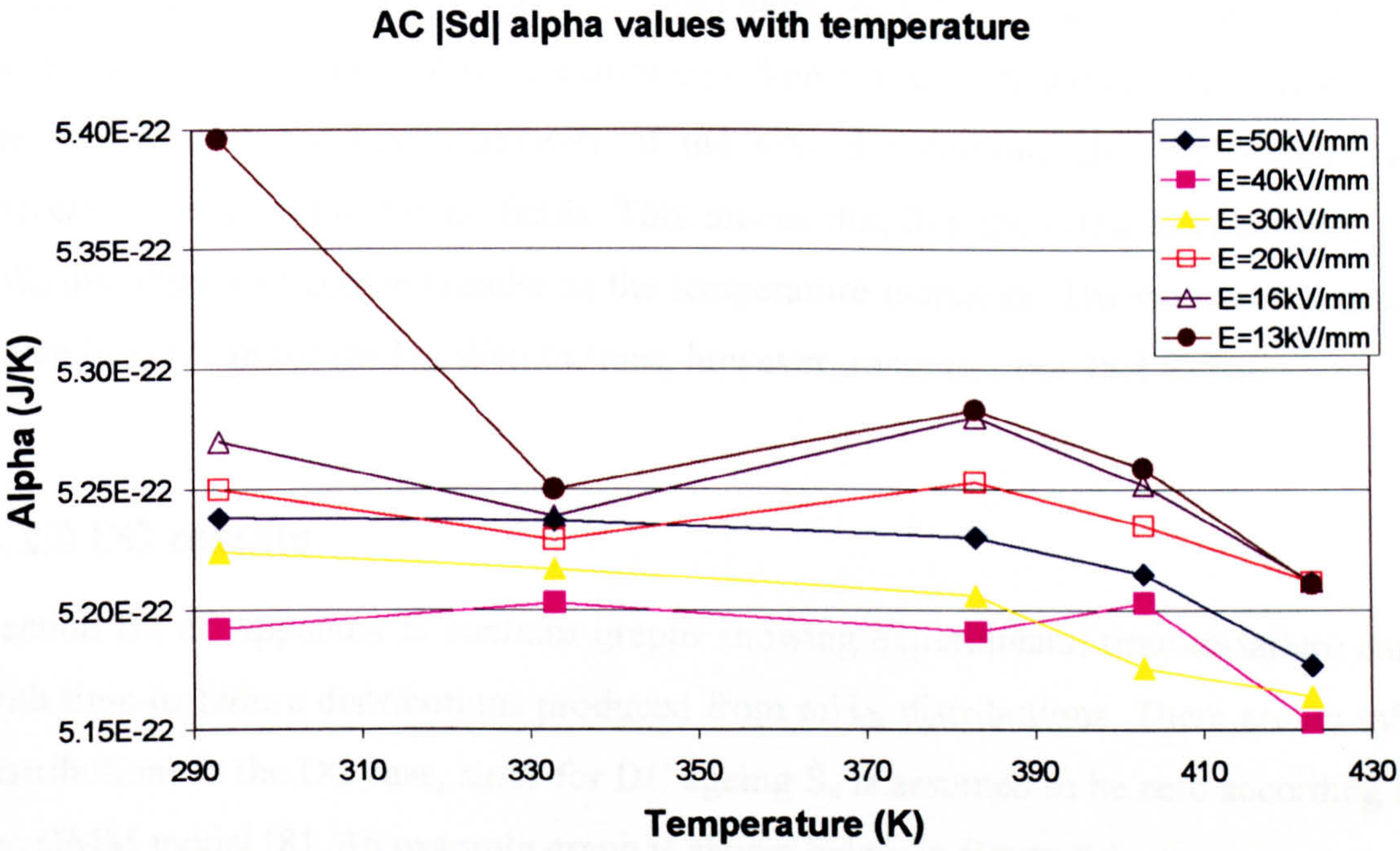

Figure 6.4

As in the case of the mH_{dk} distributions, the characteristic values in the mS_d distributions appear reasonably constant with temperature below about 383-403K. Above this temperature range, the magnitude of the characteristic mS_d appears to fall with increasing temperature at all fields. The range of α values is from $5.1x10^{-22}$J/K to $5.4x10^{-22}$J/K, which encompasses the value found of $5.2x10^{-22}$J/K found for this data in chapter 3.

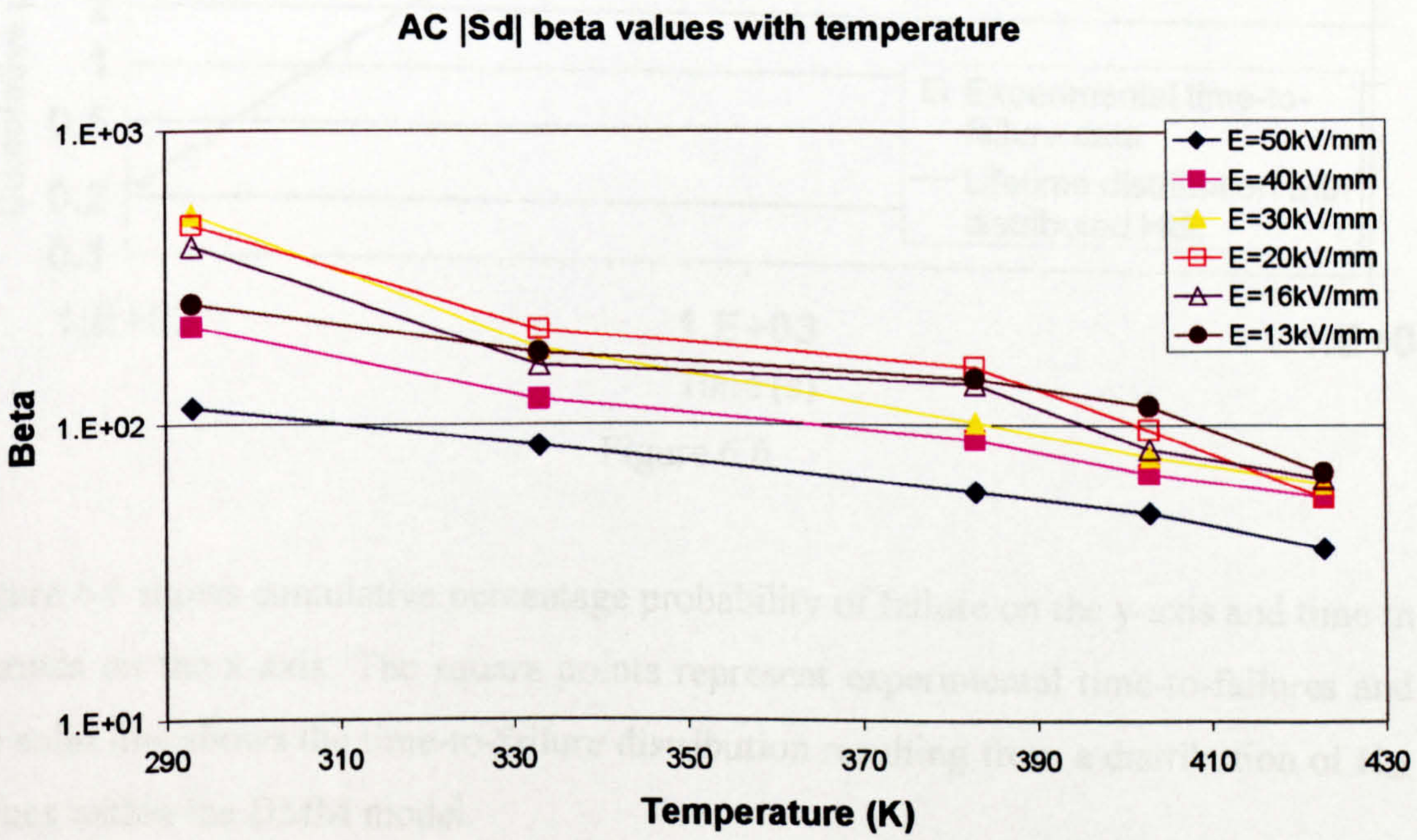

Figure 6.5

Figure 6.5 shows the variation of beta with temperature for all ageing fields, with beta on a logarithmic y-axis and temperature on a linear x-axis. It shows similar results to figure 6.3, with the beta parameter of the mS_d distributions also decreasing with increasing temperature for all fields. This means that like the mH_{dk} distributions, the mS_d distributions become broader as the temperature increases. The values of beta are much larger than for the H_{dk} distributions, however, ranging from 38.4 to 518.

6.2.3 DC results

Section B2 of Appendix B contains graphs showing experimental time-to-failure data with time-to-failure distributions produced from mH_{dk} distributions. There are no mS_d distributions in the DC case, since for DC ageing S_d is assumed to be zero according to the DMM model [8]. An example graph is shown below in figure 6.6.

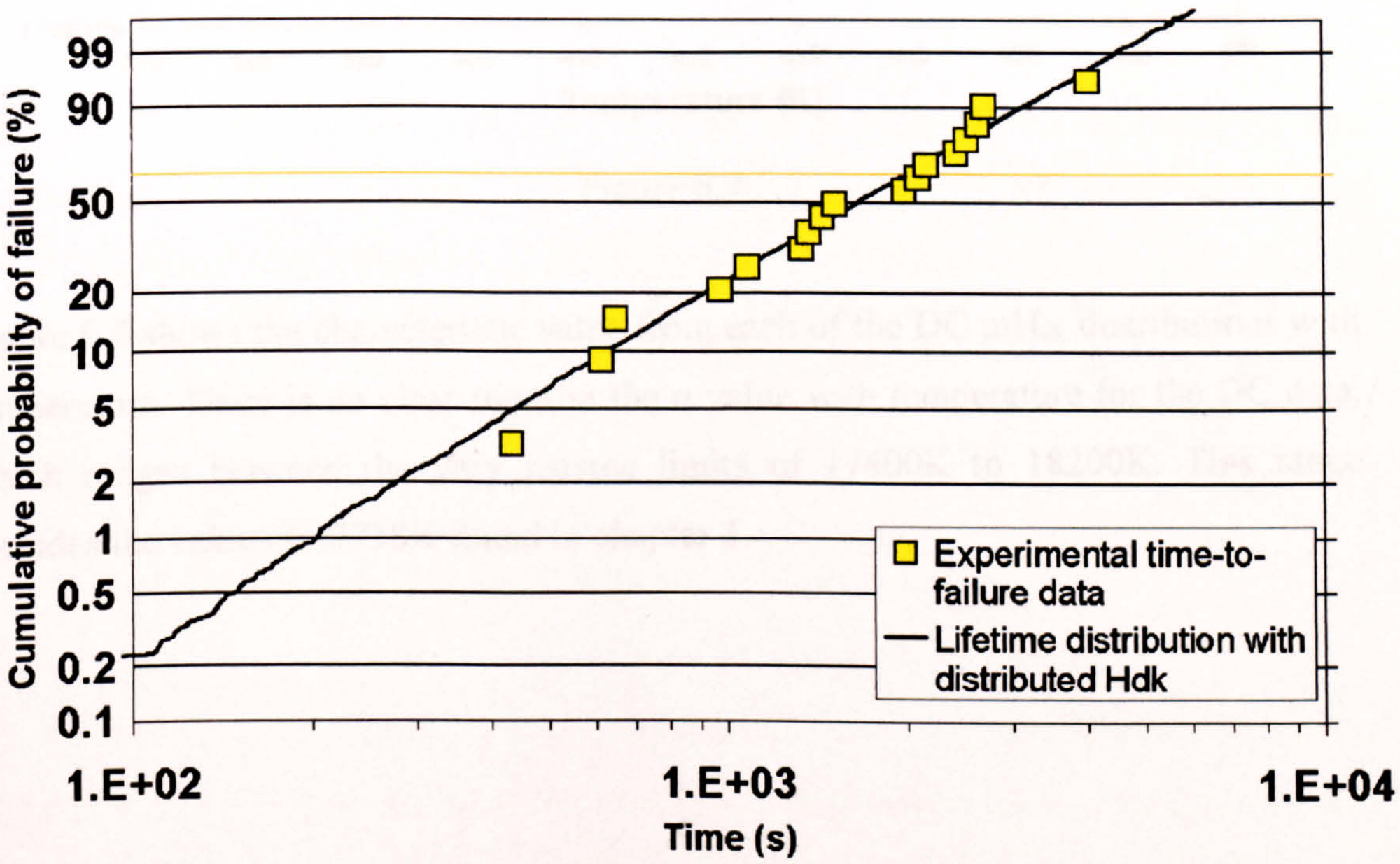

Figure 6.6

Figure 6.6 shows cumulative percentage probability of failure on the y-axis and time in seconds on the x-axis. The square points represent experimental time-to-failures and the solid line shows the time-to-failure distribution resulting from a distribution of H_{dk} values within the DMM model.

Figure 6.7 shows the change in the characteristic mH_{dk} value, α, with T, and figure 6.8 shows the change in the β parameter of the mH_{dk} distributions with T.

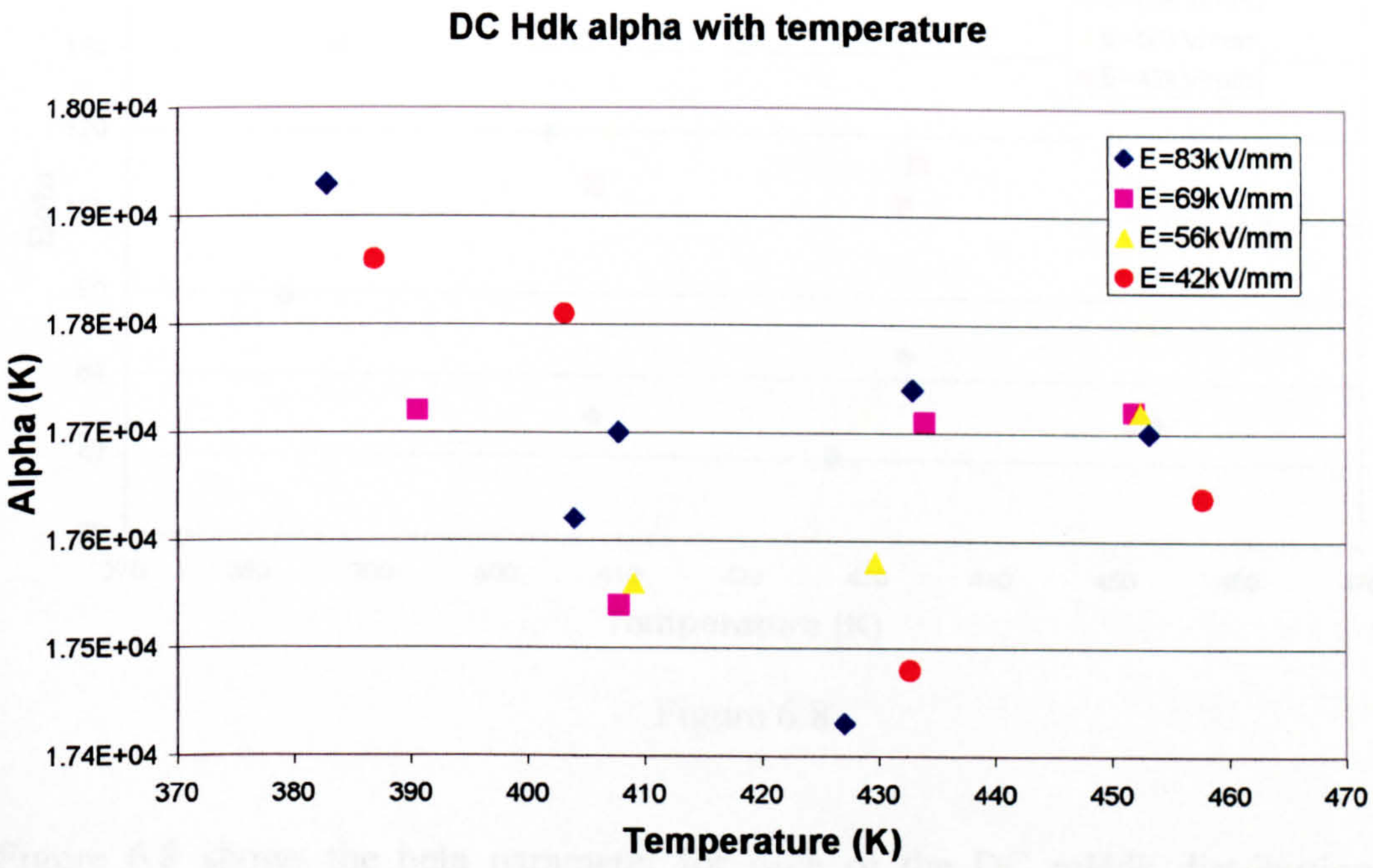

Figure 6.7

Figure 6.7 shows the characteristic value from each of the DC mH_{dk} distributions with temperature. There is no clear trend in the α value with temperature for the DC data, which ranges between the very narrow limits of 17400K to 18200K. This range includes the value of 17738K found in chapter 3.

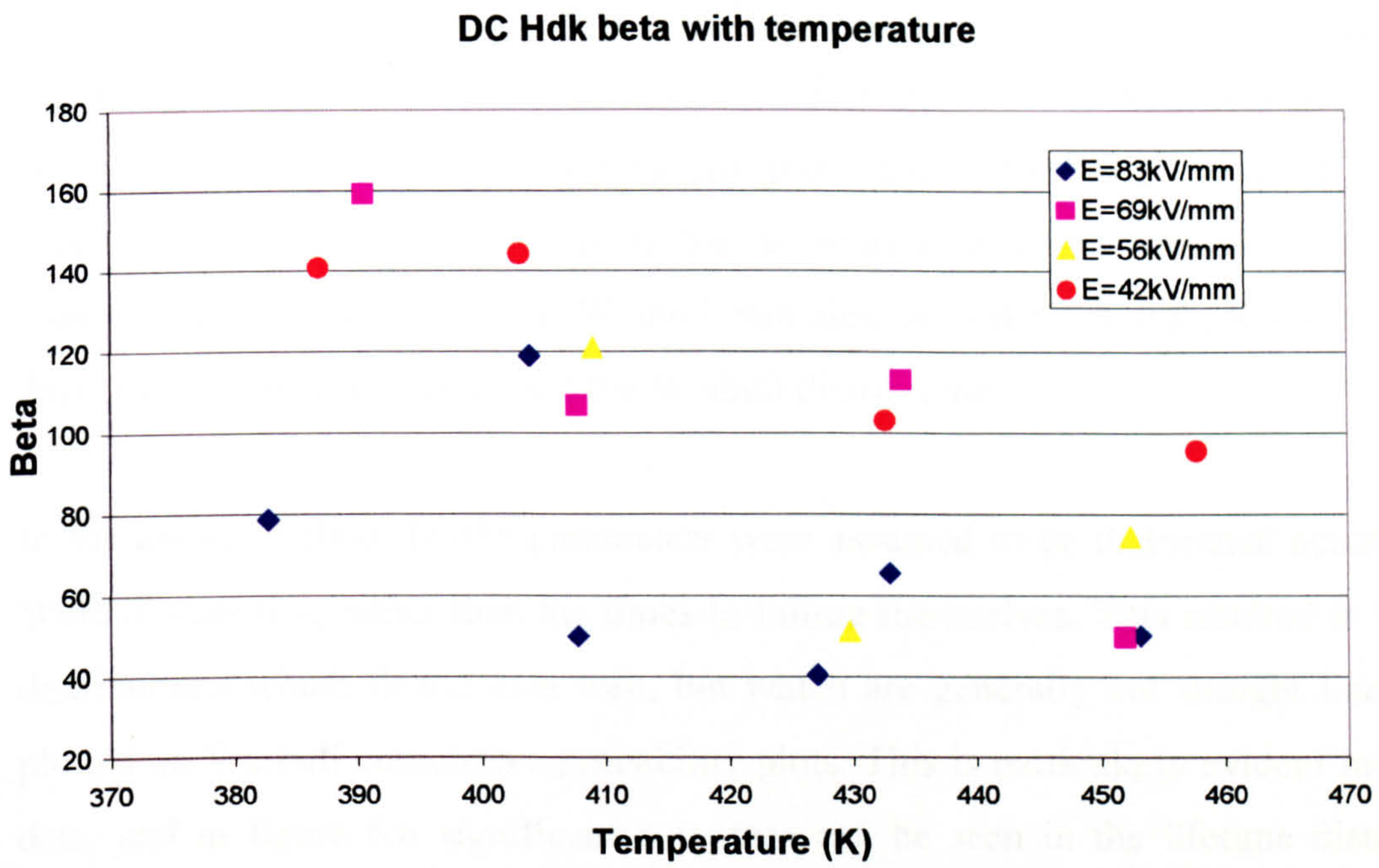

Figure 6.8

Figure 6.8 shows the beta parameter for each of the DC mHdk distributions with temperature. The beta parameters at each field can be seen to be following a downward trend with increasing temperature, though this is much less clear than in the AC case. The β values vary between 40.4 and 159. In the DC case, as in the AC case, no pattern was seen in either α or β with field, E.

6.2.4 Discussion of thin film results

Fits to experimental time-to-failure data

Figures 6.1 and 6.6, along with the graphs at other experimental conditions in Appendix B, show that the agreement between experimental time to failure data and time-to-failure distributions generated by distribution of activation energy parameters is good in most cases. Distributions of mH_{dk} and mS_d in the AC case, and mH_{dk} in the DC case, can therefore be used to accurately model observed experimental time to failure data. This suggests that it may be the difference in the smallest barriers to ageing between specimens which is responsible for the different times-to-failure observed experimentally, as proposed.

As mentioned before, polymer time-to-failure data is often assumed to be distributed according to Weibull statistics. A feature of data that has this statistical shape is that when plotted on a cumulative probability plot such as figures 6.1 and 6.6, the data should plot as a straight line. This feature is often used to test whether or not data is indeed distributed according to Weibull statistics. A best fit straight line through the data points is then used to model the Weibull distribution.

In the above method, DMM parameters were assumed to be distributed according to Weibull statistics, rather than the times-to-failure themselves. This resulted in lifetime distributions which fit the data well, but which are generally not straight lines when plotted on Weibull cumulative probability plots. This is particularly evident in the AC data, and in figure 6.6 significant curvature can be seen in the lifetime distribution generated by a distribution of mH_{dk} values. The curvature is particularly pronounced at the low probability end of the distributions.

Even when the generated lifetime distributions do appear to be reasonably good straight lines, they tend to deviate from the line that would be produced by a best-fit straight line through the data points. An example of this is shown below for DC time-to-failure data at E-83kV/mm and T=427K.

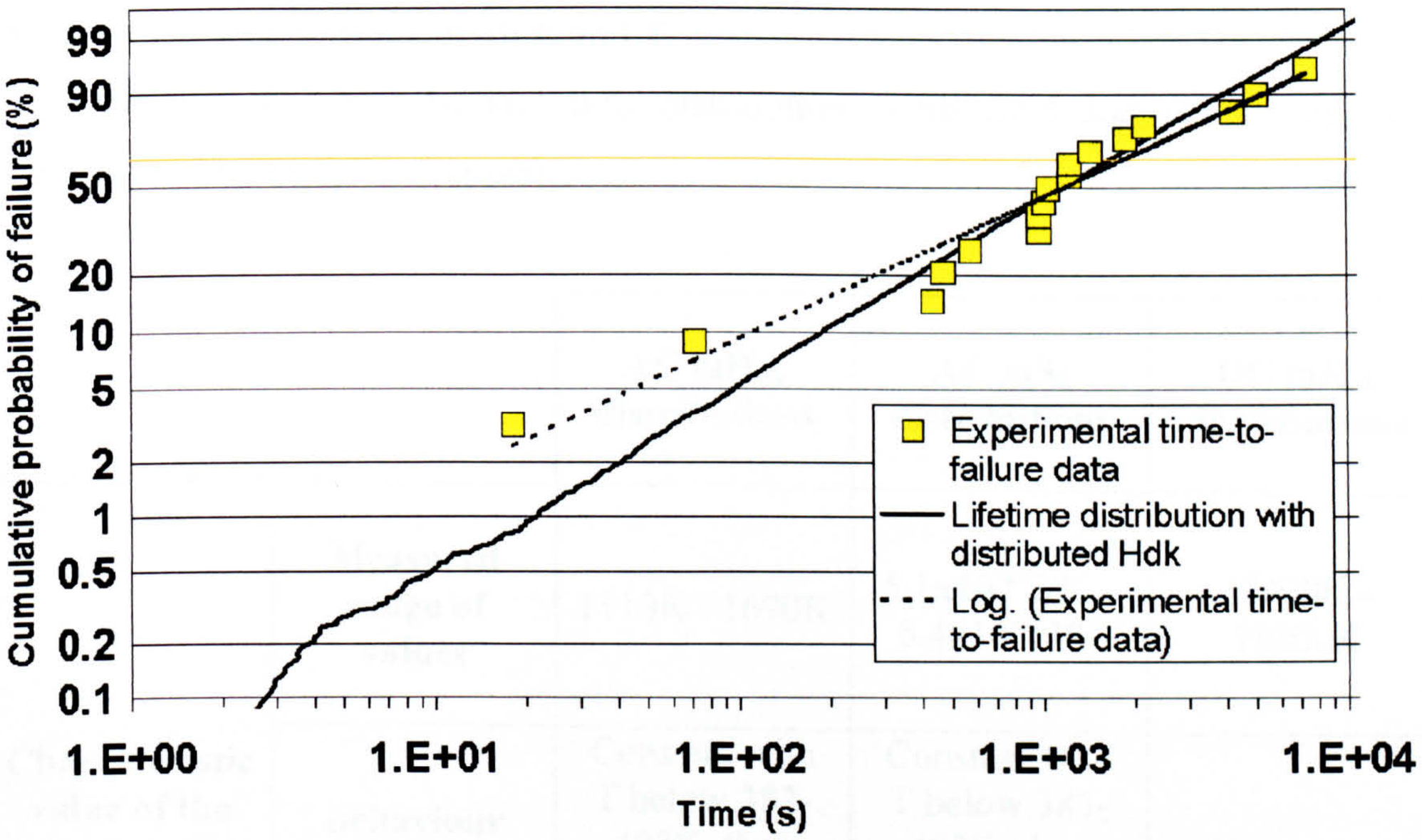

Figure 6.9

In figure 6.9, Weibull percentage cumulative probability is shown in the y-axis, with time in seconds on the x-axis. The square points are experimental data, and the solid line shows the time-to-failure distribution obtained from a distribution of H_{dk} within the DMM model. The dotted line shows a best-fit straight line through the data points. It can be seen that the best-fit line and the H_{dk} distribution line are not co-incident, and that the H_{dk} distribution line shows some curvature at very low probabilities of failure.

Depending on which of the DMM parameters is distributed within the model, the resultant fits to lifetime data may be significantly different in shape. This is true for the case shown in figure 6.1 for the H_{dk} and the S_d distributions. Both of the distributions fit the data well, so it is difficult to decide whether there is a 'better' fit for one parameter distribution that the other. It is also difficult to decide whether the best-fit straight line Weibull fit is better than the mH_{dk} or mSd distribution fits. In other words, it is hard to tell whether the lifetime data is best described as being itself distributed according to Weibull statistics, or as a function of a parameter (mH_{dk} or mS_d here) which is distributed according to Weibull statistics.

Changes in distributions with E and T

The changes in the mH_{dk} and mS_d distributions with field and temperature are summarised in the following table:

		AC mH_{dk} distributions	**AC mS_d distributions**	**DC mH_{dk} distributions**
Characteristic value of the distribution, α	**Measured range of values**	1110K - 1690K	$5.1x10^{-22}$J/K – $5.4x10^{-22}$J/K	17400K - 18200K
	Behaviour with T	Constant with T below 383-403K, then decreasing with T	Constant with T below 383-403K, then decreasing with T	No pattern
	Behaviour with E	No pattern	No pattern	No pattern
Shape parameter of the distribution, β	**Measured range of values**	2.23 - 61.7	38.4 - 518	40.4 - 159
	Behaviour with T	Falling with T at all E	Falling with T at all E	Falling with T at all E
	Behaviour with E	No pattern	No pattern	No pattern

Table 6.1

The β values for all of the minimum activation energy parameter distributions are very high. This means that the distributions of mH_{dk} and mS_d at each condition are very narrow. Such sharp mH_{dk} and mS_d distributions indicate that the energy barrier to ageing of the moieties responsible for ageing is very similar for all specimens aged at a

particular E and T. It is interesting to note that these very similar activation energies from specimen to specimen result in relatively broad lifetime distributions. For example, in the DC case, the β values for the mH_{dk} distributions range between 40 and 159, whilst for the lifetime distributions β ranged from 0.9 to 1.9. A small change in the minimum activation energy therefore has a large effect of the lifetime of a specimen, which is to be expected given the exponential dependence of lifetime on activation energy. Such a small variation in the energy barriers of the moieties responsible for breakdown from specimen to specimen seems physically reasonable, since it implies only a small change in the local environments of these moieties.

In all cases (AC mH_{dk}, AC mS_d and DC mH_{dk}), the α values do not change very much with either field or temperature according to the above data. This helps to explain why fitting the model to B63 times at all of the experimental conditions results in a good fit to each condition as in chapter 3, since it shows that mH_{dk} and mS_d do not have strong dependences on either field or temperature. This is in good agreement with the derivation of the DMM model.

Change in β with temperature

It can be seen from the results that the β value of all the mH_{dk} and mS_d distributions decreases with temperature. This means that the mH_{dk} and mS_d distributions obtained from time-to-failure data are broader at higher temperatures. The effect of broadening a Weibull probability density function while keeping the characteristic value constant as observed for all DC data, and all AC data below 383K, is shown below in figure 6.10.

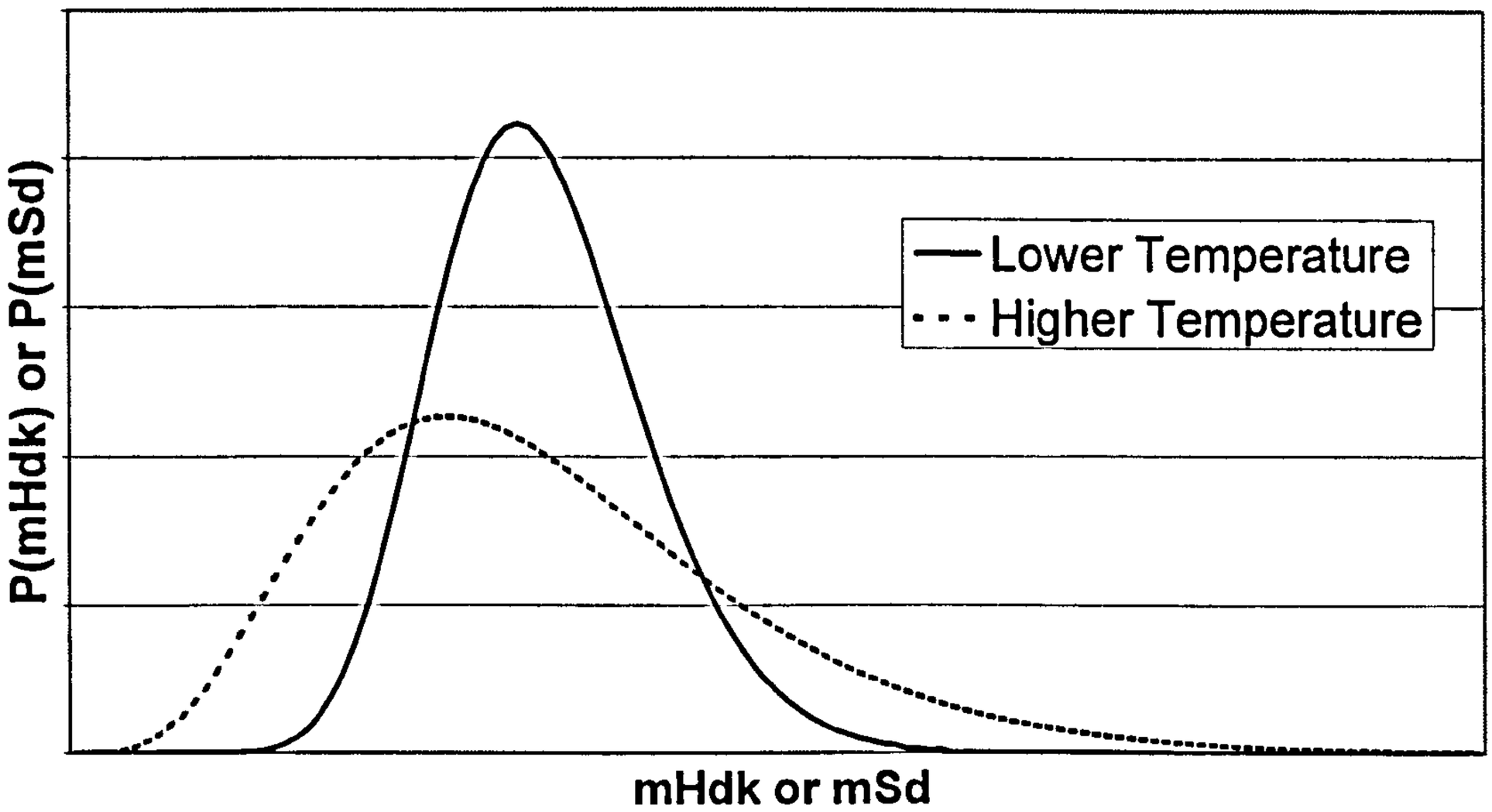

Figure 6.10

Figure 6.10 shows mH_{dk} or mS_d on the x-axis, and the Weibull probability density function $P(mH_{dk})$ or $P(mS_d)$ on the y-axis. $P(mH_{dk})$ is effectively the probability of finding a particular value of mH_{dk} in an infinite number of specimens. It can be seen that broadening the probability density function has the effect of increasing the value of $P(mH_{dk})$ or $P(mS_d)$ for low values of mH_{dk} and mS_d. In other words, the probability of finding a range of values of mH_{dk} and mS_d below the characteristic value, α, is increased. This increase must be balanced out by an increase in the probability of a range of mH_{dk} or mS_d values above α, since α remains fixed.

It should be noted that the probability density functions in figure 6.10 are for the ***minimum*** activation energy parameters in specimens aged at a particular experimental condition. An increased probability of small mH_{dk} or mS_d values means that there is an increased likelihood of finding specimens in which the lowest barrier to ageing is very small. Figure 6.10 cannot reveal information about the general shape of the global distribution of H_{dk} or S_d distributions within individual specimens, since the $P(mH_{dk})$ and $P(mS_d)$ functions describe only the probability density of the ***minimum*** H_{dk} and ***minimum*** S_d values from specimen to specimen. Narrow mH_{dk} and mS_d distributions

such as those observed, however, mean that the low value end of the global H_{dk} and S_d distributions must be very sharp.

Change in α with temperature

As well as a broadening of the minimum activation energy parameter distributions with T, the AC data shows a whole-scale movement of the mH_{dk} and mS_d distributions above 383-403K. Above this temperature range, the value of α starts to decrease with temperature. This was shown in figure 6.2 for mH_{dk} and figure 6.4 for S_d. The effect of reducing the characteristic value, α, of a Weibull probability density function is shown in figure 6.11. The value of β is the same for the two probability density functions shown.

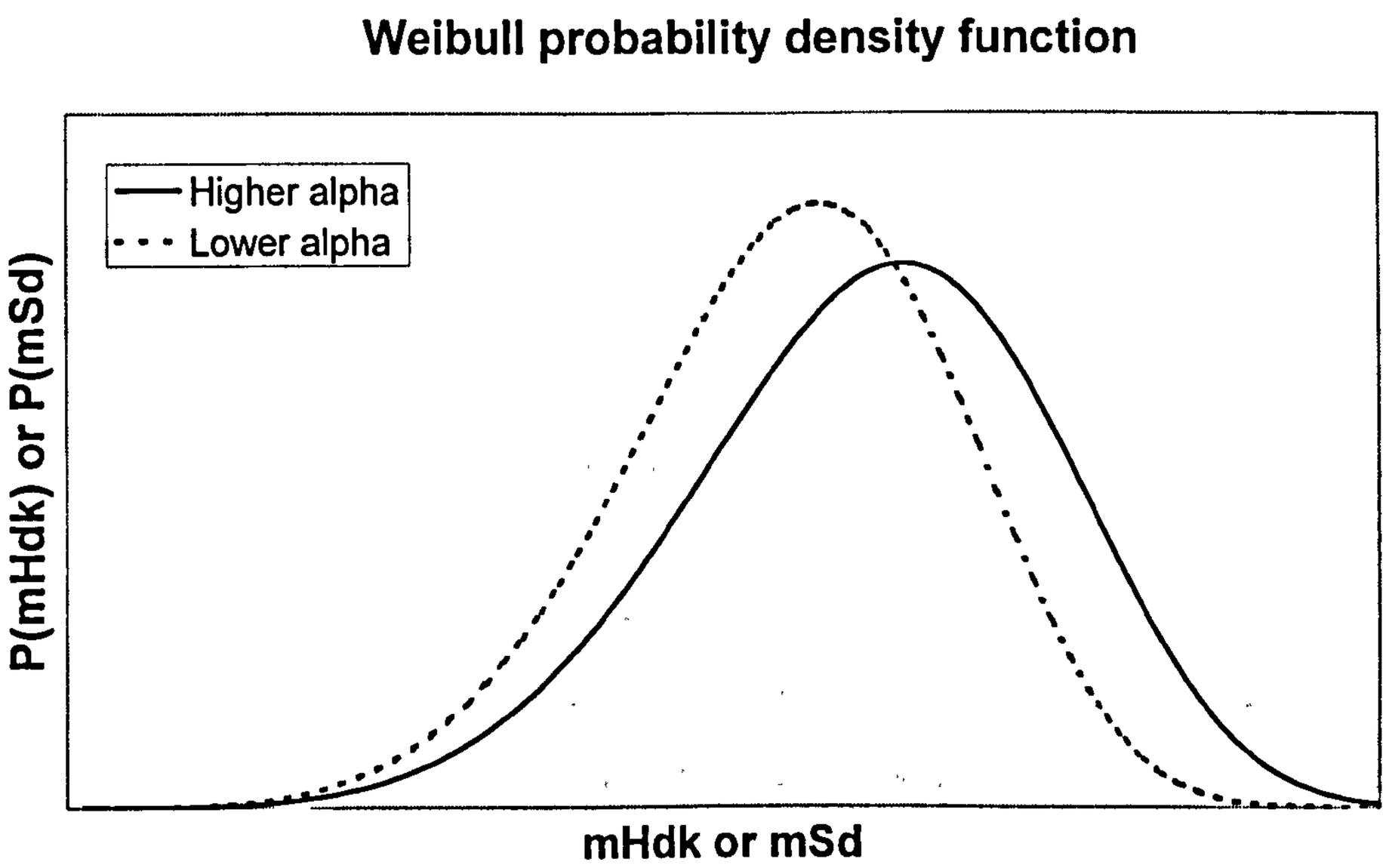

Figure 6.11

Figure 6.11 shows that decreasing the characteristic value of a distribution, α, shifts the whole probability density function to lower values of the variable. Here, this means that the probability of finding smaller mH_{dk} or mS_d values in any specimen increases significantly with temperature above 383-403K. Unlike a broadening of the distribution, there is no resultant increase in the probability of larger minimum barriers – the whole distribution moves to lower values.

Implications for the ageing process

The results provide evidence that ageing is a process whose barrier to ageing changes with temperature in the following way. Firstly, the likelihood of smaller minimum barriers to ageing increases steadily with temperature, as the distributions of minimum energy barriers broaden. This is independent of the fact that the barrier may be more easily overcome at increased T. Secondly, in the AC case above a temperature range of 383-403K, the likelihood of smaller barriers to ageing starts to increase more significantly, with a whole scale shift of the probability density function to lower values of minimum activation energy. This means that increasing T above 383-403K effectively reduces the minimum barrier to ageing in every specimen. Increasing T up to 383K for the AC data, and for all of the DC data effectively decreases the minimum barrier in some specimens, while increasing it in others. This may be explained if the ageing process is one in which rearrangement of polymer segments occurs, as suggested in, e.g. [11-14].

If ageing is a process where polymer chain segments rearrange, the activation energy of ageing must be an energetic barrier to conformational rearrangement of molecules. Such energy barriers form as the polymer solidifies. In the melt, polymer molecules have very small barriers to conformational rearrangement and the chains can move freely past one another. Barriers are then 'frozen in' as solidification occurs, so that below the glass transition temperature T_g (see Chapter 1), segmental motions cannot occur at all. Small groups of atoms will vibrate as they are heated, and the range of available motions will increase as temperature increases, but no viscous flow is possible.

Increasing the ageing temperature below T_g would therefore not reduce the minimum barrier to ageing in all specimens, but would increase the range of constrained motions available to polymer segments in each specimen. This increase in available motions may be responsible for increasing the range of observed minimum energy barriers by making conformational rearrangements easier at some sites and more difficult in others.

The barrier to segmental rearrangements would be expected to be reduced in all specimens only at temperatures above the glass transition temperature. Increasing

temperature above T_g would make it easier for all polymer chain segments in amorphous regions to rearrange, and smaller mH_{dk} and mS_d values would therefore become more likely. This implies that the moieties, or chain segments, responsible for ageing become less and less physically constrained as the temperature increases above T_g. As a result, the polymer is no longer constrained to remain globally rigid, and plastic deformations may become possible.

Unfortunately, T_g is not known for the PET specimens aged to obtain the data used in this investigation. The glass transition region for PET, however, is generally quoted in the range 342-383K [15,16,17,18]. This could therefore explain the drop in the value of α for the mH_{dk} and mS_d distributions above 383-403K in the AC case, since this range is probably above T_g.

The moieties associated with this kind of ageing process are unlikely to be those situated within crystalline parts of the polymer, since these will be firmly bound by the crystalline structure, and therefore subject to the largest activation energies for any process involving physical rearrangements. The moieties responsible for ageing are also unlikely to be those deep in amorphous regions, since it has been found that the energy barriers in the DMM model have very similar magnitudes for specimens of different materials [19]. This similarity in the magnitude of H_{dk} and S_d found for many different materials implies that the chemical composition of the polymer does not make an appreciable difference to the activation energies involved in the ageing process. This is unlikely to be the case if it is moieties in the amorphous region that are important in ageing, since the morphology of these regions, and hence the barriers to conformational rearrangement of segments in them, will depend very strongly on the constituent molecule. The same is true of the crystalline regions – the chemical composition of crystalline parts of a polymer will have a large effect on the activation energy associated with freeing chain segments.

It therefore seems likely that the ageing process is characteristic of chain sections confined to lamella surfaces, which became only partly crystallised as the polymer cooled. These will be the chains in the polymer which will be most able to move freely once they are initially freed, since they are neither bound in a rigid crystalline structure, nor are they likely to be highly tangled as in the amorphous region.

The increased freedom of these chain sections produced during the ageing reaction may eventually be sufficient to remove the constraints that prevent their crystallisation imposed during solidification. Such constraints result from a rapid cooling of a polymer melt, when some or all of the polymer chains are not allowed sufficient time to assume their lowest energy configuration (see Chapter 1). As the barrier to ageing (*i.e.* the energy barrier to physical chain rearrangements) is reduced, the sections may crystallise. Low-density regions will therefore be generated in the neighbouring amorphous regions. Such low-density regions have long been associated with breakdown in polymers, through such processes as partial discharge.

Crystallisation with field and temperature

It is suggested above that the observed behaviour of minimum activation energy barriers is consistent with the ageing process being one involving physical rearrangements such as crystallisation of polymer segments situated on lamella surfaces. The possible effects of field and temperature on crystallisation are therefore briefly discussed below.

In the absence of any external stresses, crystallisation in a polymer can only occur in a temperature range between its glass transition temperature, T_g, and the temperature at which crystallites melt, T_m. T_g for the material investigated here, as for any other polymer, depends strongly on morphological factors such as the degree of crystallisation. T_g for amorphous PET is quoted as 340K in [15], and as between 343K and 383K in [18]. Semi-crystalline PET has a T_g quoted in the range 342-353K [15,16,17]. As mentioned above, T_g for the specimens used here is not known, but is likely to be in the range 340-383K. The value of T_m for any polymer is dependent on the crystallite size, and this depends on the solidification conditions of the polymer as explained in chapter 1. This is also unknown for the particular films used here, but is usually quoted above 533K [e.g. 15]. Crystallisation is therefore only possible between these limits. For example, in [16], crystallisation in PET has been observed to occur above 363K and below 503K.

It has been suggested that in a polymer subject to a mechanical stress, the chains will be able to crystallise at lower temperatures than normal – i.e. below 363K for PET.

This effect has been observed [17] for a macroscopic compressive mechanical stress applied to a PET specimen, where crystallisation was observed just above a quoted Tg of 343K. In [17], a mechanical tension is thought to align polymer chains in such a way as to reduce the energy barrier to crystallisation.

It is possible that a similar effect may occur during electro-thermal ageing of PET. In this case, an applied electrical field may reduce the temperature at which crystallisation can occur due to the local mechanical stress caused by trapped space charge. In this investigation, AC data is available at 333K and 383K, but not in-between. Both Tg and the onset of unstressed crystallisation may occur between these limits, so it is not possible to tell at what point the ageing energy barrier begins to fall. Nonetheless, the results are consistent with the ageing process being one of crystallisation of lamella surface chains causing a free volume increase in neighbouring amorphous regions.

Difference between AC and DC results

In the DC case, all the data is above 373K and hence probably above the value of Tg for PET. However, no reduction in the characteristic barrier value with temperature is observed. It may be that the reason for this is that the ageing process is different in the AC and DC cases. However, the constancy of values of the other DMM parameters between AC and DC is contrary to this (see chapter 2).

Another possibility is that frequency effects may cause the temperature at which the energy barrier begins to fall to be different between the AC and the DC cases. The much larger values of mH_{dk} found for the DC case and the fact that mS_d is very close to zero suggest that the barrier in the DC case is related to site rearrangements, whereas in the AC case it is related to group rearrangements [11]. The increased entropy barrier in the AC case may therefore arise from the need to arrange more atoms in a particular configuration than in the DC case for the ageing reaction to proceed.

It is therefore possible that the difference between AC and DC ageing lies only in the number of polymer monomer units rearranging, and not in the process itself. The more localised the individual rearrangements are, the less likely they are to be affected by temperature. Possibly this reflects the fact that in AC fields the whole of the lamella

surface may be driven to fluctuate, whereas in DC fields it will be frozen in a specific energy configuration – rearrangement of which requires displacement of the most 'locked in' site.

6.3 Application to Power Cable Data

The time-to-failure data used here are those also used in chapter 5 [20]. Cables insulated with extruded XLPE were aged under nine different experimental conditions as described in the previous chapter. In each experiment, twelve cables were aged under the same conditions, and the tests stopped after eight of the twelve had failed. In one case (V=34.6kV and T=348K) only seven cables had failed when the experiment was stopped.

6.3.1 Method

The method to get minimum H_{dk} and minimum S_d distributions for each experimental condition is necessarily different to the method used in the film case. At each experimental V and T condition, each cable shell (as defined in chapter 4) experiences the same temperature, T, but a different field, E. Distributions of mH_{dk} and mS_d were therefore only obtainable for each value of applied voltage, V, (for which there was a TTF value) rather than for each E experienced by a particular shell.

At each experimental condition, MATHCAD was used to find the best value of H_{dk} or S_d to fit a time-to-failure at that condition. To achieve this, the minerr function was used to minimise the error in equation 6.3 for each TTF point. This was done by making equation 6.3 a constraint in a 'given' block and making either H_{dk} or S_d the argument of the minerr function. (See chapter 3 for more details on the minerr function)

$$TTF = \left[\frac{N}{\sum_{r_i=1}^{N} L_i} \right]^{\frac{1}{\beta}} \qquad 6.3$$

In equation 6.3 TTF is the time to failure of a cable aged at one particular voltage and temperature condition. N is the number of shells making up the cable insulation, and N=100 was used here for the same reasons as outlined in the last chapter. L_i is the DMM lifetime expression of the shell situated at radius r_i. L_i is therefore a function of each of the model parameters as shown in the last chapter. As for the film case, all DMM parameter values not under investigation were assigned the values found from fitting the DMM model to the B63 data. These are the values shown in table 1 of chapter 5. Also as in the thin film case, mH_{dk} and mS_d distributions were obtained independently; the value of H_{dk} from the last chapter was used in the L_i expressions when using the minerr function to find an optimal value for S_d and vice versa.

Using this method, a distribution of mH_{dk} and a distribution of mS_d values was obtained for each of the nine experimental conditions for which data were available. The distributions contained eight values (except at V=34.6kV and T=348K which only contained seven), since times-to-failure were recorded for eight cables at each condition. As mentioned in chapter 4, lifetime data of this type, where the ageing experiment is stopped before all specimens have failed is called top censored data. The resultant mH_{dk} and mS_d values were therefore also top censored, and the relevant Weibull equations were therefore used to get values for α and β of each distribution [6]. Distributions were generated in MATHCAD as above containing 10,000 values of mH_{dk} and mS_d for each experimental condition, and these were used to generate lifetime distribution curves.

6.3.2 Results

Section B3 of Appendix B contains graphs of experimental time-to-failure data with generated lifetime distributions at each of the nine experimental ageing conditions. An example is shown below:

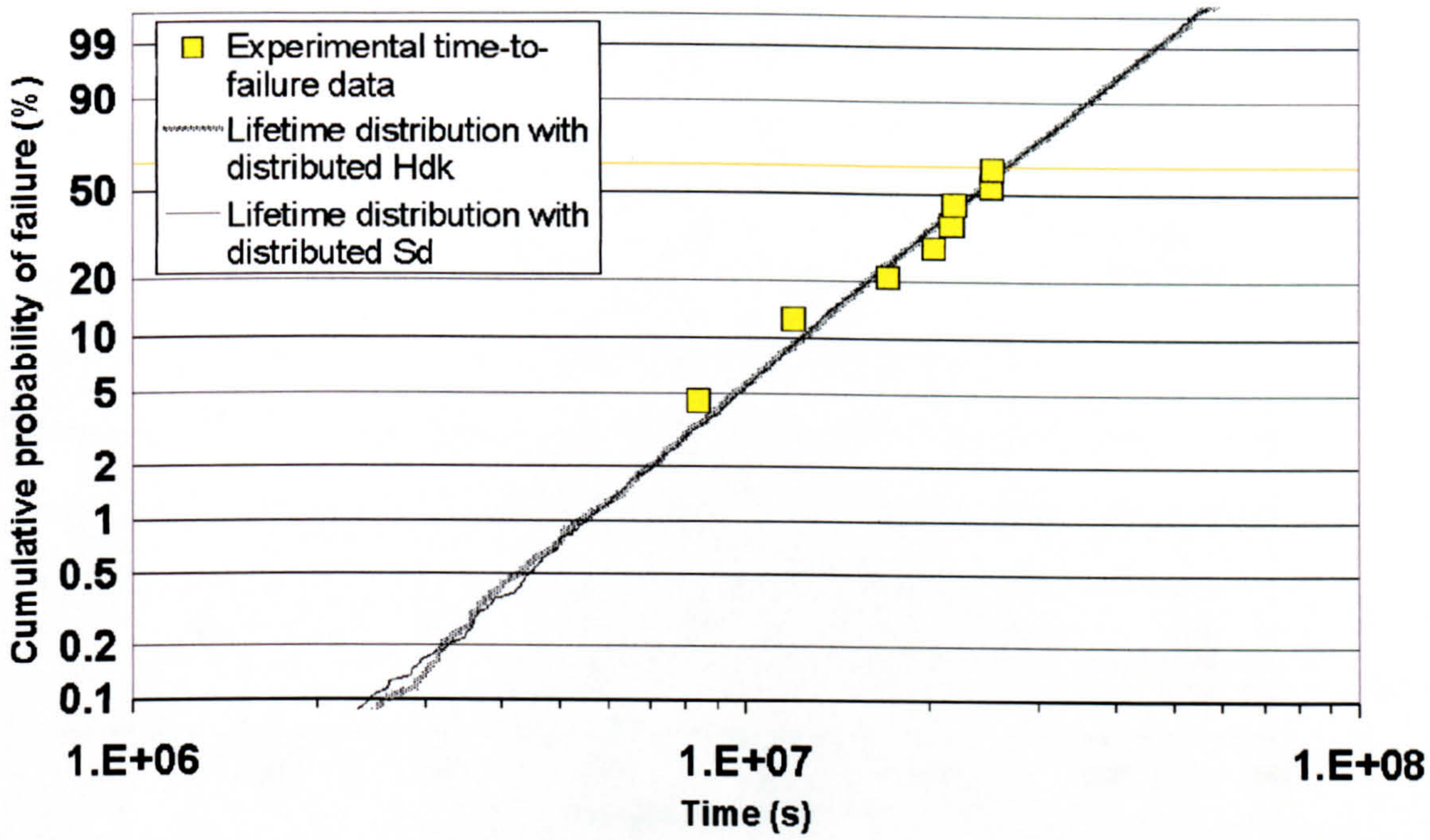

Figure 6.12

Figure 6.12 shows cumulative probability of failure on the y-axis against time in seconds on the x-axis. The square points are experimentally obtained cable times to failure. The thick grey line shown the lifetime distribution obtained from a distribution of H_{dk} values within the DMM model, while the thin black line shows the lifetime distribution resulting from a distribution of S_d values. The two lines are almost co-incident in figure 6.12 and this is also the case for the other experimental conditions as seen in Appendix B.

The changes in the values of α and β with applied voltage, V, and temperature, T, were plotted. These graphs are also presented in Appendix B. Figure 6.13 shows the variation in the β value of the nine mH_{dk} distributions with temperature, and 6.14 shows the same relationship for the mS_d distributions.

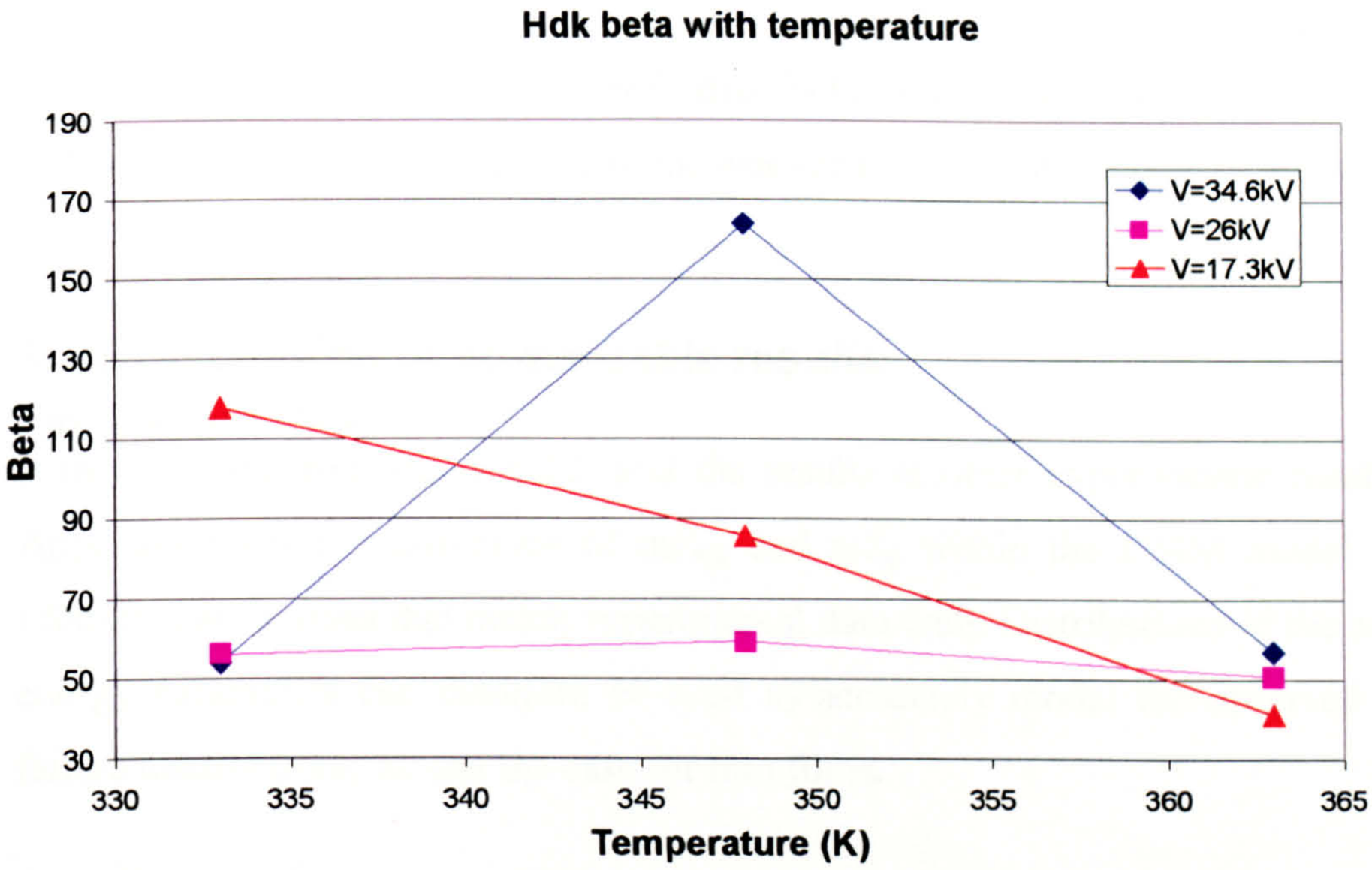

Figure 6.13

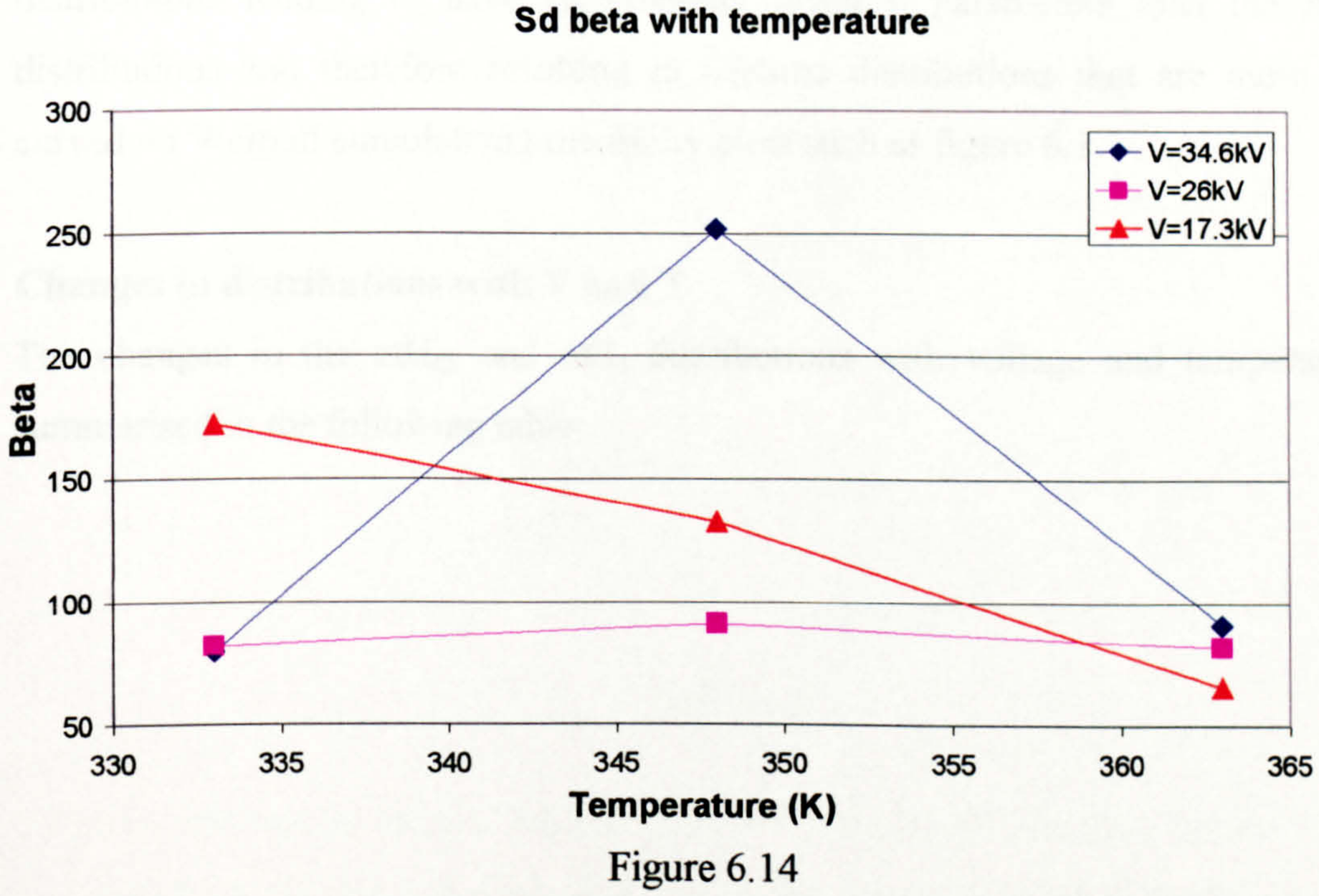

Figure 6.14

Figures 6.13 and 6.14 show variation in the shape parameters of the mH_{dk} and mS_d distributions respectively with temperature. The three lines represent β values at the three different test voltages. The shape parameters for the two sets of distributions can be seen to follow a very similar pattern, and neither shows the same trend with T at all voltages.

No trends in any of the mH_{dk} or mS_d distributions were seen with voltage, and very little change in the α of the distributions was seen with either voltage or temperature.

6.3.3 Discussion of power cable results

Fits to ageing Data

It can be seen from figure 6.12 (and the results at other experimental conditions in Appendix B) that distributions of mH_{dk} and mS_d within the DMM model result in lifetime distributions that match experimental data well. Distributions of the activation energy parameters can therefore be used to accurately model the observed time-to-failure distributions, as was the case for thin films.

In the cable case, the lifetime distributions generated by distributions of mH_{dk} and mS_d are very similar. This was not the case for the film results, with the AC mH_{dk} distributions tending to have significantly lower β parameters than the AC mS_d distributions and therefore resulting in lifetime distributions that are more sharply curved on Weibull cumulative probability plots such as figure 6.1.

Changes in distributions with V and T

The changes in the mH_{dk} and mS_d distributions with voltage and temperature are summarised in the following table:

		Cable mH_{dk} distributions	Cable mS_d distributions
Characteristic value of the distribution, α	Measured range of values	6500K - 6100K	$3.8x10^{-22}$J/K – $3.9x10^{-22}$J/K
	Behaviour with T	No consistent pattern for all applied V	No consistent pattern for all applied V
	Behaviour with V	No pattern	No pattern
Shape parameter of the distribution, β	Measured range of values	51-164	66-252
	Behaviour with T	No consistent pattern for all applied V	No consistent pattern for all applied V
	Behaviour with V	No pattern	No pattern

Table 6.2

The thin film results showed a broadening of the mH_{dk} and the mS_d distributions with temperature at all fields as discussed above. This was not found to be the case for the cable data, where the β parameters of the mH_{dk} and the mS_d distributions showed no consistent change with temperature at all applied voltages. At V=34.6kV and V=26kV, β for both the mH_{dk} and the mS_d distributions goes up and then down with increasing temperature. The value of β only decreases with temperature (as for the thin film case) for the V=17.3kV data.

The cable data do not, therefore, actively support the theory outlined in the discussion of the thin film section. However, there are several reasons why the distributions of mH_{dk} and mS_d might show different behaviour between the thin film and the cable cases.

Firstly, the time to failure data from the cable experiments is top censored. The mH_{dk} and mS_d distributions must also therefore be top censored – the largest values of mH_{dk} and mS_d from each distribution are effectively not present. This makes estimation of the α, and particularly the β parameters of the distributions very difficult. The β parameter is particularly difficult to calculate since the absent larger values in each of the distributions could significantly change the spread of the probability density function, or equivalently could significantly change the slope of the best-fit line through the cumulative probability plot. Secondly, estimation of the α and β parameters of the cable mH_{dk} and mS_d distributions is less accurate than in the film case due to the fact that fewer specimens are tested in each ageing experiment.

Both of these points mean that each of the β parameters plotted in figures 6.13 and 6.14 are much less reliable than the β parameters from the thin film ageing experiments. The behaviour they exhibit with V and T is therefore also not so reliable as for the thin film case.

Another problem with the mH_{dk} and mS_d distributions is that only one value for mH_{dk} or mS_d is found for each time-to-failure –i.e. only one value of mH_{dk} or mS_d for each aged cable. This assumes that the value of mH_{dk} or S_d is the same for every cable shell, and therefore that the material throughout each cable is morphologically and chemically identical. This may well not be the case. As mentioned previously, the by-products from manufacture and curing processes may be unevenly distributed both radially and along the length of the cable [1]. This means that the best-fit mH_{dk} or mS_d may also vary, since such products are likely to influence the barrier to ageing. Each value of mH_{dk} or mS_d in the distributions may therefore not be reliable – another reason that the cable α and β values may not be dependable.

A physical reason for the difference in results between the PET and the XLPE data could be that many of the XLPE polymer chains are likely to be physically constrained

by the cross-links between them. This would make perfect crystallisation of chain segments much more difficult in many areas of the polymer. Cross linking also means that the glass transition is a less significant process in the material, since the links between chains mean that polymer segments are locked into place more firmly.

For all these reasons it may not be very significant that the cable data do not back up the theory outlined in the discussion of the thin films results.

6.4 Summary

For AC and DC ageing of PET films, and for AC ageing of XLPE cable insulation, activation energy parameters within the DMM model can be distributed to successfully model time-to-failure distributions. The resulting time-to-failure distributions fit experimental failure data well, though in some cases they deviate significantly from Weibull distributions.

The changes in the parameter distributions for the thin film data support the theory that the ageing process is one involving conformational rearrangements of polymer segments. The barrier to ageing therefore reduces with temperatures above 383-403K. The distributions from the cables do not show the same variation with temperature. However, the accuracy of the values obtained to describe the distributions in this case is such that this discrepancy may not be significant.

7. Discussion and future work

7.1 Ageing models and fits to data

The fits to ageing data achieved by the models in chapters 3 and 5 are good considering the assumptions involved in the fitting methods. In both cases, one of the biggest assumptions is that the field strength throughout the material is as predicted by the equations derived in chapter 4. This is discussed further in 7.1.1 and 7.1.2 and 7.1.3.

One of the interesting results from the DMM model fittings in this thesis is that the value of b varies very little – the value for fitting to AC and DC films, and to XPLE cables was 0.4. In [1] values ranging from 0.4 to 0.6 are found for various polymeric systems. A similar value of b from material to material implies that the dependence of space charge magnitude and ageing on field is the same for all materials tested so far. It also implies that the electric field effect in ageing has close to a field-squared dependence, which is as assumed by the Lewis model. Further space charge measurements may help to confirm or disprove the hypothesis that space charge amount depends on the same power of applied field for all materials.

7.1.1 Electrical field strength distribution

For the cables the field was assumed to be given by equation 4.7, and for the thin films the field was assumed to be constant (equal to the applied voltage divided by the film thickness). In fact, any space charge present in either system must significantly alter the electrical field strength in its surrounding area, and this is not taken into account at all by the Lewis model.

In the Lewis model, E is assumed to accelerate ageing due to a tensile mechanical stress. This stress acts in directions orthogonal to the field, and its magnitude is proportional to E^2. Any space charge necessarily increases the value of E in a region, which will also increase the magnitude of the accelerating stress. Space charge is therefore likely to result in faster ageing and lower lifetimes than predicted.

In the DMM model, ageing is assumed to be accelerated by a local electrical field produced as a result of space charge concentrations generated by an applied electric field. Space charge is assumed to be present everywhere in the material, with the amount of charge in any region dependent on the value of E. The acceleration of ageing due to E is described by the expression C_dE^{4b} in the model, which is an approximation.

It can be seen that a more accurate or reliable expression for the field in the material, E (for the Lewis model) or space charge dependence on E (for the DMM model) would lead to better lifetime prediction. Experimental determination of the electrical field distribution in a polymeric material – even in the absence of injected space charge, if this is possible - is not straightforward. Any measuring electrodes introduced into a polymeric specimen must affect the resulting macroscopic electrical field distribution from the situation without electrodes. This would therefore be a useful experiment, but a difficult one to design.

In the case of the DMM model, an expression describing the space charge distribution dependence of applied fielding a system would very useful, since the C_dE^{4b} term could then be replaced entirely as discussed in section 4.3.1. In either case, the characterisation of space charge formation and behaviour with applied field magnitude, frequency, material, specimen geometry and temperature is an area of great interest. Experimental techniques for measurement of space charge in various materials in the form of films, cables and under both AC and DC conditions are currently under investigation by many research groups - some recent literature includes *e.g.* [2-8]. It therefore looks hopeful that a better understanding of space charge behaviour may be achievable within the next few years.

7.1.2 'Intrinsic' space charge

Space charge in this thesis has been regarded as trapped charge that has entered a polymeric specimen - either by ionisation of an impurity contained by the polymer, or by injection into the polymer from electrodes. However, in any situation in which there is a temperature or field gradient across an insulator, and a conduction process with current density j, there must be an 'intrinsic' charge distribution in addition to space

charge generated by injection and ionisation. This space charge distribution must contribute to the electrical field and space charge profiles that actually occur in cables.

The existence of this 'intrinsic' space charge can be seen by considering Poisson's law, which gives that

$$\nabla \bullet D = Q \qquad 7.1$$

Where Q is a charge density and D is electric displacement, given by

$$D = \varepsilon_r \varepsilon_0 E = \frac{\varepsilon_r \varepsilon_0 j}{\sigma} \qquad 7.2$$

Above, ε_r is the relative permittivity of the material, ε_0 is the permittivity of free space, j is current density and σ is the conductivity of the material.

Equations 7.1 and 7.2 give

$$\nabla \bullet \left(\frac{\varepsilon_r \varepsilon_0 j}{\sigma} \right) = Q \qquad 7.3$$

Assuming that ε_r is constant throughout the material, and substituting resistivity, ρ for $1/\sigma$, this simplifies to

$$\varepsilon_r \varepsilon_0 \left(\rho \nabla \bullet j + j \nabla \rho \right) = Q \qquad 7.4$$

And assuming a steady state (∇.j=0), this gives

$$\varepsilon_r \varepsilon_0 j \nabla (\rho) = Q \qquad 7.5$$

Equation 7.5 means that in any region where a spatial variation in resistivity exists, a corresponding space charge, Q must also exist. In chapter 4 an expression for ρ was given that depends on both T and E. It therefore follows that in any specimen where E and T are not spatially constant, such as in cable insulation, a space charge density must also exist. This is taken into account in chapter 4, since in the DC case the E and T dependences of ρ are included in the DC field profile distribution.

The idea of this 'intrinsic' space charge is discussed further in [9,10], which derive expressions for the field and space charge profiles in the case that ρ is dependent only

on temperature. The 'intrinsic' space charge due only to a thermal gradient is experimentally observed in [11]. This is achieved by comparison of the space charge profiles in isothermal PE plaques, and plaques subject to a temperature gradient, as measured by the LIPP method. The situation is more complex again if ε_r is not assumed to be constant, since equation 7.3 shows that any gradient the value of ε_r must also contribute to Q. It is shown in [9], however, that variation in ρ is likely to be the dominant effect for DC conditions.

7.1.3 Changes with time

In all cases in this thesis, only steady state situations have been considered. In other words it is assumed that neither the field, temperature nor space charge distributions in a material vary during the time over which the specimens are aged. In fact, on the application of a voltage across any specimen, a finite time will be taken before the electrical field stabilises, and in the case of cables under load, the temperature distribution will necessarily take time to reach equilibrium. This is particularly important since the load and voltage applied to cables in service may be switched on and off according to demand, or if part of the power delivery system becomes faulty.

In terms of ageing, it may be that the time over which such changes are effective is much smaller than the overall time to failure, and can therefore be ignored. If the time over which changes happen cannot be ignored, however, it would be necessary to know how both E and T varied with time. Expressions describing the change with time of E and T are likely to be complicated; the electrical field distribution in cable insulation during application of voltage is discussed in [12].

The question of how to then incorporate time-dependent E and T expressions into ageing models is not straightforward. A time-weighted average of field and/or temperature in the DMM or Lewis expressions may be applicable, but further experiments may need to be carried out to try to ascertain the effects of ageing a specimen at several different field or temperature levels.

7.2 Fits to cable data and volume effects

7.2.1 Fits to cable data

In chapter 5, the DMM model is fitted to cable lifetime data using the expression developed in chapter 4. Any lifetime model could have been used instead of the DMM model, since the method developed in chapter 4 can be used with any relevant lifetime expression for each shell. The method developed in chapter 4 could also be used for other geometries where E and/or T are not constant, as long as the system can be split into equal volumes over which E and T can be considered constant and can be measured or calculated.

The fits to data found in chapter 5 are good when the underlying approximations are taken into account. The expression used for E is one of the biggest assumptions involved, as mentioned above. Another source of potential error in parameter values is in the grid fit method used to find parameter values. The disadvantage of using a fitting method of this type is that it is difficult to distinguish between local and global minima in the error value. Steps were taken to try to avoid this by using many different parameter ranges to check that the solutions found were similar, and therefore likely to be accurate. An advantage of a grid search method, however, is that the initial guess values for the grid search method are not as crucial as for e.g. the Levenberg-Marquardt method used for the thin film data and in [1]. Parameter values found using the Levenberg-Marquardt algorithm are very dependent on the initial guess values, so when using this method it is important to have confidence in the initial guesses.

The data used in chapter 5 was unusual, since the insulation of each cable was kept at constant temperature. Where a temperature gradient exists due to heating by a current, using equation 4.1 to describe temperature with radius may affect the quality of fits achieved to cable data. It would be interesting to try the method on data from cables aged this way, but unfortunately none is available at the present time.

The effect of fitting to DC rather than AC cable data is also unknown, since cable ageing data available was only from AC tests. It seems likely that good fits to data may be harder to achieve in the DC case for two reasons. One is that under DC, the insulation is likely to suffer more space charge injection that in the AC case. The field

variation is therefore likely to be more radically different from theory in the DC case. However, if this were an important effect, significantly better fits might also be expected in the AC thin film data than for the DC film data in chapter 3. In fact this was not the case, as the DMM predictions for the thin films fell within just over half the 90% confidence limits for both AC and DC data.

The second reason is that the expression for E in the DC case is much more complex than the AC expression, as shown by their derivations in chapter 4. The DC expression contains more approximations than the AC expression because of the way it is derived – to try to include the effect of a varying value of ρ - and is therefore likely to be less accurate.

7.2.2 Volume effects

The possible effects of volume on the DMM parameters and on ageing are discussed in 5.4.2. It is difficult to reach firm conclusions about the effect of volume given that the comparisons are made between specimens of different materials as well as different volumes. However, from the limited data available, it seems that the two parameters most affected by volume in the DMM model are A* and C_d. A* appears to decrease for specimens of larger volumes, while C_d increases. Smaller A* implies that volume affects ageing because in a larger volume there is increased likelihood of finding areas in which only very few moieties need to be in the aged state for a breakdown process to begin. Large C_d for large volumes means an increased probability of finding areas in which space charge can have a large affect on the surrounding areas.

It therefore seems that a large volume of polymer may be more likely to fail than a smaller volume under the same conditions due to two related factors. One is that a larger volume is more likely to contain areas where a small amount of ageing can lead to breakdown. The second is that is might also contain more regions where space charge can set up larger than average electromechanical strains. More work is needed to be able to draw more firm conclusions about the role of volume in ageing, and two suggestions are made below as to how this could be achieved.

In chapter 6 the DMM model was fitted to cable data using equation 4.35. This equation was derived such that the parameter values did not depend on shell volume, so that parameter values could be compared easily to those from other fittings. It would also be possible to use equation 4.31 in place of equation 4.35. In this case, the parameter values obtained would depend on the shell volume through N, the number of shells used (see chapter 4). Carrying out a fit like this for a variety of values of N may then produce interesting results, as the effect of shell volume on the parameter values may be revealed. This could help to further the understanding of the effect of volume on ageing.

However such fittings are not straightforward, and the grid search method employed in this investigation may not be rigorous enough to be able to make meaningful comparisons between parameters produced using different values of N. A method such as a simulated annealing approach may be more appropriate [e.g. 13]. Simulated annealing fitting methods converge very slowly to a solution by choosing random parameter shifts from within a very wide range, and calculating an error function. Such methods take up considerable time and computing power, but represent a possible area of future work.

A more direct way of looking at the effect of volume would be to carry out ageing tests where volume was the main variable. Fitting and ageing model to B63 data from such experiments would then show any dependence on volume. Such data is not available at the present time, and takes a lot of time and money to produce.

7.3 Statistical variations in parameter values

In chapter 6 it was shown that distributions in H_{dk} and S_d within the DMM lifetime equation can be used to accurately model lifetime distributions for both thin film and cable ageing data. This is not necessarily so for all of the parameters within the DMM equation – for instance in [14,15] it can be seen that distribution of the C_d parameter does not generally give such a good fit as seen here.

H_{dk} and S_d do not affect the threshold field of a specimen according to the DMM model. However, it is interesting to note that assuming a distribution of parameters that do have an affect on the field threshold of ageing can have interesting results. A field

threshold exists, since at some fields, too few moieties will be in the aged state at thermal equilibrium for breakdown to occur. This field threshold depends on the DMM parameters A^*, K_d and C_d. If any of these parameters are distributed from specimen to specimen, this means that the threshold field for ageing is effectively also distributed – i.e. must be different for each specimen. Since the threshold for one particular set of specimens is generally derived from fitting to the B63 failure times, specimens within that set with smaller field thresholds than the 'typical' one may be seen to fail below the derived threshold. This is discussed further in [15], and may help to explain why experimental evidence for a field threshold is hard to produce.

As discussed in chapter 6, changes in the distributions of H_{dk} and S_d with field and temperature seem to indicate that ageing may be a process whereby polymer chain segments on lamella surfaces gain sufficient energy to crystallise. In doing so, they assume a denser configuration, and must therefore create regions of low density in the region they originally occupied. Such areas have long been associated with breakdown through processes such as partial discharge and even mechanical cracking.

It would be very interesting to try to find experimental evidence for a process of this type. Essentially this would involve looking for changes in the structure of a polymeric specimen after ageing. In [16], various techniques are used to investigate structural changes in PE and XLPE after ageing, but the area of particular interest in the investigation is the interface between the polymer and the electrode. The techniques used are therefore primarily surface techniques, which cannot reveal much information about physical changes in the bulk of the specimen.

The particular mechanism referred to above – that of crystallisation of polymer segments during ageing would be particularly interesting to investigate. Methods for investigating the degree of crystallinity of a material include X-ray diffraction, differential scanning calorimetry, density measurement techniques and infrared and Raman spectroscopy [17]. However, the change in degree of crystallinity on ageing is likely to be extremely small, and may also be very localised. Experiments to measure the effect would therefore have to be extremely sensitive, and it may be that it is not possible to experimentally measure such small changes at all.

8. Conclusions

Both of the models investigated in this thesis can be successfully fitted to characteristic lifetime data from ageing experiments involving thin films. The models can be simultaneously fitted to data from many different experimental conditions to give parameter values that have no dependence on the magnitude of the ageing field or temperature. The models are mathematically similar, and both consider ageing to be a thermally activated process that is accelerated by the application of an electrical stress. The mechanism by which an electric field is assumed to accelerate ageing is different in each case.

The DMM model can be fitted to characteristic lifetime data from ageing experiments involving cable insulation, where the field and temperature are not spatially constant. The method developed to do this could equally well be used with any other ageing model or for other insulation geometries where the field and temperature vary.

Parameter values obtained from fitting the DMM model to cable data show no large changes in magnitude from those pertaining to thin film ageing data. However, small differences in, for example, the activation energy parameters with volume or material can have a large effect on the lifetime. The effect of specimen volume on ageing is still poorly understood, and requires more research.

Narrow distributions of activation energy parameters in the DMM model can successfully model the time-to-failure distributions observed experimentally for both thin films and cables. The resulting models of time-to-failure distributions predict a lifetime distribution that matches the observed distributions of lifetime data. The predicted distribution does not retain the Weibull form over the whole lifetime range.

References

Chapter 1

[1] 'The Incorporation of Space Charge Degradation in the Life Model for Electrical Insulating Materials' by L.A. Dissado, G. Mazzanti, G.C. Montanari. IEEE Transactions on Dielectrics and Electrical Insulation Vol 2, No 6, 1995. pp1147-1158

[2] 'A new model for Electrical Ageing and Breakdown in Dielectrics' by T.J. Lewis, J.P. Llewellyn, M.J. van der Sluijs, J. Freestone, R.N. Hampton. IEEE DMMA 1996. pp.220-224

[3] 'Electrical Ageing of Extruded Dielectric Cables – a physical model' by J.L. Parpal, J.P Crine and C. Dang. IEEE Transactions on Dielectrics and Electrical Insulation Vol 4 No 2 April 1997, pp 197-209

[4] 'A general approach to the endurance of electrical insulation under temperature and voltage' by L. Simoni. IEEE Transactions on Electrical Insulation Vol EI-16 No 4 August 1981, pp277-289

[5]'Electrical Insulation Deterioration Treated as a Chemical Rate Reaction' by T.W. Dakin. AIEE transactions Vol 67, 1948, pp113-122

[6] 'A Space-charge Life Model for AC Electrical Aging of Polymers' by G. Mazzanti, G.C. Montanari, L.A. Dissado. IEEE Transactions on Dielectrics and Electrical Insulation Vol 6, No 6, 1999. pp864-875

[7] 'Thermoelectric Aging of Cable Grade XLPE' by C.L. Griffiths, J. Freestone and R.N. Hampton. IEEE ISEI 1998. pp.578-582

[8] 'Discussion of space-charge life model features in dc and ac electrical aging of polymeric materials' by L.A Dissado, G. Mazzanti, G.C. Montanari. IEEE Annual report CEIDP, 1997. pp36-40

[9] 'Solid State Physics' by J.R. Hook and H.E. Hall. Published by John Wiley and Sons Ltd. 1996. ISBN: 0 471 92805 4

[10] 'Electrical degradation and breakdown in polymers' by J.C. Fothergill and L.A. Dissado. Published by P. Peregrinus for IEE, London, 1992. ISBN: 0 86341 196 7

[11] 'Polymer Chemistry An introduction' by R.B. Seymour and C.E. Carraher Jr. Published by Marcel Dekker, Inc. ISBN: 0-8247-6979-1.

[12] 'Chemical Crystallography' by C. Bunn. Published by Oxford University Press 1961. ISBN:

[13] 'Crystals – their role in nature and science' by C. Bunn. Published by Academic Press Inc. 1964.

[14] 'Glass structure by spectroscopy' by J. Wong and C.A. Angell. Published by Marcel Dekker, Inc, 1976. ISBN: 0-8247-6468-4

[15] 'The structure of non-crystalline materials' by Y. Waseda. Published by McGraw-Hill Inc, 1980. ISBN: 0-07-068426-X

[16] 'Investigation of the Structural Changes in LDPE and XLPE Induced by High Electrical Stress' by P.W.C. Sayers. PhD Thesis submitted to the University of Wales, September 2001.

[17] 'An introduction to polymer chemistry' by W.R. Moore. Published by University of London Press, 1963.

[18] 'Anelastic and Dielectric Effects in Polymeric Solids' By N.G. McCrum, B.E. Read and G. Williams. Published by Dover Publications, Inc. 1991. ISBN: 0-486-66752-9.

[19] 'The X-ray measurement of the Amorphous Content of Polythene Samples' by J.L. Matthews, H.S. Peiser and R.B. Richards. Acta Crystallographica 1949 Vol 2, p85-90.

[20] 'Polymer chemistry: an introduction' by G. Challa. Published by Ellis Horwood, 1993. ISBN: 0134896912.

[21] 'The micro-physics of charge in solid dielectrics' By T.J. Lewis. Published in 'Space Charge in Solid Dielectrics' by The Dielectrics Society Edited by J.C. Fothergill and L.A. Dissado. ISBN: 0-9533538-0-X

[22] 'The pulsed-electro-acoustic method for the measurement of the dynamic space charge profile within insulators' by J.M. Alison. Published in 'Space Charge in Solid Dielectrics' by The Dielectrics Society Edited by J.C. Fothergill and L.A. Dissado. ISBN: 0-9533538-0-X

[23] 'Pulsed Electroacoustic Method For Measurement Of Space-Charge Distribution In Power-Cables Under Both Dc And Ac Electric-Fields' by R.S. Liu, T. Takada, N. Takasu. J PhysD-Applied Physics 26 (6):pp. 986-993 , 1993

[24] 'Molecular modelling of electron trapping in polymer insulators' by M. Meunier and N. Quirke. Journal of Chemical Physics Volume 113, Number 1, July 2000. pp. 369-376

[25] 'Molecular modelling of electron trapping in polymer insulators: Chemical defects and impurities' by M. Meunier and N. Quirke. Journal of Chemical Physics Volume 115, Number 6, August 2001. pp 2876-2881.

Chapter 2

[1] 'The Incorporation of Space Charge Degradation in the Life Model for Electrical Insulating Materials' by L.A. Dissado, G. Mazzanti, G.C. Montanari. IEEE Transactions on Dielectrics and Electrical Insulation Vol 2, No 6, 1995. pp1147-1158

[2] 'The Role of Trapped Space Charges in the Electrical Aging of Insulating Materials' by L.A. Dissado, G. Mazzanti, G.C. Montanari. IEEE Transactions on Dielectrics and Electrical Insulation Vol 4, No 5, 1997. pp496-506

[3] 'Discussion of space-charge life model features in dc and ac electrical aging of polymeric materials' by L.A. Dissado, G. Mazzanti, G.C. Montanari. IEEE Annual report CEIDP, 1997. pp36-40

[4] 'A Space-charge Life Model for ac Electrical Aging of Polymers' by G. Mazzanti, G.C Montanari, L.A. Dissado. IEEE Transactions on Dielectrics and Electrical Insulation Vol 6, No 6, 1999. pp864-875

[5] 'A new model for Electrical Ageing and Breakdown in Dielectrics' by T.J. Lewis, J.P. Llewellyn, M.J. van der Sluijs, J. Freestone, R.N. Hampton. IEEE DMMA 1996. pp.220-224

[6] 'Ageing – A Perspective' by T.J. Lewis. IEEE Electrical Insulation Magazine, 2001. pp 6-16

[7] 'Electrokinetic properties of metal-dielectric interfaces' by T.J. Lewis, J.P. Llewellyn, M.J. van der Sluijs. IEE Proceedings-A Vol 140, No 5, September 1993. pp.385-392

[8] 'Electrically induced mechanical Strain in Insulating Dielectrics' by T.J. Lewis, J.P. Llewellyn, M.J. van der Sluijs. IEEE Annual report CEIDP, 1994. pp 328-333.

[9] 'Electromechanical Effects in XLPE Cable Models' by T.J. Lewis, J.P. Llewellyn, M.J. van der Sluijs, J. Freestone, R.N. Hampton. IEEE ICSD 1995. pp. 269-273.

[10] 'Electric Field-Induced Viscoelastic Changes in Insulating Polymer Films' by P. Connor, J.P. Jones, J.P Llewellyn and T.J. Lewis. IEEE CEIDP 1998, pp27-30.

[11] 'Thermoelectric Aging of Cable Grade XLPE' by C.L. Griffiths, J.Freestone and R.N. Hampton. IEEE ISEI 1998. pp.578-582

[12] 'Investigation of the Structural Changes in LDPE and XLPE Induced by high Electrical Stress' by P.W. Sayers, T.J. Lewis, J.P Llewellyn and C.L. Griffiths IEE Conf Pub No 473 DMMA 2000. pp. 403-407

[13] 'The Importance of Mechanical Properties for Increasing the Electrical Endurance of Polymeric Insulation' by C.L. Griffiths, S. Betteridge, J.P. Llewellyn and T.J. Lewis. IEE Conf Pub No 473. DMMA 2000 pp. 408-411

[14]'Electrical Ageing of Extruded Dielectric Cables – a physical model' by J.L. Parpal, J.P. Crine and C. Dang. IEEE Transactions on Dielectrics and Electrical Insulation Vol 4 No 2 April 1997, pp 197-209

[15]'A Molecular Model to Evaluate the Impact of Aging on Space Charges in Polymer Dielectrics' by J.P. Crine. IEEE Transactions on Dielectrics and Electrical Insulation Vol 4 No 5 October 1997, pp487-495

[16]'A general approach to the endurance of electrical insulation under temperature and voltage' by L. Simoni. IEEE Transactions on Electrical Insulation Vol EI-16 No 4 August 1981, pp277-289

[17] 'Electric strength of Polymers' by J. Artbauer. JPhys D: Appl Phys. 29, 1996. pp. 446-456

[18] 'Electrical Insulation Deterioration Treated as a Chemical Rate Reaction' by T.W. Dakin. AIEE transactions Vol 67, 1948, pp113-122

[19] Charge transport in polymers' by T.J. Lewis. Annual Report of the Conference on Electrical Insulation and Dielectric Phenomena 1976. pp 533-561

[20] 'Charge transport, charge injection and breakdown in polymeric insulators' by T.J. Lewis. Journal of Physics D Vol 23, 1990, pp1469-1478

[21] 'The Micro-Physics of Charge in Solid Dielectrics' by T.J. Lewis. Proceedings of the Annual Meeting of the Dielectrics Society. Published by The Dielectrics Society 1998. ISBN: 0-9533538 0 X

[22] 'A mechanical origin for electrical ageing and breakdown in polymeric insulation' by P. Connor, J.P. Jones, J.P. Llewellyn and T.J. Lewis. IEEE International Conference on Conduction and Breakdown in Solid Dielectrics 1998. pp434-438

[23] 'Investigation of the Structural Changes in LDPE and XLPE Induced by High Electrical Stress' by P.W.C. Sayers. PhD Thesis submitted to the University of Wales, September 2001.

[24] 'Interim report on Project entitled: 'Electromechanical endurance model and failure in High Voltage Cables' Project No W 01/03/01' by C.L Griffiths for BICC Cables Ltd.

[25] 'Short-term Techniques for the Inference of Electrical Threshold of PET' by G. C. Montanari, I. Ghinello, A. Motori, S. Gubanski, D. Das Gupta. IEEE Transactions on Dielectrics and Electrical Insulation, Vol 5, No 1, Feb 1998. pp. 148-153.

[26] 'The electrical degradation threshold of polyethylene material, investigated by space charge and conduction current measurements' by G.C. Montanari. IEEE Transactions on Dielectrics and Electrical Insulation 2000. pp. 309-315.

Chapter 3

[1] 'Electrical degradation and breakdown in polymers' by J.C. Fothergill and L.A. Dissado. Published by P. Peregrinus for IEE, London, 1992. ISBN: 0 86341 196 7

[2] IEEE Draft Standard P930: 'IEEE Guide for the statistical analysis of electrical insulation breakdown data' by J.C. Fothergill

[3] 'Weibull statistics in dielectric breakdown; theoretical basis, applications and implications' by L.A. Dissado, J.C. Fothergill, S.V. Wolfe and R.M. Hill. IEEE Transactions on Electrical Insulation Vol EI-19 No 3 June 1984, pp227-233

[4] 'Theoretical basis for the statistics of dielectric breakdown' by L.A. Dissado. Journal of Physics D Vol 23, 1990, pp1582-1591

[5] 'Estimating the Cumulative Probability of Failure Data Points to be Plotted on Weibull and other Probability Paper' by J.C. Fothergill. IEEE Transactions on Dielectrics and Electrical Insulation Vol 25 No 3, June 1990, pp 489-492

[6] PET lifetime data – private communication from Stanislaw Gubanski.

[7] 'A Space-charge Life Model for AC Electrical Aging of Polymers' by G Mazzanti, G.C. Montanari, L.A. Dissado. IEEE Transactions on Dielectrics and Electrical Insulation Vol 6, No 6, 1999. pp864-875

[8] 'Discussion of space-charge life model features in dc and ac electrical aging of polymeric materials' by L.A. Dissado, G. Mazzanti, G.C. Montanari. IEEE Annual Report CEIDP, 1997. pp36-40

[9]'Numerical Recipes in FORTRAN, Second Edition' by W. H. Press, S.A. Teukolsky, W.T. Vetterling, B.P Flannery, Cambridge University Press, 1992. ISBN 0 521 43064 X

[10] 'Inverse Problem Theory' by A. Tarantola. Elsevier Science Publishers, 1987. ISBN 0 444 42765 1

[11] 'The Incorporation of Space Charge Degradation in the Life Model for Electrical Insulating Materials.' L.A. Dissado, G. Mazzanti, G.C. Montanari. IEEE Transactions on Dielectrics and Electrical Insulation Vol 2, No 6, 1995. pp1147-1158.

[12] 'The Role of Trapped Space Charges in the Electrical Aging of Insulating Materials' by L.A. Dissado, G. Mazzanti, G.C. Montanari. IEEE Transactions on Dielectrics and Electrical Insulation Vol 4, No 5, 1997. pp496-506

Chapter 4

[1] 'BICC Electrical Cables Handbook' Edited by G.F. Moore. Published by Blackwell Science Ltd 1998. ISBN: 0 632 04075 0

[2] 'Power and Communication Cables Theory and applications' Edited by R. Bartnikas and K.D. Srivastava. Published by IEEE Press, 2000.ISBN 0-07-135385-2

[3] 'Charges and Discharges in HVDC Cables – In particular in mass-impregnated HVDC cables' by M. Jeroense. PhD thesis submitted to the University of Delft and published by Delft University Press 1997. ISBN: 90-407-1438-X

[4] 'Thermal dielectric breakdown with cylindrical electrodes' by B.L. Beers and J.J .O'Dwyer. Journal of Applied Physics Vol 54 No 7, 1983, pp4083-4086

[5] 'Measurement of space charge in XLPE insulation under 50 Hz AC electric stresses using the LIPP method' by Y.F.F. Ho, G. Chen, A.E. Davies, S.G. Swingler, S.J. Sutton, R.N. Hampton, S. Hobdell. IEEE Transactions on Dielectrics and Electrical Insulation 9 (3), 2002 pp.362-370

[6] 'Pulsed Electroacoustic Method For Measurement Of Space-Charge Distribution In Power-Cables Under Both Dc And Ac Electric-Fields' by R.S. Liu, T. Takada, N. Takasu. Journal Of Physics D-Applied Physics 26 (6): Jun 14 1993 pp.986-993.

[7] 'Field Distribution in HVDC cables: dependence on insulating materials' by B. Aladenize, R. Coelho, J.C. Assier. Jicable 1999 pp557-560.

[8] 'Development of XLPE cable under DC voltage' by M. Satoru, T. Tanaka, H. Muto. Jicable 1999 pp527-532.

[9] 'Research and Development of DC XLPE cable and associated factory joint' by K. Terashima, M. Asano. Jicable 1999 pp543-548.

[10] 'Theory of Stress Distribution in Insulation of High-Voltage DC Cables: Part 1' by C.K. Eoll. IEEE TEI Vol E1-10, No. 1, March 1975. pp.27-35.

[11] The Development of a High Voltage DC Cable' Prepared by The Okonite Company. EPRI EL-606 Project 7818.

[12] 'On the Intrinsic Space Charge in a DC Power Cable' by B. Aladenize, R. Coelho, P. Mirabeau. CEIDP 1996. pp. 278-282

[13] 'Calculation of Electrical stresses in DC Cable Insulation' by F.H. Buller. IEEE Trans. on PAS, Vol. PAS-86, No. 10, October 1967 pp. 1169-1178

[14] 'Design and Development of DC Cables' by J.M. Oudin, M. Fallou and H. Thevenon. IEEE Trans. on PAS, Vol. PAS-86, No. 3, March 1967, pp. 304-311

[15] 'HVDC extruded cables – parameters for determination of stress' by B. Weedy and D. Chu. IEEE Transactions on Power Apparatus and Systems, Vol. PAS-103, No 3, March 1984, pp 662-667.

[16] 'The effect of paper properties on the temperature and stress dependence of the resistivity of impregnated laminates' by F. Chang, R.N. Hampton, S.B. Hobdell. 8th International DMMA, 2000. pp. 474-479,

[17] 'The influence of the semicon-insulation interface on the thermally stimulated current spectra of XLPE cable samples' by S.B. Hobdell, T.J. Lewis, J.P. Llewellyn, S.M. Moody. IEEE ICSD 1998. pp581-584

[18] Development of the new polymer insulating materials for HVDC cable' by N. Yoshifuji, T. Niwa, T. Takahasi, H. Miyata, G. Luoni. IEEE Transactions on Power Delivery, Vol 7, No 3, July 1992 pp. 1053-1059.

[19] 'Development of ± 250kV DC XLPE Cables – Long-Term Performance Verification Test' by K. Fujii, K. Terashima, H. Suzuki, N. Hozumi, M. Hara, Y.

Murata, K. Watanabe, M. Yoshida. International Conference on Electrical Engineering 1997, pp774-777

[20] 'High Performance HVDC polymer cable' by T. Tanaka, K. Kunii, T. Nakatsuka, H. Miyata, T. Takahashi. Published in Jicable 1999, paper C9.8

[21] 'Space charge Behaviour in Full-Size 250kV DC XLPE Cables' by T. Takeda, N. Hozumi, H. Suzuki, K. Fujii, K. Terashima, M. Hara, Y. Murata, K. Watanabe, M.Yoshida. IEEE Transactions on Power Delivery, Vol 13, No 1, Jan 1998 pp. 28-38

[22] IEEE Draft Standard P930: 'IEEE Guide for the statistical analysis of electrical insulation breakdown data' by J.C. Fothergill

[23] 'Volume dependence of Electric Strength of Polymers' by V.M. Morton and A.W. Stannett. Published in Proc. IEE Vol. 115, No 12, Dec 1968, pp 1857

[24] 'The Influence of test method on the Weibull parameters of extruded cable insulation' by R.J. Jackson and S.G. Swingler. IEE 4th International DMMA Conf Pub no. 239, 1984. pp 92-95.

[25] 'Electrical degradation and breakdown in polymers' by J.C. Fothergill and L.A. Dissado. Published by P. Peregrinus for IEE, London, 1992. ISBN: 0 86341 196 7

Chapter 5

[1] BICC company report 'Analysis of Accelerated Ageing Tests On Extruded XLPE and EPR Power Cables Carried Out By EPRI at the Marshall Technology Centre of BICC' by F. Chang, 1998. EPRI report RP-2713-02.

[2] IEEE Draft Standard P930: 'IEEE Guide for the statistical analysis of electrical insulation breakdown data' by J Fothergill

[3] 'A Space-charge Life Model for ac Electrical Aging of Polymers' by G. Mazzanti, G.C. Montanari, L.A. Dissado. IEEE Transactions on Dielectrics and Electrical Insulation Vol 6, No 6, 1999. pp.864-875

Chapter 6

[1] 'Multi-stress electrical and thermal ageing of HV extruded polymeric cables: mechanism and methods'. By L. Markey, G.C. Stevens, L.A. Dissado and G.C. Montanari. IEE DMMA 200 Conf Pub No. 473. pp. 413-418

[2] 'Electrical degradation and breakdown in polymers' by J.C. Fothergill and L.A. Dissado. Published by P. Peregrinus for IEE, London, 1992. ISBN: 0 86341 196 7

[3] L. A. Dissado, S.J. Urban and P.A. Norman, 'Breakdown Statistics of the Space-charge ageing model for polymeric insulation' IEEE CEIDP 1996 pp129-132

[4] 'Statistical Theory of Extreme Values and Some Practical Applications' a series of lectures by E.J. Gumbel. Published by U.S Department of Commerce National Bureau of Standards Applied Mathematics Series No. 33. Issued Feb 1954

[5] 'Extreme Value Distributions Theory and Applications' by S. Kotz and S. Nadarajah. Published by Imperial college Press 2000. ISBN: 1860942245

[6] IEEE Draft Standard P930: 'IEEE Guide for the statistical analysis of electrical insulation breakdown data' by J.C. Fothergill

[7] 'Theoretical basis for the statistics of dielectric breakdown' by R.M. Hill and L.A. Dissado. JPhys C: Solid State Phys., 16, 1983 pp. 2145-2156.

[8] 'Weibull statistics in dielectric breakdown; theoretical basis, applications and implications' by L.A. Dissado, J.C. Fothergill, S.V. Wolfe and R.M. Hill. IEEE transactions on Electrical Insulation Vol EI-19 No 3 June 1984, pp227-233

[9] 'Theoretical basis for the statistics of dielectric breakdown' by L.A. Dissado. Journal of Physics D Vol 23, 1990, pp1582-1591

[10] PET lifetime data – private communication from Stanislaw Gubanski.

[11] 'The physics of electrical ageing in semi-crystalline insulating polymers by L. A. Dissado. Proc. 32nd Symp. On Electrical and Electronic Insulating Material and Applications in Systems, Nagano, Japan (sponsor IEEJ), S2-1, 2000, pp.9-16

[12] 'Investigation of the Structural Changes in LDPE and XLPE Induced by High Electrical Stress' by P.W.C. Sayers. PhD Thesis submitted to the University of Wales, September 2001

[13] 'Investigation of the Structural Changes in LDPE and XLPE Induced by high Electrical Stress' by P.W. Sayers, T.J. Lewis, J.P. Llewellyn and C.L. Griffiths IEE DMMA 2000 Conf Pub No 473. pp. 403-407

[14] 'The Importance of Mechanical Properties for Increasing the Electrical Endurance of Polymeric Insulation' by C.L. Griffiths, S. Betteridge, J.P. Llewellyn and T.J. Lewis. IEE DMMA 2000 Conf Pub No 473. pp. 408-411

[15] 'Anelastic and Dielectric Effects in Polymeric Solids' by N. G. McCrum, B.E. Read and G. Williams. Published by Dover Publications, Inc, 1991. ISBN: 0-486-66752-9

[16] 'Crystallisation of Polyethylene Terephthalate' by W.H. Cobbs and R.L. Burton. Journal of Polymer Science, 10, No. 3, 1953. pp275-290

[17] 'Crystallisation of PET with strain, strain rate and temperature' by J.O. Fernandez and G.M. Swallowe. Journal Mat. Sci., 35, 2000. pp.4405-4414.

[18] 'Electrical conduction in polyethylene terephthalate and polyethylene films' by D.M. Taylor and T.J. Lewis. J. Phys. D: Appl. Phys., 1971, Vol4. pp.1346-1357.

[19] 'A Space-charge Life Model for AC Electrical Aging of Polymers' by G. Mazzanti, G.C. Montanari, L.A. Dissado. IEEE TDEI Vol 6, No 6, 1999. pp864-875

[20] BICC company report 'Analysis of Accelerated Ageing Tests On Extruded XLPE and EPR Power Cables Carried Out By EPRI at the Marshall Technology Centre of BICC' by F. Chang, 1998. EPRI report RP-2713-02.

Chapter 7

[1] 'A Space-charge Life Model for ac Electrical Aging of Polymers' by G. Mazzanti, G.C. Montanari, L.A. Dissado. IEEE Transactions on Dielectrics and Electrical Insulation Vol 6, No 6, 1999. pp.864-875

[2] 'Measurement of space-charge distributions in solid insulators under rapidly varying voltage using the high-voltage, high-speed pulsed electro-acoustic (PEA) apparatus' A. See, J.C. Fothergill, L.A. Dissado, J.M. Allison. Meas. Sci. Technol. Vol 12 (2001) pp. 1227-1234.

[3] 'High resolution multidimensional space charge measurement using elastic wave methods' by S. Hole and J. Lewiner. Phys. Rev. B, 64, 2001. art. no. 104106.

[4] 'Space charge measurements in power cables using a modified PEA system' by M. Fu, G. Chen, A.E. Davies, J.G. Head. IEE DMMA 2000, Conf Pub No. 473. pp. 74-79

[5] 'Space Charge Observation of a Filler Free Epoxy resin' by K. Fukunaga, T. Maeno and V. Griseri. CEIDP 2000 pp.125-127

[6] 'Recent advances in space charge measurement and extruded HVDC cable design' by P. Mirebeau, A. Toureille, R. Coelho, H. Janah, J. Matallana, P. Horquebie, S. Agnel and D. Sy. 7th Int Conf on AC-DC Power Transmission 2001. IEE Conf. Pub. No. 485. pp. 44-48

[7] 'Space Charge Measurement Using Pulsed Electroacoustic Technique and Signal recovery' by A. Vaquez, G. Chen, A.E. Davies and R. Bosch. J. Eur. Cheram. Soc, 19 1999. pp.1219-1222.

[8] 'Dependence of space-charge trapping threshold on temperature in polymeric DC cables' by G.C. Montanari, G. Mazzanti, F. Palmieri, G. Perego, S. Gerra. IEEI ICSD 2001. pp. 81-84.

[9] 'Charge Buildup in Lossy Dielectrics with Induced Inhomogeneities' by R. Coelho, B. Aladenize, F. Guillaumond. IEEE Trans. DEI Vol4, No 5, October 1997. pp. 477-486

[10] 'On the intrinsic space charge in a DC power cable' by B. Aladenize, R. Coelho, F. Guillaumond, P. Mirebeau. Journal Of Electrostatics Vol 39 (4) 1997 pp. 235-251

[11] 'Space charge profiles in low density polyethylene samples containing a permittivity/conductivity gradient' by K.R. Bamberry, R.J. Fleming, J.T. Holboll. J.Phys. D 34 2001. pp.3071-3077.

[12]'Charges and Discharges in HVDC Cables – In particular in mass-impregnated HVDC cables' by M. Jeroense. PhD thesis submitted to the University of Delft and published by Delft University Press 1997. ISBN: 90-407-1438-X

[13] 'Inverse Problem Theory' by A. Tarantola. Elsevier Science Publishers, 1987. ISBN 0 444 42765 1

[14] 'Breakdown Statistics of the Space-charge ageing model for polymeric insulation' L.A. Dissado, S.J. Urban and P.A. Norman, CEIDP 1996 pp129-132

[15] 'Predicting electrical breakdown in polymeric insulators: from deterministic mechanism to failure statistics' by L.A. Dissado. IEEE Trans. DEI, vol 9, 2002 to be published October 2002

[16] 'Investigation of the Structural Changes in LDPE and XLPE Induced by High Electrical Stress' by P.W.C. Sayers. PhD Thesis submitted to the University of Wales, September 2001.

[17] 'Electrical degradation and breakdown in polymers' by J.C. Fothergill and L.A. Dissado. Published by P. Peregrinus for IEE, London, 1992. ISBN: 0 86341 196 7

Appendix A

Section A1 of this appendix contains the FORTRAN code used to generate parameter values for the DMM model applied to cable data, as described in chapter 5. In all cases, a C at the start of a line indicates a comment, which is ignored by the compiler.

Section A2 has details of the compiling and running of the FORTRAN program.

In order for the program to work, the following text files need to be set up:

- VOLTAGES.TXT, containing the test voltage for each set of cables.
- TEMPERATURES.TXT containing test.
- MYALPHAS.TXT containing B63 lifetime values for each set of cables.

A1. FORTRAN Code

The function of each of the following modules is described in Chapter 5. The code is presented below.

A1.1 MAIN.F – main program

```
PROGRAM MAIN


REAL   L
REAL   RIN
REAL   ROUT
REAL   PI
REAL   NMAX

REAL   RADIUS
REAL   RADII
REAL   FIELD
REAL   EVALS
REAL   V
REAL   HDK
REAL   SD
REAL   C
REAL   B
REAL   BETA
REAL   KD
REAL   ASTAR
REAL   INVLIVES
REAL   T
REAL   INVLIFETIME
REAL   ALPHA
REAL   INVSUM
```

```
REAL   ERROOR,ERRTSM
REAL   PRELIFE

REAL   ERR,ERRT1,ERRTOT,H1,H2,A1,A2,S1,S2,B1,B2,C1,C2,K1,K2
INTEGER P,G,I,U,W,O
INTEGER M,K,J,S,D,E,F,X,OP,N
CHARACTER no


DIMENSION     V(100)
DIMENSION     T(100)
DIMENSION     ALPHAS(1000)
PI=3.14
BETA=3.5
ERRT1=30000000.0

C          The user is asked for the cable dimensions

PRINT*,'Please enter cable dimensions:'
PRINT*,'Length in mm'
READ*,L
PRINT*,'Core radius in mm'
READ*,RIN
PRINT*,'Outer insulation radius in mm'
READ*,ROUT

VTOT=PI*L*(ROUT**2-RIN**2)
PRINT*,VTOT

PRINT*,'HOW MANY VOLTAGES DO YOU HAVE?'
READ*,F

IF (F.LT.2) THEN
PRINT*,'NOT ENOUGH VOLTAGES'
STOP
ELSE
CONTINUE
ENDIF

PRINT*,'AND HOW MANY TEMPERATURES?'
READ*,E

IF (E.LT.2) THEN
PRINT*,'NOT ENOUGH TEMPERATURES'
STOP
ELSE
CONTINUE

ENDIF

PRINT*,'HOW MANY DATA POINTS ALTOGETHER?'
READ*,S

IF (S.LT.6) THEN
PRINT*,'NOT ENOUGH DATA POINTS'
STOP
ELSE
CONTINUE

ENDIF
```

```
C       Asks the user for a beta value

PRINT*,'Enter a value for beta (suggested value is mean of TTF sets)'
READ*,BETA



C       Reading in alpha, voltage and temperature values from text files

OPEN(15,'MYALPHAS.TXT')
OPEN(25,'VOLTAGES.TXT')
OPEN(35,'TEMPERATURES.TXT')



DO 80 N=1,S
READ(15,'(F15)',END=1000)ALPHAS(N)

READ(25,'(F15)',END=2000)V(N)

READ(35,'(F15)',END=3000)T(N)
80      CONTINUE

1000    CLOSE(15)
2000    CLOSE(25)
3000    CLOSE(35)
C4000   CLOSE(45)



C       Asks the user how many layers to use, and how many parameter points in

the ranges, which are specified next.

PRINT*,'HOW MANY LAYERS WOULD YOU LIKE TO USE?
6 RECOMMENDED NUMBER IS 100'
READ*,NMAX
NMAX=NMAX+1

999     PRINT*,'HOW MANY POINTS IN EACH PARAMETER RANGE?
6 RECOMMENDED IS 7'
READ*,X

ERRT1=30000000.0

OPEN(10,'UFALLVALS.TXT')
OPEN(20,'UFERROR.TXT')
OPEN(30,'UFSD.TXT')
OPEN(40,'UFHDK.TXT')
OPEN(50,'UFKD.TXT')
OPEN(60,'UFCD.TXT')
OPEN(70,'UFASTAR.TXT')
OPEN(80,'UFB.TXT')



C       Now asks the user for some initial parameter values for the DMM model.
```

```
PRINT*,'Please enter limits for Sd. Suggested for first run is -1E-22 to

-10E-22'


PRINT*,'To accept suggestions type 1, to enter own values type 0 then

values'
READ*,RS
IF (RS.EQ.1) THEN
S1=-1E-22
S2=-10E-22
ELSE
READ*,S1,S2
ENDIF
RS=0

PRINT*,'Please enter limits for Hdk. Suggested for first run is 500 to

5000.'

PRINT*,'To accept suggestions type 1, to enter own values type 0, then

values'

READ*,RS
IF (RS.EQ.1) THEN
H1=500
H2=5000
ELSE
READ*,H1,H2
ENDIF

RS=0

PRINT*,'Please enter limits for Kd. Suggested for first run is 50 to 500'

PRINT*,'To accept suggestions type 1, to enter own values type 0 then values'
READ*,RS
IF (RS.EQ.1) THEN
K1=50
K2=500
ELSE
READ*,K1,K2
ENDIF
RS=0

PRINT*,'Please enter limits for Cd. Suggested for first run is 0.5 to 5'
PRINT*,'To accept suggestions type 1, to enter own values type 0 then

values'
READ*,RS
IF (RS.EQ.1) THEN
C1=0.5
C2=5.0
ELSE
READ*,C1,C2
ENDIF
RS=0
```

```
PRINT*,'Please enter limits for Astar. Suggested for first run is 0.1 to

1'

PRINT*,'To accept suggestions type 1 etc'
READ*,RS
IF (RS.EQ.1) THEN
A1=0.1
A2=1.0
ELSE
READ*,A1,A2
ENDIF

RS=0


PRINT*,'Please enter limits for b. Suggested for first run is 0.1 to 1'
PRINT*,'To accept suggestions type 1, to enter own values type 0 then

values'
READ*,RS
IF (RS.EQ.1) THEN
B1=0.1
B2=1.0
ELSE
READ*,B1,B2
ENDIF


C       These next loops calculate the required number of parameter values in the specified limits

DO 190 P=1,X
SD=S1+(((S2-S1)/(X-1))*(P-1))


DO 180 G=1,X
HDK=H1+(((H2-H1)/(X-1))*(G-1))

DO 200  I=1,X
KD=K1+(((K2-K1)/(X-1))*(I-1))

DO 220  U=1,X
C=C1+(((C2-C1)/(X-1))*(U-1))

DO 240  W=1,X
ASTAR=A1+(((A2-A1)/(X-1))*(W-1))


DO 260  D=1,X
B=B1+(((B2-B1)/(X-1))*(D-1))


C       This loop calculates radius values, field at each radius, and then1/lifetime for each cable. It puts
these values in a matrix called INVLIVES.

ERRTOT=0
DO 100 N=1,S
```

```
INVSUM=0
DO 120 K=1,NMAX-1

INVLIVES=INVLIFETIME(HDK,SD,KD,B,ASTAR,C,FIELD(V(N),
6       ROUT,RIN,RADIUS(K,VTOT,NMAX,L,RIN,ROUT)),T(N),BETA)
INVSUM=INVSUM+INVLIVES
120                     CONTINUE
PRELIFE=(NMAX/INVSUM)**(1.0/BETA)


C       This works out the error function for each calculated lifetime and the

data

ERR=ERROOR(PRELIFE,ALPHAS(N))
ERRTOT=ERRTOT+ERR

100     CONTINUE

C       Here, the best error value so far is recorded, along with the associated

parameter values.

IF (ERRTOT.LT.ERRT1) THEN
ERRTSM=ERRTOT
GOODHDK=HDK
GOODSD=SD
GOODKD=KD
GOODAST=ASTAR
GOODB=B
GOODBETA=BETA
GOODC=C
PRINT*, ERRTSM,GOODSD,GOODHDK,GOODKD,
6                       GOODC,GOODAST,GOODB,GOODBETA

WRITE(10,'((2(2X,G14.7),6(2X,F12.7)))') ERRTOT,
6               GOODSD,GOODHDK,GOODKD,
6                       GOODC,GOODAST,GOODB,GOODBETA


WRITE(20,'(G14.7)') ERRTOT
WRITE(30,'(G14.7)') GOODSD
WRITE(40,'(F12.7)') GOODHDK
WRITE(50,'(F12.7)') GOODKD
WRITE(60,'(F12.7)') GOODC
WRITE(70,'(F12.7)') GOODAST
WRITE(80,'(F12.7)') GOODB


ELSE
ERRTSM=ERRT1

ENDIF


ERRT1=ERRTSM
```

```
260       CONTINUE
240       CONTINUE
220       CONTINUE
200       CONTINUE

180       CONTINUE


C         This prints the outer loop number, so that the progress of the program can be observed.

PRINT*,P
190       CONTINUE
CLOSE(10)
CLOSE(20)
CLOSE(30)
CLOSE(40)
CLOSE(50)
CLOSE(60)
CLOSE(70)
CLOSE(80)

C         After all specified parameters have been tried, the lowest error is

printed to the screen with the parameter values

PRINT*,'The lowest generated error is',ERRTSM
PRINT*,'The corresponding parameter value set is'
PRINT*,'Hdk=',GOODHDK
PRINT*,'Sd=',GOODSD
PRINT*,'Kd=',GOODKD
PRINT*,'C=',GOODC
PRINT*,'A*=',GOODAST
PRINT*,'b=',GOODB

C         The user in then advised that they can quit the program, or run it again with different parameter
values

PRINT*,'To get a good fit it is usually necessary to search around
6the initial best fit parameters.'
PRINT*,'To run the program again with smaller parameter ranges
6 type 1, otherwise type 0 to quit the program'

READ*,OP

IF(OP.EQ.1) THEN
GOTO 999
ELSE
PRINT*,'Program ended'
GOTO 99
ENDIF



99        STOP
END
```

A1.2 RADIUS.F – function to calculate shell radii

```
FUNCTION RADIUS(N,VTOT,NMAX,L,RIN,ROUT)



REAL VTOT
REAL ROUT
REAL RIN
REAL L
REAL PI
REAL NMAX
REAL RADIUS

INTEGER N

PI=3.14

        RADIUS=((((N-1)*((VTOT/((NMAX-1)*PI*L))+(RIN**2)))-((N-2)*(RIN**2)))**0.5)
END
```

A1.3 FIELD.F – function to calculate field for each shell

```
FUNCTION FIELD(V,ROUT,RIN,R)

        REAL V
        REAL ROUT
        REAL RIN
        REAL R

        FIELD=V/(R*LOG(ROUT/RIN))

        END
```

A1.4 LIFETIME.F – function to calculate predicted lifetime for each experimental condition

```
FUNCTION INVLIFETIME(HDK,SD,KD,B,ASTAR,C,E,T,BETA)

        REAL HDK
        REAL SD
        REAL KD
        REAL B
        REAL ASTAR
        REAL C
        REAL BETA
        REAL E
        REAL T
        REAL H
        REAL K
        REAL INVLIFETIME
        REAL AEQ
        REAL BETA

        H=6.63 E -34
```

```
      K=1.38 E -23
C     PRINT*, H



      AEQ=1.0/(1.0+(EXP((KD-(C*(E**(4.0*B))))/T)))
      CDEB=C*(E**(4.0*B))
      HKT=H/(2.0*K*T)

C     PRINT*,AEQ-ASTAR

      IF (AEQ.GT.ASTAR) THEN

      INVLIFETIME=1.0/(((HKT*(EXP(-SD/K))*
     6                  (EXP((HDK-(CDEB/2.0))/T))*
     6                  (-LOG((AEQ-ASTAR)/AEQ)))/
     6                  COSH((KD-CDEB)/(2.0*T)))**BETA)

      ELSE
            INVLIFETIME=0.0
C           PRINT*,'INFINITE CONDITION'

      ENDIF
      END
```

A1.5 ERROR.F – function to calculate error between data and predictions

```
FUNCTION ERROOR(PRELIFE,ALPHA)

      REAL ALPHA
      REAL PRELIFE



            ERROOR=(log(PRELIFE)-log(ALPHA))**2


      END
```

A2. Compiling and running the program

Compiling

- The following modules must be compiled into an executable FORTRAN file:
    1. RADIUS.F
    2. FIELD.F
    3. LIFETIME.F
    4. ERROR.F
    5. MAIN.F

  A command to do this on the Leicester University IRIX system is:

  'f77 –ouf RADIUS.F FIELD.F LIFETIME.F ERROR.F MAIN.F'

  This compiles the units into an executable file called 'uf'
- The executable can then be run, simply by typing 'uf'

Running

To carry out the calculations, the program asks the user for the following

- Cable length, core radius and outer radius of cable.
- The number of V and T conditions under which tests have been carried out
- The total number of experimental conditions
- The β value for the data (it suggest using the mean value from the TTF sets)
- A value for N – the number of shells that the insulations should be spit into. This number should be as large as possible without making the run-time too long.
- The number of steps required in each parameter range – i.e. the number of values of each parameter to test in the range specified next.
- A maximum and minimum value for each of the parameters. It makes suggestions for each one, which can be accepted or rejected. The suggestions represent a very wide range of parameter values, so are most useful on a first run through.

The program will then run, printing on the screen successively better parameter sets with their associated error as they are encountered. The program also outputs to the

screen the loop number of the outer-most loop so that the progress of the calculations can be assessed.

After the initial run, the best parameter set from that run is displayed. The user can end the program then, or chose to re-run the program with a different parameter value range. This is so that the parameter range can be narrowed down to give smaller and smaller errors compared with the data.

The successively better parameter sets and error values outputted to the screen are also output to the following text files:

- Error plus all parameter values in UFALLVALS.TXT
- Error values only in UFERROR.TXT
- Sd values only in UFSD.TXT
- Hdk values only in UFHDK.TXT
- C' values in UFCD.TXT
- Kd values in UFKD.TXT
- A* values in UFASTAR.TXT
- b values in UFB.TXT

Appendix B

Graphs showing experimental time-to-failure data with the corresponding time-to-failure distributions predicted by H_{dk} (and S_d for the AC data) distributions are presented below. Section B1 shows the data for the AC PET thin film data, and B2 shows the data for the DC PET film data. In section B3, the results from the XLPE cable data are presented.

B1. AC Data

These graphs show the Weibull cumulative probability of failure on the y-axis, against time in seconds on the x-axis. Each graph shows experimental time-to-failure points as squares. The thin black line in each case corresponds to the failure distribution predicted by an S_d distribution as explained in Chapter 6. The broader grey lines show the time-to-failure distributions predicted by H_{dk} distributions within the DMM model.

The experimental condition to which each graph corresponds is shown below the graphs.

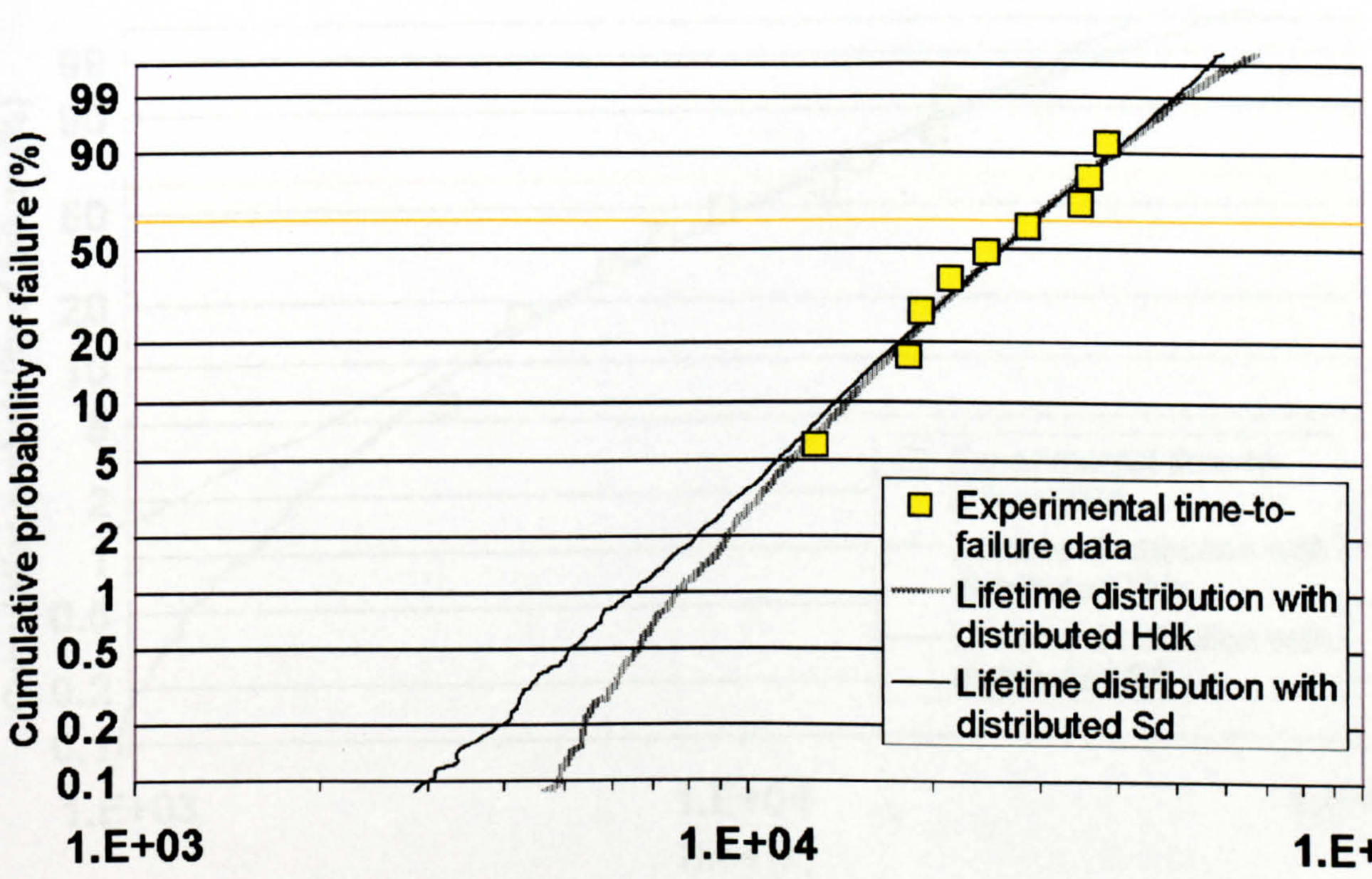

Figure B1.1 E=50kV/mm T=293K

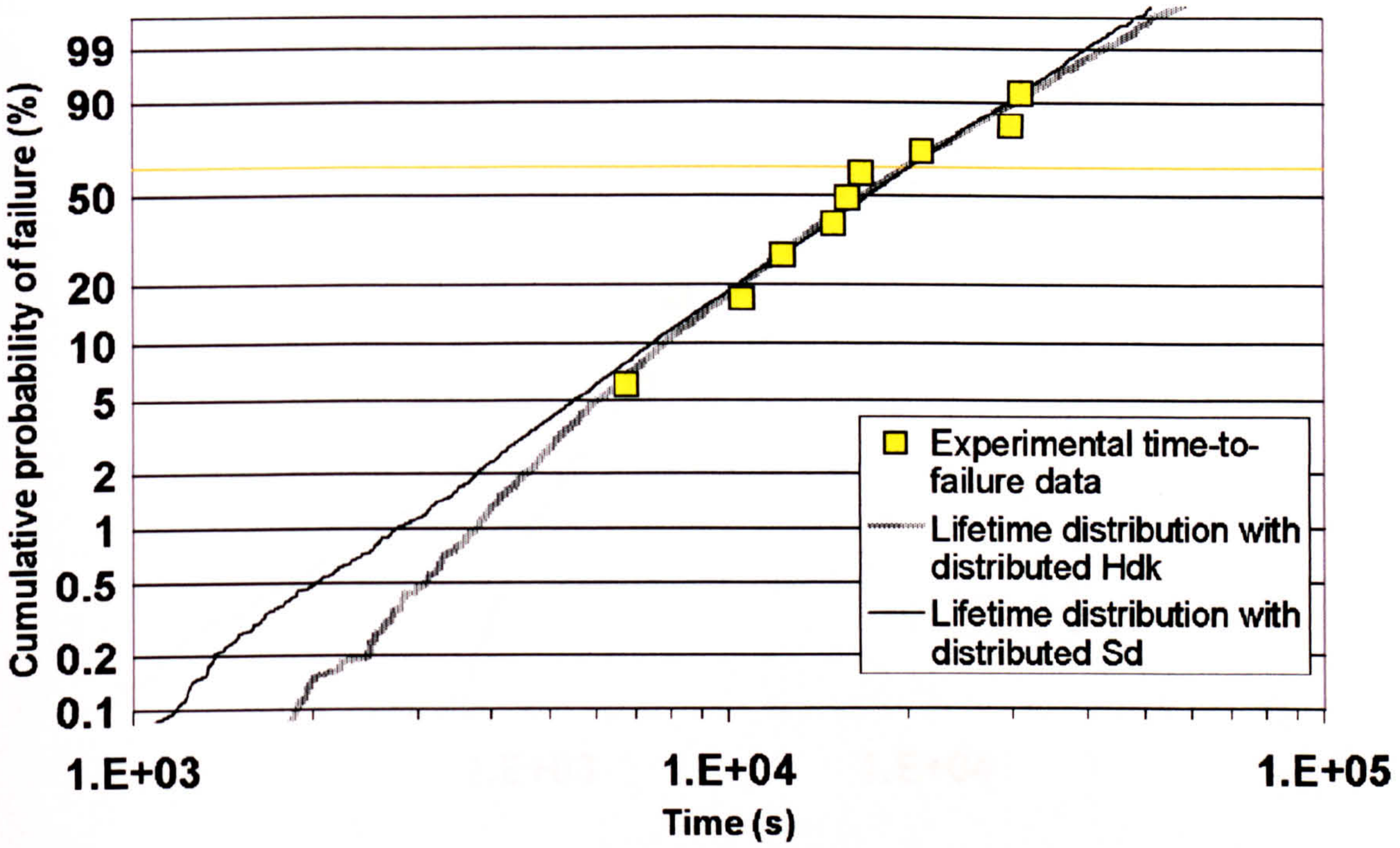

Figure B1.2 E=50kV/mm T=333K

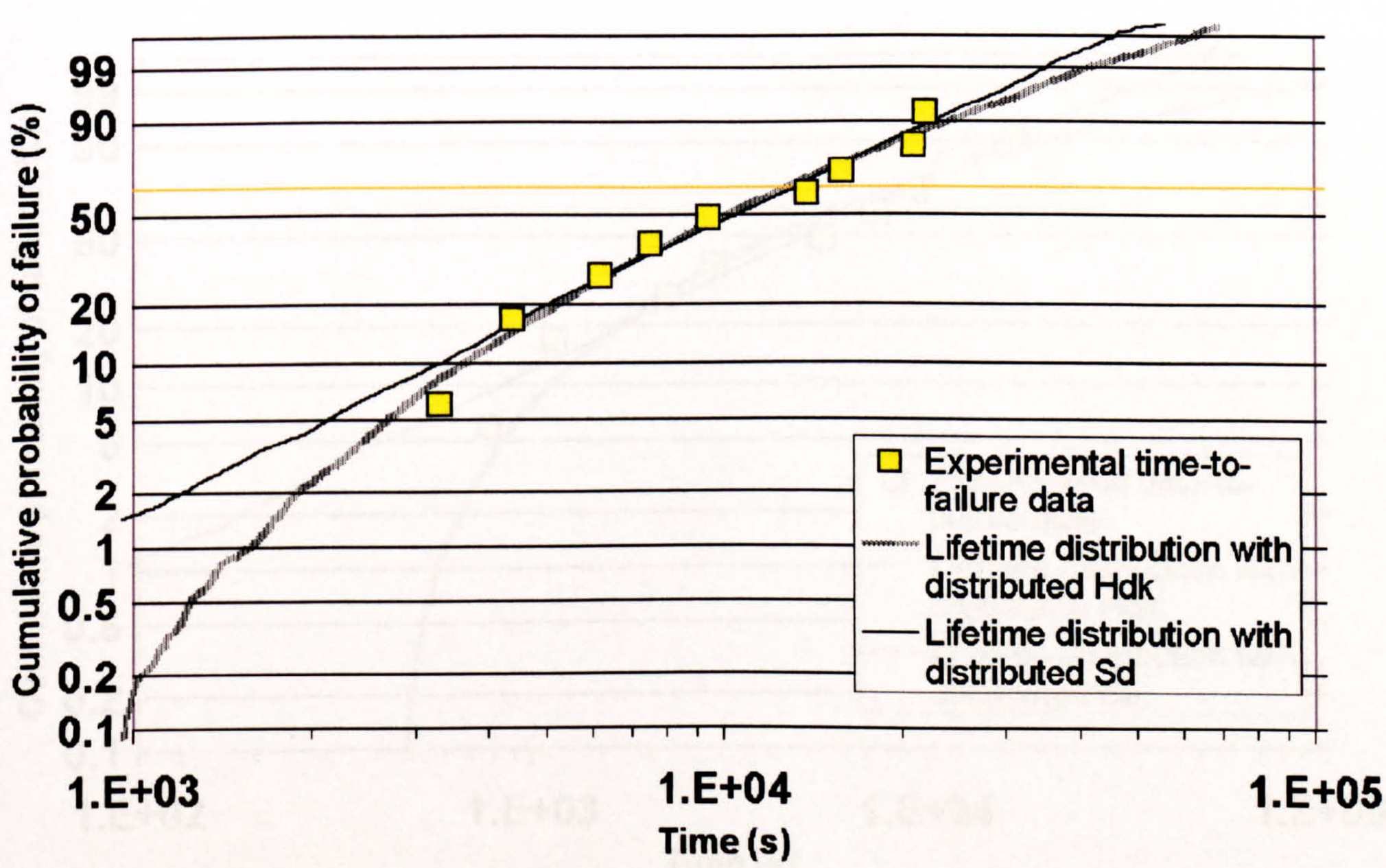

Figure B1.3: E=50kV/mm T=383K

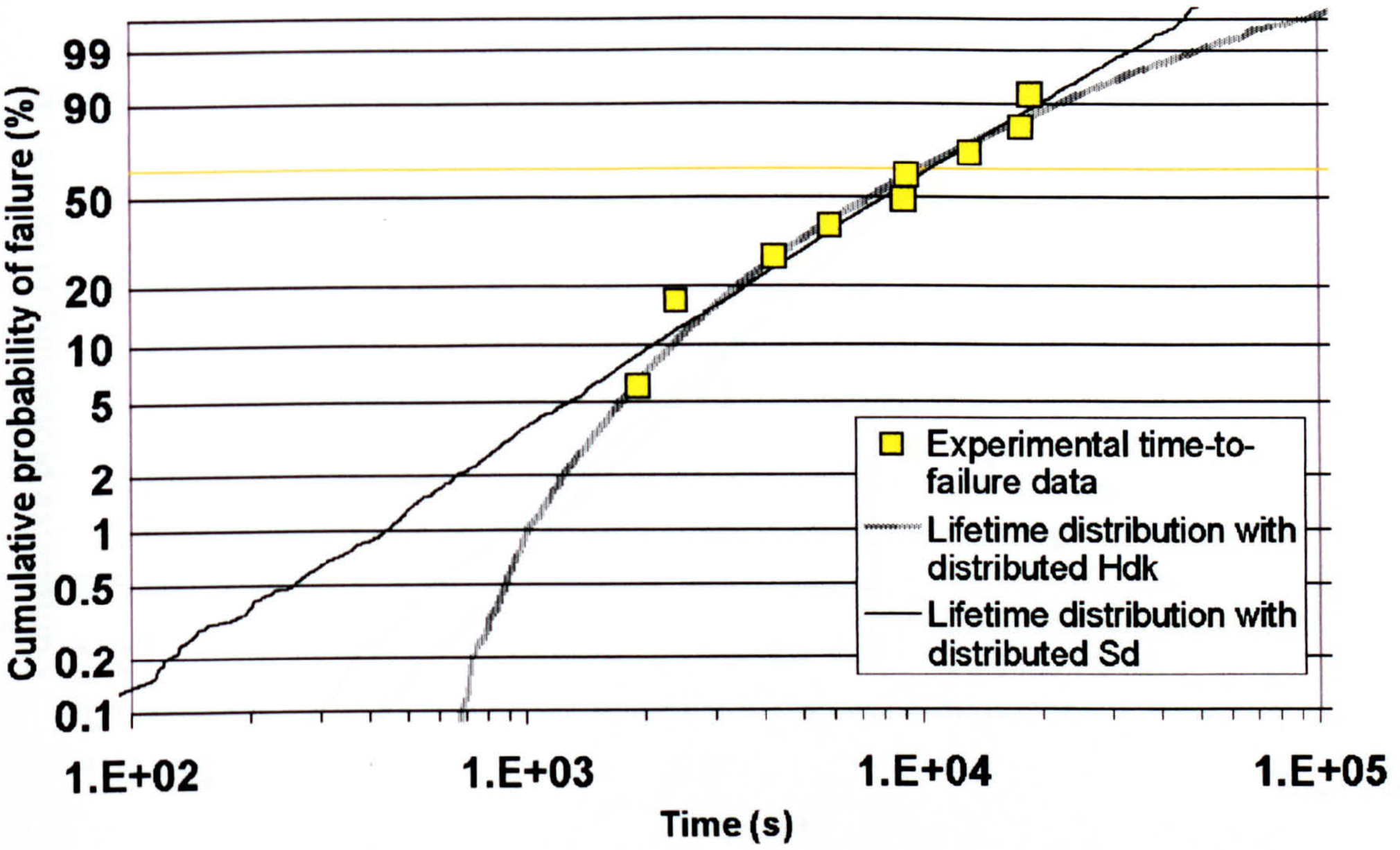

Figure B1.4 E=50kV/mm T=403K

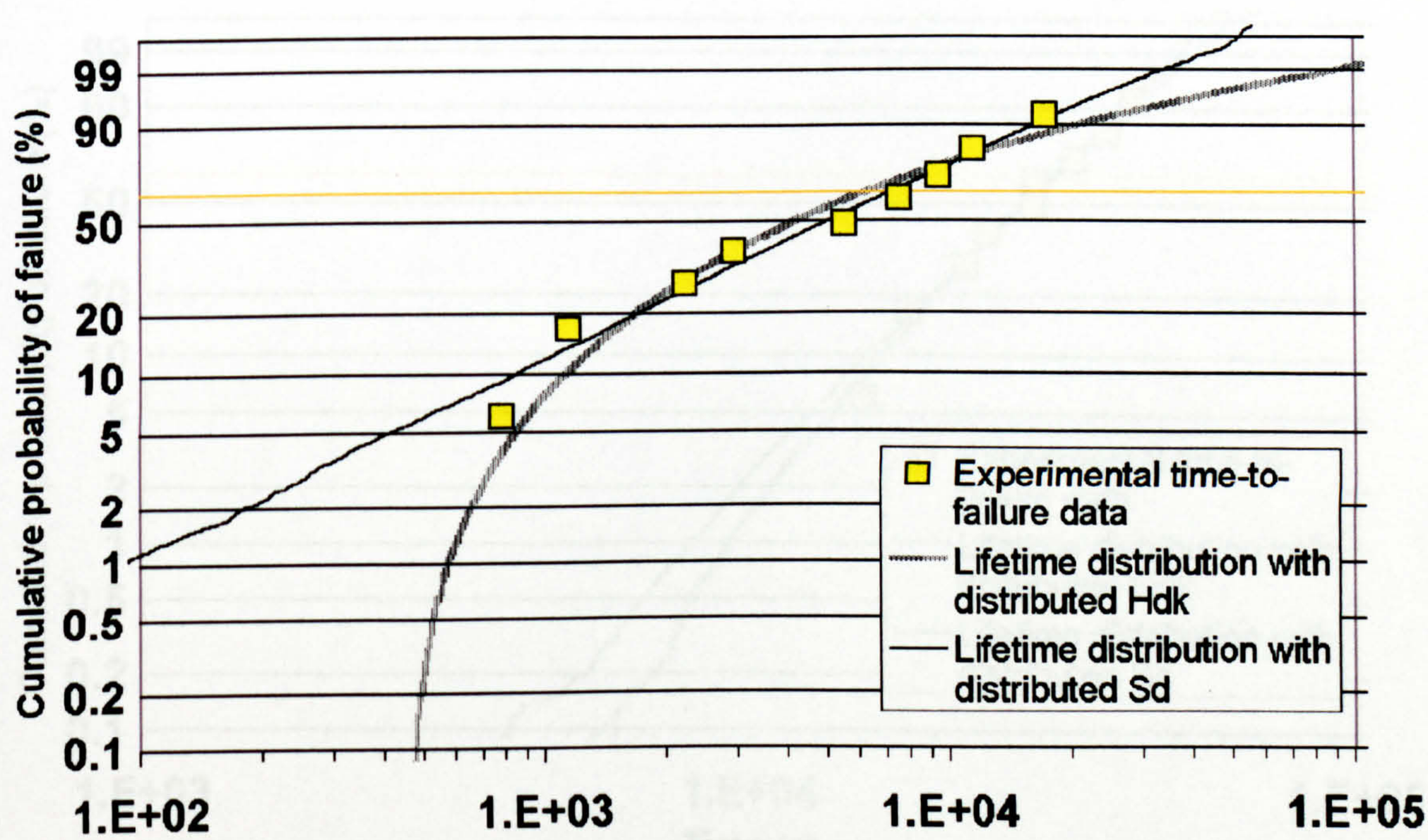

Figure B1.5 E=50kV/mm T=423K

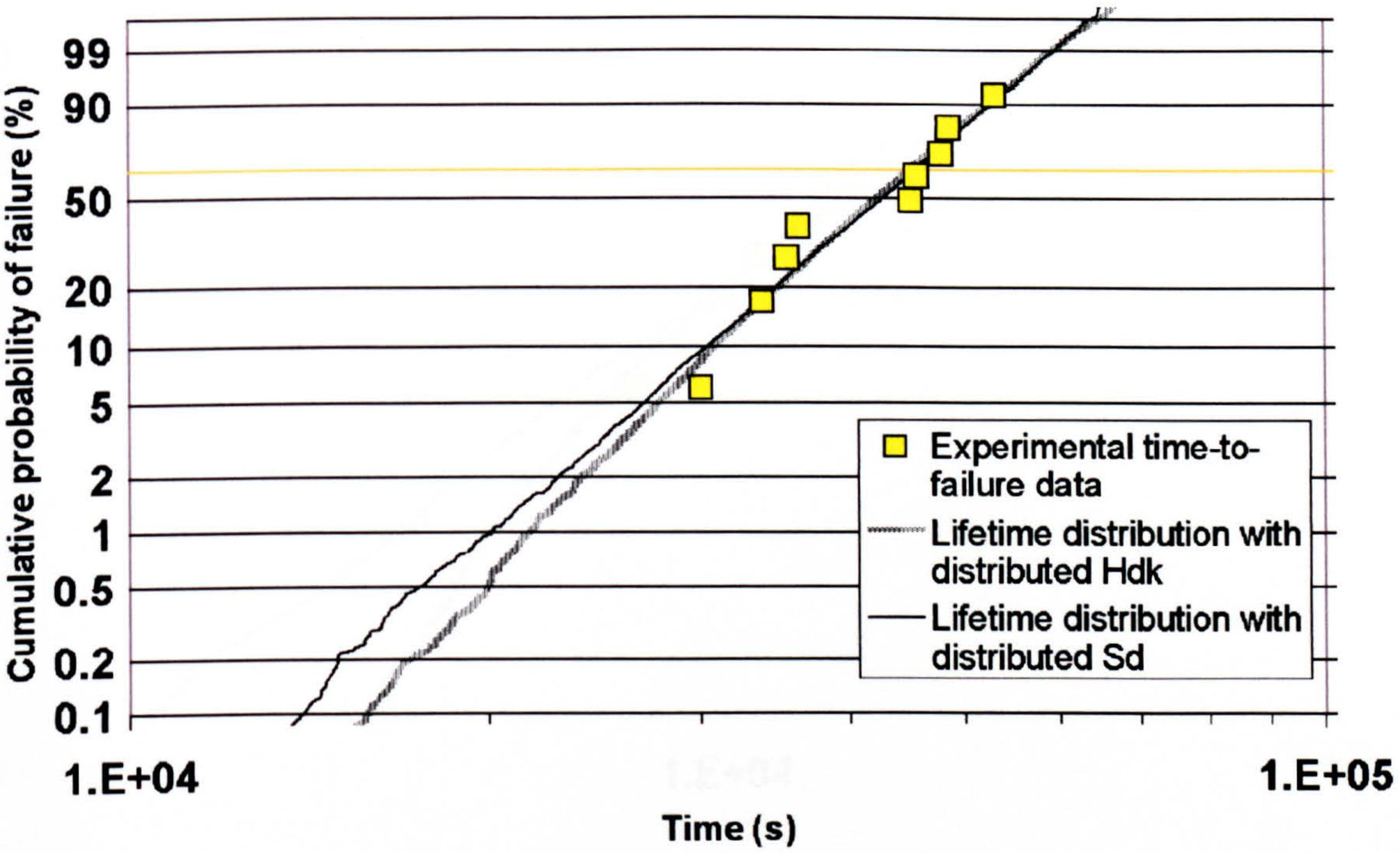

Figure B1.6 E=40kV/mm T=293K

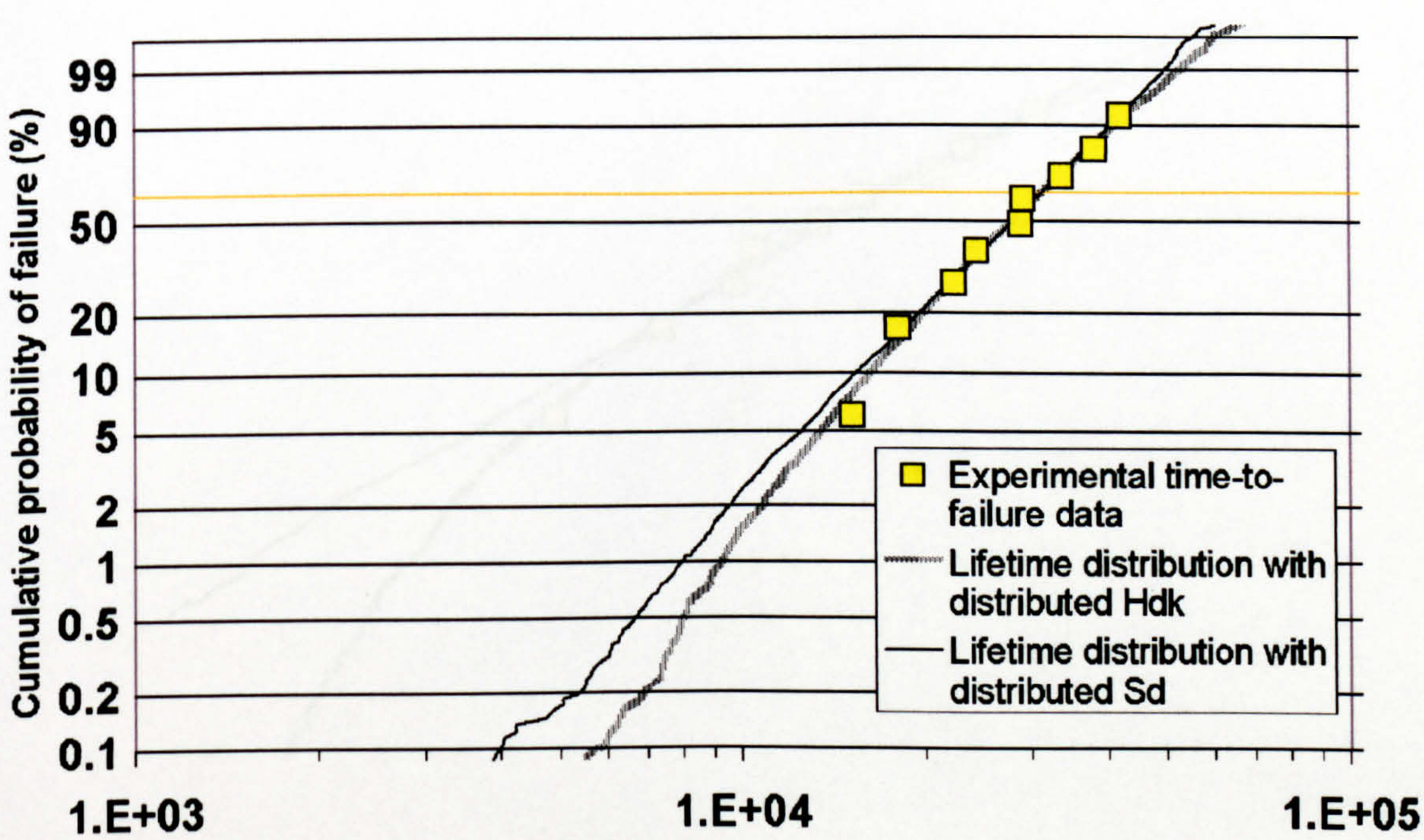

Figure B1.7 E=40kV/mm T=333K

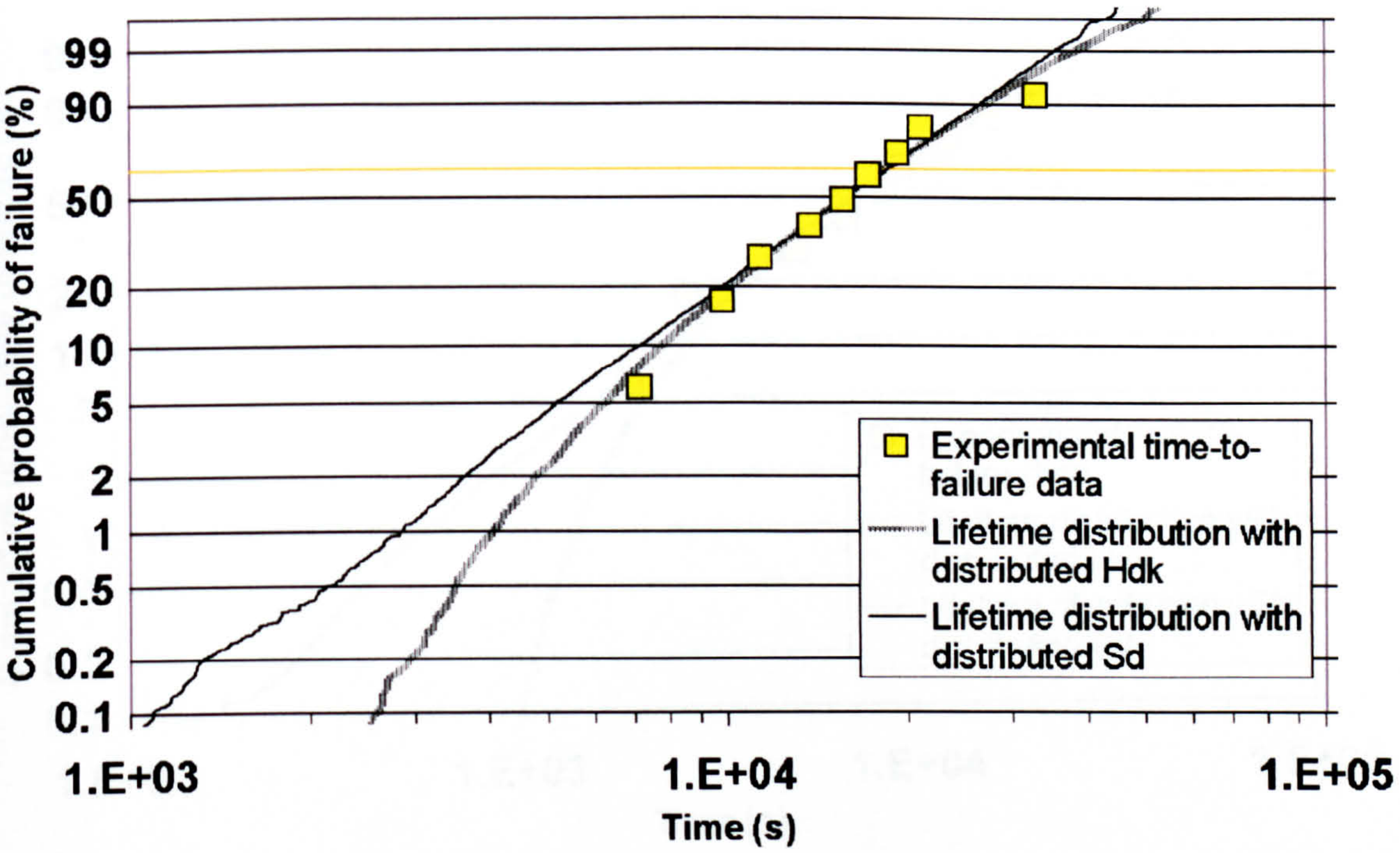

Figure B1.8 E=40kV/mm T=383K

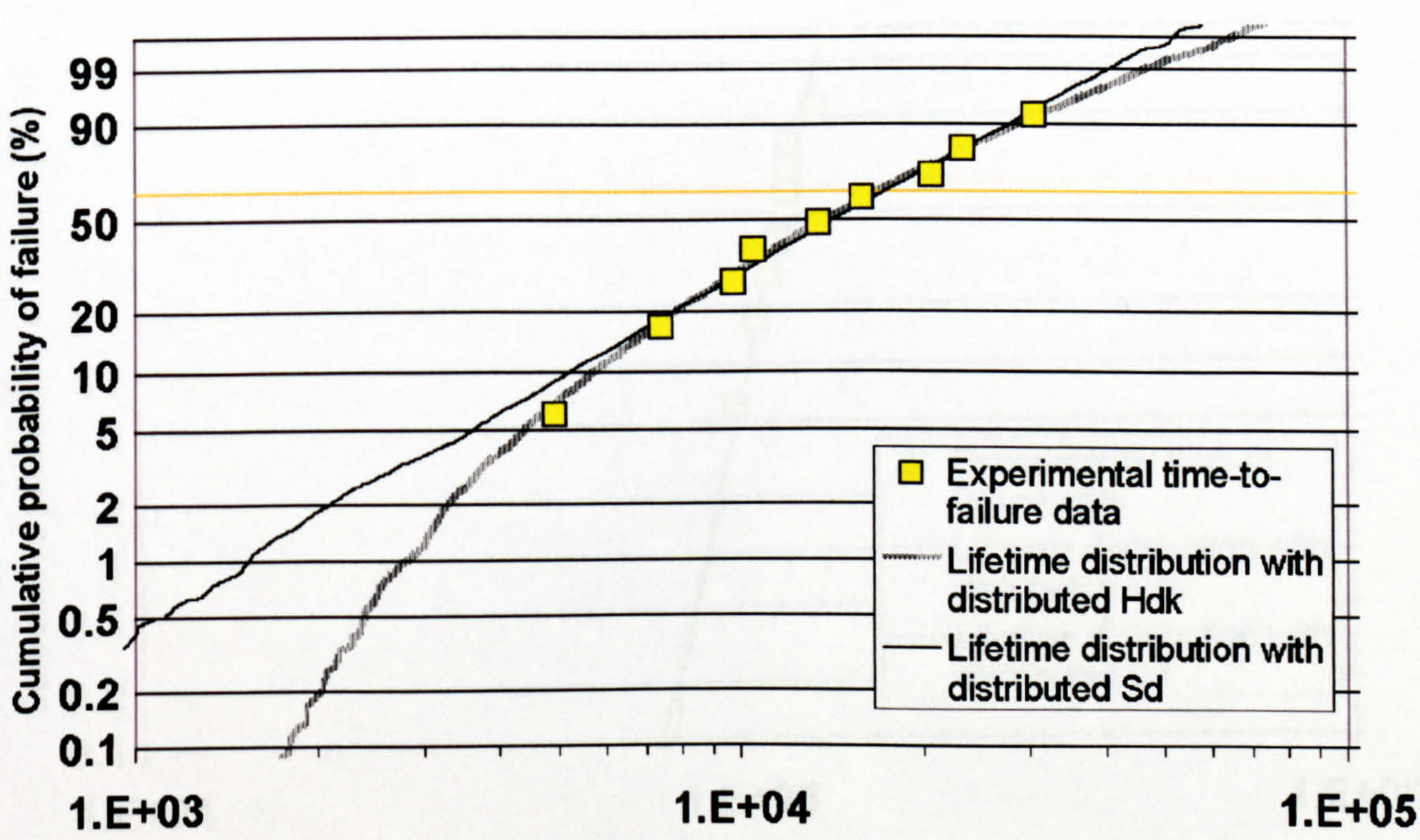

Figure B1.9 E=40kV/mm T=403K

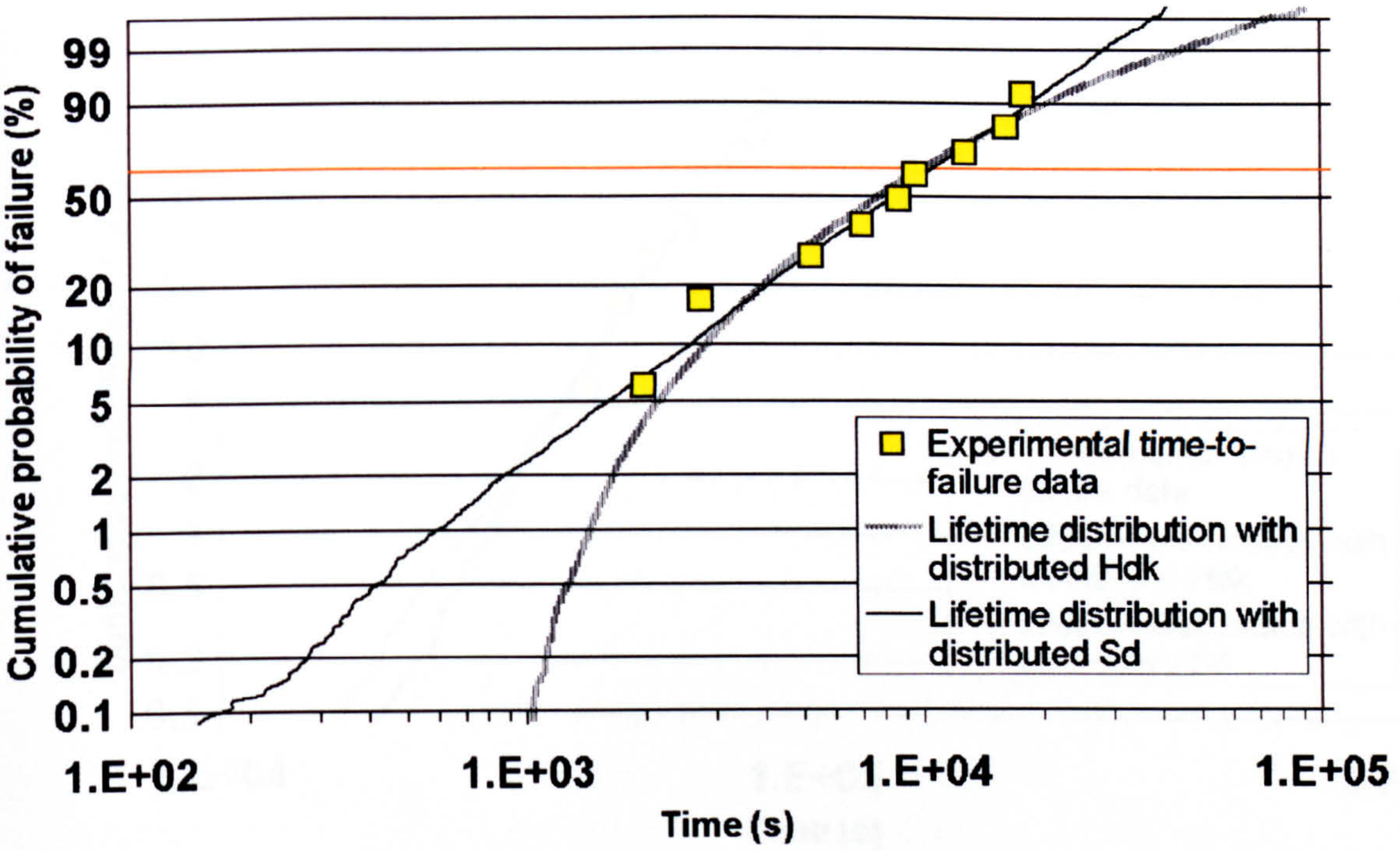

Figure B1.10 E=40kV/mm T=423K

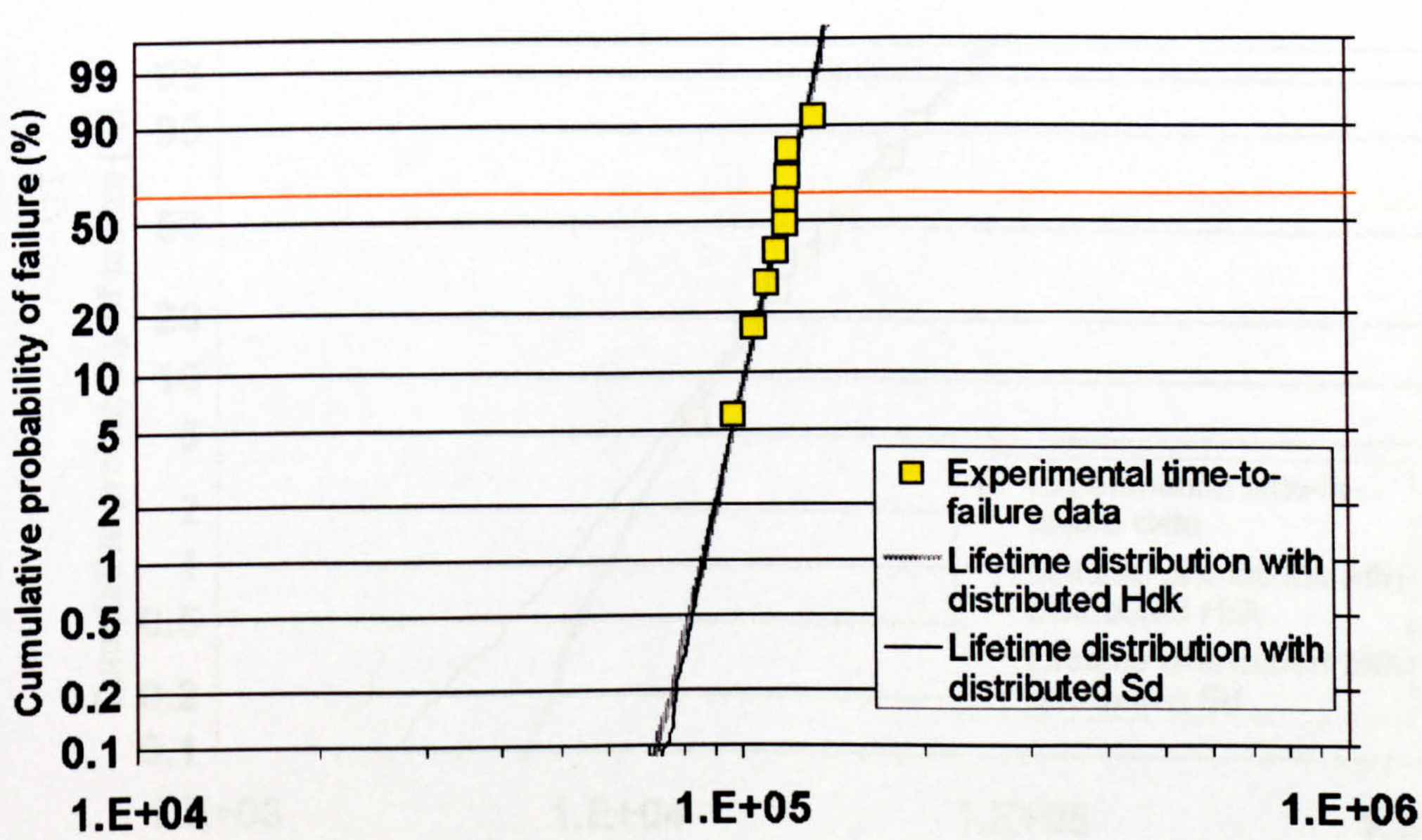

Figure B1.11 E=30kV/mm T=293K

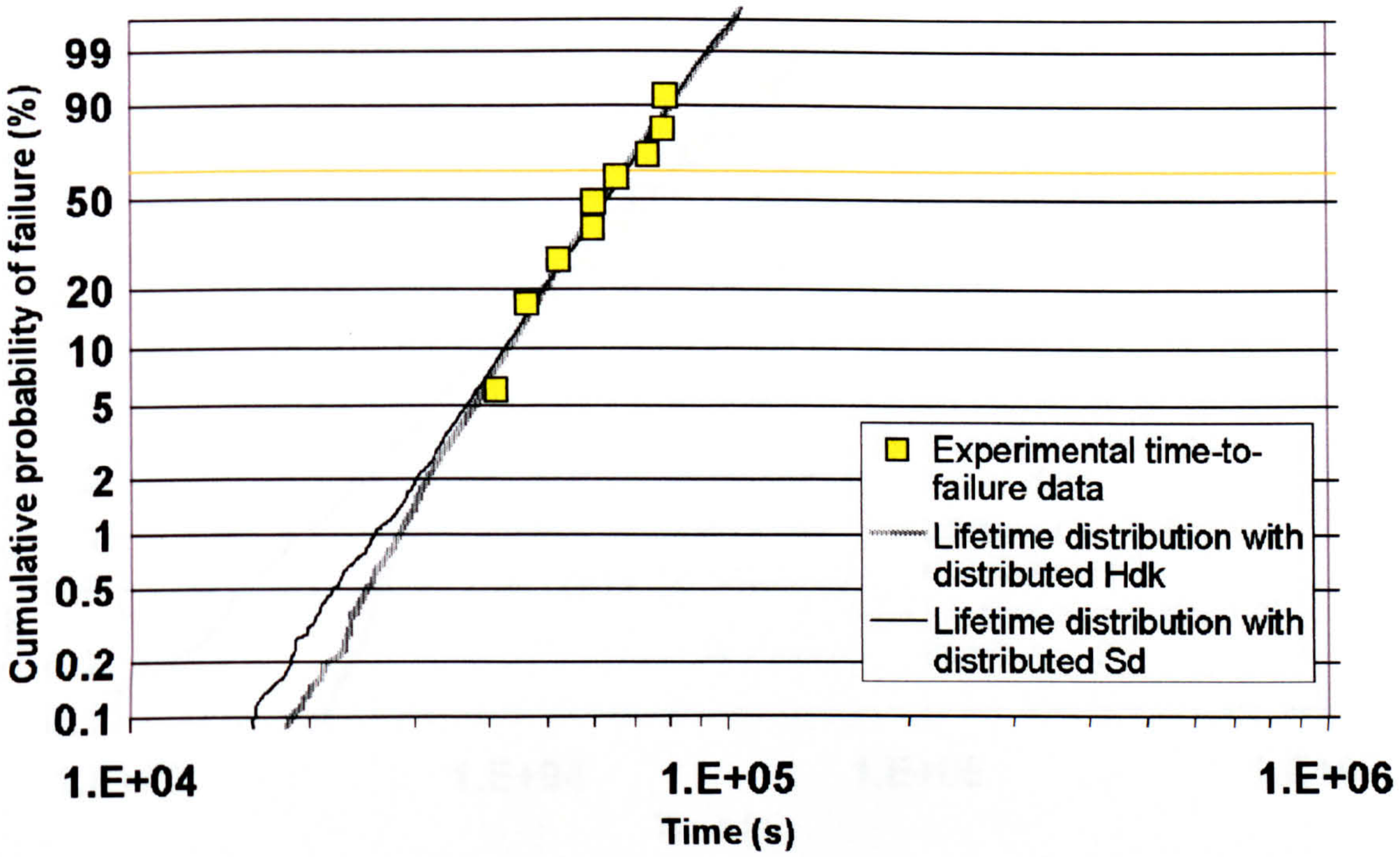

Figure B1.12 E=30kV/mm T=333K

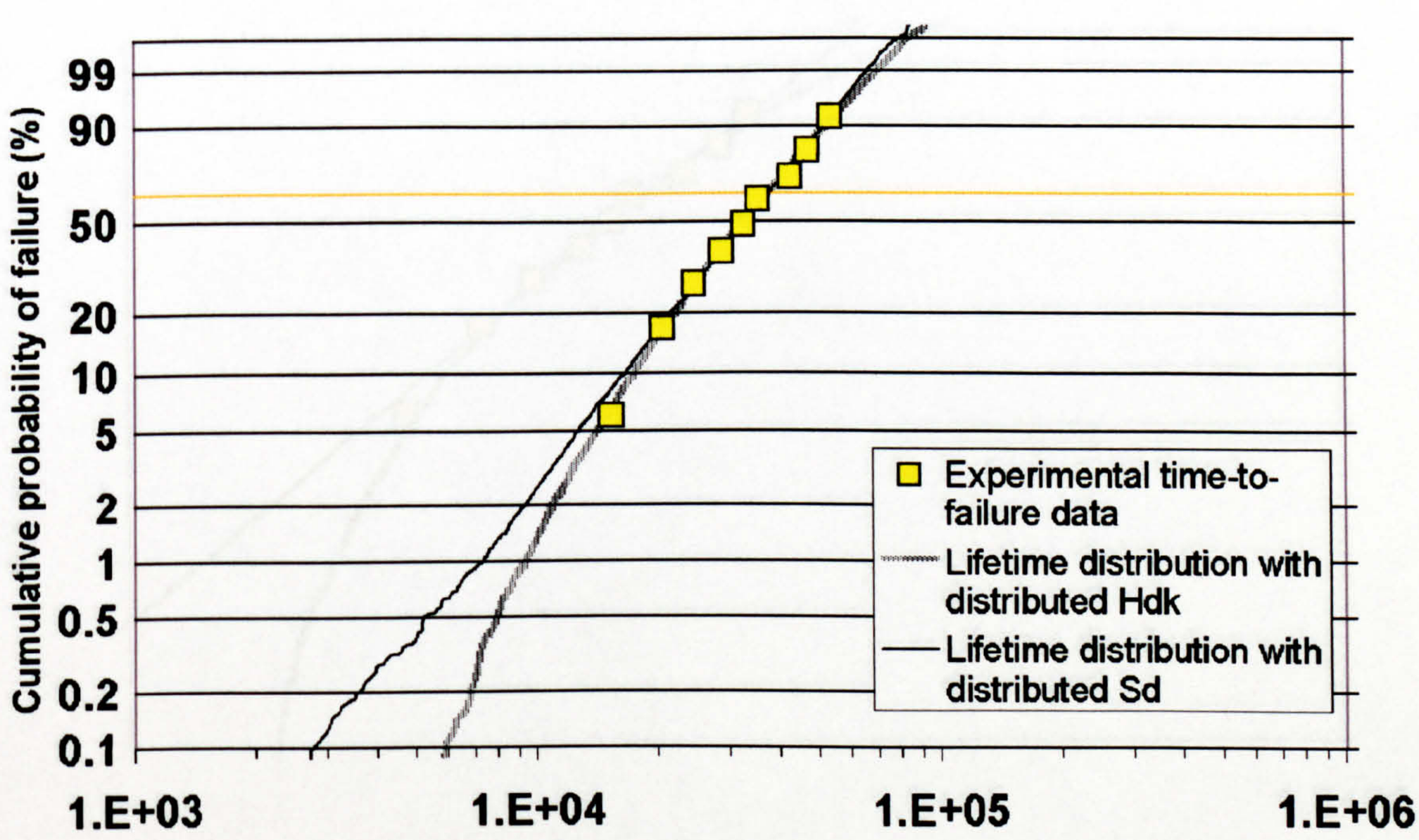

Figure B1.13 E=30kV/mm T=383K

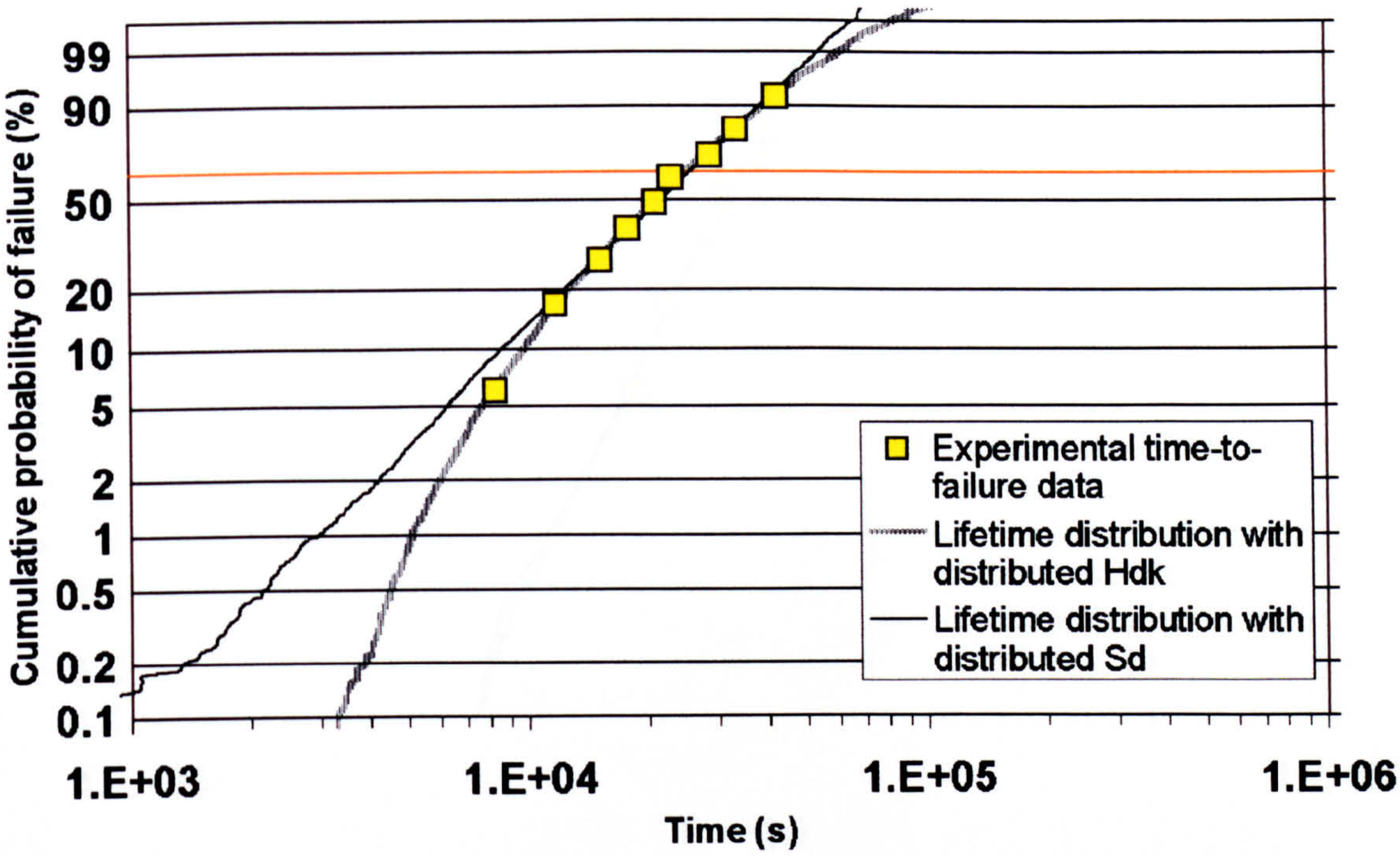

Figure B1.14 E=30kV/mm T=403K

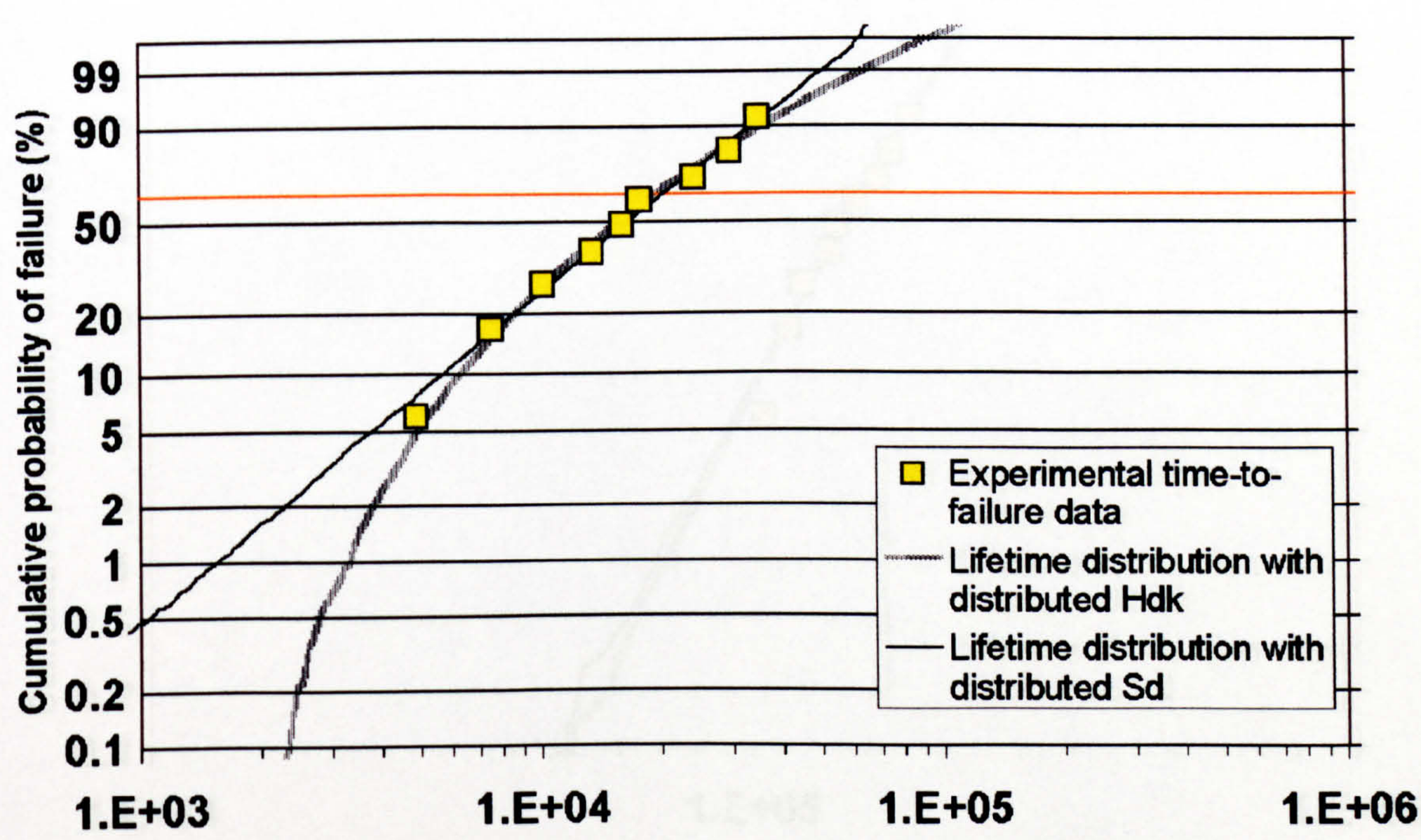

Figure B1.15 E=30kV/mm T=423K

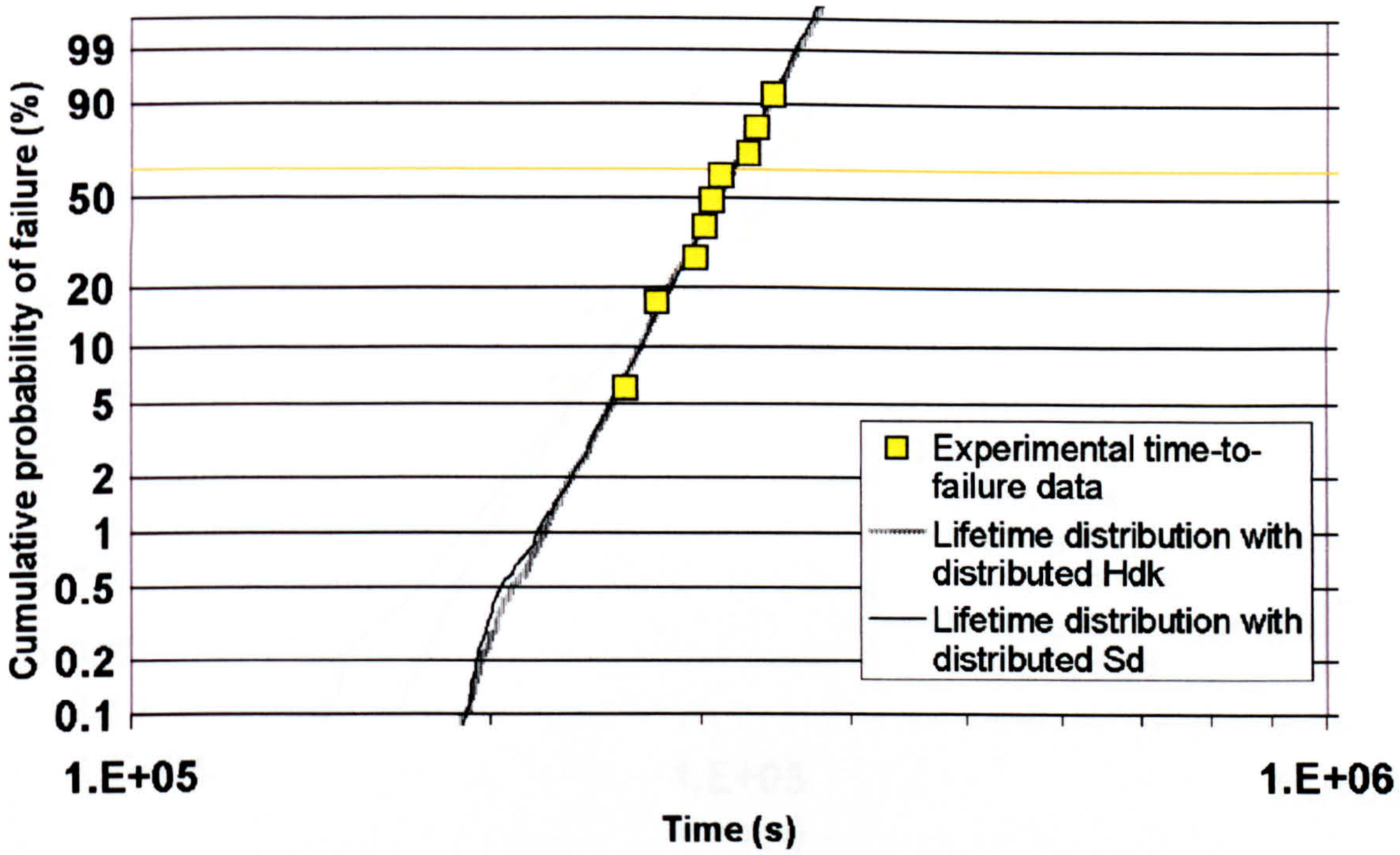

Figure B1.16 E=20kV/mm T=293K

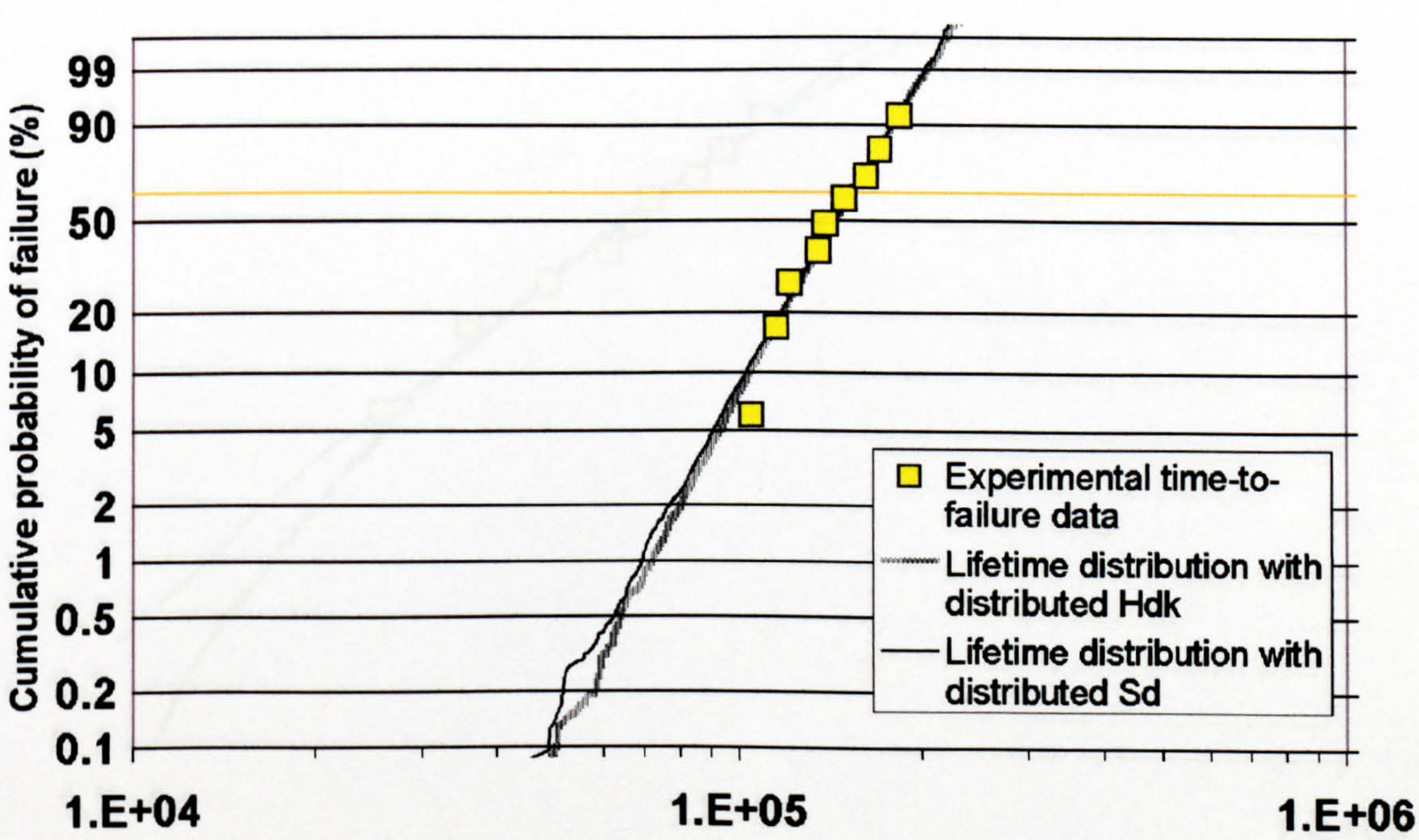

Figure B1.17 E=20kV/mm T=333K

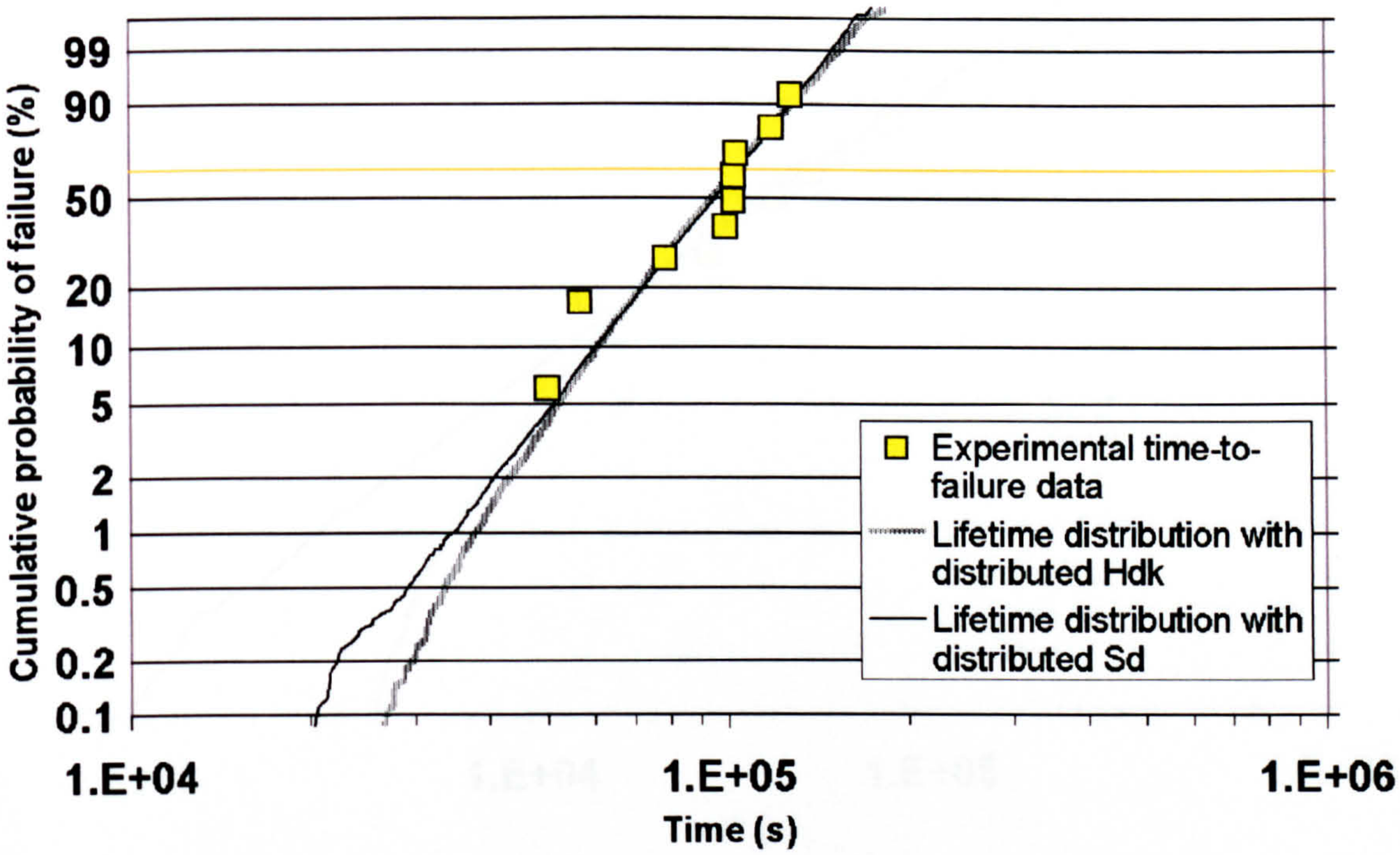

Figure B1.18 E=20kV/mm T=383K

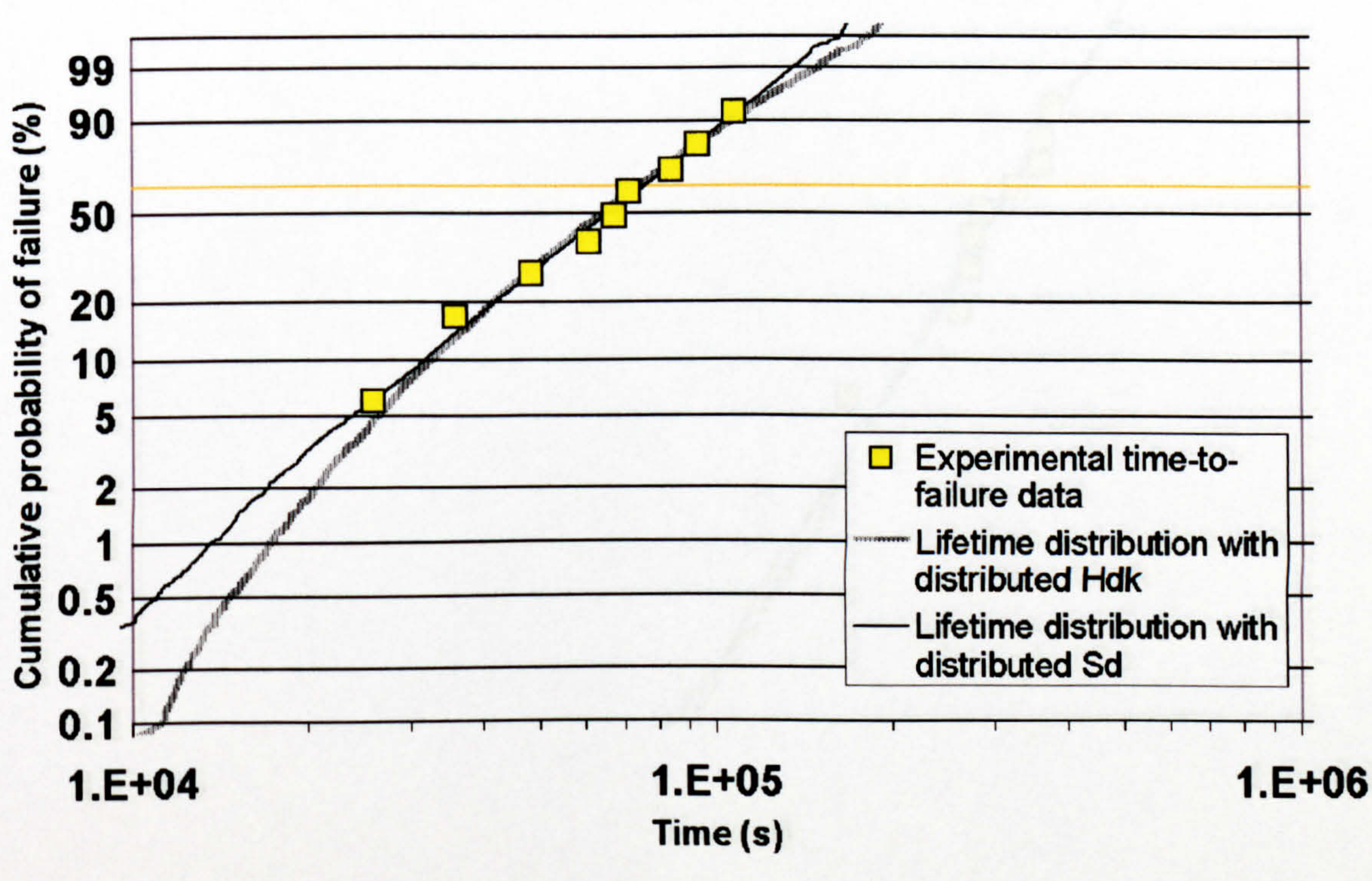

Figure B1.19 E=20kV/mm T=403K

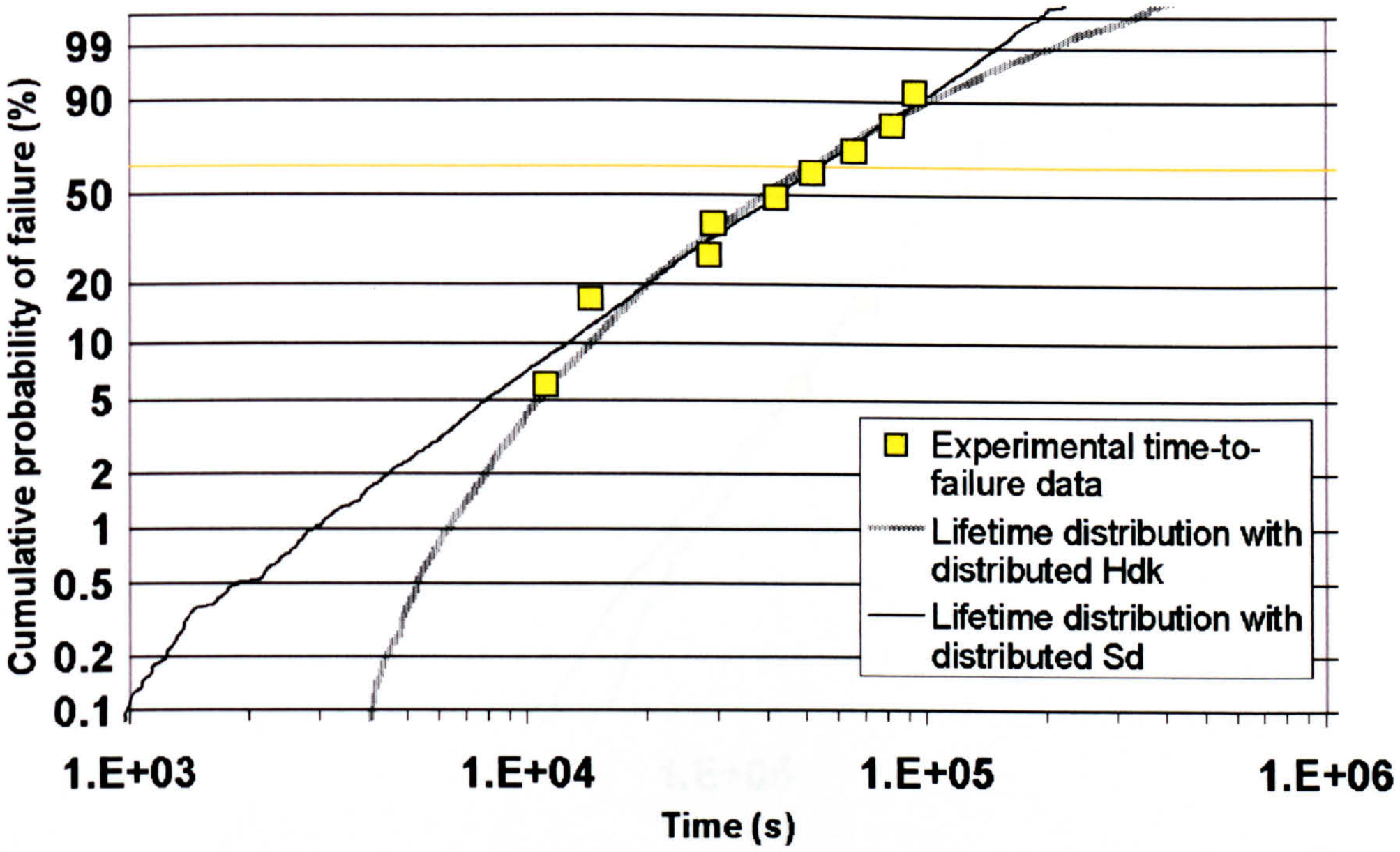

Figure B1.20 E=20kV/mm T=423K

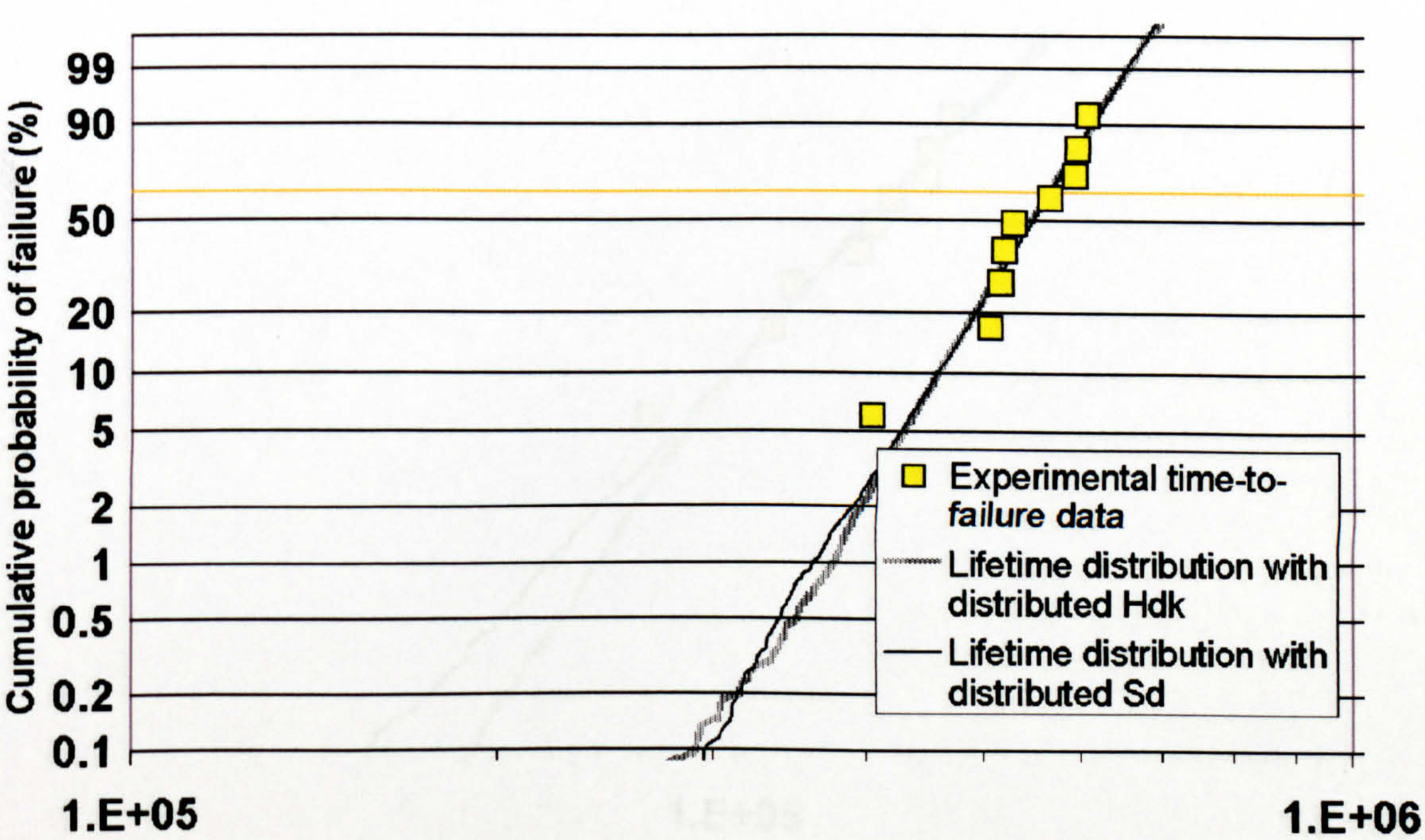

Figure B1.21 E=16kV/mm T=293K

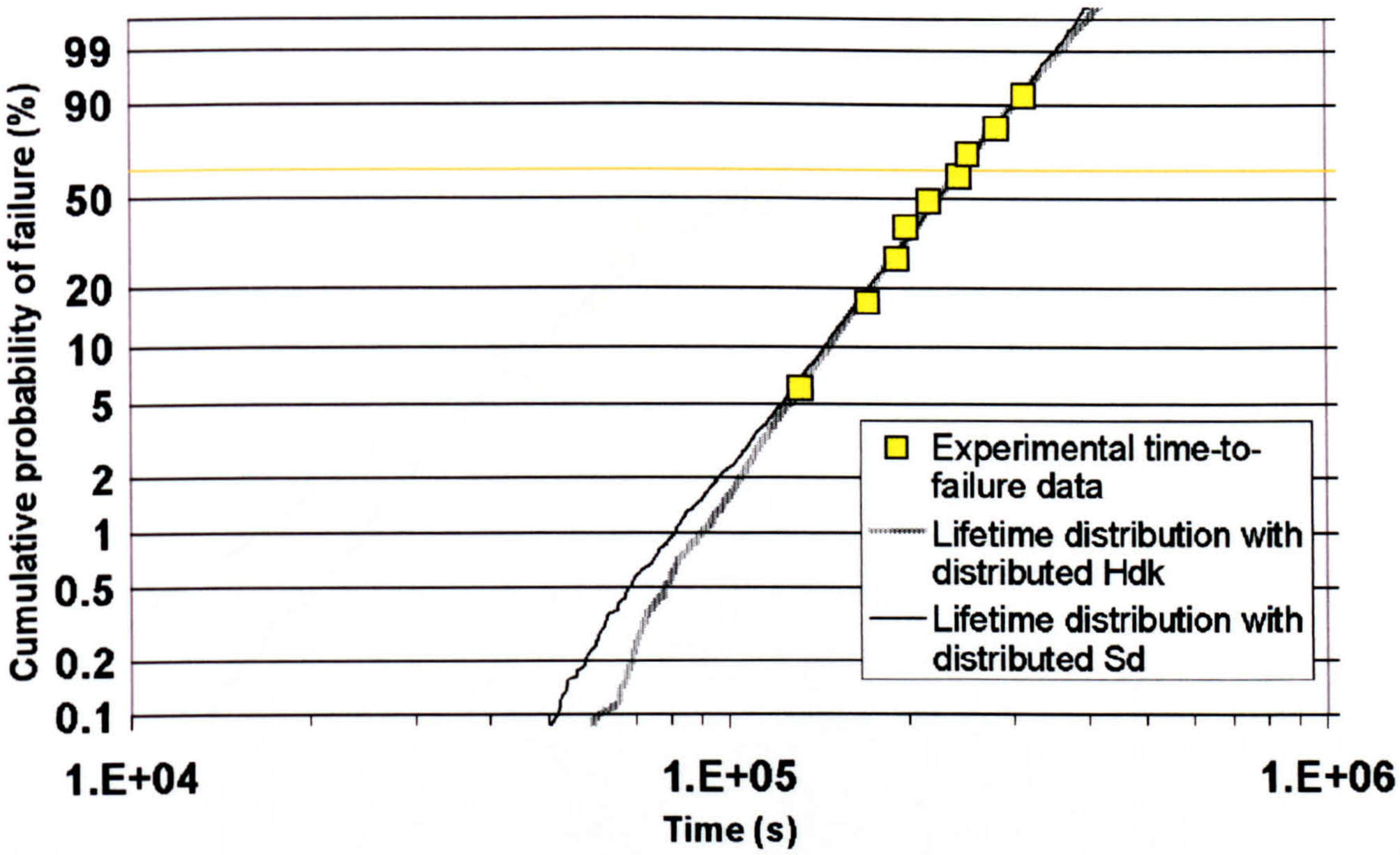

Figure B1.22 E=16kV/mm T=333K

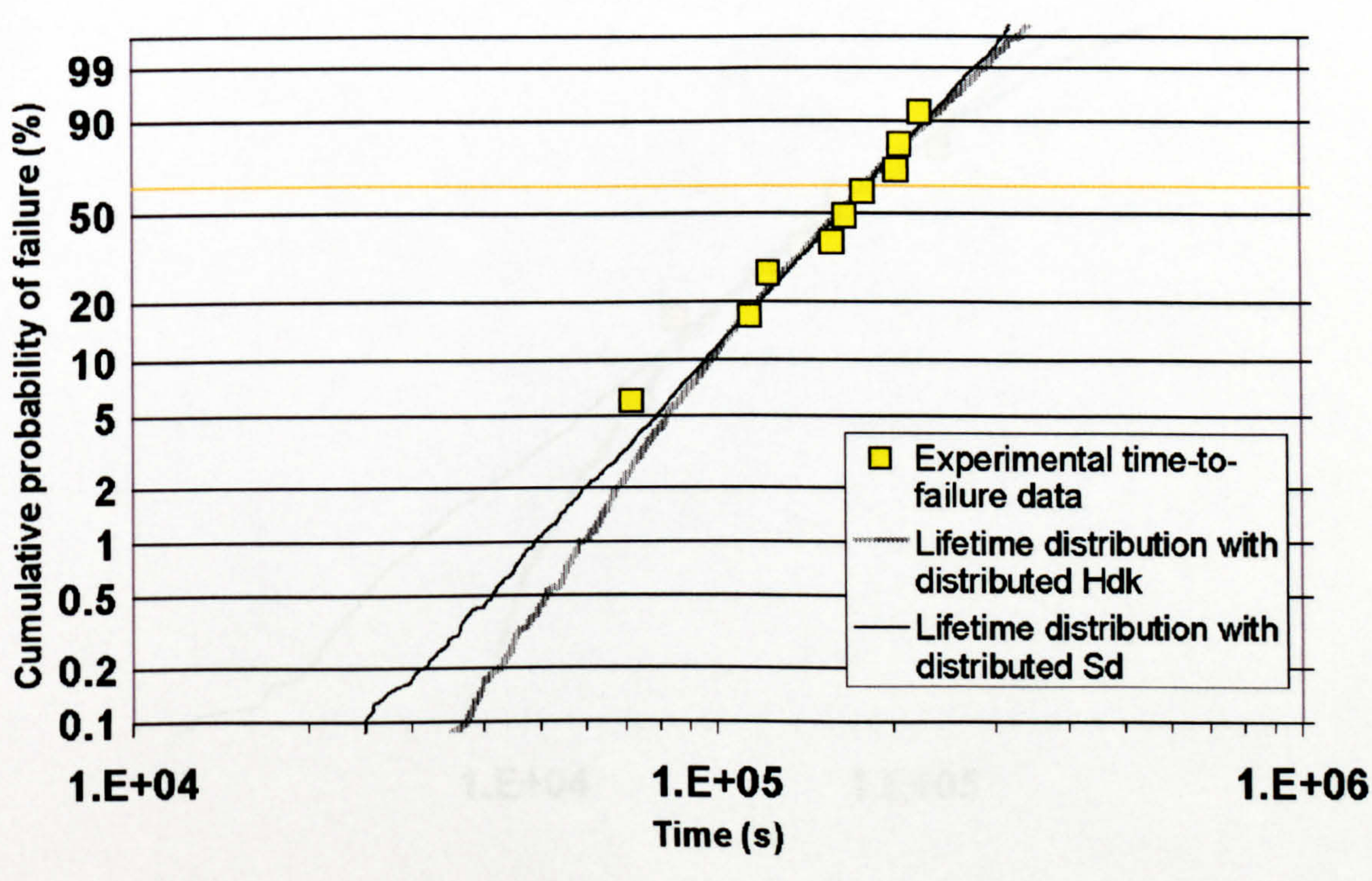

Figure B1.23 E=16kV/mm T=383K

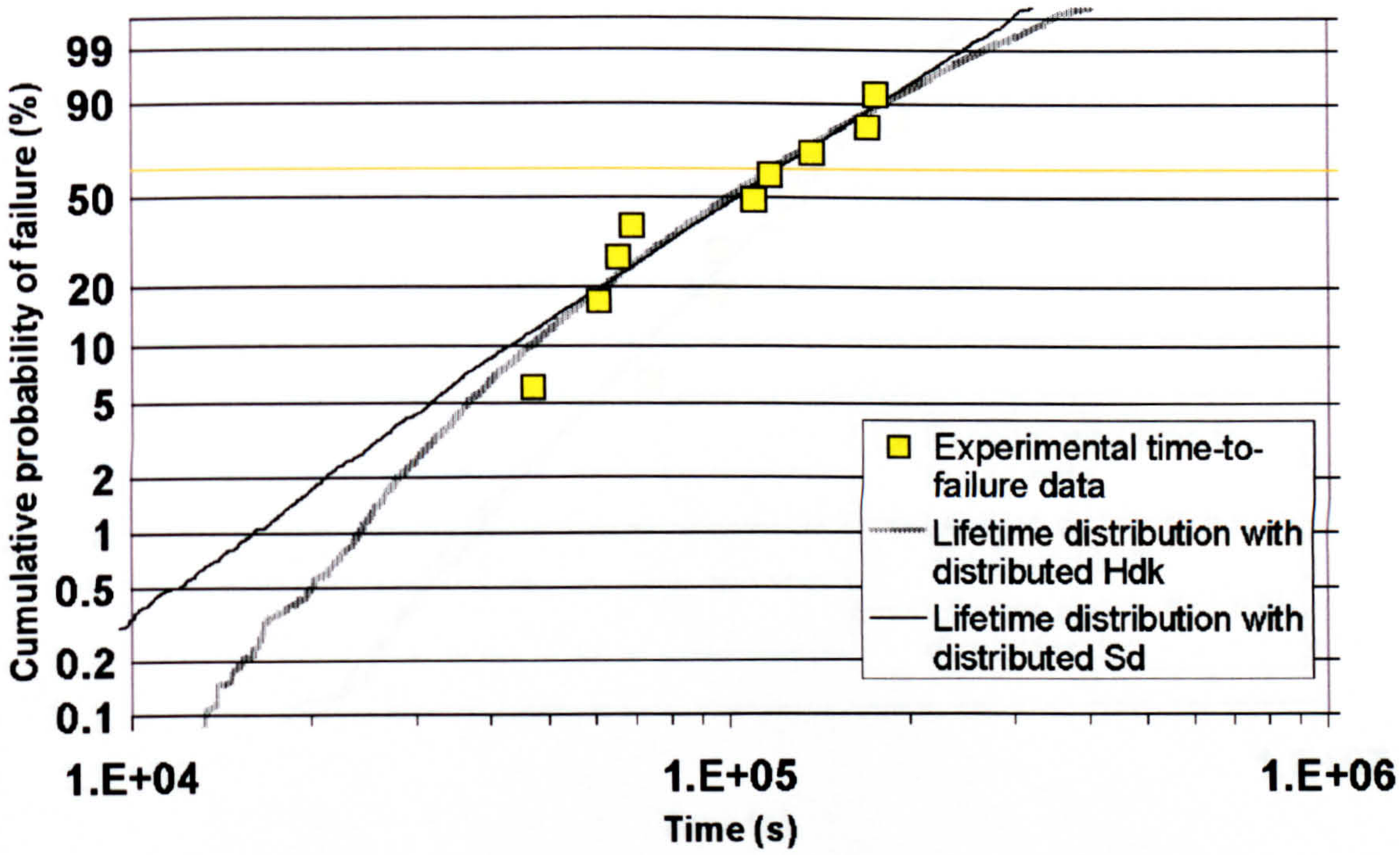

Figure B1.24 E=16kV/mm T=403K

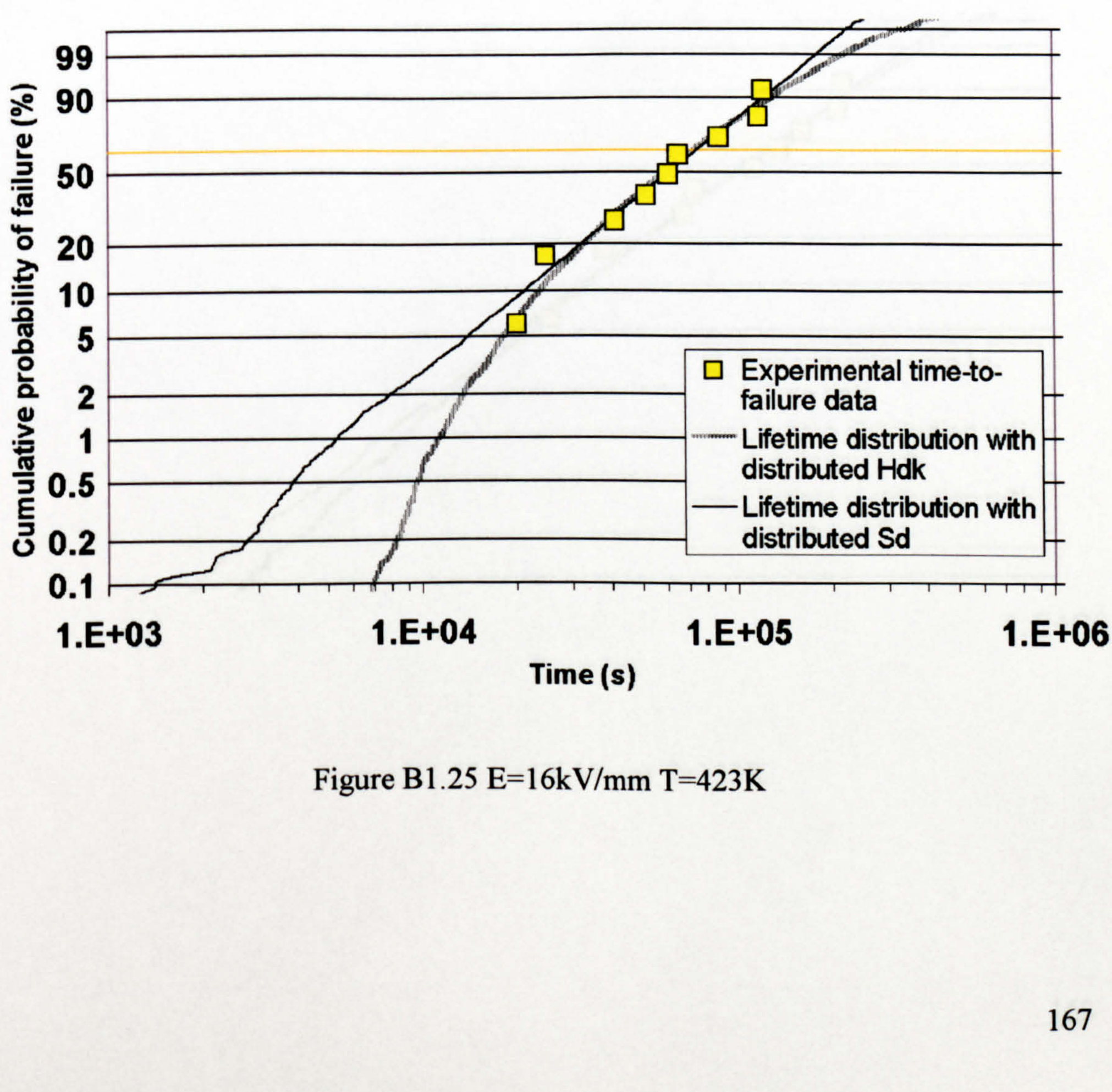

Figure B1.25 E=16kV/mm T=423K

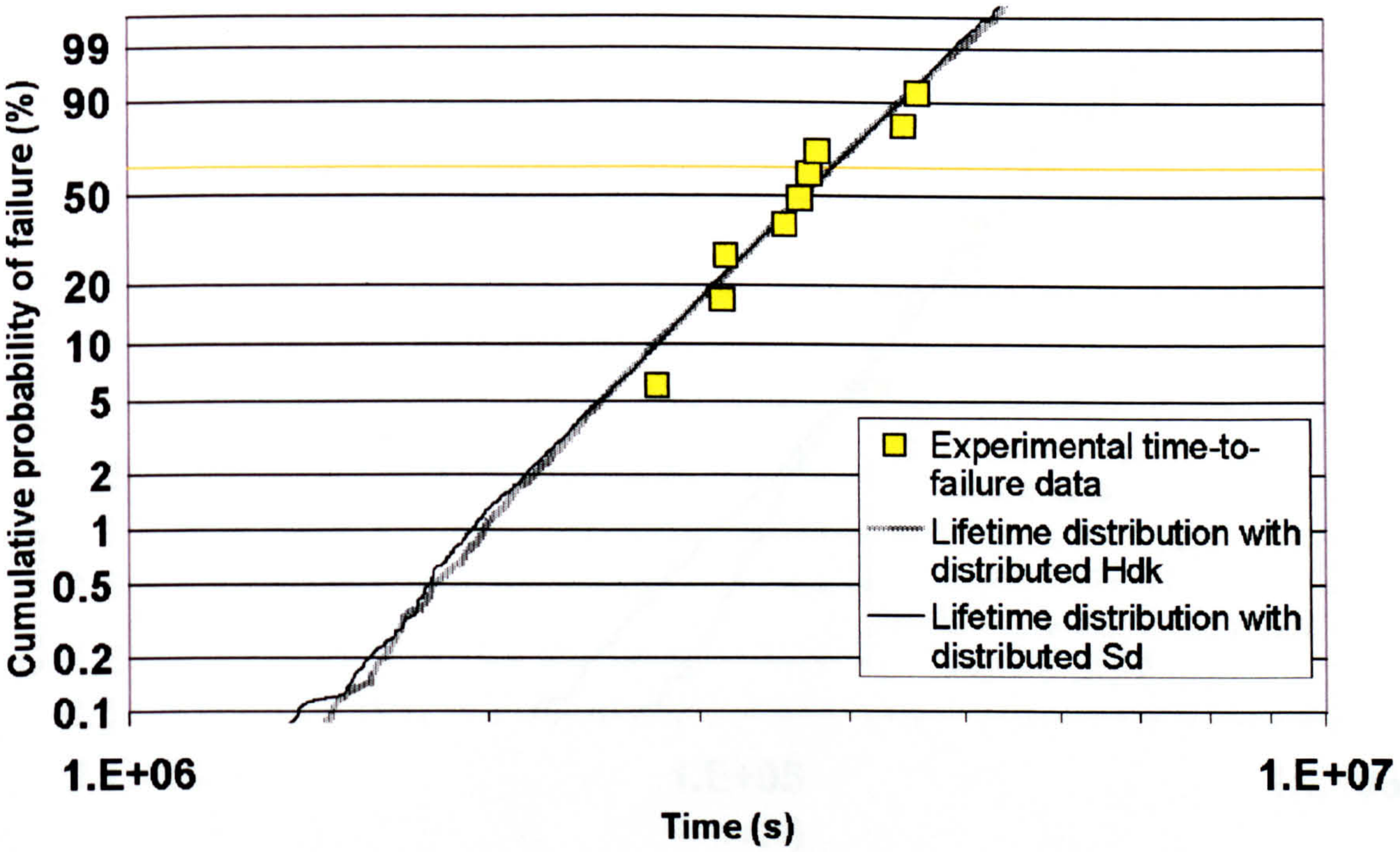

Figure B1.26 E=13kV/mm T=293K

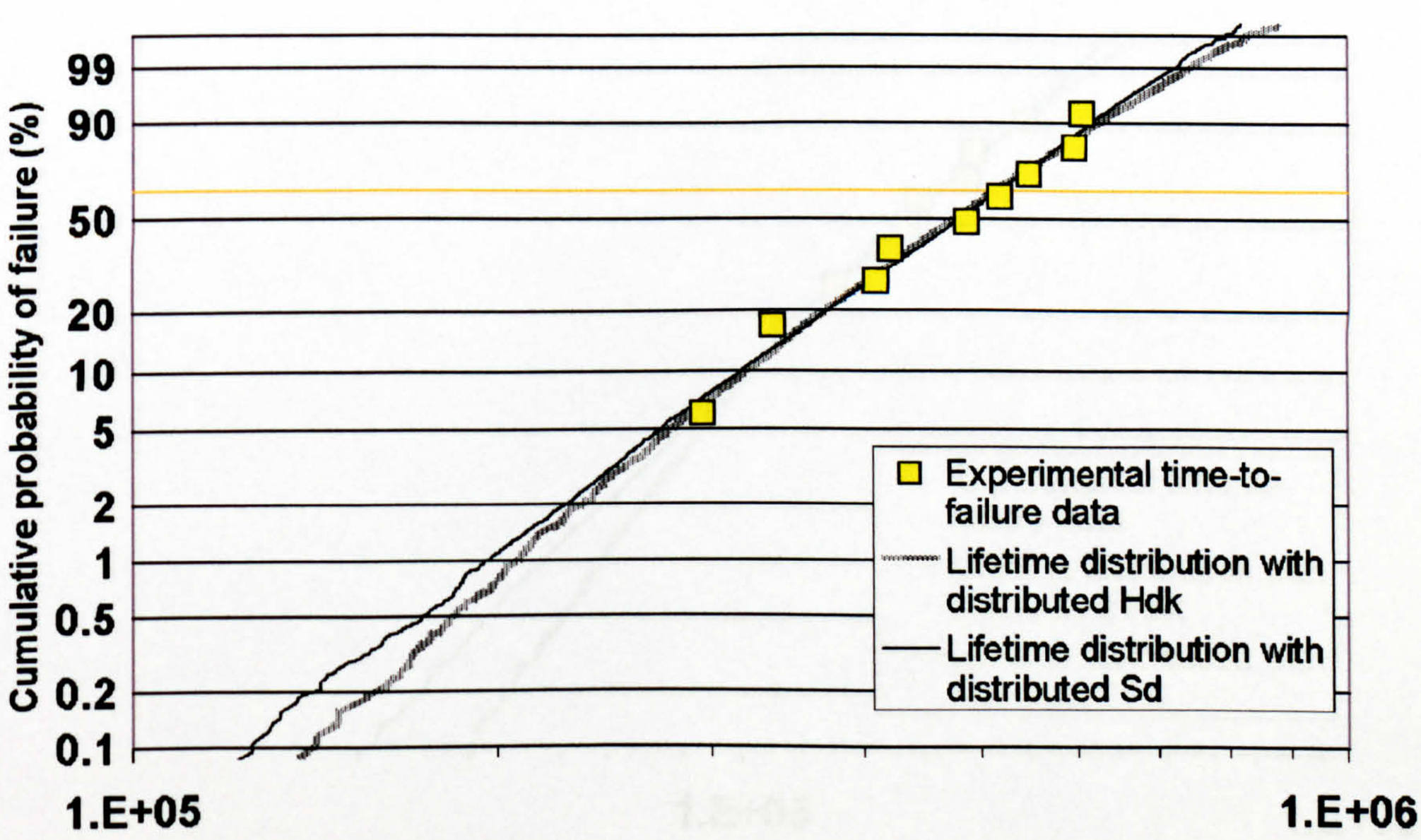

Figure B1.27 E=13kV/mm T=333K

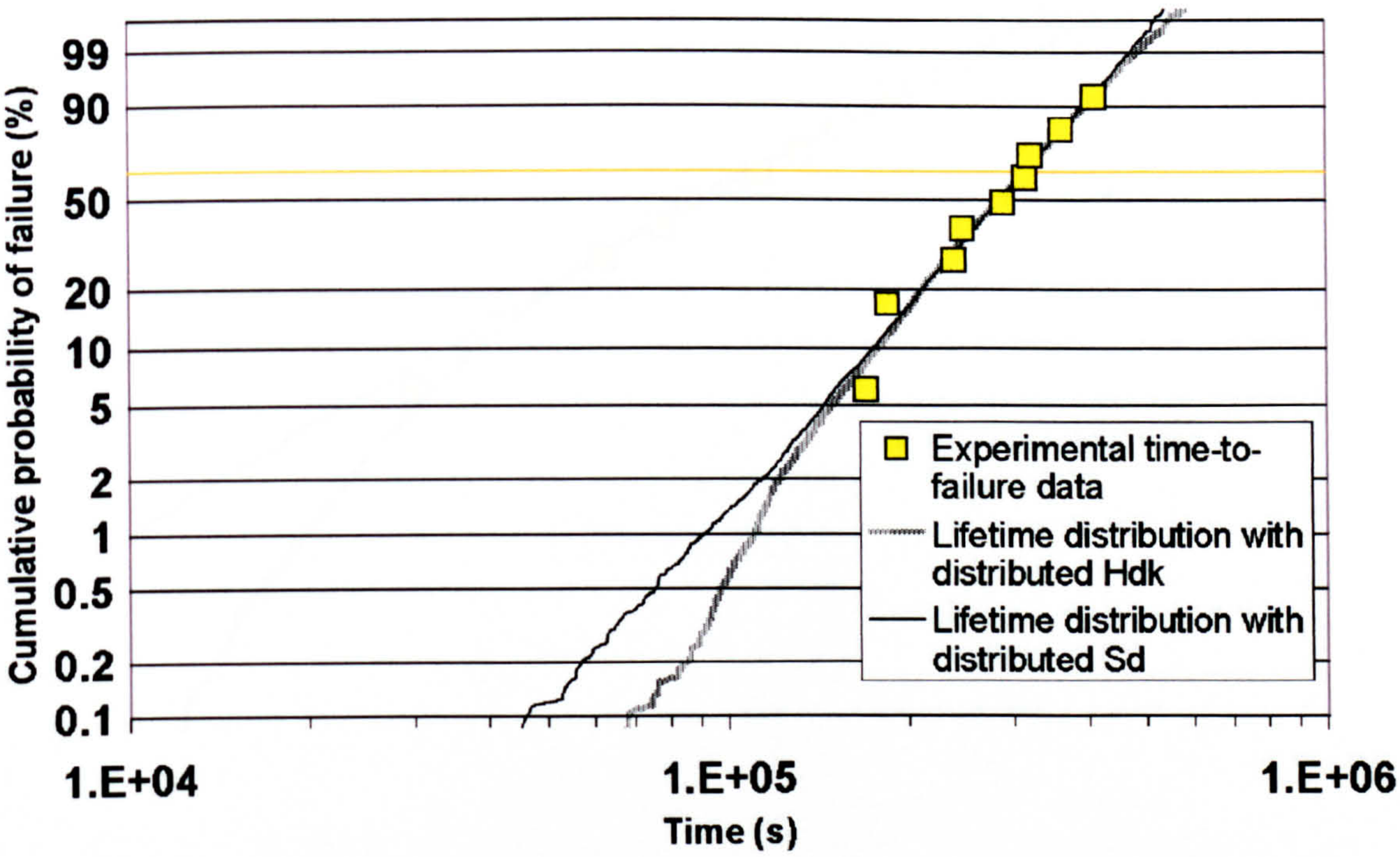

Figure B1.28 E=13kV/mm T=383K

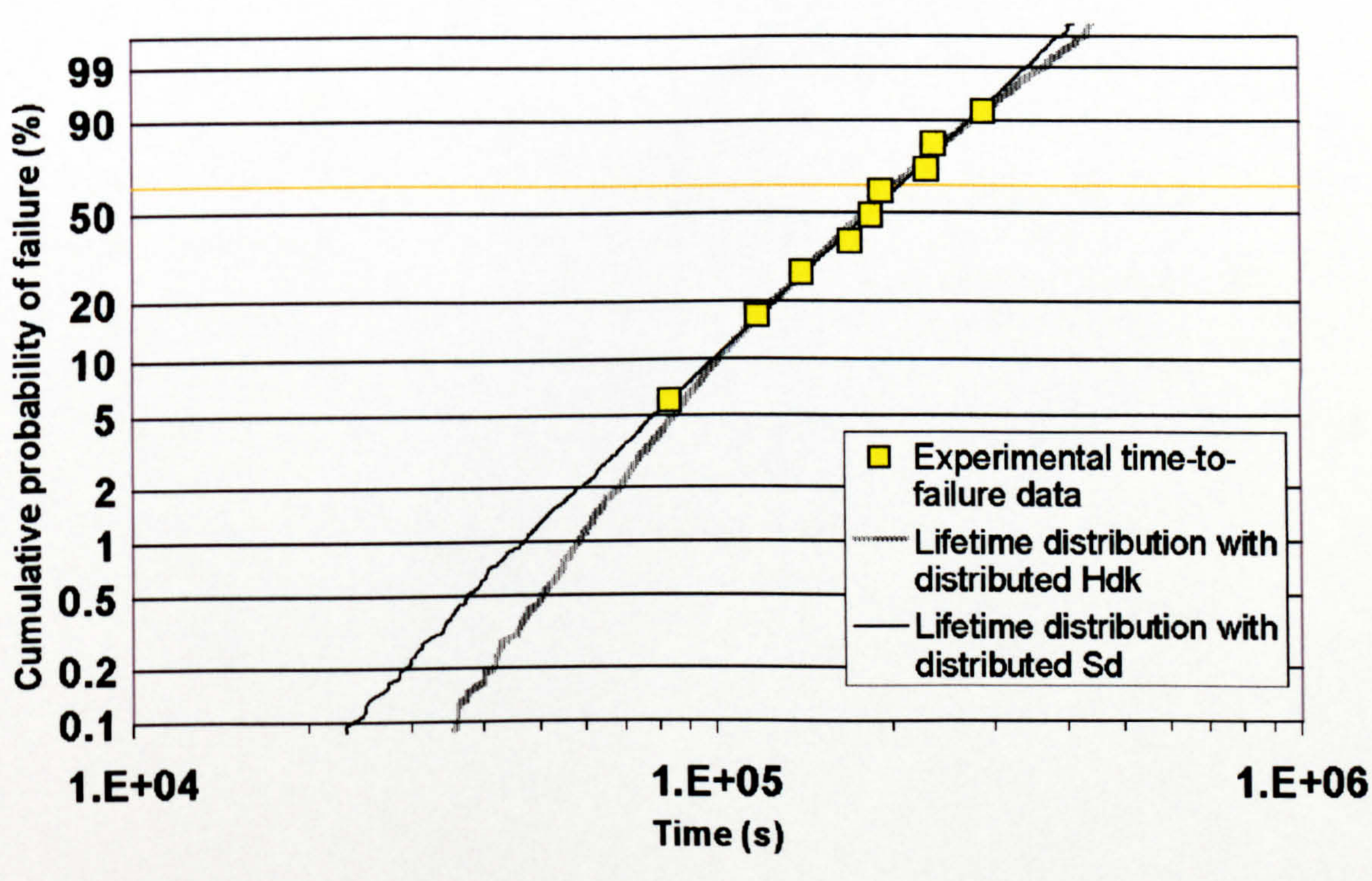

Figure B1.29 E=13kV/mm T=403K

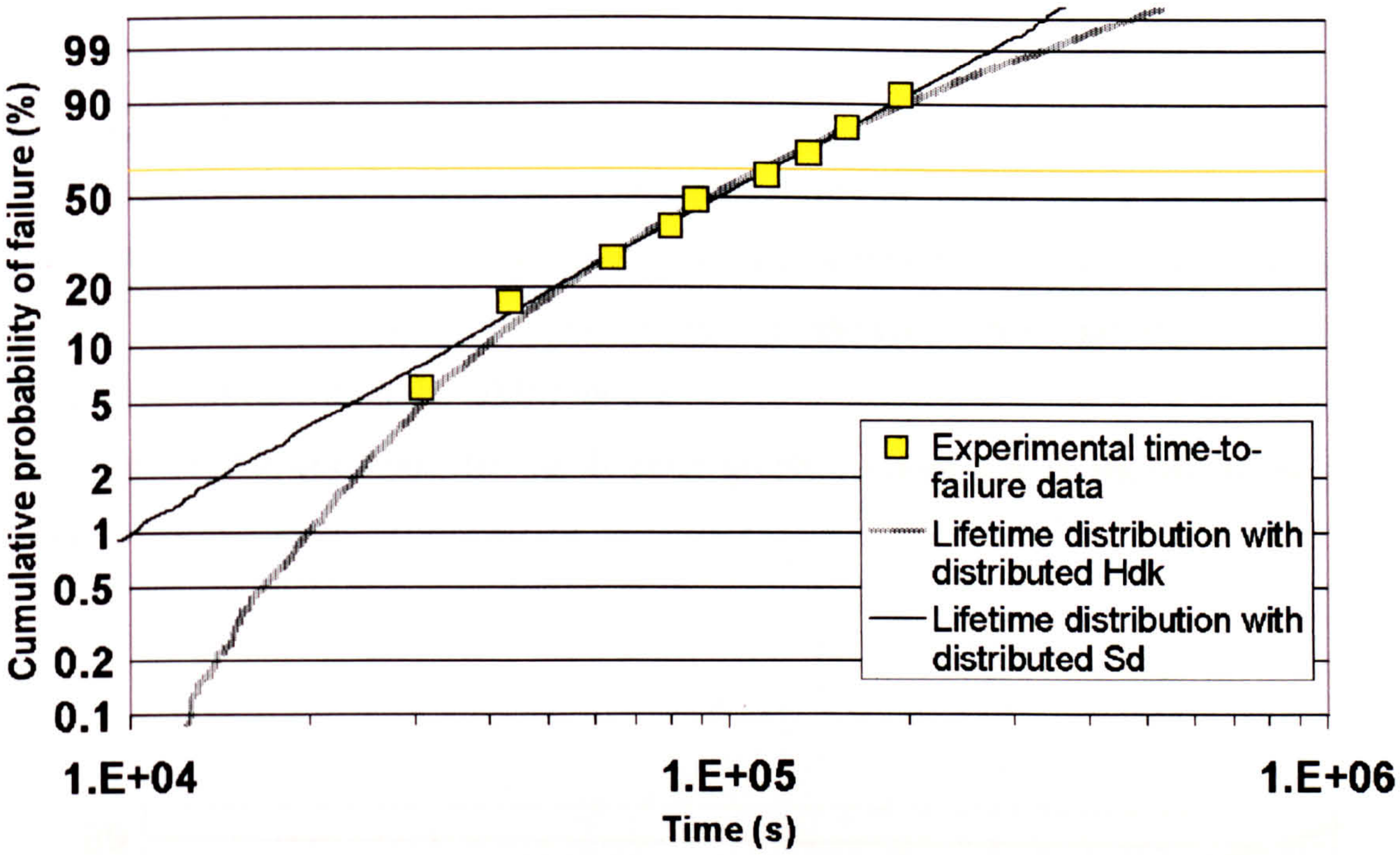

Figure B1.30 E=13kV/mm T=423K

B2. DC Data

These graphs show the Weibull cumulative probability of failure on the y-axis, against time in seconds on the x-axis. Each graph shows experimental time-to-failure points as squares. The black line in each case corresponds to the failure distribution predicted by an H_{dk} distribution within the DMM model.

The experimental condition to which each graph corresponds is shown below the graphs.

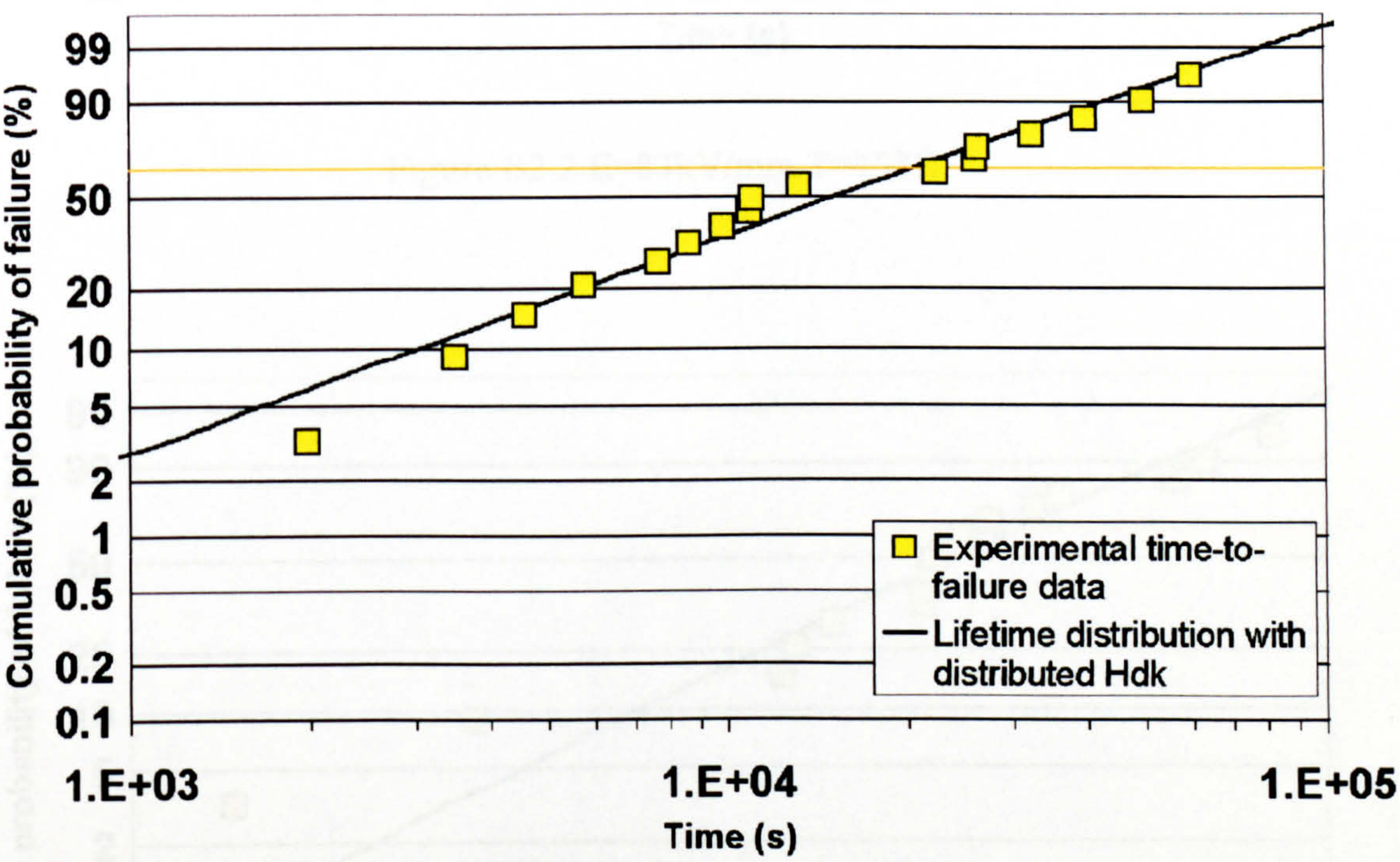

Figure B2.1 E=83kV/mm T=408K

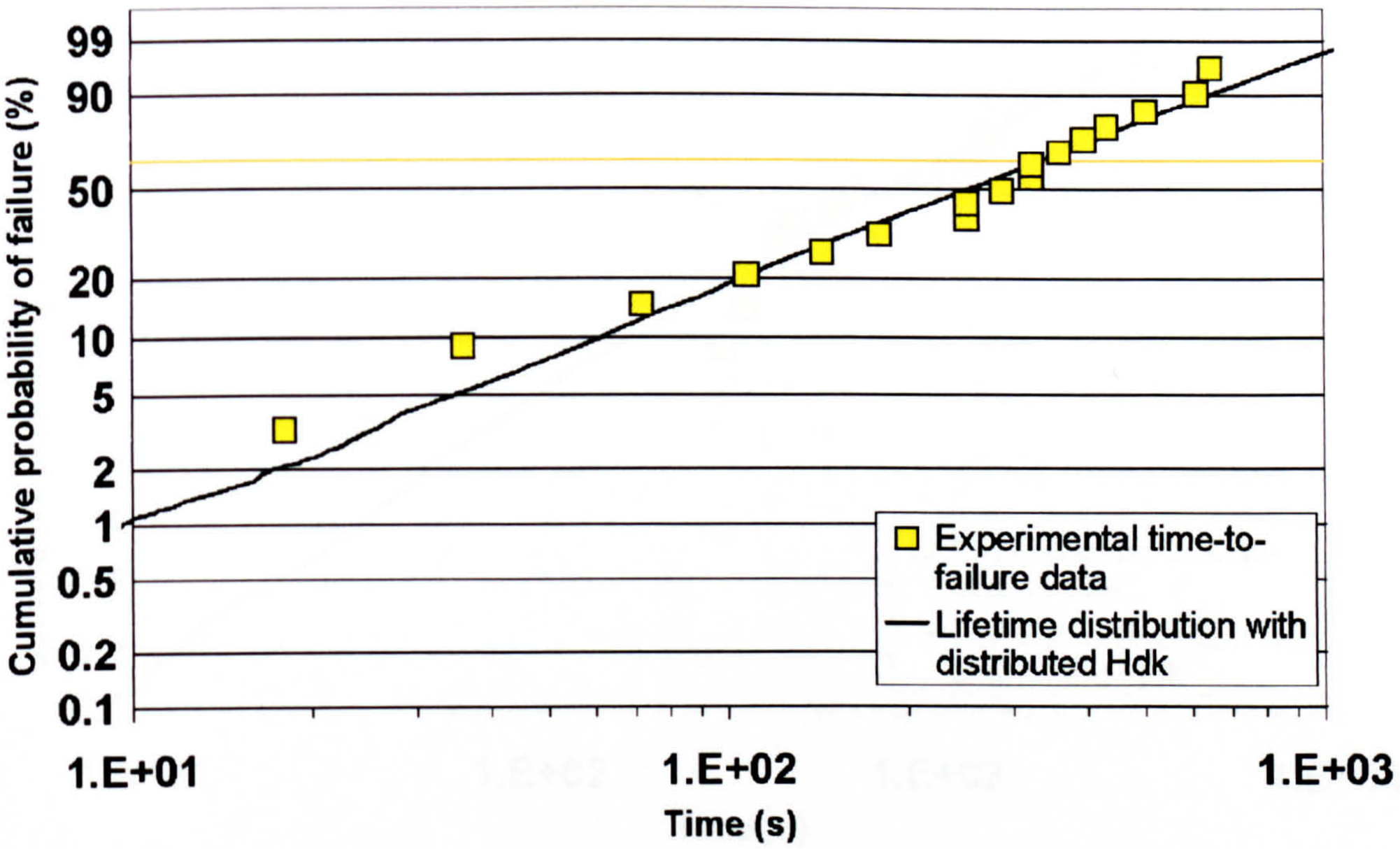

Figure B2.2 E=83kV/mm T=453K

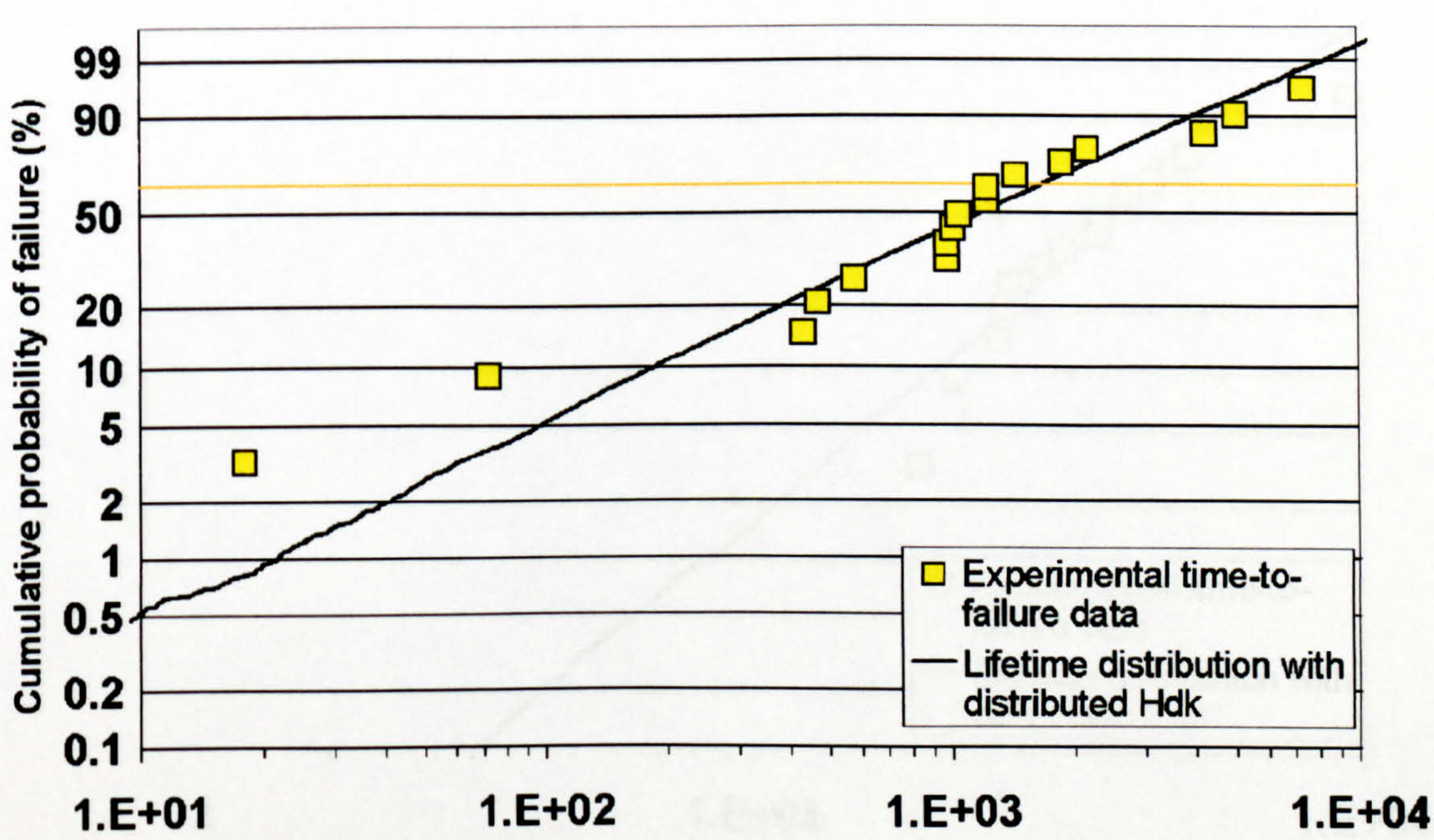

Figure B2.3 E=83kV/mm T=427K

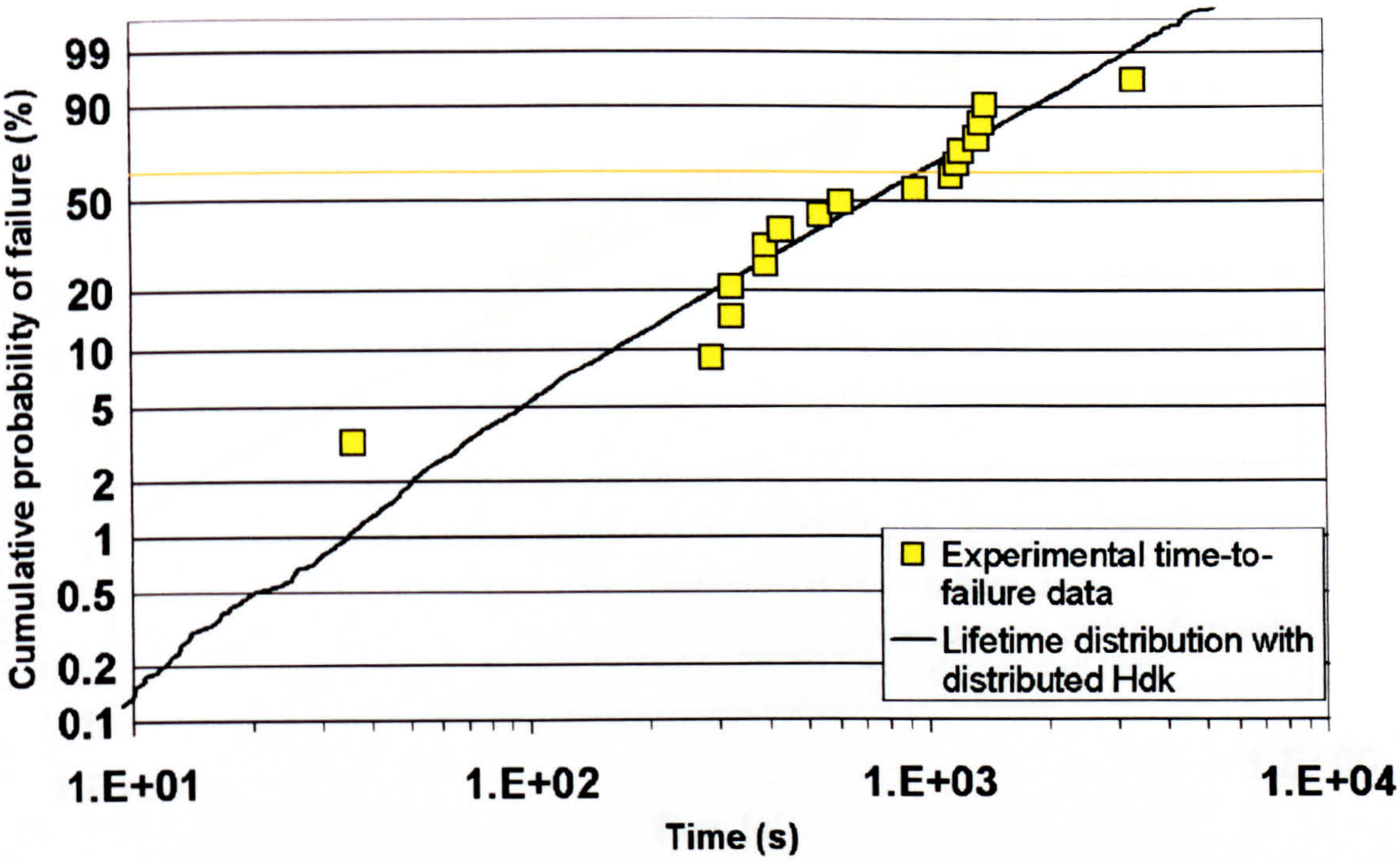

Figure B2.4 E=69kV/mm T=452K

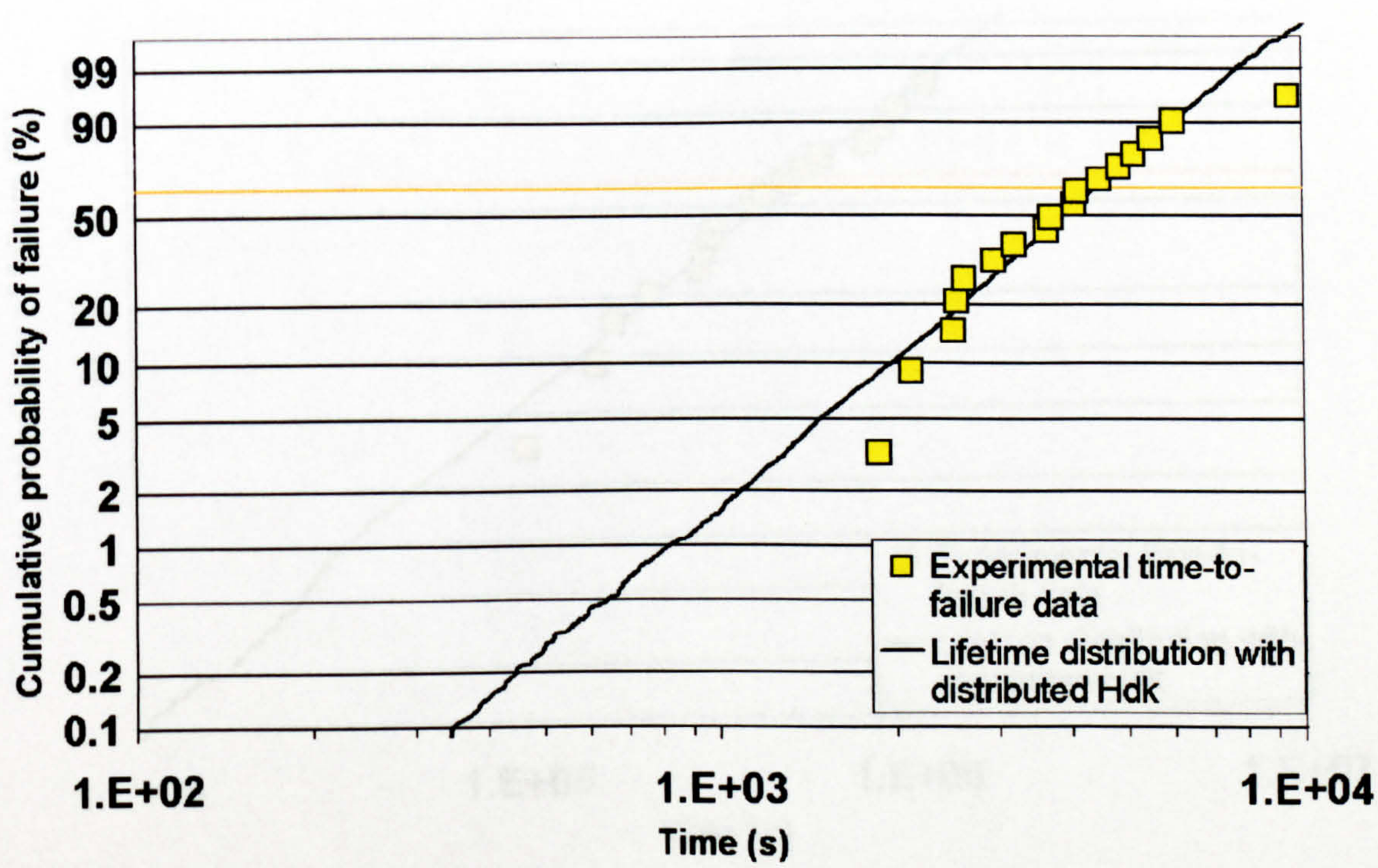

Figure B2.5 E=69kV/mm T=434K

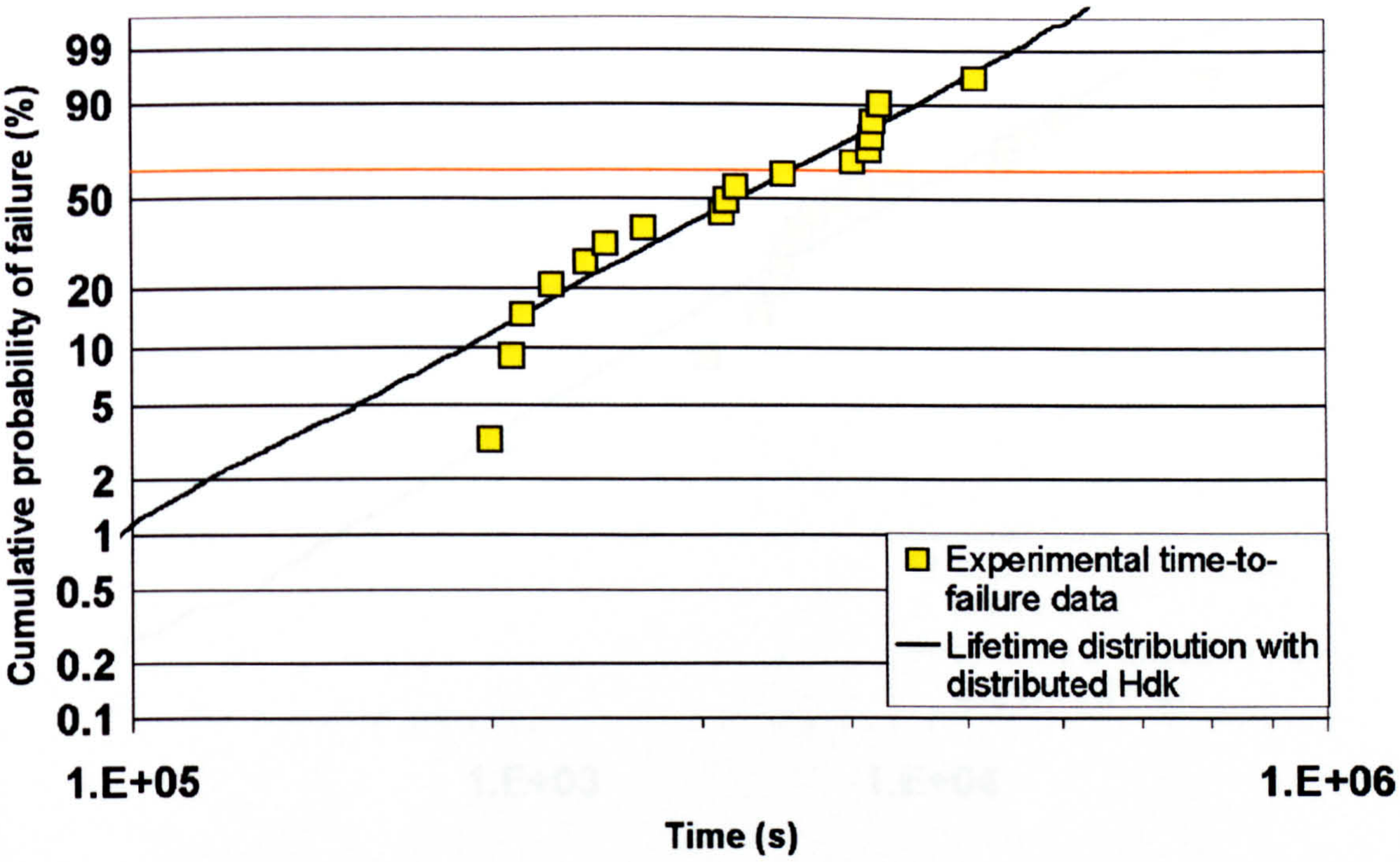

Figure B2.6 E=69kV/mm T=391K

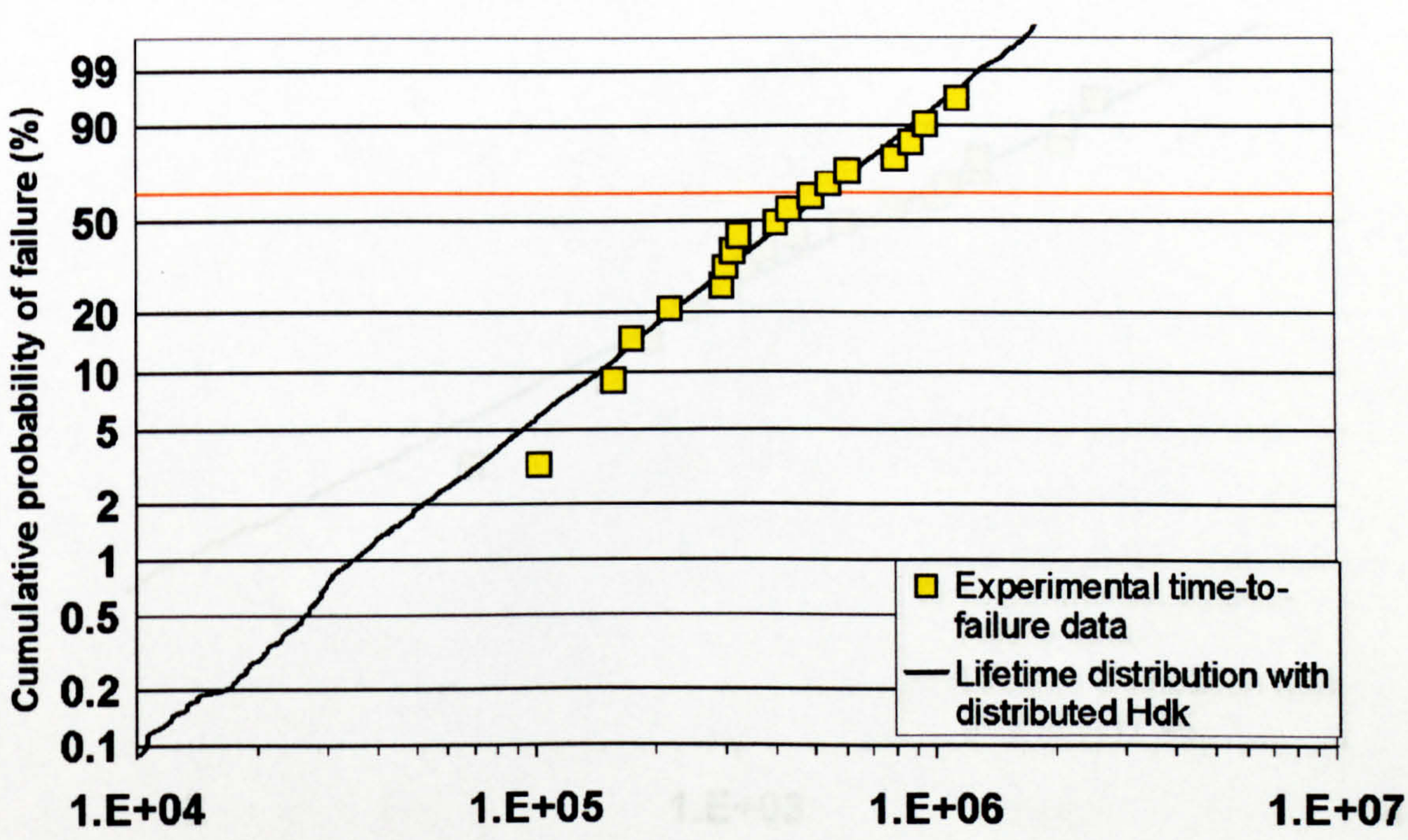

Figure B2.7 E=83kV/mm T=383K

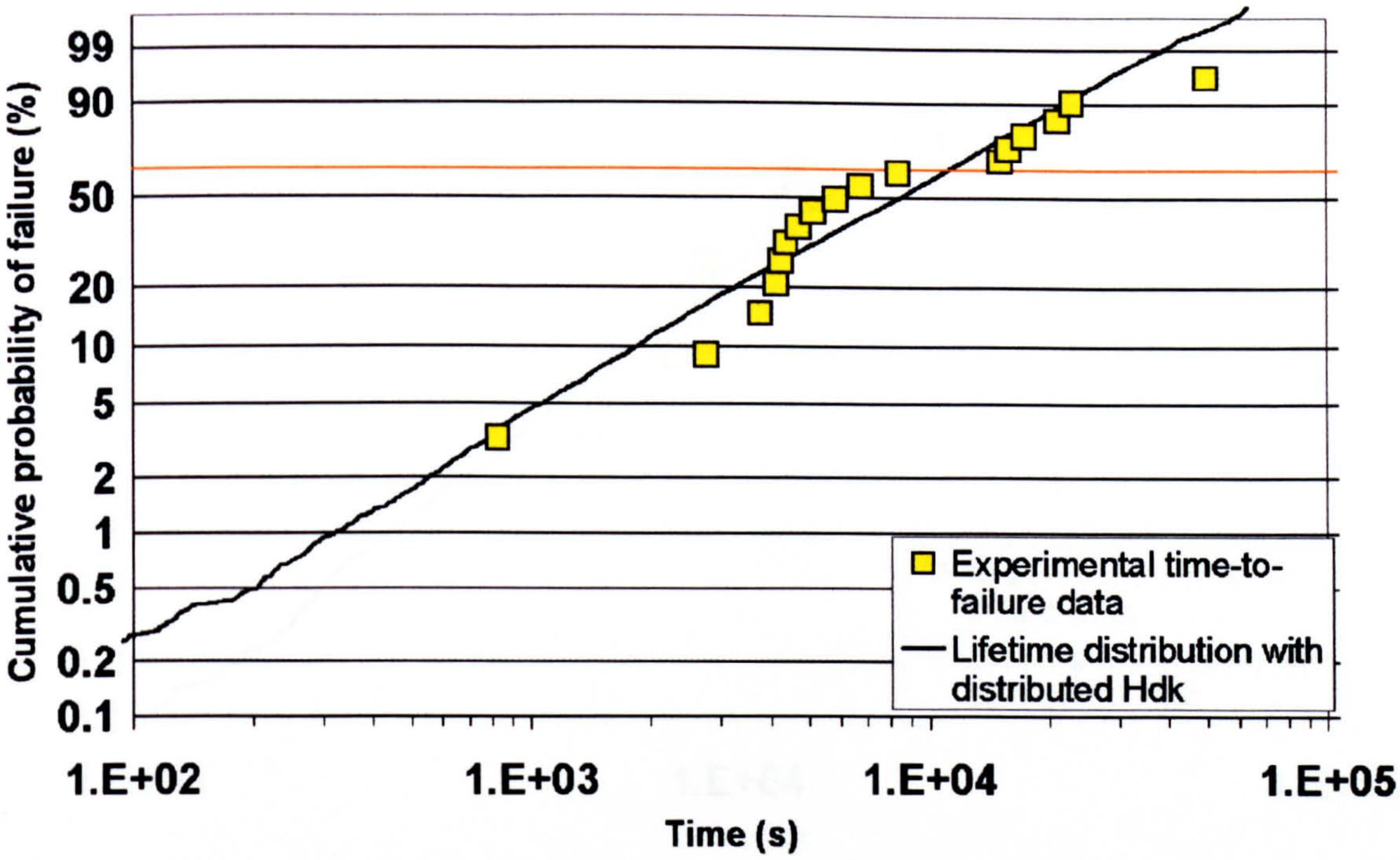

Figure B2.8 E=56kV/mm T=430K

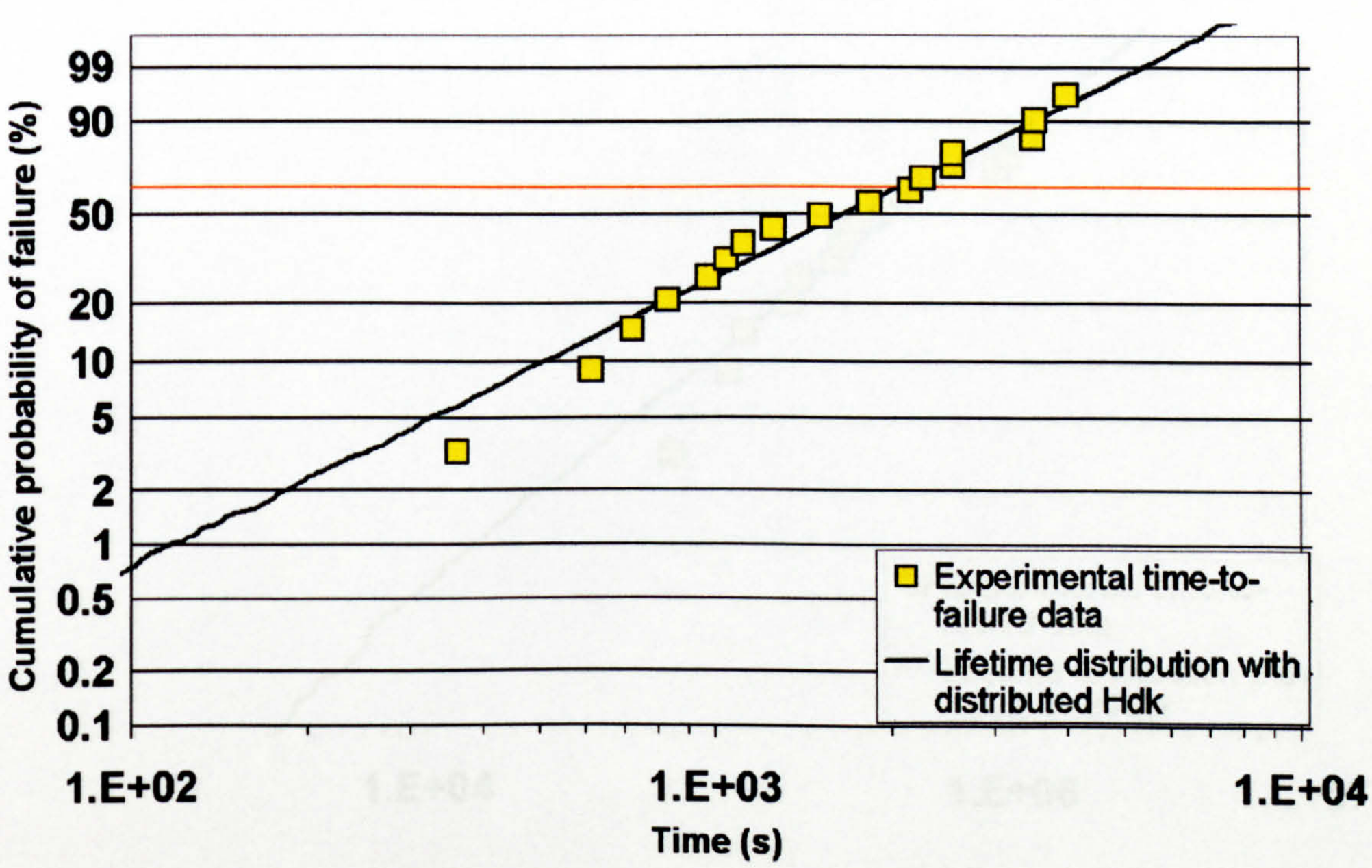

Figure B2.9 E=83kV/mm T=433K

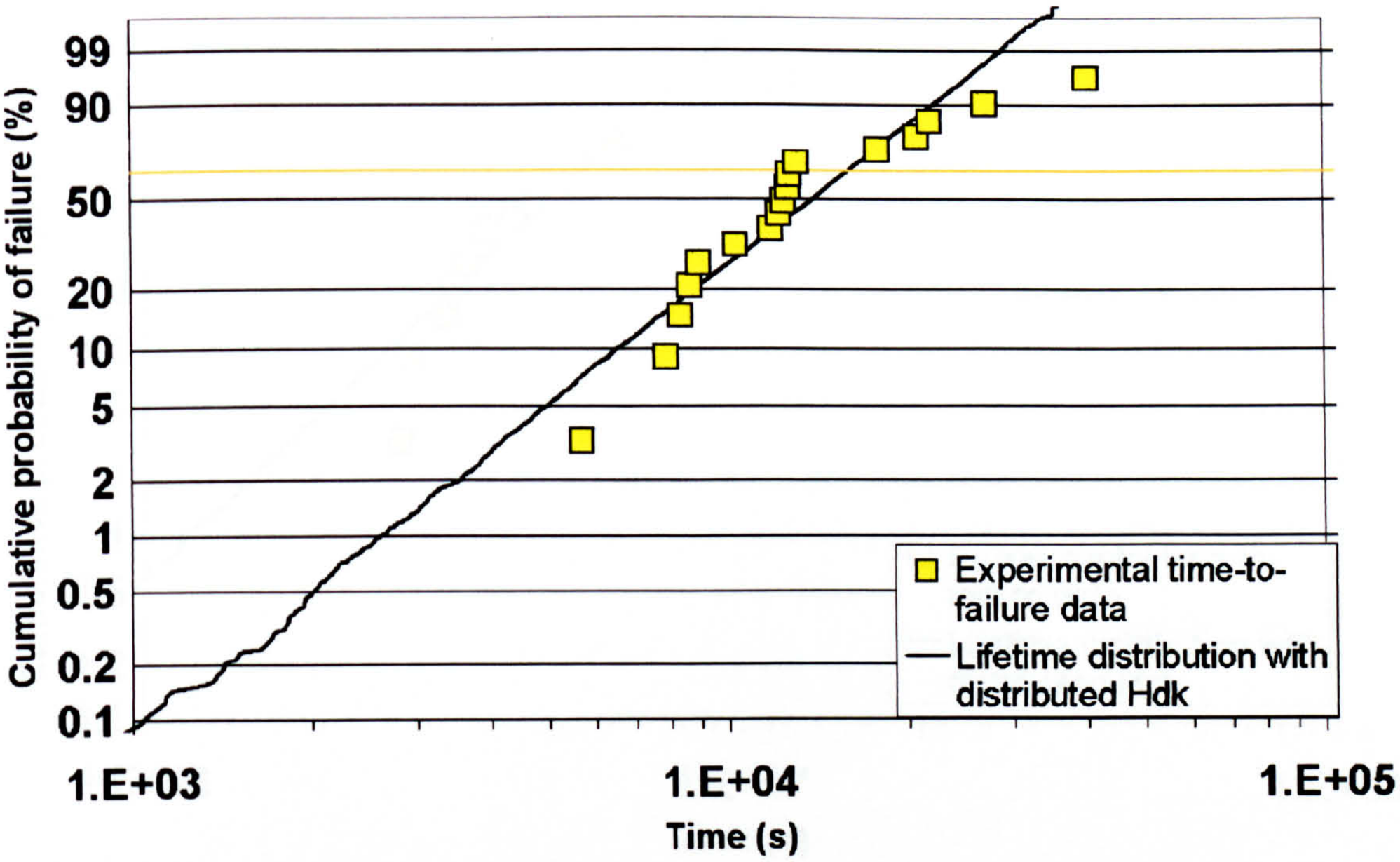

Figure B2.10 E=24kV/mm T=433K

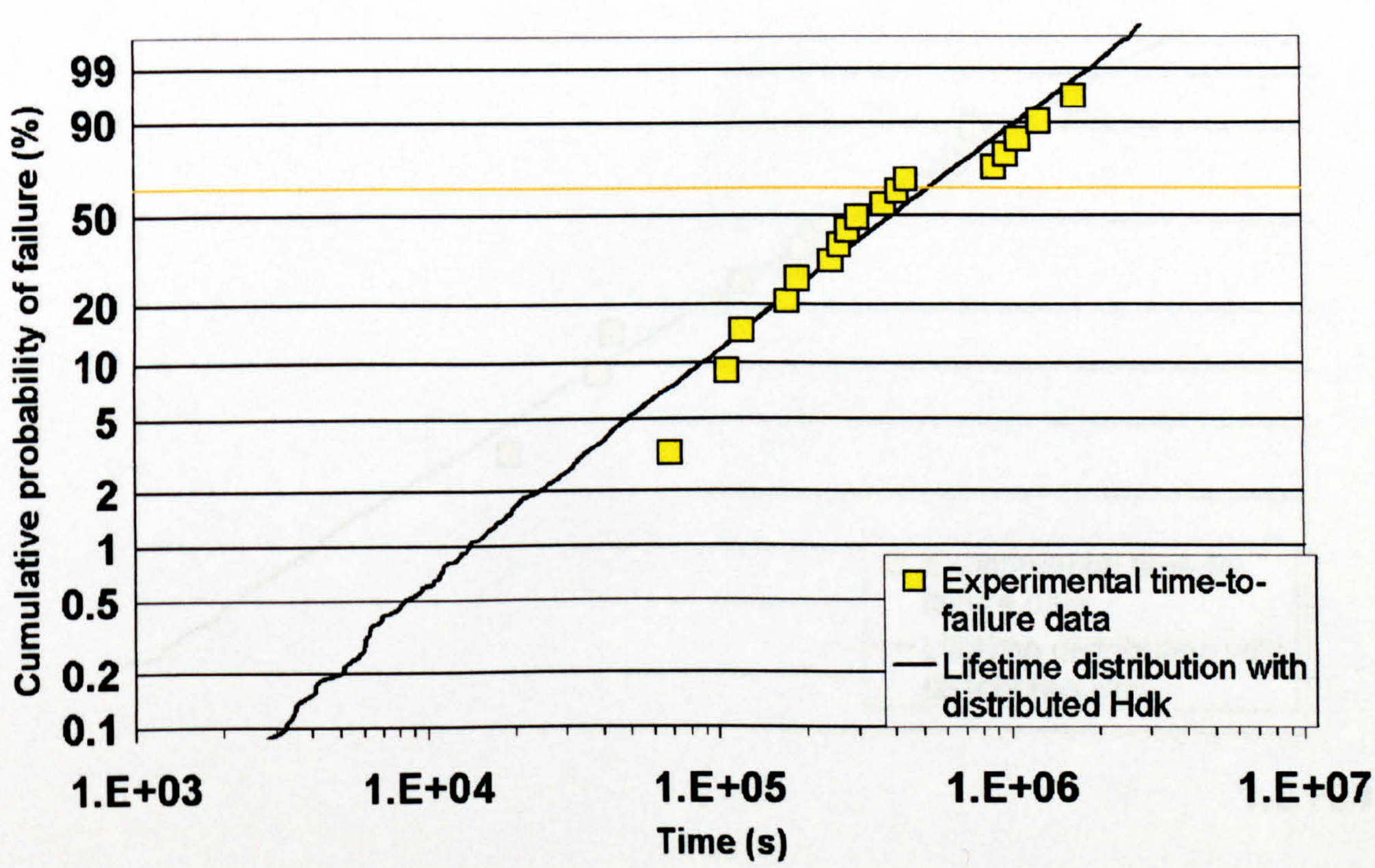

Figure B2.11 E=28kV/mm T=431K

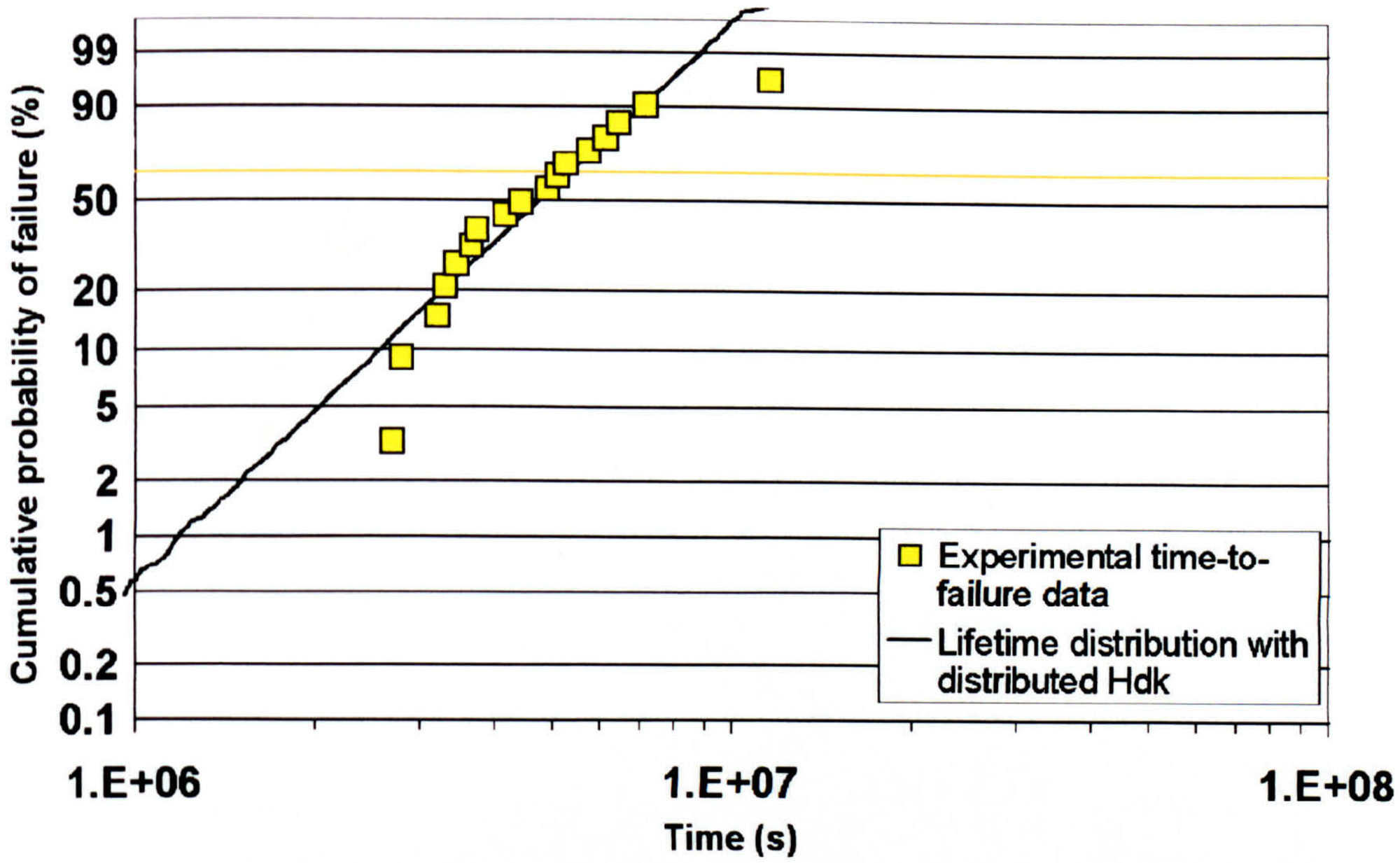

Figure B2.12 E=41kV/mm T=387

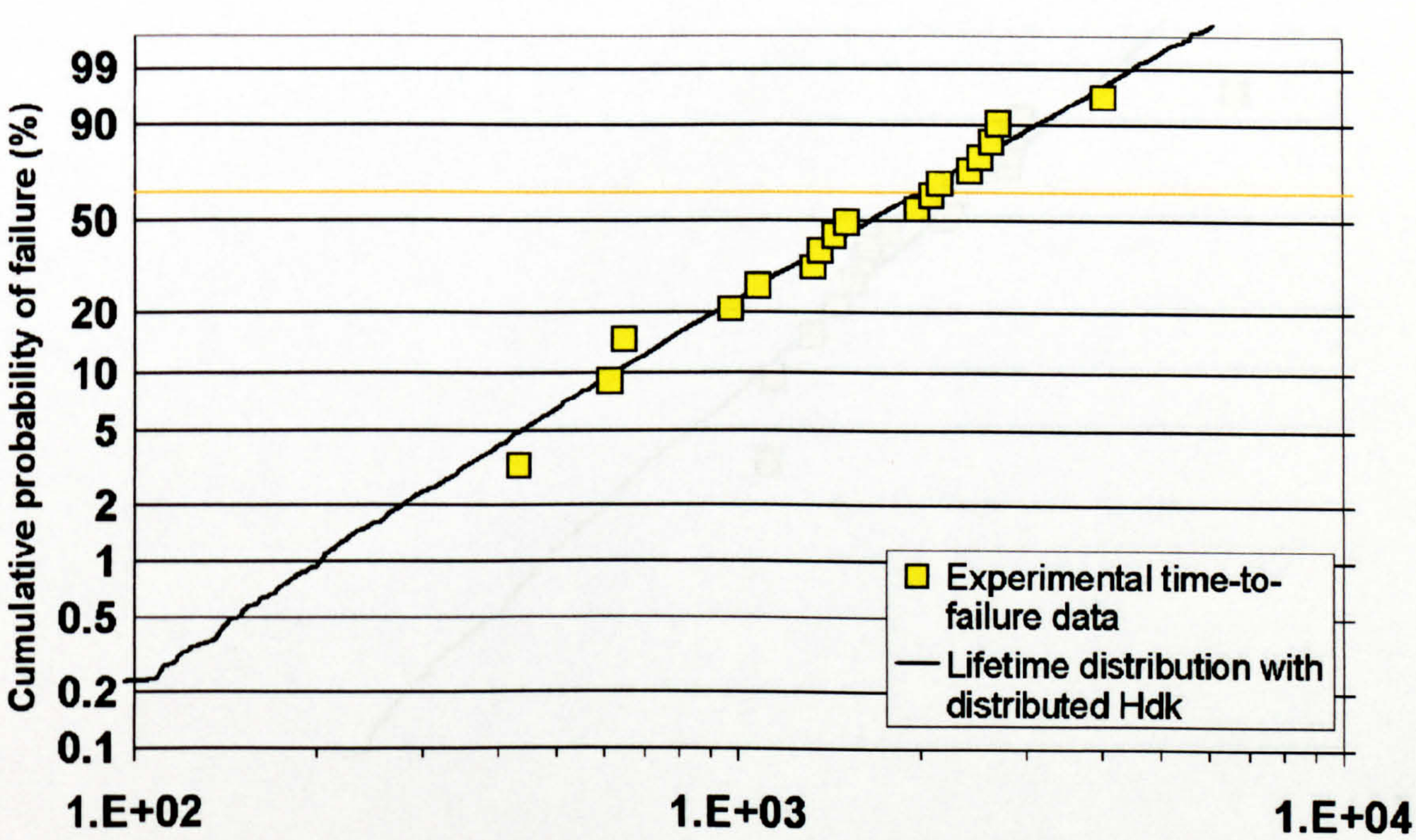

Figure B2.13 E=56kV/mm T=452K

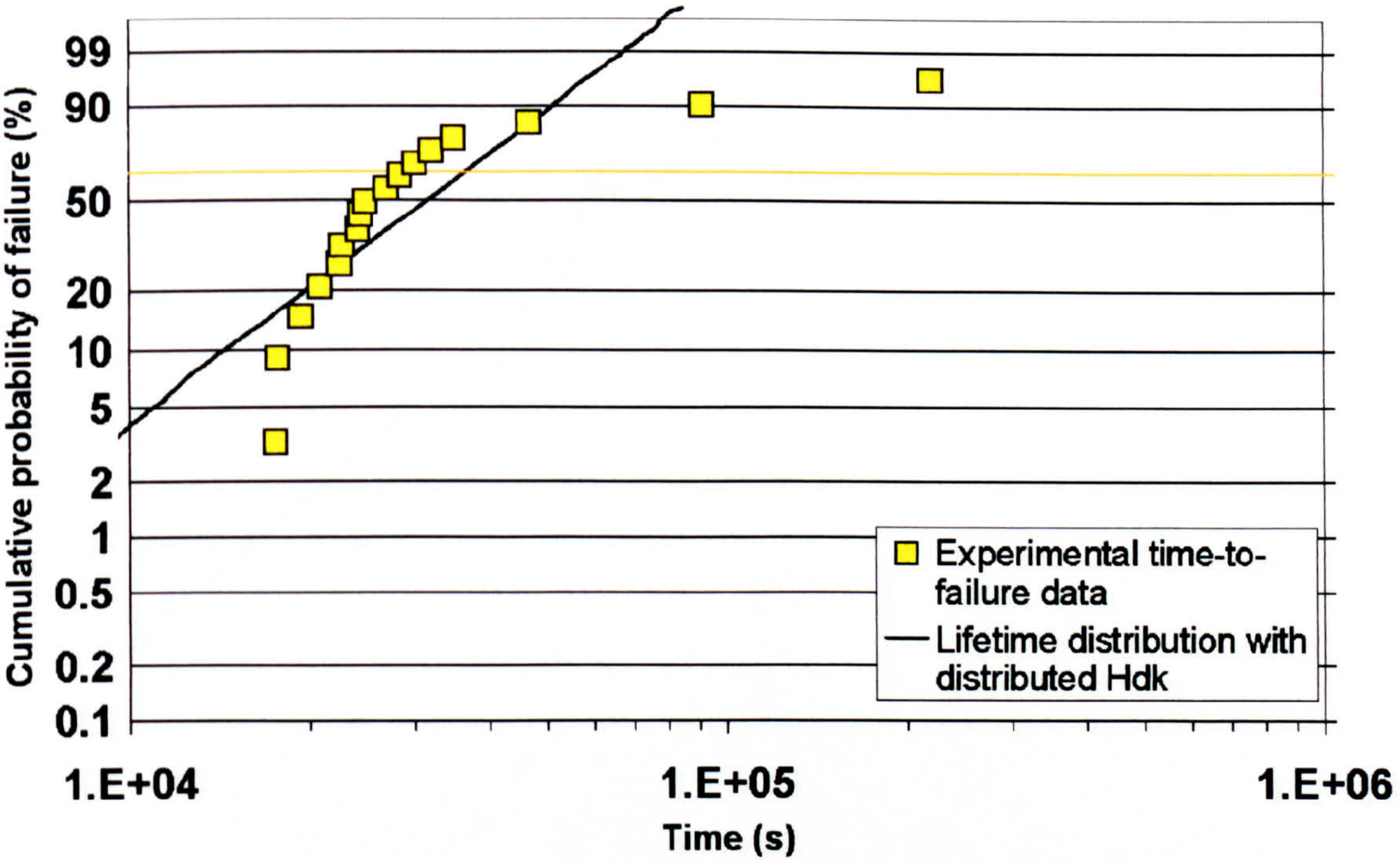

Figure B2.14 E=69kV/mm T=408K

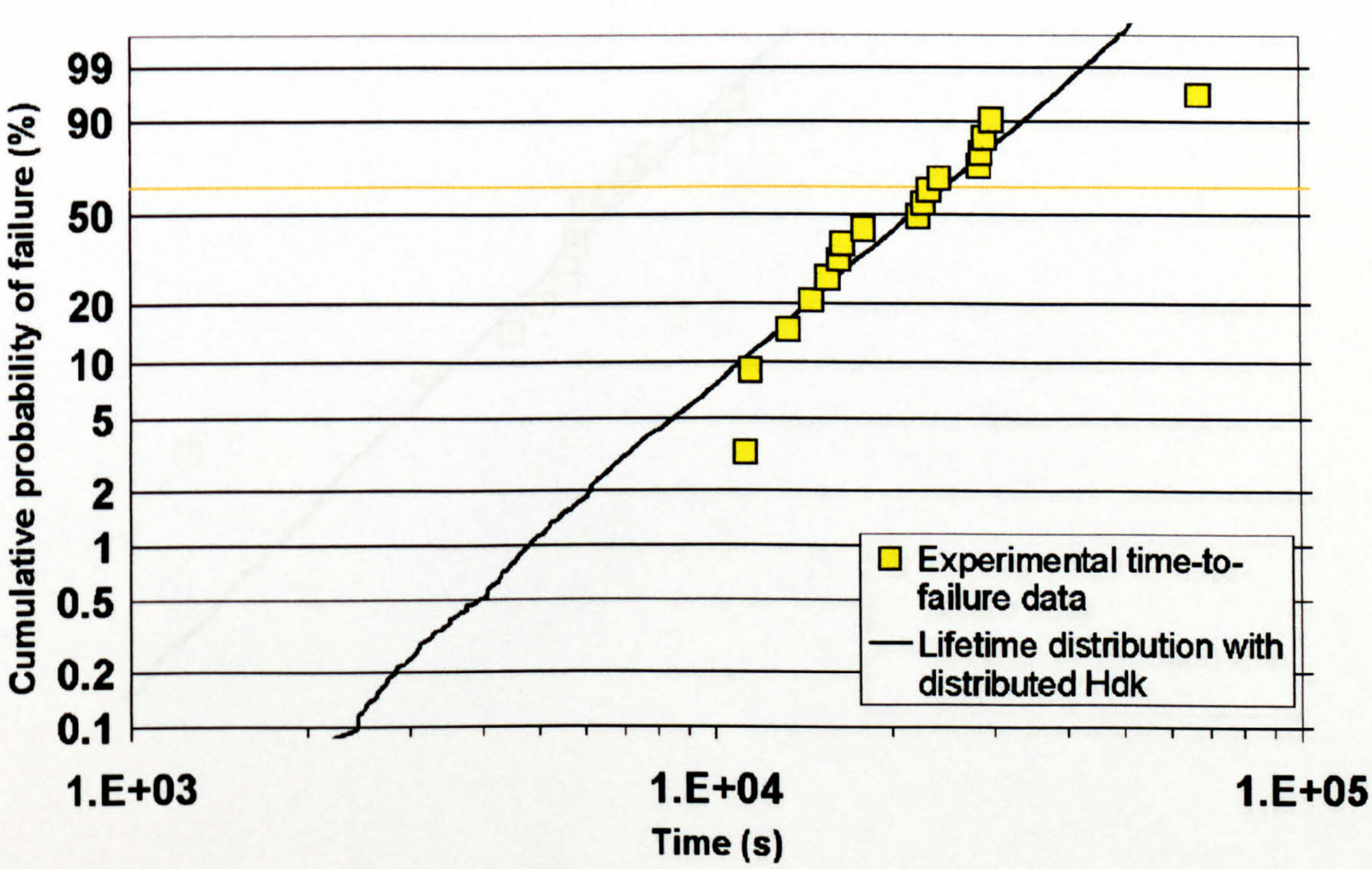

Figure B2.15 E=83kV/mm T=404K

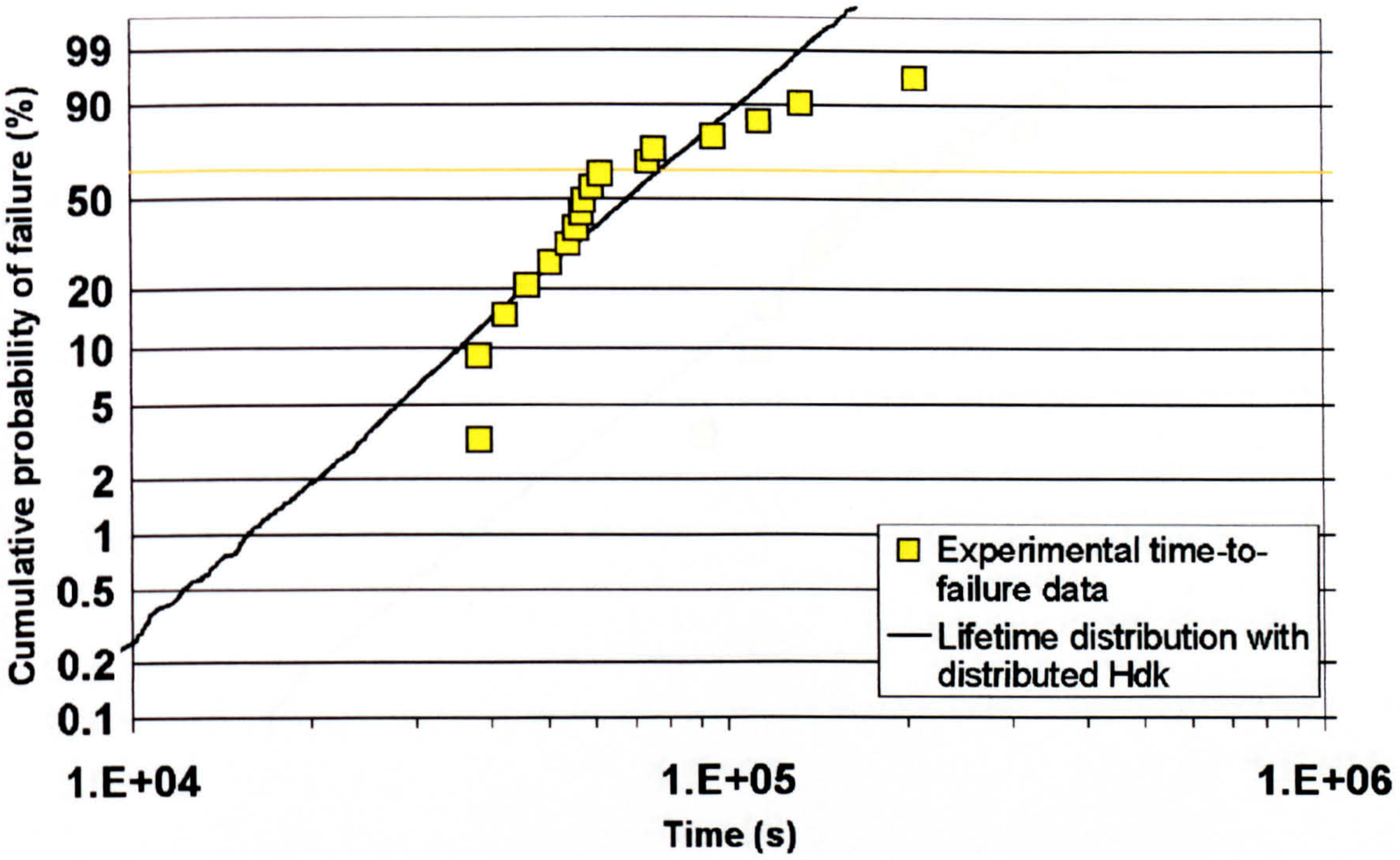

Figure B2.16 E=56kV/mm T=409K

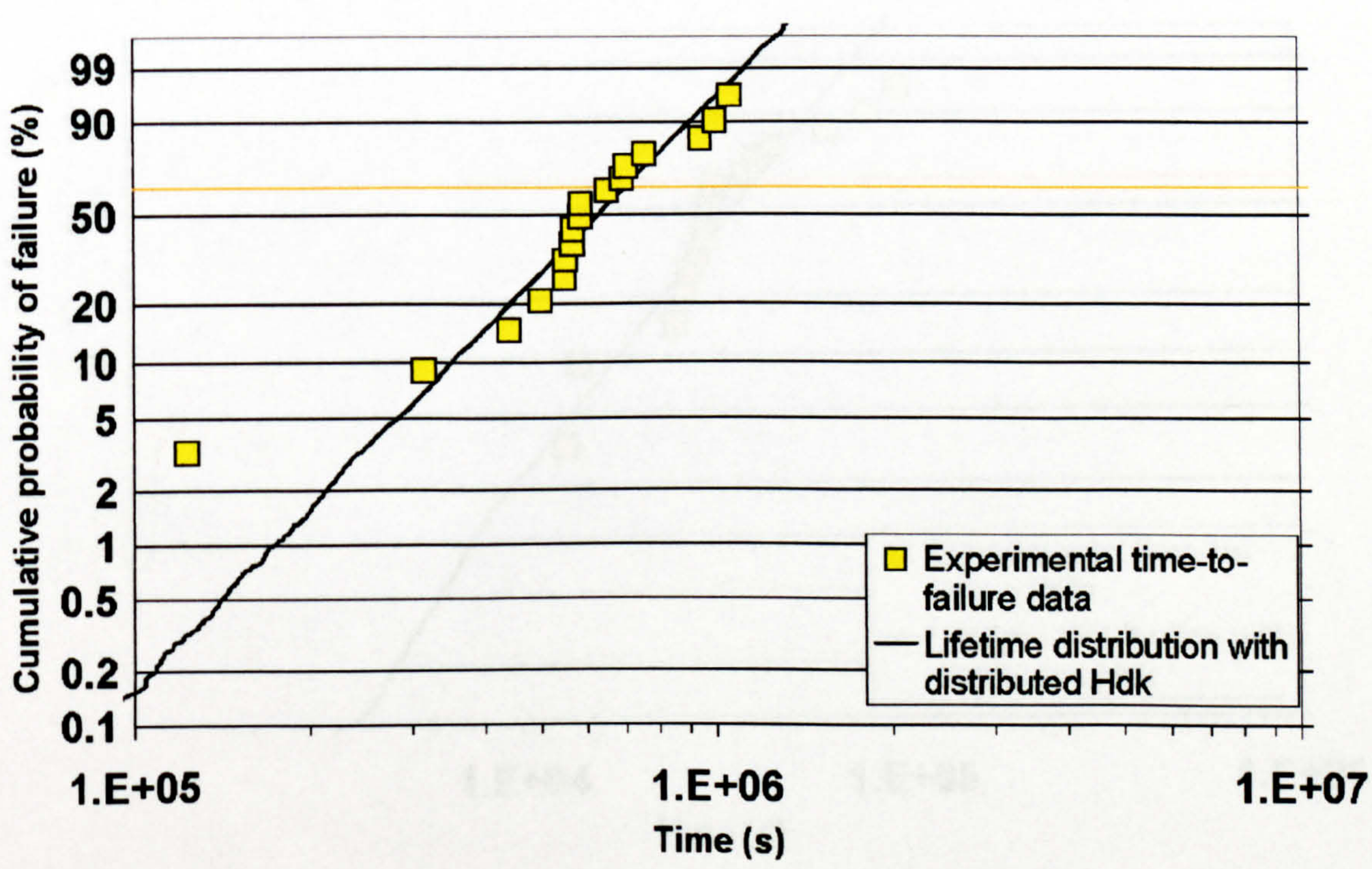

Figure B2.17 E=42kV/mm T=403K

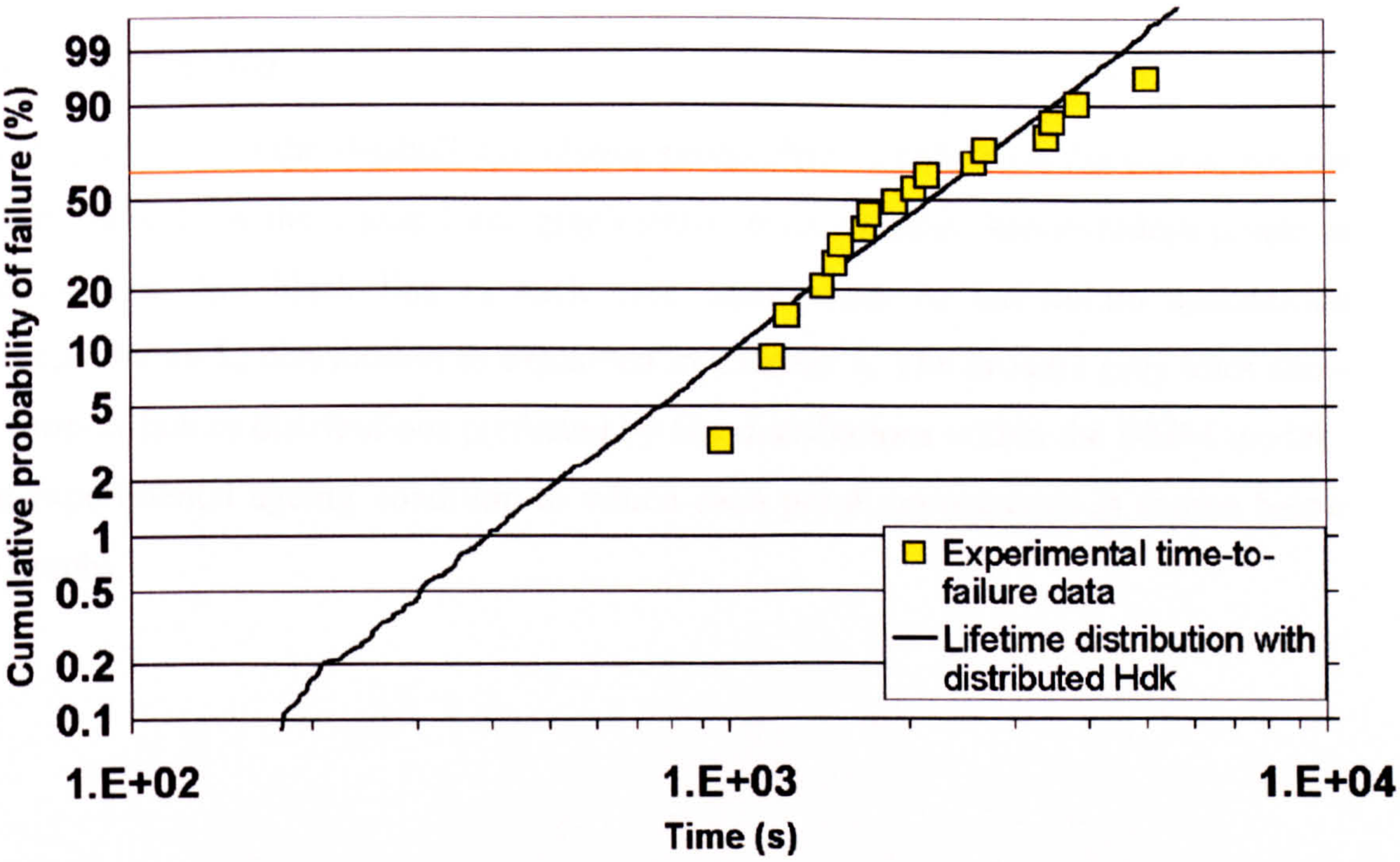

Figure B2.18 E=42kV/mm T=458K

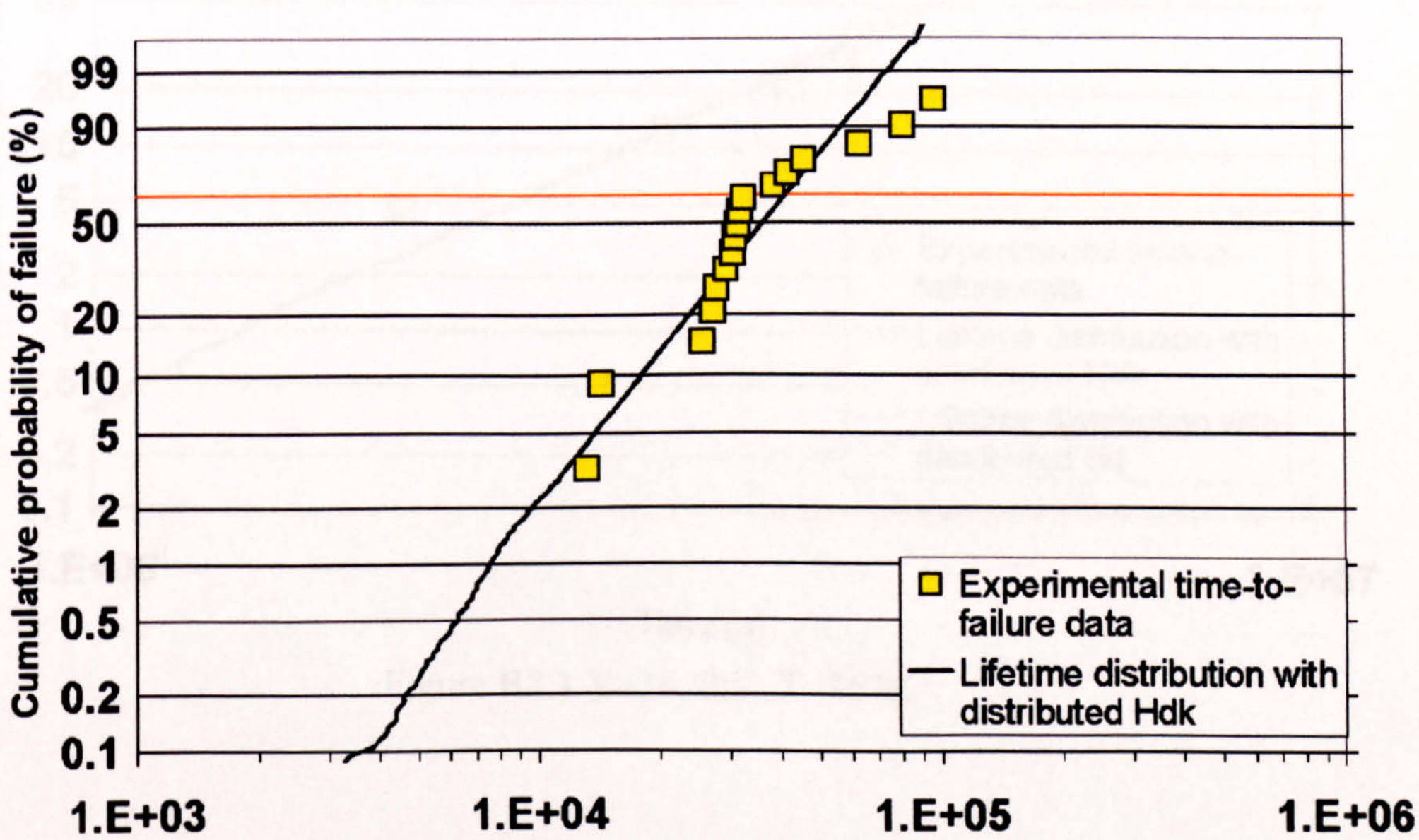

Figure B2.19 E=28kV/mm T=453K

B3. Cable Data

These graphs show the Weibull cumulative probability of failure on the y-axis, against time in seconds on the x-axis. Each graph shows experimental time-to-failure points as squares. The thin black line in each case corresponds to the failure distribution predicted by an S_d distribution as explained in Chapter 6. The broader grey lines show the time-to-failure distributions predicted by H_{dk} distributions within the DMM model. The experimental ageing condition to which each graph corresponds is shown below the graphs.

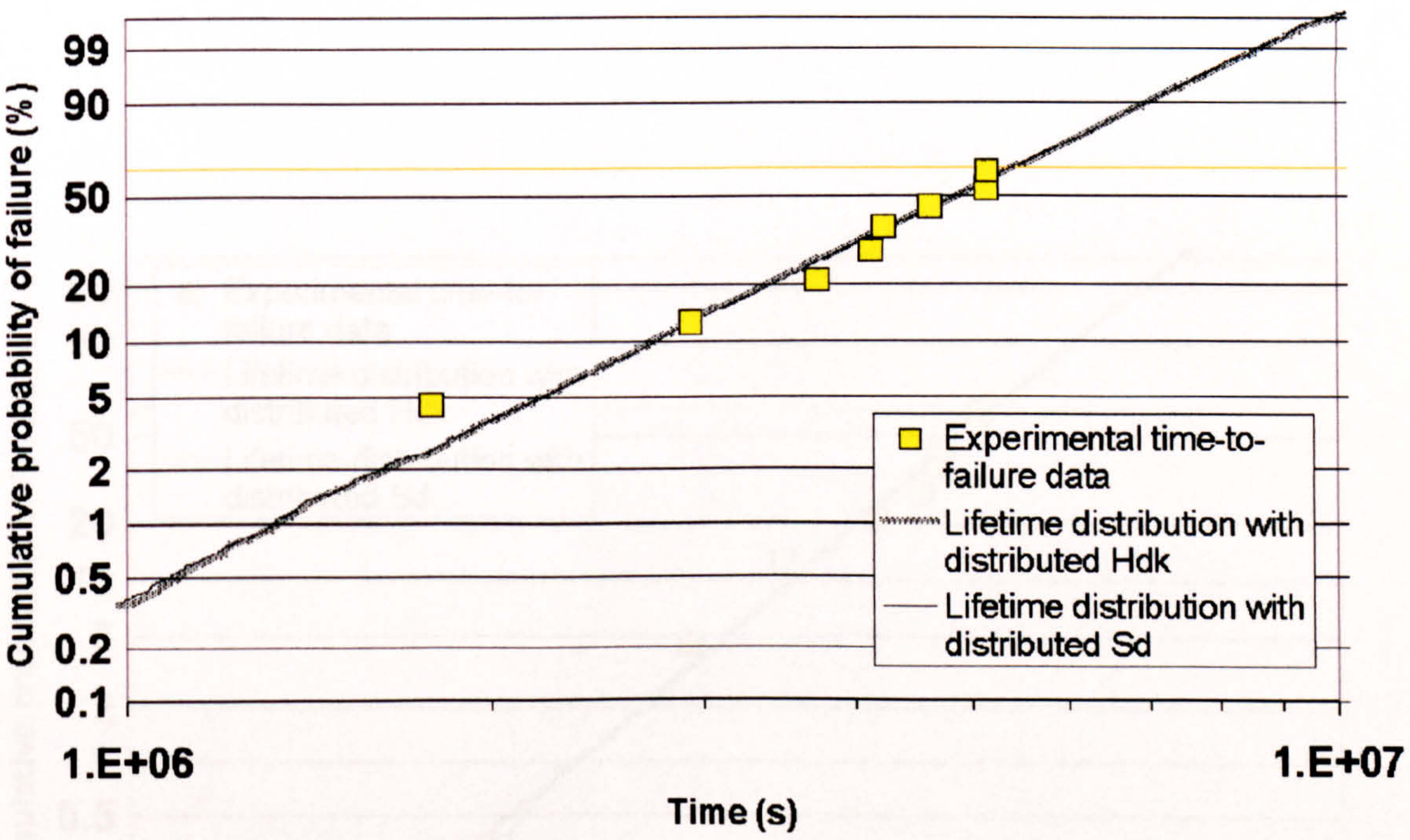

Figure B3.1 V=34.6kV, T=363K

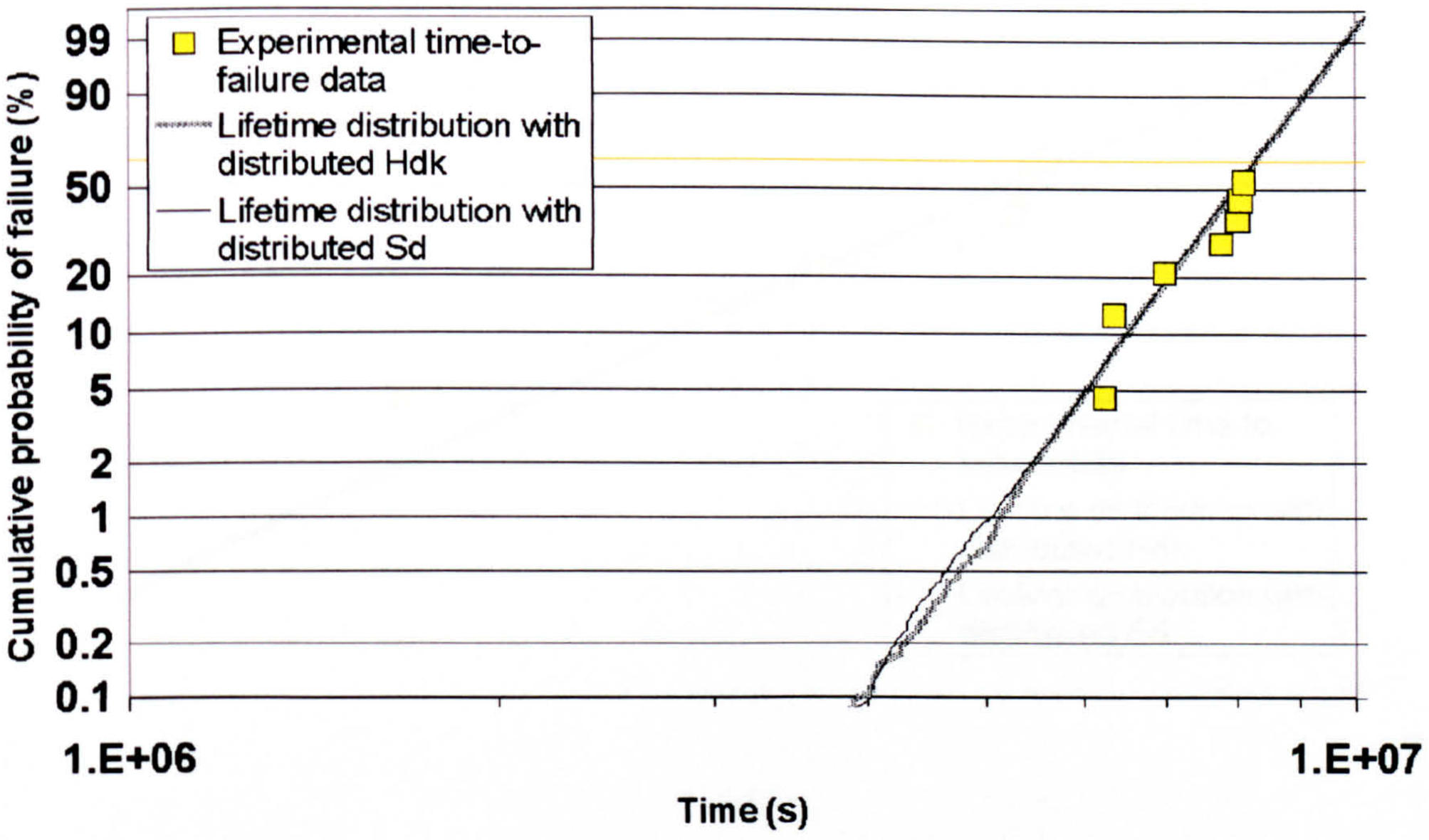

Figure B3.2 V=34.6kV, T=348K

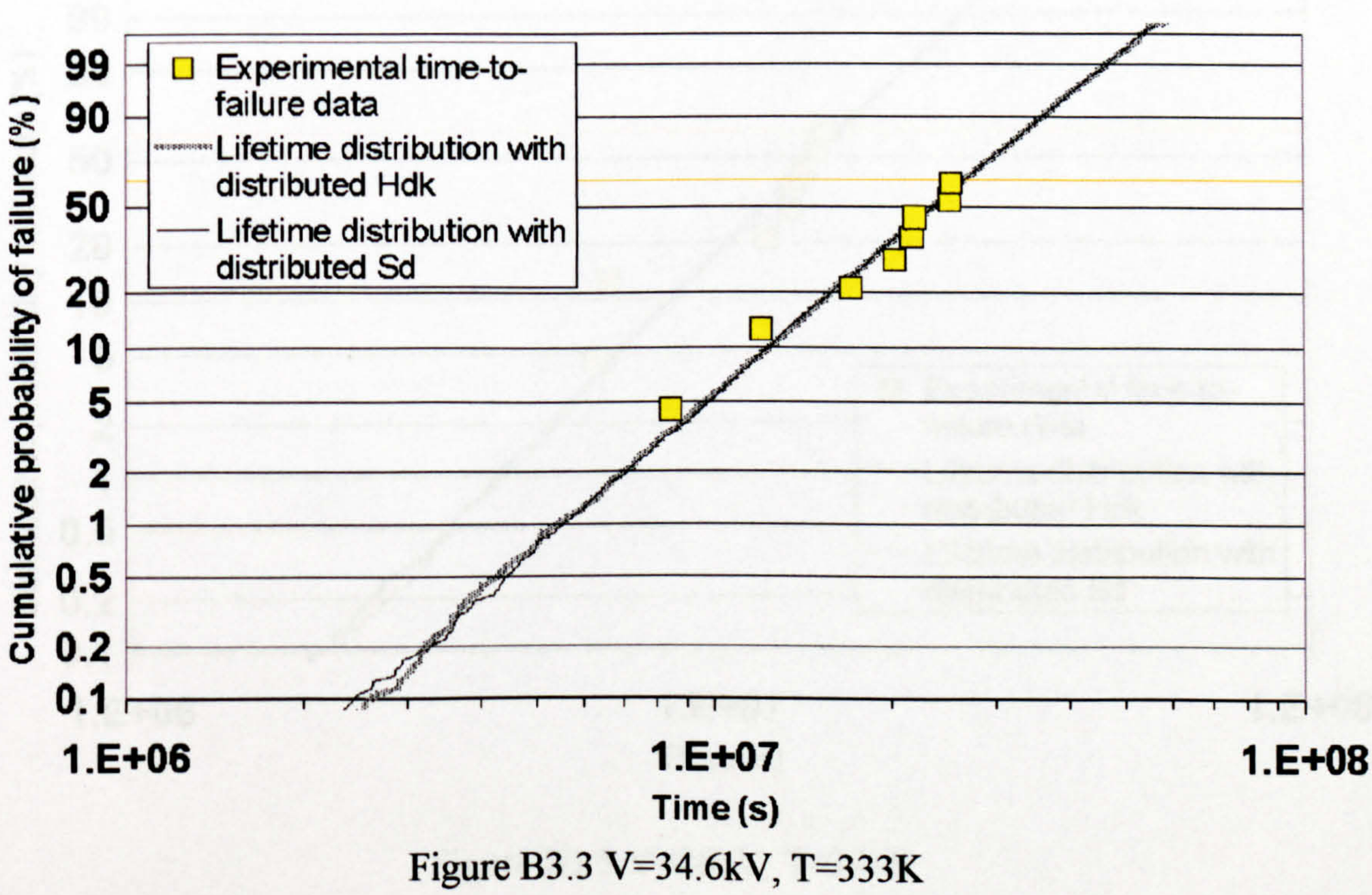

Figure B3.3 V=34.6kV, T=333K

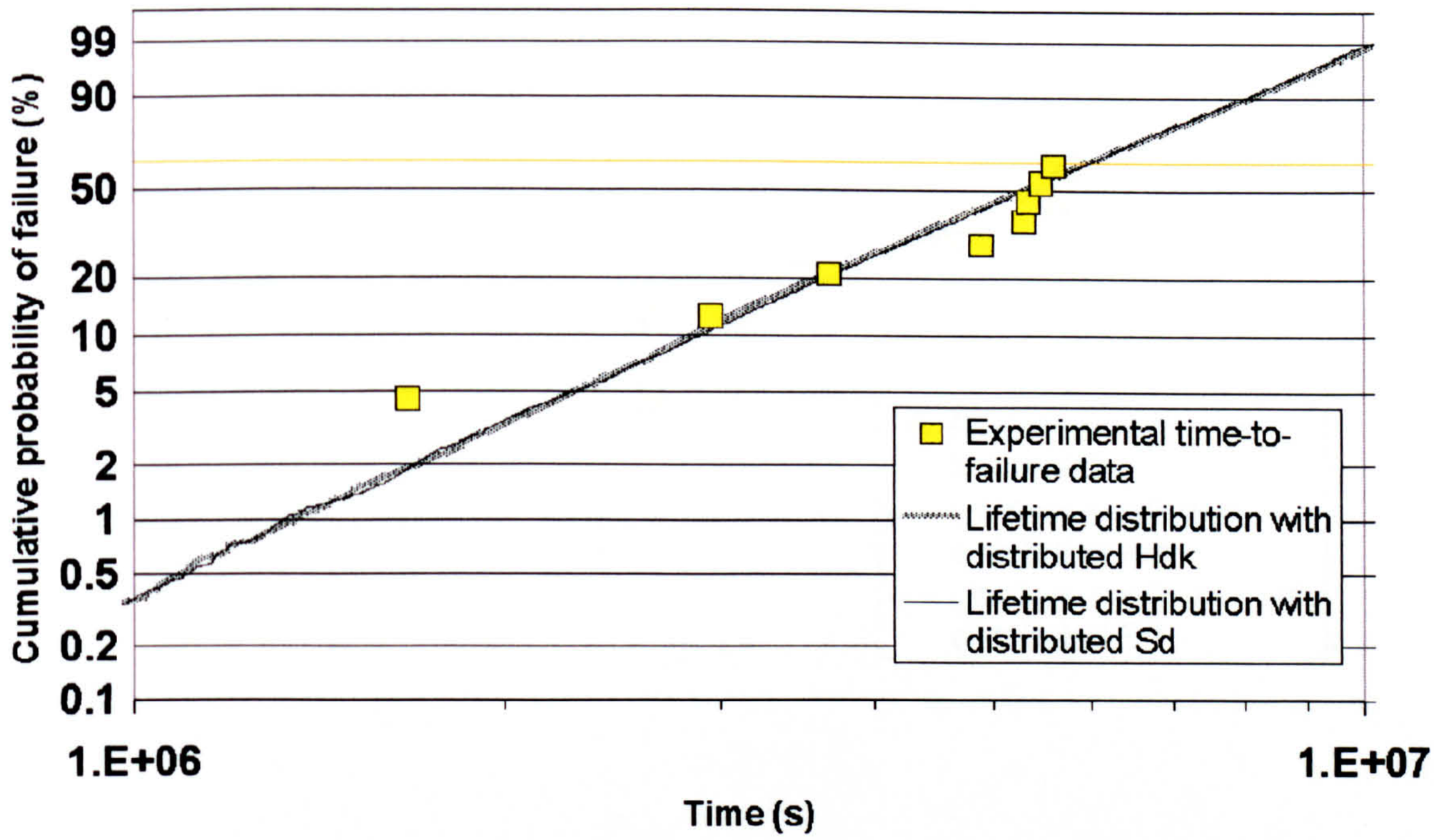

Figure B3.4 V=26kV, T=363K

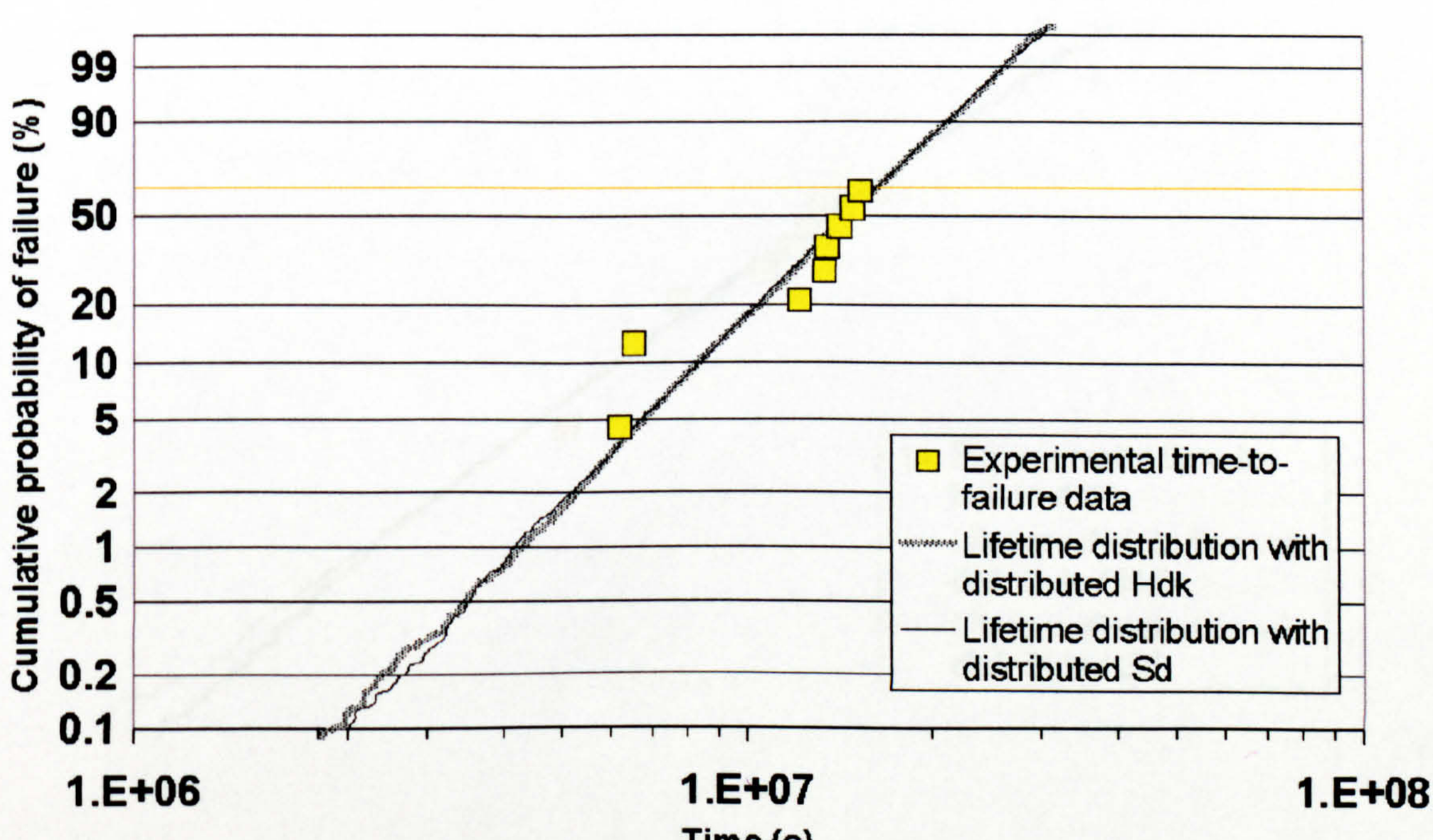

Figure B3.5 V=26kV, T=348K

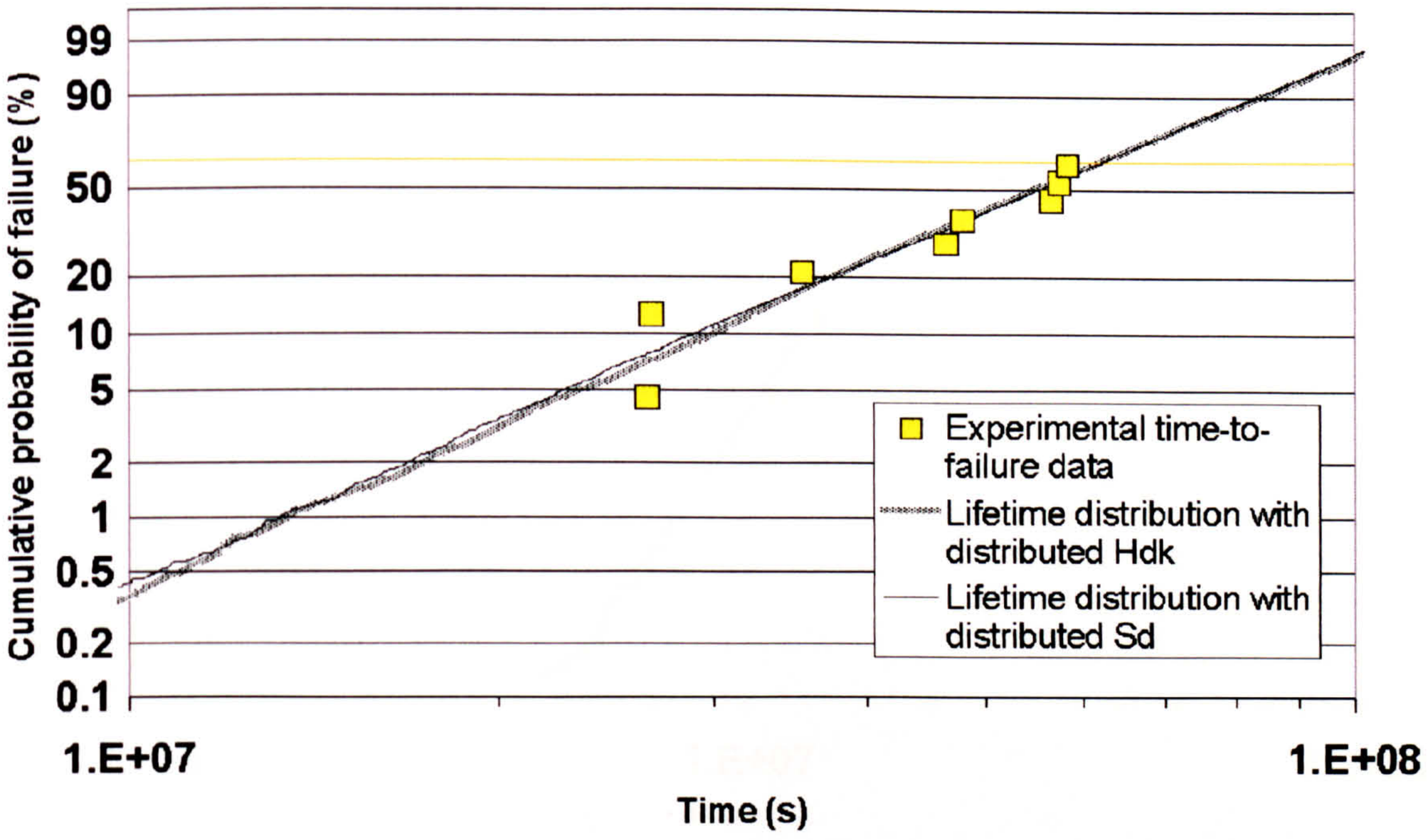

Figure B3.6 V=26kV, T=333K

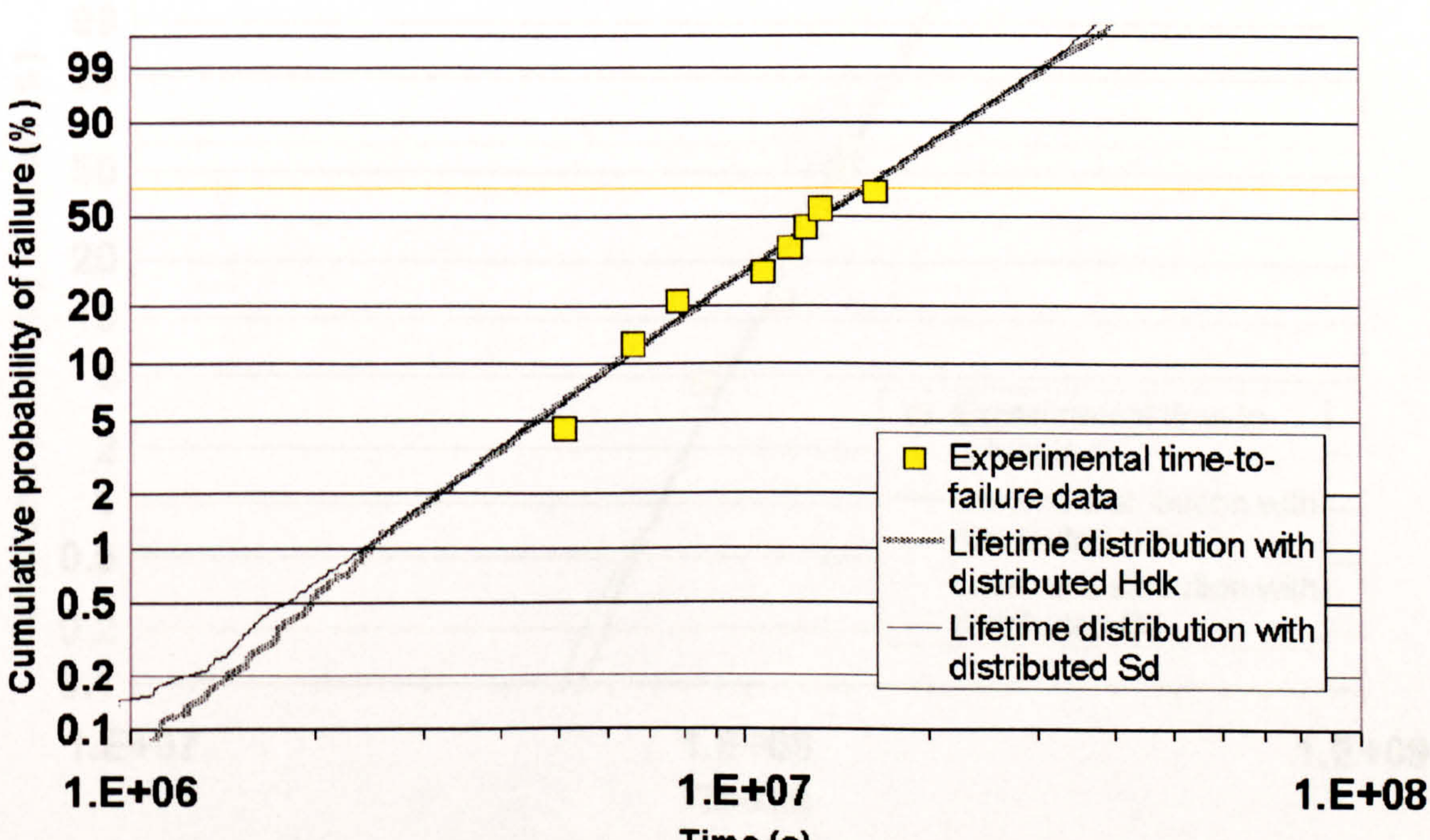

Figure B3.7 V=17.3kV, T=363K

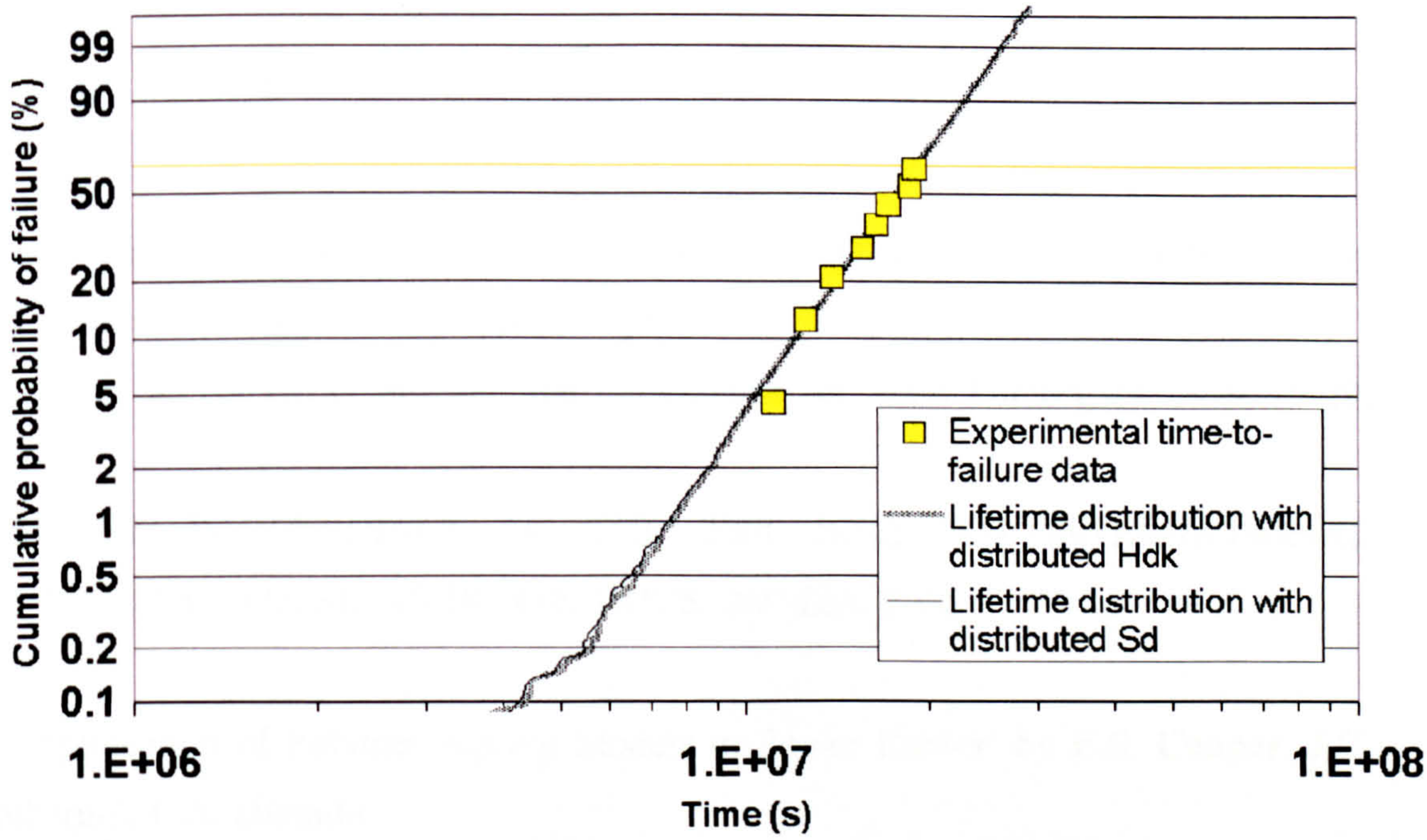

Figure B3.8 V=17.3kV, T=348K

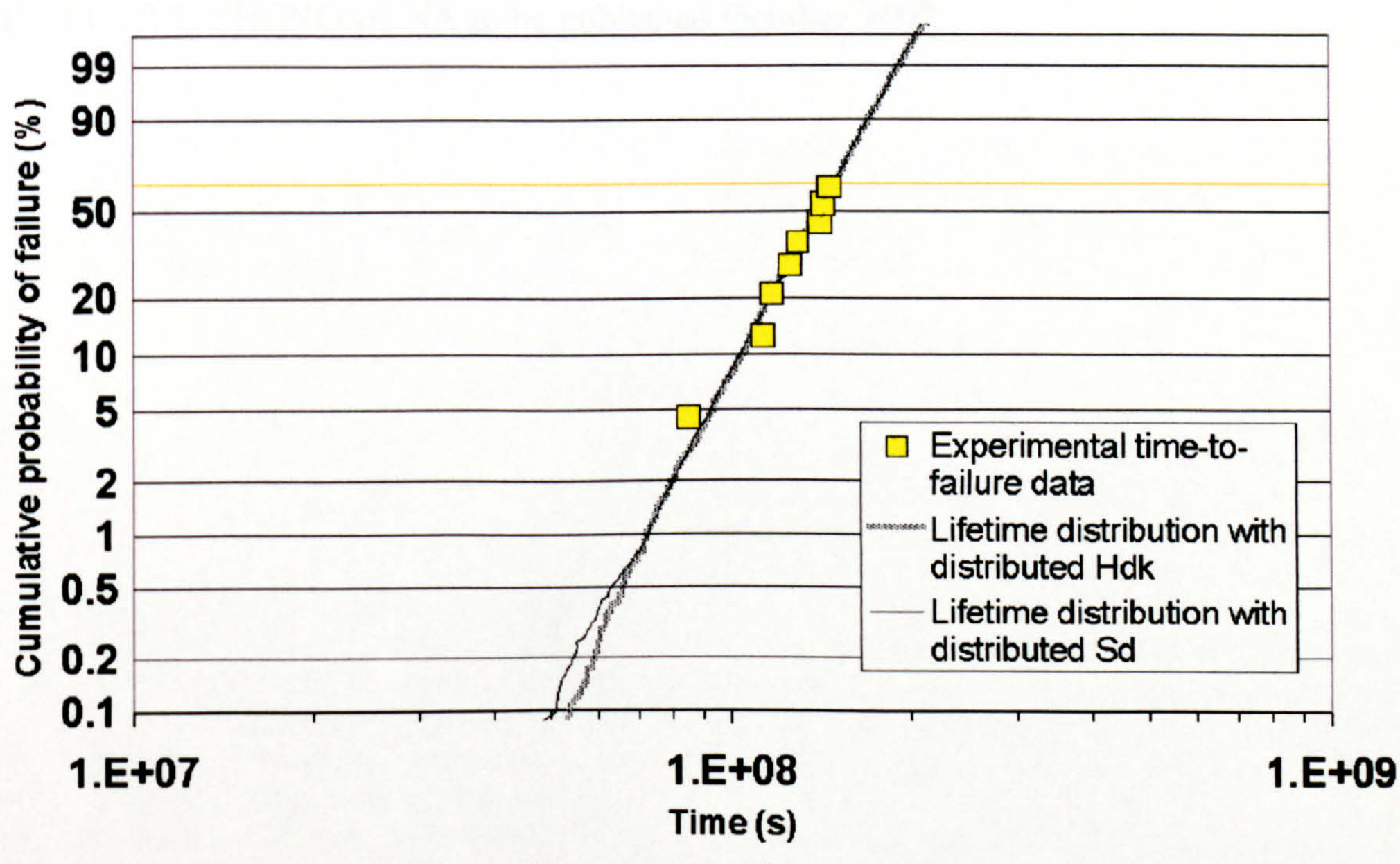

Figure B3.9 V=17.3kV, T=333K

Publications

1. 'Material Morphology and Energy Barriers to Electrical Ageing' by **E.S. Cooper,** J.C. Fothergill, L.A. Dissado, R.N. Hampton.
Presented at 7th IEEE International Conference on Solid Dielectrics, JUN 25-29, 2001
ICSD '01: PROCEEDINGS OF THE 2001 IEEE 7TH INTERNATIONAL CONFERENCE ON SOLID DIELECTRICS, 260-263, 2001

2. 'Application of Polymer Ageing Models to Power Cables' by **E.S. Cooper,** J.C. Fothergill, L.A. Dissado.
To be presented at 2002 IEEE Conference on Electrical Insulation and Dielectric Phenomena
ANNUAL REPORT CONFERENCE ON ELECTRICAL INSULATION AND DIELECTRIC PHENOMENA to be published October 2002.

Material Morphology and Energy Barriers to Electrical Ageing

E.S. Cooper, J.C. Fothergill, L.A. Dissado
Department of Engineering, University of Leicester, Leicester, LE1 7RH, UK

R. N. Hampton*
BICC Cables, Erith, Kent, DA8 1HS, UK

BACKGROUND

Various theories of electro-thermal ageing of high voltage polymeric insulation have been proposed recently, L. A Dissado et al [1], G. Mazzanti et al [2], T. J. Lewis et al [3], J. P. Crine [4], all of which can successfully fit experimental lifetime data, Griffiths et al [5]. However, each model predicts one single time to failure for a set of identical specimens subject to the same electrical field, E, and temperature, T except as discussed in L. A. Dissado et al [6]. In reality, this is not the case; a distribution of breakdown times is observed. Prediction of this distribution is attempted in this investigation, by a distribution of activation energy parameters within the Dissado-Montanari-Mazzanti (DMM) lifetime model [1], [2]. Investigation of the form of the parameter distributions, and how they change with field and temperature, then gives some insight into the ageing process. The analysis carried out should apply equally well to other lifetime models, since they all contain an activation energy term.

The DMM model predicts a time to failure of polymeric insulation subject to a given electrical stress and temperature as shown below in equation (1).

$$L(E,T) = \frac{\frac{h}{2kT}\exp\left(\frac{-S_d}{k}\right)\exp\left(\frac{H_{dk} - \frac{C_d E^{4b}}{2}}{T}\right)\left(-\ln\left(\frac{A_{eq}(E,T) - A^*}{A_{eq}(E,T)}\right)\right)}{\cosh\left(\frac{K_d - C_d E^{4b}}{2T}\right)}$$

L is predicted lifetime, k is Boltzmann's constant, h is Planck's constant and the C_dE^{4b} term describes the effect of the applied field. The model describes the ageing process in terms of groups of atoms, or moieties within the polymer, undergoing a reversible reaction from a reactant state, to a less energetically favourable product state leading to the initiation of local degradation. This reaction is characterised by an activation energy per moiety, #G, which is made up of an enthalpy part, H_{dk}, and an entropy part, S_d. As a polymer specimen moves towards thermal equilibrium, it moves towards an equilibrium in terms of the number of moieties in each of these states. If the fraction of moieties in the product state, A, exceeds a critical fraction, A^* in any localised area, then the insulator is considered to have broken down, since failure in that area becomes inevitable. Catastrophic electrical failure may not yet have occurred, but the insulation can no longer sustain the function for which it was designed.

The DMM model yields one lifetime prediction if all specimens of the same material at a particular temperature and field possess the same values of the governing parameters. Actual experimental results produce a Weibull distribution of lifetimes, J. C. Fothergill and L. A. Dissado [7]. This is because polymers are not homogeneous on an atomic scale, and consequently each of the moieties in a polymeric specimen will have an individual set of parameters describing its own ageing kinetics. The DMM lifetime model contains terms which describe this degradation process, and the values of these are generally obtained by fitting the model to the characteristic lifetime of experimentally obtained lifetime data. However, in each specimen, there will actually be a distribution of physical properties related to ageing, and there must therefore also be a distribution in the model parameters describing the process. Failure will be determined by the most extreme parameter values accessible to a particular specimen [7], so the parameter values obtained by fitting the life expression to the characteristic life will be characteristic values in the extreme value distribution of each parameter.

INVESTIGATION

Extreme value (EV) distributions of activation entropy, S_d, and activation enthalpy, H_{dk}, for the ageing process were investigated, using time to failure data for PET films subject to both AC and DC stress, Gubanski [8]. The AC tests were carried out on films of 50μm thickness, and the DC tests on 36μm films. In the AC case, H_{dk} and S_d distributions were obtained separately; H_{dk} was kept constant while the S_d values were obtained and vice versa. In the DC case S_d was assumed to be zero [2], and only the H_{dk} distribution was investigated.

To investigate the H_{dk} and S_d EV distributions, equation (1) was rearranged in terms of the parameter of interest. This gave an equation in which H_{dk} or S_d was expressed in terms of the other model parameters, E, T and the time to failure. The other model parameters were assumed to have their characteristic values for PET – calculated using the Levenberg-Marquardt algorithm and published in the literature [2]. For each time to failure datum at a known E and T, an H_{dk} or an S_d value was calculated. Each value generated in this way was assumed to be the minimum H_{dk} or S_d value for the specimen, mH_{dk} or mS_d. This is reasonable, since the moieties

with the smallest energy barriers age the material quickest, and lead to failure before any of the others, i.e. they are the 'weakest links'. Each lifetime experiment, comprising a set of identical specimens at a certain E and T, typically tested 9 specimens in the AC case, and 17 in the DC case. The above procedure therefore resulted in a set of 9 mH_{dk} values and mS_d values for each AC test, and 17 mH_{dk} values for each DC test. Since the sets of mH_{dk} and mS_d values were assumed to be minimum values, an approach using extreme value statistics was suitable for their analysis. Reciprocals of mH_{dk} and mS_d were used since an appropriate distribution to model them is the second extreme value distribution $\Lambda_2(z)=\exp(-Z^{\beta})$ with $Z=1/mH_{dk}/\alpha$ or $1/mS_d/\alpha$. This gives the cumulative probability of finding a parameter value greater than Z, i.e. a smaller value of mH_{dk} or mS_d than $1/\alpha$.

The probability density appropriate to this distribution is $Z^{\beta-1}\exp(-Z^{\beta})$, which has the same form as the Weibull function; Weibull graphs can therefore be plotted. When the generated values of $1/mH_{dk}$ and $1/mS_d$ were ranked and plotted in this way, good straight lines were obtained, and these were therefore used to obtain β, the shape parameter, and α the characteristic value of $1/mH_{dk}$ or $1/mS_d$. Values of α and β were calculated for each of the data sets. Large simulated sets data sets of $1/mH_{dk}$ and $1/mS_d$ values were then produced with these α and β characteristics using a Monte Carlo technique. These large distributions were in turn used to generate distributions of lifetime values, using the DMM model and the relevant E and T values. The generated cumulative probabilities were compared to the original experimental data, and found to be a good fit in both AC and DC cases. Examples are shown in **fig 1.** An investigation was then carried out into the effect of temperature and field on the distributions of $1/mH_{dk}$ and $1/mS_d$. The DMM model assumes that values of H_{dk} and S_d for a given insulation do not change with E or T. It was therefore expected that the characteristic values of the $1/mH_{dk}$ and $1/mS_d$ distributions would be reasonably independent of E and T, but that shape parameters might change.

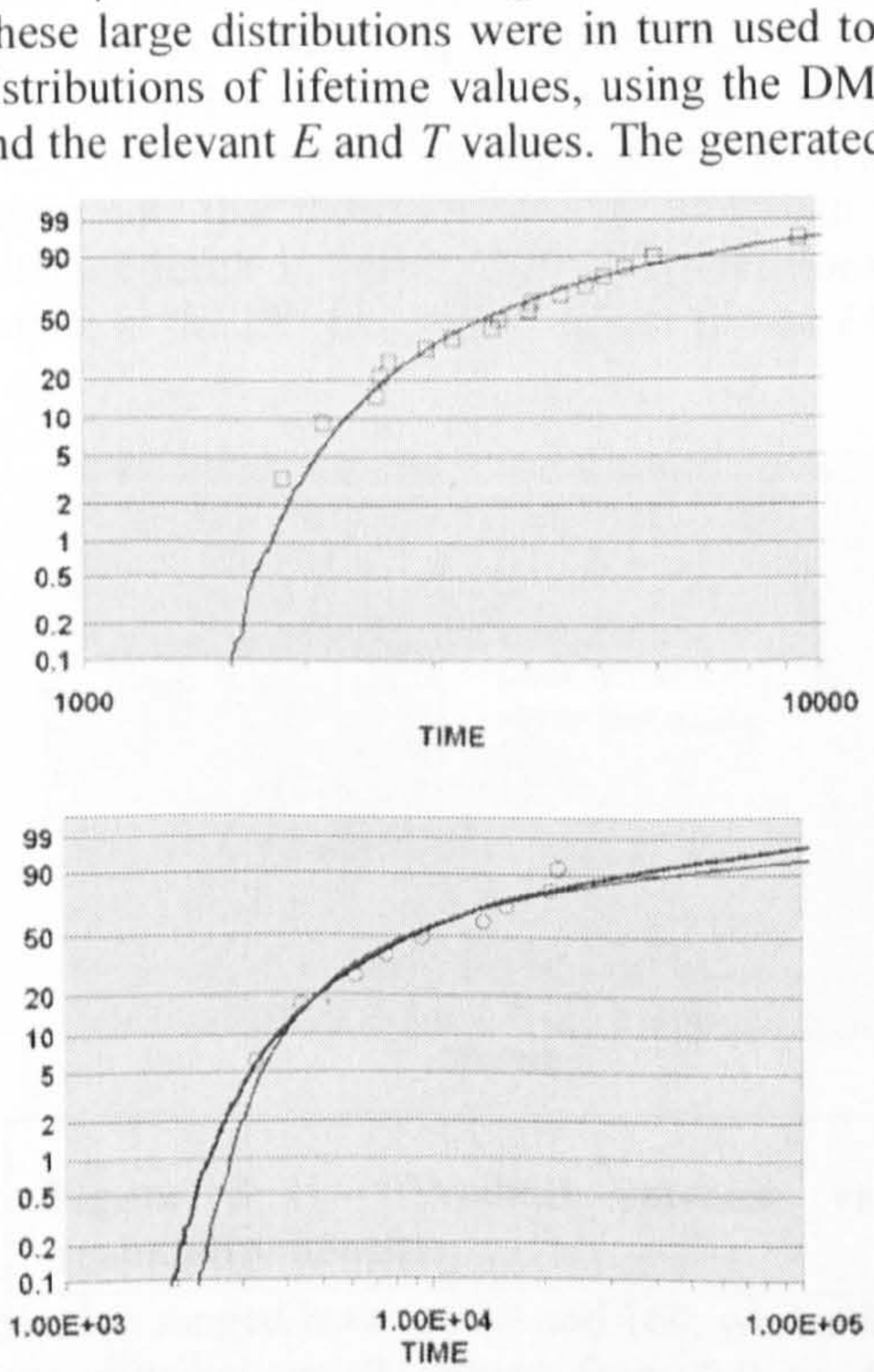

Figure 1 – Weibull cumulative probability with time. Squares are from DC lifetime data, circles from AC lifetime data. Solid lines are from calculated $1/mH_{dk}$ and $1/mS_d$ distributions.

RESULTS

AC results

AC time-to-failure data were available in the range 20°C to 150°C and 10 to 50 kV/mm. Over this range, the $1/mH_{dk}$ and$1/mS_d$ distributions appeared not to be dependent on field. There were, however, various temperature effects. For both the $1/mH_{dk}$ and $1/mS_d$ distributions, the β parameter was found to decrease with increasing temperature. This means that both the distributions became wider with greater temperature. The β parameter was in all cases large ($1.5<\beta<50$ for $1/mH_{dk}$ and $30<\beta<430$ for $1/mS_d$), which means that the distributions of minimum activation energies were all sharp. The α parameter in both distributions appeared to remain independent of temperature until it reached between 60°C and 110°C, a range encompassing the glass transition temperature, T_g, of PET. $1/\alpha$ then began to fall with increasing temperature, L.A. Dissado [9]. Plots of the Weibull parameters with temperature are shown for the AC $1/mH_{dk}$ distributions in **figures 2a and 2b**.

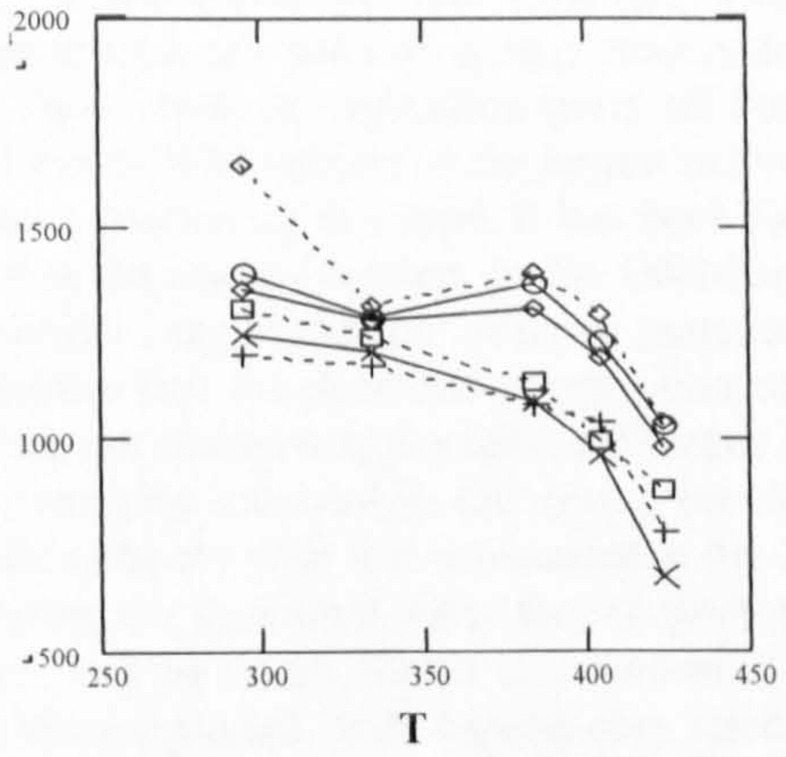

Figure 2a – calculated characteristic mH_{dk} values with temperature for various field strengths.

DC results

DC lifetime data were available in the range 28 to 83kV/mm and from 109°C to 180°C, which is probably above the Tg of PET. As in the AC case, field strength had no effect on either of the Weibull parameters of the $1/mH_{dk}$ distribution. The values of β in the DC case are even greater than in the AC case ($40<\beta<160$), which means that the distributions are narrower still. Increased

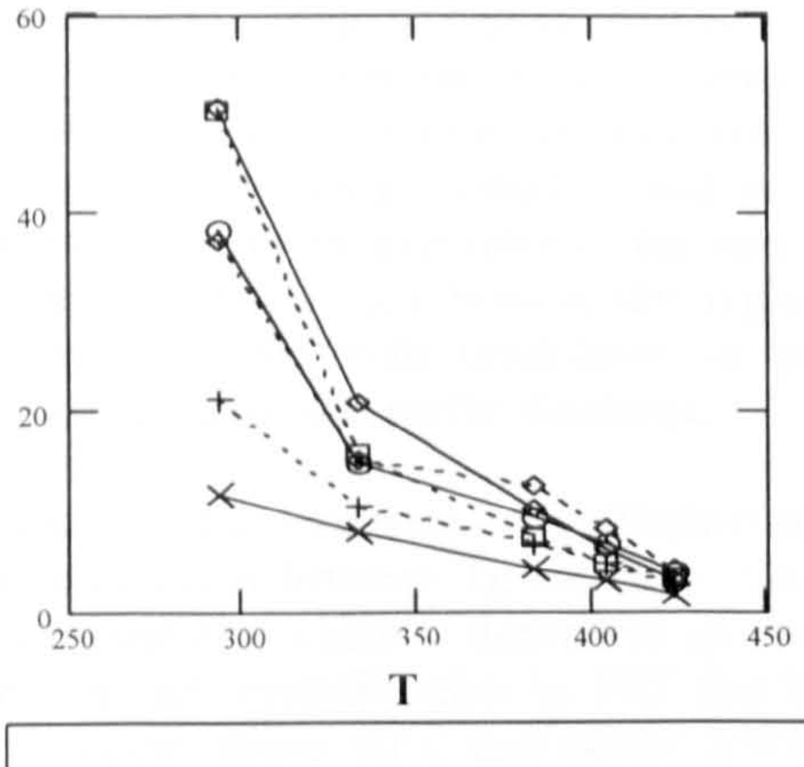

Figure 2b – calculated β parameters with temperature for $1/mH_{dk}$ distributions at various field strengths

temperature caused a reduction in the value of β, and therefore a broadening of the $1/mH_{dk}$ distribution. The characteristic value of the $1/mH_{dk}$ distribution did not change significantly.

DISCUSSION OF RESULTS

Figure 3 shows the form of the $1/mH_{dk}$ and the $1/mS_d$ probability densities. $P(1/mH_{dk})$ is the probability density of the largest values of $1/H_{dk}$ and hence the smallest values of H_{dk} in an infinite number of specimens. The sharp $1/mH_{dk}$ distributions indicate that the minimum activation energies of the ageing process in specimens at a particular E and T are all very similar – they are clustered closely around a characteristic value. It is interesting to note that these very similar minimum activation energies result in broad lifetime distributions. For example, in the DC case, the β values for the $1/mH_{dk}$ distribution ranged between 39 and 160, whilst for the lifetime distributions β ranged from 0.9 to 1.9. Small changes in minimum activation energy have a large effect on the resultant lifetime – particularly at higher temperatures. This is to be expected since lifetime depends exponentially on activation energy. A small variation in the parameters seems physically reasonable,

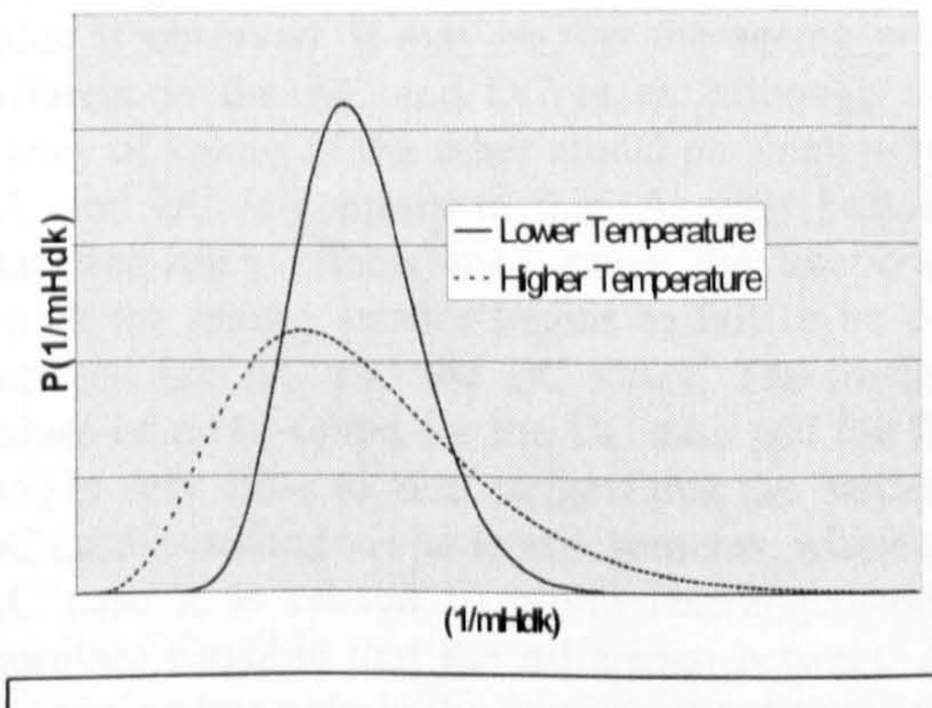

Figure 3 – Weibull extreme value probability density.

since it implies only a small change in the local environment of each moiety involved in ageing.

At higher temperatures the distribution density of $1/mH_{dk}$ values, $P(1/mH_{dk})$ becomes broader, and this must be due to an increased probability of smaller H_{dk} values in the continuous distribution. The value of $<mH_{dk}>$, which is equal to $1/\alpha$, however, remains constant (until the temperature reaches between 60 and 100°C in the AC case). This increase in probability of activation energies lower than $<mH_{dk}>$ must be balanced by a decrease in the probability of a range of energies above $<mH_{dk}>$. This may be explained if the ageing process is assumed to be one in which rearrangement of polymer segments occurs. The activation energy of this process is an energetic barrier to conformational rearrangement of molecules. Such activation energies form as the polymer solidifies. In the melt, the polymer molecules have very small barriers to conformational rearrangement and the chains can move freely past one another. Barriers are then 'frozen in' as solidification occurs, so that below the glass transition temperature Tg, segmental motions cannot occur at all. Small groups of atoms can vibrate as they are heated, and the range of motions will increase as temperature increases, but no viscous flow is possible.

At temperatures above 60°C to 110°C, i.e. above T_g, the AC results show a whole-scale movement of the $1/mH_{dk}$ and $1/mS_d$ distributions, as $1/\alpha$ (and hence $<mH_{dk}>$ and $<mS_d>$) start to decrease with temperature, as shown for $1/mH_{dk}$ in **fig 2a**. The polymer is no longer constrained to remain globally rigid above these temperatures - the activation energy can therefore begin to decrease, and plastic deformations become possible. The moieties associated with this kind of ageing process are unlikely to be those deep in crystalline parts of the polymer, since these will be subject to the largest activation energies for a process of this type. It has been found, however, that the energy barriers in the DMM model have very similar magnitudes for different materials [2], and this implies that the chemical composition of the polymer does not make an appreciable difference to the activation energies involved in the ageing process. This is unlikely to be the case if it is moieties in the amorphous region that are important, since the morphology of these regions, and hence the barrier distribution to conformational rearrangement, will depend very strongly on the constituent molecule. The same is true of the crystalline regions – the chemical composition of crystalline parts of a polymer will have a large effect on the activation energy associated with freeing chain segments. It therefore seems likely that the breakdown process is characteristic of chain sections confined to the lamella surfaces, which became only partly crystallised as the polymer cooled. These will be the chains which will be most able to move freely once they are initially freed, since they are neither part of a rigid crystalline structure, nor are they likely to be highly tangled as in the amorphous region. The increased freedom of these chain

sections produced during the ageing reaction may eventually be sufficient to remove the constraints on their crystallisation imposed during solidification. Consequently, the sections may crystallise, and low-density regions will therefore be generated in the neighbouring amorphous regions. Such low-density *regions have* long been associated with breakdown in polymers, through such processes as partial discharge.

In the absence of any stresses, crystallisation in a polymer can only occur between Tg and Tm – the melting point of crystallites, which is dependent on the crystallite size. In fact, crystallisation in PET has been observed to occur above 90°C and below 250°C, W.H. Cobbs and R. L. Burton [10]. It is possible that in a polymer subject to a stress, the chains will be able to crystallise at lower temperatures than normal – i.e. below 90°C for PET. This effect has been observed, J. O. Fernandez and G.M. Swallowe [11] for a macroscopic compressive mechanical stress applied to a PET sample, where crystallisation was observed just above a quoted Tg of 70°C. In this case, a mechanical tension is thought to align polymer chains in such a way as to reduce the energy barrier to crystallisation. A similar reduction in activation energy may occur for an applied electrical stress via local mechanical stress caused by trapped space charge. In this investigation, AC data is available at 60°C and 110°C, but not in-between. Both Tg and the onset of unstressed crystallisation occur between these limits, so it is not possible to tell at what point the ageing energy barrier begins to fall. Nonetheless, the results are consistent with the ageing process being one of crystallisation of lamella surface chains causing a free volume increase in neighbouring amorphous regions.

In the DC case, all the data is above 100°C and hence above Tg. No reduction in the characteristic barrier value is observed. It may be that the ageing process is different in the AC and DC cases, although the constancy of values of the other model parameters between AC and DC is contrary to this. Another possibility is that frequency effects may cause the temperature at which the energy barrier begins to fall to be different between the AC and the DC cases. The much larger values of mH_{dk} found for the DC case and the fact that mS_d is very close to zero suggest that the barrier in the DC case is related to site rearrangements, whereas in the AC case it is related to group rearrangements. It is therefore possible that the difference between AC and DC ageing lies only in the number of polymer monomer units rearranging and not in the process itself. The more localised the individual rearrangements are, the less likely they are to be effected by temperature. Possibly this reflects the fact that in AC fields the whole of the lamella surface may be driven to fluctuate, whereas in DC fields it will be frozen in a specific energy configuration – rearrangement of which requires displacement of the most 'locked in' site.

*Now at Borealis AB, Sweden

CONCLUSION

A distribution of the parameters representing activation energy of the ageing process within the DMM lifetime model has been shown to model experimental lifetime distributions of PET films well. The results imply small differences *in the local environments of the moieties* involved in the ageing process Very small changes in the minimum activation energy values have a pronounced effect on the resultant lifetimes of polymer specimens. Changes in the distributions of activation energies with field and temperature can be explained by assuming the ageing process to be one whereby polymer segments on lamella surfaces crystallise to create free volume within the polymer.

ACKNOWLEDGEMENT

We thank EPSRC and BICC Cables/Pirelli, for their support, Dr S. Gubanski for the unpublished statistical lifetime data and the University of Leicester for study leave for Professor John Fothergill.

REFERENCES

1. L. A Dissado, G. Mazzanti and, G. C. Montanari 'The Role of Trapped Space Charges in the Electrical Aging of Insulating Materials' IEEE Trans. DEI, 4 No. 5, pp496-506, 1999.
2. G. Mazzanti, G. C. Montanari and L. A Dissado 'A Space-charge Life Model for ac electrical Aging of Polymers' IEEE Trans DEI, 6, , pp864-875, 1999.
3. T. J. Lewis, P. Llewellyn, M. J. van der Sluijs, J. Freestone, R. N. Hampton, 'A New Model for Electrical Ageing and Breakdown in Dielectrics' 7th DMMA, pp23-26, 1996.
4. J. P. Crine 'A Molecular Model to Evaluate the Impact of Aging on Space Charges in Polymer Dielectrics' IEEE Trans. DEI 4 No. 5, pp487-495, 1997.
5. C. L. Griffiths, S. Betteridge and R. N. Hampton 'Thermoelectric ageing of cable grade XLPE in dry conditions' IEEE ICSD pp279-282, 1997
6. L. A. Dissado, S. J. Urban and P.A. Norman, 'Breakdown Statistics of the Space-charge ageing model for polymeric insulation' CEIDP pp129-132, 1996
7. J. C. Fothergill and L.A. Dissado, 'Electrical degradation and breakdown in polymers'. (P. Peregrinus for IEE, London, :ISBN 0 86341 196 7, 1992)
8. S. Gubanski, private communication.
9. L. A. Dissado, 'The Physics of Electrical Ageing in Semi-crystalline Insulating Polymers', 32nd Symposium on Electrical and Electronic Insulating Materials and Applications in Systems, pp9-16, 2000.
10. W.H. Cobbs and R. L. Burton 'Crystallisation of Polyethylene Terephthalate' Journal of Polymer Science, **10**, No. 3, pp275-290, 1953.
11. J. O. Fernandez and G.M. Swallowe, 'Crystallisation of PET with strain, strain rate and temperature' Journal Mat. Sci., **35**, pp4405-4414, 2000.

Application of polymer ageing models to power cables

E.S. Cooper, J.C. Fothergill & L.A. Dissado
Department of Engineering, University of Leicester, Leicester, LE1 7RH, UK

Abstract: Ageing models have been developed to predict the lifetime of polymeric insulation subject to electro-thermal stresses. We present here a method for applying the models to situations in which the field is not constant over the whole specimen, as for cable geometry. The method has been applied to characteristic lifetime data from AC ageing experiments on cables. The results are presented, and the effect of insulation volume upon the model parameters is discussed.

Introduction

The aim of polymer lifetime models is to predict the working lifetime of polymeric insulation subject to thermal and electrical stresses. Such theories have been developed by a number of authors [1-4]. The model used in this work is that developed by Dissado et al – abbreviated here to the DMM model. For this model [1] the lifetime equation is given in terms of applied electrical field, E and temperature, T, by (1)

$$L(E,T) = \frac{\frac{h}{2kT}\exp\left(\frac{-S_d}{k}\right)\exp\left(\frac{H_{dk}-\frac{C_dE^{*b}}{2}}{T}\right)\left(-\ln\left(\frac{A_{eq}(E,T)-A^*}{A_{eq}(E,T)}\right)\right)}{\cosh\left(\frac{K_d-C_dE^{*b}}{2T}\right)} \quad (1)$$

L is predicted lifetime, k is Boltzmann's constant, h is Planck's constant. The model describes the ageing process in terms of moieties within the polymer undergoing a reversible reaction from a reactant state, to a less energetically favourable product state leading to the initiation of local degradation. The difference in free energy between the reactant and product states is called K_d. The reaction is characterised by an activation energy per moiety, #G, which is made up of an enthalpy part, H_{dk}, and an entropy part, S_d with #G ($=kH_{dk}$,$-TS_d$). As a polymer specimen evolves from the as-prepared state towards thermodynamic equilibrium, the concentration of moieties in each of these states alters. If the fraction of moieties in the product state, A, exceeds a critical fraction, A^* in any localised area, then the insulator is considered to have broken down, since failure in that area becomes inevitable. The C_d and b parameters in (1) describe the effect of an applied field on #G, which is reduced by an amount equal to C_dE^{*b} on application of a field, E.

Equation (1) can be fitted to data from ageing experiments to give values for the parameters in the model, and from these values, information can be drawn about the ageing process. In fact in any polymer specimen, each reacting moiety must have its own value of H_{dk}, S_d and K_d, and A^*, C_d and b may vary with location in the specimen. Fitting (1) to the characteristic lifetime from any given set of ageing experiments gives the characteristic value for each parameter, and these must be thought of as typical of the specimens that have been aged. In the case of thin film ageing experiments, the fitting is straightforward. Ageing tests on sets of identical specimens under various E and T conditions can be analysed using Weibull statistics to obtain the characteristic lifetime, B63, for each experimental condition. The RHS of (1) containing the relevant E and T values can then be set directly equal to each B63 to yield parameter values. In fact, according to the model, the parameters should be independent of E and T, so this should be done simultaneously for all available E, T and B63 data.

Any dependence of the failure times on polymer specimen volume or size must naturally be reflected in the parameter values obtained using (1), through B63. A volume effect on insulation lifetime is often assumed by e.g. cable manufacturers, but little is known about the way in which volume affects the ageing process and polymer lifetime.

For the thin film case, the temperature, T, and field, E, experienced by each film can be considered spatially constant. In systems such as power cables this assumption cannot be made. The insulation of a power cable under load experiences a radially varying temperature distribution due to Ohmic heating in the core as shown [5].

$$T(r) = T_1 + \left(\frac{W \times Th}{2\pi}\ln\left(\frac{R_O}{r}\right)\right) \quad (2)$$

$T(r)$ is the temperature at radius r, T_1 is the temperature outside the cable and R_O is the cross sectional radius of the cable. W is the power dissipated per unit length along the cable core by the current, and Th is the thermal resistivity of the cable insulation. The insulation also experiences a radially varying electrical stress distribution, as shown in (3) for an AC case [6].

$$E(r) = \frac{V}{r \ln\left(\frac{R_O}{R_I}\right)} \quad (3)$$

In (3) *E(r)* is the electrical stress at radius *r*. R_O is the cable radius as before, and R_I is the cross sectional radius of the cable core. *V* is the voltage of the core relative to the outer edge of the cable, which is generally earthed. This radial variation in *E* and *T* makes fitting the ageing models to lifetime data from cable ageing experiments more difficult than in the thin film case, and a method is presented here for doing this.

Fitting method

Substituting (2) and (3) into (1) gives a lifetime prediction for cable insulation that is radius dependent. In order to fit this radially dependent lifetime prediction to the B63 value from cable ageing experiments, the insulation is first split into *N* concentric shells. Each shell is at radius r_i from the centre of the cable core, Figure 1. These shells should be thin enough that *E* and *T* can be considered constant over their volume. Equal volume shells are used in this investigation, so that the ratio of the cable insulation volume, *VC*, to the volume of each shell, *VS*, is *N*.

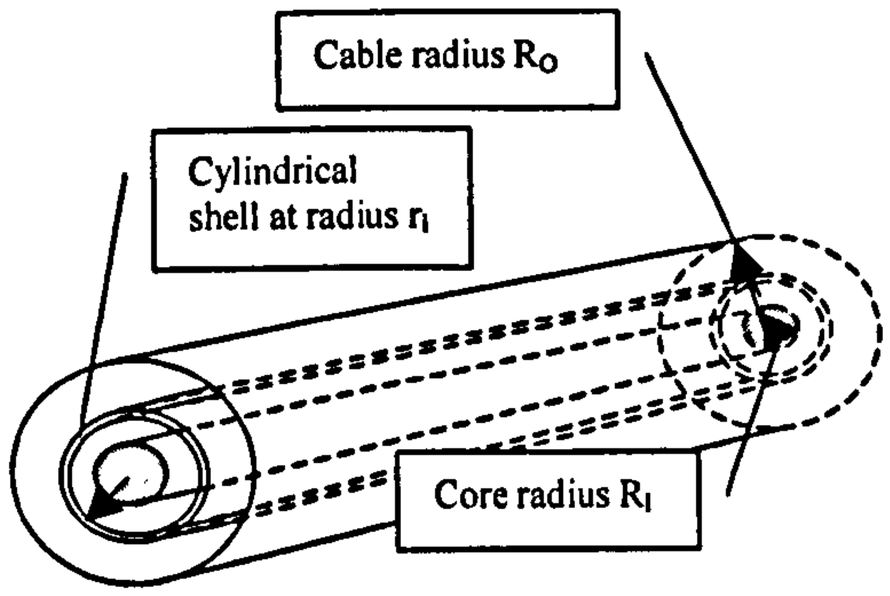

Figure 1 - Example shell at radius r_i

Each shell experiences E_i and T_i according to its position r_i and (2) and (3). Substituting E_i and T_i into equation (1) then provides a lifetime expression for each shell in terms of r_i and the DMM parameters. These *N* lifetime expressions then need to be fitted to the B63 value for each experimental ageing condition to give parameter values. An expression linking the lifetime expressions of the shells and the experimental B63 value is therefore required, and this can be obtained via probability equations.

Assuming that any insulation system can be considered as made up of many smaller insulation volumes, and that failure in any one of the volumes will cause the entire insulation to fail, the following equation can be used.

$$PS(L) = \prod_{i=1}^{N} PS(S)_i \quad (4)$$

Where *PS(L)* is the probability of survival at time t of a large volume of insulation, made up of *N* components. $PS(S)_i$ is the probability of survival at time t of the ith, smaller component. If the values of *PS(S)* are all the same, this leads to

$$PS(L) = PS(S)^N \quad (5)$$

Assuming that *PS(L)* and *PS(S)* are Weibull distributions with the same β values, (4) can be used to derive an expression for the characteristic lifetime of a large volume of insulation, B63 in terms of the characteristic lifetimes of a set of smaller volumes of insulation, L_i.

$$\frac{1}{B63^{\beta}} = \sum_i \left(\frac{1}{L_i^{\beta}}\right) \quad (6)$$

In this case, B63 is the characteristic lifetime of a cable set, and L_i is an expression for the lifetime of the 'i'th shell. Parameter values obtained from fitting this equation will necessarily depend on the volume of the cable insulation through B63 in the same way as for thin films. However, they will also have a dependence on the shell volume (or equivalently a dependence on *N*), since the probabilities in (4) are volume dependent.

Parameters that depend on both *VC* and *N* have the disadvantage that direct comparisons between cable and film experiments are then difficult, since parameters from film experiments will only depend on the total insulation volume. To get parameter values from cable experiments that only depend on *VC*, it is necessary to 'scale up' the probability of failure of each shell to the total insulation volume. In other words, it is necessary to work out the probability of failure that each shell would have if it had the volume of the whole insulation. This can be obtained using (7).

$$PS(SS) = PS(SH)^N \quad (7)$$

Where *PS(SS)* is the probability of survival of the scaled up shell, and *PS(SH)* is the probability of survival of the shell. Equation (4) shows that taking the product of the *PS(SS)* values would then give the probability of survival of a volume of insulation *N* times bigger than *VC*. Using (4) and (7) therefore gives

$$\prod_{i=1}^{N} PS(SS)_i = \prod_{i=1}^{N} [PS(SH)]^N{}_i = PS(NV) \quad (8)$$

Where *PS(NV)* is the probability of survival of an insulation specimen with volume *N* times bigger than *VC*. To get the probability of survival of insulation of volume *VC* (i.e. of the total cable insulation), (5) can be used again with (8) to give

$$PS(VC) = PS(NV)^{\frac{1}{N}} = \left[\prod_{i=1}^{N} PS(SS)_i\right]^{\frac{1}{N}} \quad (9)$$

Where *PS(VC)* is the probability of survival of the cable. Using this equation, and assuming again that the probabilities of survival are all Weibull distributions with the same shape parameter, the following equation is derived

$$\frac{1}{B63^{\beta}} = \frac{1}{N}\sum_{i}\left(\frac{1}{L_i{}^{\beta}}\right) \quad (10)$$

L_i is now an expression for the lifetime of a scaled up shell – i.e. an expression for the lifetime that a shell would have if it had volume *VC*. Substituting (1) for each L_i and fitting the equation to experimental B63 data results in parameter values that have no dependence on *N*, and depend only on the total volume of insulation, *VC* through B63.

As in the thin film case, the parameters should have no dependence on *E* or *T*, so the function to be minimised is

$$\sum_{J}\left[\left\{\log(B63_J) - \log\left(\left[\frac{N}{\sum_{i}\left(\frac{1}{L_i{}^{\beta}}\right)}\right]^{\frac{1}{\beta}}\right)_J\right\}^2\right] \quad (11)$$

$B63_J$ is the Jth experimental characteristic lifetime value. In (11), logs are used due to the extreme non-linearity of (1). Squares are used to ensure a good fit for all B63 values.

Application of the method

The above fitting method was applied to data from sets of cables aged under nine different AC voltage and temperature conditions. Twelve cables were aged under each of the nine experimental conditions. The cables had core radii of 5.9mm surrounded by XLPE insulation of 4.4mm thick. Equation (11) was minimised using a grid search method implemented in FORTRAN, the output of which was the error function magnitude with values for each of the DMM parameters.

Results

The parameters obtained above can be used to plot lifelines – i.e. lines showing predicted cable lifetime with applied voltage. The lifelines for the optimal parameter set obtained are shown in figure 2 with the experimental B63 data from the cable tests. The experimental B63 data points are shown as crosses with their 90% confidence limits shown as error bars. Lifelines corresponding to the temperatures under which experiments were conducted are shown as lines. The error function for this parameter set has a value of 0.85.

The parameters obtained are shown in table 1, along with the parameter values found from fitting the model to PET film samples and XLPE insulated mini-cables [1]. These other fittings were carried out using the Levenberg-Marquardt algorithm to minimise the difference between experimental data and the DMM lifetime predictions, which is a more sophisticated method than a grid search. A grid search was used here due to the higher level of complexity of the equation to be minimised.

TABLE 1	Parameters from this investigation	Parameters for AC ageing of PET	Parameters for AC ageing of mini-cables
Sd (J/K)	-4.0E-22	-5.2E-22	-5.6E-22
Hdk (K)	6000	1274	1448
Kd (K)	250	103	229
C_d (J(mm/kV)^{4b})	2.25	1 593	1.376
A*	0.35	0.485	0.38
b	0.5	0.39	0.425

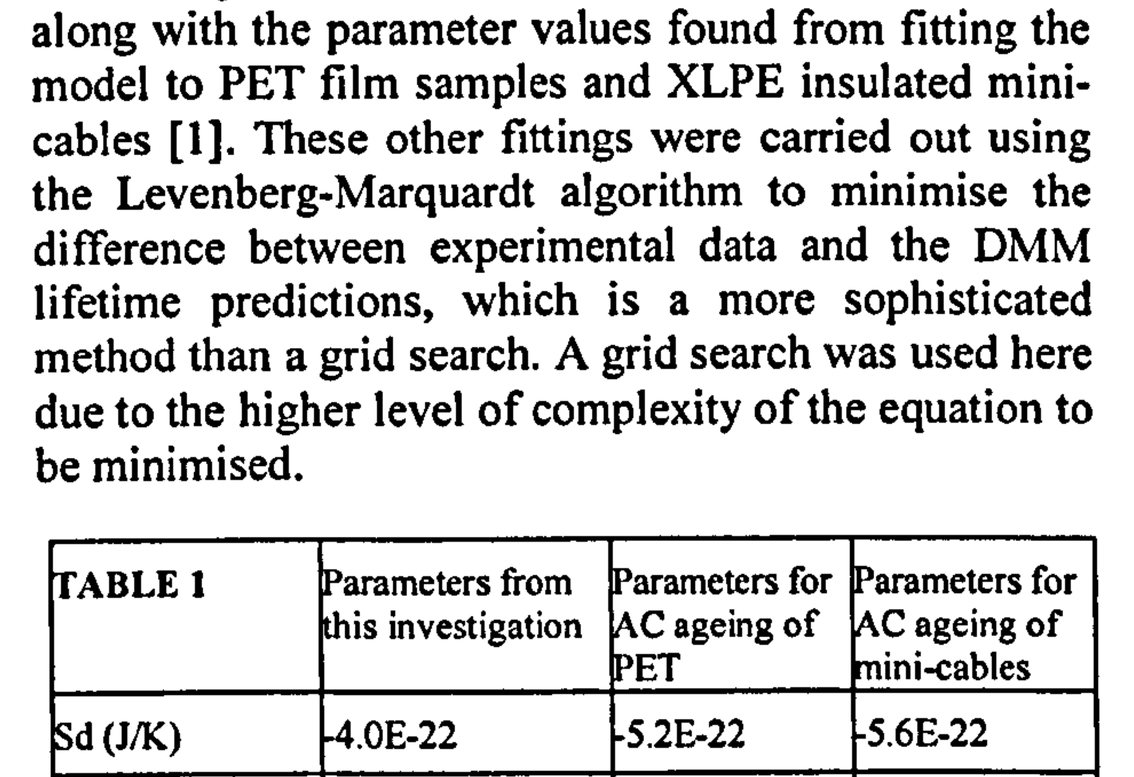

Figure 2 - Lifelines with data

Discussion

The match between the data and the lifelines obtained using the parameters from the fitting method can be seen to be fairly good, with the model being within the 90% confidence limits for four of the nine data points. The parameters were allowed to vary over wide ranges in the grid search fitting, and the magnitudes of the model parameters obtained are all similar in magnitude to those obtained in previous fittings for XLPE mini-cables and PET thin films. This suggests that the method works well, and supports the theory that the

ageing process is the same for each of the materials studied.

Any dependence of specimen lifetime on volume must be reflected in the magnitudes of the DMM parameter values obtained from fitting to the data. The question of how specimen volume affects parameter values in table 1, however, is not clear, since the parameters obtained are all for different materials, as well as for different volumes. It is therefore not possible to separate out differences due to volume from differences due to material morphology and chemical composition. The volume of insulation used in this investigation, however, is considerably larger than in the other two cases.

It is possible to speculate on which of the DMM parameter values might be affected by volume. The idea that a larger volume of insulation will fail faster than a smaller volume is essentially based on the fact that a larger volume must contain more moieties that can take part in the ageing process. Thus the likelihood of finding moieties that are in some way more susceptible to ageing, or can age faster is increased.

It is possible that a larger volume of polymer may contain more moieties with very low #G values, and this may be responsible for the shorter lifetimes observed in larger polymer specimens. The values obtained show however, that the *characteristic* value of #G is actually very similar for all three of the parameter sets. Over a range of temperatures from 20°C to 100°C the ratio of the energy barrier magnitudes is never more than 1.2:1. This would imply that the ageing process is very similar in each of the specimens regardless of material or volume. The differences in the magnitudes of the parameters between this investigation and the others may be due more to the different fitting methods used than any physical reason. However it should be noted that because #G appears in an exponential form in (1) a small decrease in its value will reduce the characteristic lifetime substantially.

It is also possible that A^* could vary from area to area of specimen. If so, in a larger volume of polymer there must be an increased likelihood of finding areas where fewer moieties need to be in the aged state for breakdown to be initiated. As a result the sample will require less local energy concentration ($\propto K_d A^*$) for the initiation of failure. The differences in *characteristic* A^* found so far imply that the samples with larger volumes require lower energies and hence probably a lower threshold field with a concomitant reduction in lifetime.

C_d and b describe the effect of a field on the barrier to ageing, #G. On the application of an electrical field of magnitude E, #G is reduced by an amount equal to $C_d E^b$, and this acts to accelerate the ageing reaction. Large values of C_d and b for a set of specimens therefore indicate that the ageing reaction is accelerated strongly by the electrical field. A greater volume of polymer is more likely to contain sites at which this is the case – i.e. sites at which the field can have a strong influence on the ageing process. According to the model such sites will be those that have greater ability to trap charge and store electro-mechanical energy. They may be expected to have a bigger electrostriction coefficient, and/or smaller bulk modulus and relative permittivity than the average. Variations in these material characteristics seem likely on a microscopic scale, which makes these two parameters the most likely to have a volume dependency. The data in table 1 seems to support this to some extent, with the largest polymer volume showing the largest values of C_d and b. These parameters are also likely to be material dependent, however, so this is by no means conclusive.

Conclusions

The method outlined above for fitting the DMM model to data from ageing experiments involving cables has been shown to produce results that match experimental data well. The parameter values so obtained are consistent with values obtained from fitting the model to data from ageing tests involving other polymeric materials, supporting the theory that the ageing process is the same in each. The question of how volume affects ageing in polymers is still poorly understood, and requires further research, but it seems that the DMM parameters C_d and b, which describe the effect of the field on ageing, are the ones most likely to have volume dependence.

References

[1] G Mazzanti, G.C Montanari, L. Dissado, 'A Space-charge Life Model for ac Electrical Aging of Polymers' IEEE TDEI vol 6, pp864-875, 1999.

[2] T. J. Lewis, J. P. Llewellyn, M. J. van der Sluijs, J. Freestone, R. N. Hampton, 'A New Model for Electrical Ageing and Breakdown in Dielectrics' IEE DMMA Conf. Pub. 430, pp220-224, 1996.

[3] J. P. Crine, 'A Molecular Model to Evaluate the Impact of Aging on Space Charges in Polymer Dielectrics'. IEEE TDEI vol 4, pp487-495, 1997

[4] J. Artbauer, 'Electric strength of Polymers'. JPhysD. vol 2, pp446-456, 1996.

[5] C.K Eoll, 'Theory of Stress Distribution in Insulation of High-Voltage DC Cables: Part 1' IEEE Trans. EI, vol E1-10, pp27-35, 1975.

[6]Edited by G. F. Moore, 'Electrical Cables Handbook' Blackwell Science Ltd 1998. ISBN: 0 632 04075 0